

**Independent University**

**Bangladesh (IUB)**

**IUB Academic Repository**

---

Electrical and Electronics Engineering

Article

---

2015-12

# Artifact Characterization, Detection and Removal from Neural Signals

Islam, Md Kafiul

National University of Singapore

---

---

<http://dir.iub.edu.bd:8180/handle/123456789/261>

*Downloaded from IUB Academic Repository*

# Artifact Characterization, Detection and Removal from Neural Signals

**Md Kafiul Islam**


*B.Sc. in EEE, Islamic University of Technology, Dhaka, Bangladesh*

A THESIS SUBMITTED  
FOR THE DEGREE OF DOCTOR OF PHILOSOPHY  
DEPARTMENT OF ELECTRICAL AND COMPUTER ENGINEERING  
NATIONAL UNIVERSITY OF SINGAPORE

2015

## Declaration

I hereby declare that the thesis is my original work and it has been written by me in its entirety. I have duly acknowledged all the sources of information which have been used in the thesis. This thesis has also not been submitted for any degree in any university previously.



---

Md Kafil Islam

November 2015

# Dedication

I dedicate this thesis to my beloved parents especially my father who has always dreamed of my doctoral degree and therefore has provided for me the best education he could afford since beginning. On the other hand, dedication to my mother who has sacrificed everything in her life to raise me, educate me and suffer for me. I also dedicate my thesis to my new-born son Afraz who has been a blessing and inspiration for my life since he was born. I have learned the true value of parenting after becoming a father which inspires me to realize and appreciate even more about the role of my own parents in my life.



## Acknowledgments

First and foremost, all the praises be to Almighty Allah for His endless blessings, mercy and guidance upon me. Thank to Allah for bestowing me with wisdom and sustaining me with countless supports throughout this study period.

I would like to express my utmost gratitude to my supervisor Dr. Zhi Yang. Since the beginning of my research study, he has been guiding me with so much skills and care; especially I am quite thankful to him for his invaluable sharing of ideas, inspiration, advices, discussions and above all, great patience.

I am also very grateful to Dr. Amir Rastegarnia for his continuous guidance and encouragement throughout the study. His insights, comments, critical assessments and ideas for improvements have always sharpened my views, and helped me to refine my works. I also express my thanks to his wife Dr. Azam Khalili as well for her supports.

I am thankful towards our research group members Anh Tuan Nguyen, Mohammad Reza Keshtkaran, Xu Jian, Zhou Yin, and others. Specially Anh Tuan Nguyen who helped me to write down the MATLAB code during artifact database synthesis.

My deepest thanks to my parents for whom I have come to this far where I am now and special thanks to my better-half who always encouraged me and stood by my side during my difficult times.

# Contents

<b>Summary</b>	<b>vi</b>
<b>List of Tables</b>	<b>ix</b>
<b>List of Figures</b>	<b>xi</b>
<b>1 Introduction</b>	<b>1</b>
1.1 Background	1
1.1.1 <i>In-Vivo</i> Neural Recording	1
1.1.1.1 Single and Multi-Unit Recording (Spikes)	5
1.1.1.2 Local Field Potentials	6
1.1.2 Electroencephalography (EEG)	7
1.2 Thesis Motivation	8
1.2.1 Artifact Removal from <i>In-Vivo</i> Neural Recording	8
1.2.1.1 The Signal and Artifact Characteristics	9
1.2.1.2 Deficiency of Available Algorithms	9
1.2.2 Artifact Reduction from Scalp EEG	11
1.2.2.1 Artifact Reduction for Seizure Detection	11
1.2.2.2 Artifact Reduction for BCI Experiments	13
1.3 Thesis Objectives	15
1.4 Overview and Contributions	16
1.4.1 Overview	16
1.4.2 Original Contributions	17
<b>2 Artifacts</b>	<b>20</b>
2.1 Characterization ( <i>In-Vivo</i> Neural Recording)	20
2.1.1 Sources	21
2.1.2 Types	23
2.1.3 Properties	25
2.2 Artifact Spectrum vs. Neural Signal Spectrum	26
2.3 Dynamic Range	28
2.3.1 Real Data	29
2.3.2 Synthesized Data	30
2.3.3 Calculation of Dynamic Range	31

2.3.4	Spectral Domain Analysis . . . . .	35
2.4	Artifact Characterization in EEG . . . . .	36
2.4.1	Internal/Physiological Artifacts . . . . .	36
2.4.2	External Artifacts . . . . .	37
<b>3</b>	<b>Literature Review</b>	<b>39</b>
3.1	Introduction . . . . .	39
3.2	Existing Artifact Handling Methods . . . . .	41
3.2.1	Artifact Avoidance . . . . .	41
3.2.2	Artifact Detection . . . . .	42
3.2.2.1	Machine Learning . . . . .	43
3.2.3	Artifact Rejection . . . . .	43
3.2.4	Artifact Removal . . . . .	44
3.2.4.1	Regression . . . . .	44
3.2.4.2	Blind Source Separation . . . . .	45
3.2.4.3	Time-Frequency Representation . . . . .	48
3.2.4.4	Wavelet Transform . . . . .	49
3.2.4.5	Empirical Mode Decomposition . . . . .	51
3.2.4.6	Adaptive Filtering . . . . .	52
3.2.4.7	Wiener Filtering . . . . .	53
3.2.4.8	Bayesian Filtering . . . . .	54
3.2.4.9	Spatial Filtering . . . . .	55
3.2.4.10	Hybrid Methods . . . . .	56
3.2.4.11	Statistical Features . . . . .	61
3.3	Comparison between Methods . . . . .	64
3.3.1	Removal Performance . . . . .	65
3.3.2	Automatic or Semi-Automatic . . . . .	65
3.3.3	Real-time/Online Implementation . . . . .	66
3.3.4	Single or Multi-Channel . . . . .	66
3.3.5	Robustness . . . . .	67
3.3.6	Reference Channel . . . . .	67
3.3.6.1	EOG . . . . .	68
3.3.6.2	ECG . . . . .	68
3.3.6.3	Eye Tracker . . . . .	69
3.3.6.4	Accelerometer . . . . .	70
3.3.6.5	Gyroscope . . . . .	70
3.3.6.6	Contact Impedance Measurement . . . . .	71
3.3.6.7	Motion Captured Camera . . . . .	71
3.4	Effects of Artifacts in EEG-Based Applications . . . . .	76
3.4.1	Epilepsy Monitoring . . . . .	76
3.4.2	BCI Applications . . . . .	76
3.4.3	Patient Monitoring . . . . .	77
3.4.4	Sleep Study . . . . .	78
3.4.5	Other Applications: Neurological Diseases . . . . .	78
3.5	Discussion . . . . .	79
3.5.1	Current Status . . . . .	79

3.5.1.1	FORCe	80
3.5.1.2	FASTER	80
3.5.1.3	LAMIC	80
3.5.1.4	PureEEG	81
3.5.1.5	OSET	81
3.5.1.6	MARA	81
3.5.1.7	AAR	82
3.5.1.8	ADJUST	82
3.5.2	Future Direction	83
3.5.2.1	Probability Mapping	83
3.5.2.2	Standard Performance Evaluation	84
3.5.2.3	Ground Truth Data	85
3.5.2.4	Recommendation	86
3.6	Conclusions	87
<b>4</b>	<b>Artifact Detection and Removal from <i>In-Vivo</i> Neural Recording: Algorithm Design</b>	<b>89</b>
4.1	Introduction	90
4.2	Time Series Analysis of Neural Signal	91
4.2.1	Spectrogram	92
4.2.2	Correlation Analysis	93
4.2.3	Coherence Analysis	94
4.3	Data Modeling	95
4.4	Proposed Algorithm	97
4.4.1	Artifact Labeling	98
4.4.1.1	SWT Decomposition	99
4.4.1.2	Threshold Calculation	101
4.4.2	Filtering	104
4.4.3	Detection	106
4.4.4	Signal Reconstruction	106
4.5	Experiments	107
4.5.1	Experiment on Real Data	110
4.5.2	Experiment on Synthesized Data	111
4.5.2.1	Efficiency Metrics	111
4.6	Results and Discussion	116
4.6.1	Effect of Filtering	116
4.6.2	Quantitative Evaluation	117
4.6.3	Qualitative Analysis	121
4.6.4	Comparison with Other Methods	121
4.7	Optimum Parameter Selection	126
4.7.1	Unsupervised Selection of Mother Wavelets	126
4.7.2	Calculation and Optimization of Threshold Parameters	131
4.7.2.1	Optimization of $k_A$ and $k_D$	132
4.8	Conclusion	133

<b>5</b>	<b>Artifact Reduction from Scalp EEG for Epilepsy Seizure Monitoring: Algorithm Design</b>	<b>138</b>
5.1	Introduction	139
5.2	EEG Characteristics	143
5.2.1	EEG Rhythm	144
5.2.2	Epileptic Seizures	145
5.3	Proposed Algorithm	146
5.3.1	Reference Generation	147
5.3.2	Preprocessing	147
5.3.3	Wavelet decomposition	149
5.3.4	Denoising	150
5.3.5	Decision	152
5.3.6	Reconstruction	153
5.3.7	Overall Process Flow	154
5.4	Methods and Experiments	155
5.4.1	Data Collection	155
5.4.2	Data Synthesis	157
5.4.2.1	Semi-Simulated	157
5.4.2.2	Fully-Simulated	157
5.5	Performance Evaluation	158
5.5.1	Metrics for Artifact Removal	159
5.5.2	Metrics for Seizure Detection	160
5.5.2.1	Feature Extraction	161
5.5.2.2	SVM Classification	163
5.6	Results and Discussion	165
5.6.1	Qualitative Evaluation	165
5.6.1.1	Real Data	165
5.6.1.2	Semi Simulated	165
5.6.1.3	Fully Simulated	166
5.6.2	Quantitative Evaluation	167
5.6.2.1	Artifact Removal Results	168
5.6.2.2	Comparison with Other Methods	169
5.6.2.3	Seizure Detection Results	170
5.7	Optimum Parameter Selection	175
5.8	Conclusions	175
<b>6</b>	<b>Artifact Reduction for EEG-based BCI Application: Algorithm Design</b>	<b>180</b>
6.1	Introduction	181
6.2	Proposed Method	185
6.2.1	Artifact Detection: Probability Mapping	185
6.2.2	SWT-Based Artifact Removal	189
6.2.2.1	Preprocessing	189
6.2.2.2	Wavelet Decomposition	191
6.2.2.3	Denoising	192
6.2.2.4	Decision	193

6.2.2.5	Reconstruction	195
6.3	Methods/Data Collection	195
6.3.1	Data Collection	195
6.3.2	Data Synthesis	196
6.4	Performance Evaluation	196
6.4.1	Artifact Removal Performance Metrics	196
6.4.2	BCI Performance Metrics	197
6.5	Results and Discussion	198
6.5.1	Qualitative Evaluation	198
6.5.1.1	Real Data	198
6.5.1.2	Simulated	198
6.5.2	Quantitative Evaluation	200
6.5.2.1	Artifact Removal	201
6.5.2.2	Comparison with Other Methods	202
6.5.2.3	BCI Performance	204
6.6	Conclusions	207
6.7	Tuning of Parameter $K$ for MI-BCI Application	207
<b>7</b>	<b>Conclusion and Future Work</b>	<b>210</b>
7.1	Contributions	210
7.2	Future Works	211
7.2.1	Improvements on Current Work	212
7.2.1.1	Artifact Removal from <i>In-Vivo</i> Neural Signals	212
7.2.1.2	Artifact Removal from EEG	213
7.2.2	Other Possible Applications of Current Work	214
7.2.2.1	Neural Signals	214
7.2.2.2	Non-Neural Biomedical Signals	215
7.2.2.3	Software GUI for Complete Solution	215
	<b>Bibliography</b>	<b>216</b>
<b>A</b>	<b>Source Codes and Artifact Templates</b>	<b>247</b>
A.1	Open Source MATLAB Codes for Artifact Removal	247
A.1.1	Artifact Removal from <i>In-Vivo</i> Neural Signals	247
A.1.2	Artifact Removal from EEG for Seizure Detection Application	248
A.1.3	Artifact Detection and Removal from EEG for BCI Application	248
A.2	Artifact Templates	248
A.2.1	<i>In-Vivo</i> Neural Recording	248
A.2.2	EEG Recording	248
	<b>Author's Publications</b>	<b>250</b>

# Summary

Extracellularly recorded neural data from *in-vivo* experiments provide higher spatio-temporal resolution and SNR compared with non-invasive brain signal recordings. While the recorded data can be corrupted by artifacts, especially under a less constrained recording protocol, the detection and removal of artifacts as a part of neural signal preprocessing procedure without distorting the signal-of-interest, play an important role. However, due to very limited knowledge of the appeared artifacts and the broad spectral content of *in-vivo* neural data, it is difficult to apply available artifact removal algorithms directly on *in-vivo* neural recordings and thus poses a great challenge to decode the underlying brain information properly. The first objective of this thesis is to investigate the artifacts usually found in the *in-vivo* neural recordings and then characterize them in a systematic way (first ever attempt to the best of our knowledge). Our second objective is to develop an algorithm for automatic artifact detection and removal without distorting the signals of interest.

Apart from *in-vivo* neural recordings, EEG has been the most preferred way of brain recordings in clinical studies, lab experiments, patient

health monitoring, diagnosis and many other applications due to its non-invasiveness and affordability benefits . In scalp EEG-based applications, as the electrodes are placed on the scalp, become most prone to external artifacts including physiological ones. Consequently artifact detection and removal also from EEG recordings become one of the most faced challenges and therefore an active research problem in EEG signal processing community. Many attempts have been made till now to develop suitable methods for artifact detection and removal with the help of recent advancement in signal processing techniques and algorithms. However, each of them lacks from some practical issues and there is no complete solution yet which indicates the future need for removal algorithms to be more application-specific; e.g. in brain-computer interface (BCI) or epilepsy seizure detection applications. This research gap motivates us to design artifact removal algorithms for two of the most popularly used EEG-based applications i.e. epilepsy seizure monitoring and BCI studies. The proposed EEG artifact reduction methods are automatic, independent of artifact types, do not require a reference channel, can work for both single and multi channels and most importantly application-specific.

In order to evaluate the proposed methods quantitatively in comparison with available state-of-the-art methods, different artifact types have been extracted from real recordings for simulating artifact templates and hence to build a synthesized neural database on which the methods are applied. Extensive testing shows that the proposed algorithms can remove around



50 – 80% of artifacts on average which correspond to SNR increment of about 10 – 15 dB without almost no distortion to signal of interest and outperform the counterpart methods with a large margin. In addition, the effects of artifact removal on the later-stage processing have also been evaluated that result in significant performance improvement in terms of neural spike detection, seizure detection and BCI classification which proves the efficacy of the proposed methods. Thus this work is expected to provide a useful platform in neural signal analysis and processing area for future brain research.

# List of Tables

2.1	Summary of artifact classification from different perspectives.	23
2.2	Summary of dynamic range change due to artifacts. . . . .	30
2.3	Different types of artifacts and their origins. . . . .	37
3.1	Comparative analysis of artifact removal methods found in literature published in recognized journals: Part-A IEEE articles . . . . .	73
3.2	Comparative analysis of artifact removal methods found in literature published in recognized journals: Part-B Elsevier articles . . . . .	74
3.3	Comparative analysis of artifact removal methods found in literature published in recognized journals: Part-C other articles . . . . .	75
4.1	Correlation coefficient between 8 different channels from a same electrode recording shown in Figure 2.2 (left plot) to detect global type-0 artifacts. . . . .	94
4.2	The frequency bands of the respective SWT coefficients and corresponding signal components for a 10-level decomposition. Here two typical sampling frequencies for extracellular neural recordings are considered (i.e. 40 kHz and 30 kHz) and the maximum recording bandwidth is assumed to be half of the sampling frequency. . . . .	101
4.3	Quantitative comparison of proposed method with other methods on artifact removal for different artifact SNR ( $SNR_{Art}$ ). . . . .	136
4.4	Improvement in FPR and TPR for proposed method in comparison with other methods for different data RMS thresholds. . . . .	137
5.1	The frequency bands of EEG rhythms and seizure activities. . . . .	144
5.2	The frequency bands of wavelet coefficients after performing level-8 SWT on the raw EEG data which has a typical sampling frequency of 256 Hz. Coefficients that correspond to the seizure activities (0.5 Hz $\sim$ 30 Hz) are from $d_3$ to $d_8$ . . . . .	149

5.3	Pseudo code for the separation of seizures from artifacts. The decision is made by the similarity based thresholding. .	151
5.4	Quantitative metrics of artifact removal results for different artifact SNR ( $SNR_{Art}$ ). . . . .	179
5.5	Quantitative metrics of artifact removal results for different artifact durations ( $\Delta T_{Art}$ ). The mean values are highlited with bold face in the final row. . . . .	179
6.1	Illustration of SWT coefficients in relation to EEG rhythms, artifacts and relevant BCI studies in their corresponding frequency bands. . . . .	190
6.2	Pseudo-code for the decision stage during denoising SWT coefficients. . . . .	194
6.3	Quantitative metrics of artifact removal results for corresponding artifact SNR ( $SNR_{Art}$ ) and artifact duration ratio ( $T_{Art}(\%)$ ) for two different cases: one is without considering probability mapping and the other is after considering probability mapping. . . . .	206

# List of Figures

1.1	A typical experimental set-up for <i>in-vivo</i> extracellular neural recording of spontaneous neural activity from a freely moving subject. . . . .	2
1.2	A typical closed loop neural system for BCI or neural prostheses applications. . . . .	4
1.3	Illustration of an idealized intracellular action potential shows its various phases as the action potential passes a point on a cell membrane (a). A schematic diagram showing a field potential recording in response to a stimulus from rat hippocampus by an intracellular (1) and an extracellular electrode (2) (b). . . . .	6
1.4	An illustration of EEG based epilepsy seizure monitoring and detection. Adopted from [14]. . . . .	8
2.1	Illustration of different artifact sources for <i>in-vivo</i> neural recording. . . . .	22
2.2	Example of global artifacts from two different datasets. . . .	23
2.3	An example of irregular (top) and periodic (bottom) artifacts. . . .	24
2.4	Different types of artifact present at <i>in-vivo</i> recordings. . . .	26
2.5	(a), (b), and (c): manually labeled type-1, type-2, and type-3 artifact segments collected from recorded data. (d), averaged type-1 and type-2 artifact power spectrum in comparison with LFP. (e), type-3 artifact spectrum and spike spectrum. Spikes are randomly selected from two different templates. . . . .	28
2.6	An example of effect of artifact on dynamic range can be seen in two time domain database of <i>in-vivo</i> neural data recorded from two different subjects. Left plot is from human epilepsy data and right plot is from rat hippocampus data. . . . .	31
2.7	Synthesized artifact templates for type-1, type-2 and type-3. . . . .	31

2.8	The simulation result for both full spectrum neural signal and spike signal contaminated with different artifact templates with respect to different artifact amplitudes. Top plot is for rat hippocampus data and bottom plot is for human epilepsy data. . . . .	32
2.9	Illustration of different ADC resolution noise floor in comparison with neural signal power in spectral domain to choose the right ADC resolution in order to achieve minimum 10 dB SNDR for full-spectrum neural recording. . . . .	33
3.1	Trend of research on artifact detection and removal from EEG in terms of publication history since year 2000 until present indexed by Google Scholar. The search criteria include both the keywords Artifact(s)/Artefact(s) and EEG(s)/Electroencephalography/Electroencephalogram(s) that present in the title of published journal articles and conference papers. . . . .	40
3.2	Machine learning classification for identifying artifactual epoch from clean EEG epoch. . . . .	44
3.3	Illustration of blind source separation technique. . . . .	46
3.4	A 3-level DWT filter bank for decomposition (collected from [74]). . . . .	48
3.5	Typical use of adaptive filtering in canceling physiological artifacts with available artifact source channel as reference [80]. . . . .	53
3.6	General process flow of EMD-BSS and Wavelet-BSS methods. . . . .	54
3.7	Process flow of the hybrid BSS-SVM algorithm. . . . .	58
3.8	Process flow of the hybrid REG-BSS methodology. . . . .	59
3.9	Process flow of the hybrid ICA-ARX methodology. . . . .	59
3.10	Process flow of EMD algorithm to generate IMFs. . . . .	60
4.1	Upper trace: real neural data contaminated with both type-1 and type-2 artifacts; Lower trace: Spectrogram of that neural data showing the justification of using BPF at 150-400 Hz as there is significant artifact power in this band corresponding to the temporal location of artifacts. . . . .	93
4.2	Coherence analysis between clean reference data and artifact-contaminated data which clearly shows that type-1 and type-2 artifacts can be detected between 150 Hz to 400 Hz as the coherence is minimum at this band while coherence for type-3 artifact becomes lower after few kHz. . . . .	95
4.3	Comparison in amplitude histogram of LFP for reference, artifactual and reconstructed signal. . . . .	96
4.4	Corresponding time course data for the histogram of three signals shown in Figure 4.3. . . . .	97
4.5	Overview of the proposed algorithm. . . . .	98

4.6	An example of all the signals at different stages (as mentioned in the proposed algorithm flow in Figure 4.5) in the same temporal domain is provided. A 10-level SWT decomposition is performed to an artifactual signal with Haar basis wavelet. (a): artifactual signal, $r(n)$ ; (b): reconstructed signal, $r'(n)$ ; (c): $x_b(n)$ obtained from band-pass filtering $r(n)$ at 300 Hz - 5 kHz; (d): A zoom-in version of (c) showing few spikes; (e): $x_s(n)$ obtained from band-pass filtering $r_n$ at 150 Hz - 400 Hz; (f): $x_h(n)$ obtained from high-pass filtering $r(n)$ at 5 kHz; (g)-(h): The final approximate coefficient before and after thresholding respectively; (i)-(j): The detail coefficients before and after thresholding respectively. . . . .	99
4.7	(a) Type-3 artifact contaminated neural data and (b) Effect of HPF at 5 KHz for detecting type-3 artifact; Effect of band pass filtering at 150-400 Hz for detecting type-1 (c) and type-2 (d) artifacts. . . . .	105
4.8	The comparison between two threshold functions: hard and garrote in terms of spike detection on the reconstructed signal where it is obvious that garrote outperforms the hard threshold. . . . .	108
4.9	Artifact removal algorithm applied to a raw <i>in-vivo</i> data recorded from the hippocampus of a rat. The plot is the time course data where both type-1 and type-2 artifacts are present. . . . .	108
4.10	A Comparison in field potentials and spike data when there are no visually detectable artifacts (A small data segment from Figure 4.9 after low-pass filtering at 200 Hz and band-pass filtering at 300 Hz - 5 kHz are performed to get LFP and spike data respectively). The proposed algorithm nearly perfect reconstructs the original data when there is no artifact present. . . . .	109
4.11	Illustration of the synthesis process to generate artifactual data. . . . .	112
4.12	Artifact removal example by the proposed method where the artifactual signal (synthesized) is corrupted by all four types of artifact. The top plot shows the three different time course signals of reference, artifactual and reconstructed. The bottom plot is the zoom-in version of the previous plot highlighted on the artifact affected regions. . . . .	113
4.13	The effect of filtering along with SWT in comparison with only SWT during wavelet-denoising for artifact removal is obvious for the time course neural sequences presented in the plots for raw artifactual data with spikes, reconstructed with SWT only and reconstructed with SWT along with filtering respectively. . . . .	117

4.14	ROC curve evaluating neural spike detection accuracy to illustrate the effect of filtering in combination with SWT compared with only SWT. . . . .	118
4.15	Amount of distortion to neural signal in terms of spectral distortion (top) and root mean square error, RMSE (bottom) before and after artifact removal for different artifact SNR. . . . .	118
4.16	Amount of artifact removal in terms of Lambda, $\lambda$ (top) and amount of SNR improvement, $\Delta$ SNR (bottom) for different artifact SNR after artifact removal is performed. . . . .	119
4.17	An example of overlapping of different artifact types in temporal domain in a synthesized artifactual data. . . . .	120
4.18	Amount of distortion to neural signal in terms of root mean square error, RMSE (top) and spectral distortion (bottom) before and after artifact removal for different artifact duration. . . . .	122
4.19	Amount of artifact removal in terms of lambda, $\lambda$ (top) and amount of SNR improvement, $\Delta$ SNR (bottom) for different artifact duration after artifact removal is performed. . . . .	123
4.20	SNDR comparison between signals before (artifactual) and after (reconstructed) artifact removal. The SNDR values are averaged over 200 iterations. . . . .	124
4.21	Comparison of computational latency for artifact removal from in-vivo neural recordings for processing of every 1 sec data segment. . . . .	126
4.22	Example of spike-liked artifacts produced after wICA algorithm is applied on artifactual signal. The upper trace is the superimposed representation of reconstructed signal on artifactual signal and the lower trace is the spike data after and before artifact removal derived from the upper-trace data after BPF is performed from 300 Hz to 5 kHz. . . . .	127
4.23	The decomposition and reconstruction structures of wavelet filters . . . . .	127
4.24	Correlation value vs. $\alpha$ . . . . .	129
4.25	Performance metrics (amount of artifact removal) vs. $\alpha$ . . . . .	129
4.26	Performance metrics (amount of distortions) vs. $\alpha$ . . . . .	130
4.27	Correlation value vs. $k_A$ . . . . .	133
4.28	Performance metrics vs. $k_A$ . . . . .	134
4.29	Correlation value vs. $k_D$ . . . . .	135
4.30	Performance metric, $SNDR$ vs. $k_D$ . . . . .	135
5.1	An example of real seizure segment marked by the epilepsy specialist from MIT-CHB database. . . . .	145
5.2	The overall process flow of the proposed method. . . . .	146
5.3	EEG experiment performed. . . . .	156
5.4	Illustration of the synthesis process to generate artifactual EEG data with seizure segment. . . . .	156

5.5	Process flow for validation of seizure detection. . . . .	157
5.6	The removal result after the proposed algorithm is applied on our recorded EEG. . . . .	163
5.7	The removal result after the proposed algorithm is applied on an artifact-free seizure segment labeled and collected from MIT-CHB dataset. The reconstruction is almost perfect when there is no visible artifact. . . . .	164
5.8	Artifact removal result applied to fully-simulated dataset-1. The plot is a time course data where all six types of artifacts are present. Note that, not all of the artifacts are removed or attenuated. The reason is that in order to preserve the seizure events, the amount of artifact reduction has been compromised. . . . .	166
5.9	Six types of different simulated artifacts that mimicking real artifacts found in the typical scalp EEG recording environments. The application of proposed artifact removal algorithm can almost successfully remove such artifacts most of the time without distorting the background EEG signals. The black, red and blue traces denoting reference, artifactual and reconstructed simulated EEG data respectively. . .	167
5.10	The removal result after the proposed algorithm is applied on the semi-simulated EEG data. . . . .	168
5.11	SNDR for signals before and after artifact removal clearly shows the improvement in signal quality over the entire frequency band. . . . .	169
5.12	Comparison of proposed method with respect to few available artifact removal methods in terms of the quantitative metrics. . . . .	170
5.13	Comparison of proposed method with respect to few available artifact removal methods in terms of the computational time required to process each 1 second of data in MATLAB simulation. . . . .	171
5.14	An example of false alarms due to artifacts is illustrated where sample entropy is chosen as a feature to separate seizure from non-seizure (normal) events. Artifact removal can significantly reduce the false alarms by reducing the amount of artifacts. . . . .	172
5.15	False positive ( $FP$ ) before and after artifact removal (shown on top) and improvement of false positive ( $\Delta FP$ ) in percentage (shown on bottom) are plotted with respect to different data sequence/channel no. For seizure detection purpose, SampEn is used as feature and SVM as classifier. . . . .	172
5.16	ROC curve for seizure detection in scalp EEG to illustrate the effect of artifact removal on the seizure detection performance. . . . .	173



5.17	Different features from EEG data for seizure and non-seizure events calculated for each data segment of time window 1 sec.	173
5.18	Process flow for automatically selection of wavelet parameters for algorithm optimization in terms of best performance metrics.	176
5.19	An illustration of selecting the best mother wavelet by optimizing the parameter alpha with the help of performance metrics vs. alpha plot.	177
5.20	An illustration of selecting the best threshold parameter $k_A$ by the help of performance metrics vs. $k_A$ plot.	178
5.21	An illustration of selecting the best threshold parameter $k_D$ by the help of performance metrics vs. $k_D$ plot.	178
5.22	An illustration of selecting the best threshold parameter $k_A$ and $k_D$ by the help of performance metric (Avg. SNDR Improvement) vs. $k_A$ or $k_D$ plot.	179
6.1	Segmenting EEG sequences into epochs and calculating corresponding probability of being artifactual	188
6.2	Proposed structure to create probability mapping and subsequently to remove artifacts from EEG	189
6.3	Illustration of the synthesis process to generate artifactual EEG data for quantitative evaluation of proposed artifact removal.	196
6.4	The removal result after the proposed algorithm is applied on our recorded EEG.	199
6.5	The removal result after the proposed algorithm is applied on real BCI dataset collected from BCI Competition-IV.	200
6.6	Fully simulated EEG data sequence with different types of artifacts before and after artifact removal (upper plot) and their corresponding probability map (lower plot). The time window duration in this case is chosen as 1 sec	200
6.7	Six types of different simulated artifacts that mimicking real artifacts found in the typical scalp EEG recording environments. The application of proposed artifact removal algorithm can almost successfully remove such artifacts most of the time without distorting the background EEG signals. The black, red and blue traces denoting reference, artifactual and reconstructed simulated EEG data respectively.	201
6.8	Selected epochs with probability more than threshold for artifact correction and their corresponding amount of artifact removal in %.	202
6.9	SNDR improvement in frequency domain for signals before and after artifact removal.	203
6.10	Comparison of proposed method with respect to few available artifact removal methods in terms of the quantitative metrics.	204

6.11	Comparison of proposed method with respect to few available artifact removal methods in terms of the computational time required to process each 1 second of data in MATLAB simulation. . . . .	205
6.12	ROC curve plotted for signals before and after artifact removal from the BCI output using LDA Classifier and Windowed Means as features from BCILAB tool. . . . .	205
6.13	Error Rate for signals before and after artifact removal from the BCI output using LDA Classifier and Windowed Means as features from BCILAB tool. . . . .	206

# List of Acronyms

<b>AAR</b>	<u>A</u> utomatic <u>A</u> rtifact <u>R</u> emoval
<b>ADJUST</b>	<u>A</u> utomatic EEG artifact <u>D</u> etector based on <u>J</u> oint <u>U</u> se of <u>S</u> patial & <u>T</u> emporal features
<b>ANN</b>	Artificial Neural Network
<b>AP</b>	Action Potential
<b>APF</b>	Adaptive Predictor Filter
<b>ARX</b>	Auto-Regressive exogenous
<b>ASD</b>	Automatic Seizure Detector
<b>ASIC</b>	Application Specific Integrated Circuit
<b>BCG</b>	Ballistocardiography
<b>BCI</b>	Brain Computer Interface
<b>BMI</b>	Brain Machine Interface
<b>BPF</b>	Band-Pass Filter
<b>BSS</b>	Blind Source Separation
<b>CBSS</b>	Constrained Blind Source Separation
<b>CC</b>	Correlation Coefficient
<b>CCA</b>	Canonical Component Analysis
<b>CWT</b>	Continuous Wavelet Transform
<b>DWT</b>	Discrete Wavelet Transform
<b>EAS</b>	Ensemble Average Subtraction
<b>EAWICA</b>	Enhanced Automated Wavelet-ICA
<b>ECG</b>	Electrocardiography
<b>ECoG</b>	Electrocorticography

<b>EEG</b>	Electroencephalography
<b>EMD</b>	Empirical Mode Decomposition
<b>EEMD</b>	Ensemble Empirical Mode Decomposition
<b>EMG</b>	Electromyography
<b>ERP</b>	Event Related Potential
<b>FASTER</b>	<u>F</u> ully <u>A</u> utomated <u>S</u> tatistical <u>T</u> hresholding for <u>E</u> EG artifact <u>R</u> ejection
<b>FLNN-ANFIS</b>	Functional link neural network with Adaptive Neural Fuzzy Inference System
<b>FLN-RBFN</b>	Functional Link Neural Network with adaptive Radial Basis Function Networks
<b>fMRI</b>	Functional Magnetic Resonance Imaging
<b>fNIRS</b>	Functional Near-Infra-Red Spectroscopy
<b>FOOBI</b>	Fourth-order Tensor Method
<b>FORCE</b>	Fully Online and automated artifact Removal for BCI
<b>GUI</b>	Graphical User Interface
<b>HFO</b>	High Frequency Oscillations
<b>HHT</b>	Hilbert Huang Transform
<b>HPF</b>	High-Pass Filter
<b>ICA</b>	Independent Component Analysis
<b>IIR</b>	Infinite-Impulse-Response
<b>JBSS</b>	Joint Blind Source Separation
<b>LAMIC</b>	Lagged Auto-Mutual Information Clustering
<b>LDA</b>	Linear Discriminant Analysis
<b>LFP</b>	Local Field Potential
<b>LPF</b>	Low-Pass Filter

<b>MARA</b>	Multiple Artifact Rejection Algorithm
<b>MCA</b>	Morphological Component Analysis
<b>MI</b>	Mutual Information
<b>MSE</b>	Mean Squared Error
<b>OSET</b>	<u>O</u> pen- <u>S</u> ource <u>E</u> lectrophysiological <u>T</u> oolbox
<b>PCA</b>	Principal Component Analysis
<b>PPG</b>	Photoplethysmogram
<b>PSD</b>	Power Spectral Density
<b>RBF-ANN</b>	Radial Basic Function based Artificial Neural Network
<b>RLS</b>	Recursive Least Squares
<b>RRMSE</b>	Relative Root-Mean-Squared Error
<b>SNDR</b>	Signal to Noise and Distortion Ratio
<b>SNR</b>	Signal-to-Noise Ratio
<b>STF-TS</b>	Space–Time–Frequency Time/Segment
<b>STFT</b>	Short Term Fourier Transform
<b>SVD</b>	Singular Value Decomposition
<b>SVM</b>	Support Vector Machine
<b>SWT</b>	Stationary Wavelet Transform
<b>TDSEP</b>	Temporal Decorrelation Source Separation
<b>UBSS</b>	Underdetermined Blind Source Separation
<b>UDWT</b>	Un-Decimated Wavelet Transform
<b>WNN</b>	Wavelet Neural Network
<b>WPT</b>	Wavelet Packet Transform

# Chapter 1

## Introduction

This chapter introduces the background of the current study by describing both invasive and non-invasive neural signals at first, followed by the motivation of this thesis by describing the challenges faced during pre-processing of these neural data due to artifacts and the limitations of the existing methods to handle the issues. Then the objectives of this thesis are presented. Finally the chapter introduction and contributions of each chapter are presented.

### 1.1 Background

#### 1.1.1 *In-Vivo* Neural Recording

Extracellular neural data recorded from awake behaving animals can be used to investigate brain information processing and data storage (e.g. how memory works). Recently, due to the advancement in new record-



Figure 1.1: A typical experimental set-up for *in-vivo* extracellular neural recording of spontaneous neural activity from a freely moving subject.

ing technologies and computational power, *in-vivo* neural recording experiments on such freely behaving animals have been possible that provide a greater means to directly relate neural activity to behavior than in the intact animal or *in-vitro* recordings. Besides, such recorded extracellular *in-vivo* neural signals provide better spatio-temporal resolution than other recording techniques of brain signals, e.g. EEG, MEG, fMRI, fNIRS [1, 2, 3, 4, 5, 6]. However, during such behavioral experiments, especially in less constrained environment, the recorded neural data are severely corrupted by various environment and recording artifacts, mostly due to the random movement of subject (as shown in Figure 1.1). Artifacts in neural recordings can be defined as some abnormal activities that originate from sources other than brain. In general, the appeared artifacts in the recorded neural data saturate the recording electronics and cause serious mistake in interpretation of recorded neural information [7]. Hence as a part of neural

data preprocessing procedure, the detection and removal of such offending artifacts without distorting the signal of interest, play an important role for proper processing of neural signals in the subsequent stages to decode the neural information accurately. In order to develop a complete neural processing system (e.g. open-loop system in basic neuroscience research or closed-loop in neural prostheses or invasive brain-computer interface (BCI)) that works in real-time (required for closed-loop system, although for basic neuroscience studies offline processing is enough), an automatic algorithm which is able to detect and remove artifacts on-the-fly, implemented in an on-chip neural signal processor integrated with the analog front-end circuitry, therefore is extremely necessary.

An example of such neural system is shown in Figure 1.2 where brain signals, recorded using electrode array, are amplified by analog front-end circuitry followed by digitization process by ADC. The post-ADC digital signals are processed in two stages: Preprocessing where artifacts, interferences are removed and Neural Signal Processing where actual signal processing and analysis are performed (e.g. spike detection/sorting). Finally output of signal processing block is transmitted through a bidirectional telemetry interface and then based on the decision, specific feedback in terms of stimulation is provided either to the brain (e.g. epileptic seizure suppression) or other parts of the body (e.g. muscle to control a prosthetic hand) or sometimes to control an external device (e.g. mouse cursor, wheel chair, etc.) depending on the application.



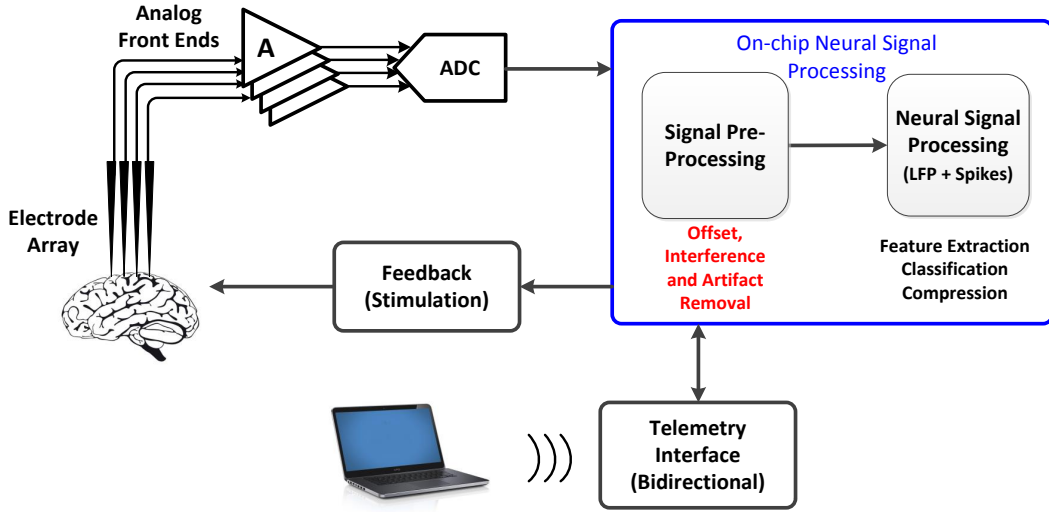


Figure 1.2: A typical closed loop neural system for BCI or neural prostheses applications.

*In-Vivo* neural signal recorded from extracellular space consists of both fast action potentials and slow field potentials and usually has a wide dynamic range starting from few  $\mu\text{V}$  up to few mV [6]. The amplitude of extracellular action potentials (spikes) can vary depending on the recording site from the soma as the spike amplitude decreases rapidly with distance from soma [6]. The variation can be from as low as  $0.1 \mu\text{V}$  (recording site is about  $300 \mu\text{m}$  away from soma) up to as high as  $100 \mu\text{V}$  (if recording electrode tip is closest to soma). While in other literatures it is mentioned that the dynamic range of extracellular action potentials is approximately between  $20 \mu\text{V}$  to  $5 \text{mV}$  [8]. Moreover, very often such recording is severely corrupted by different types of artifacts and interferences especially in less constrained recording environment, e.g. experiments with behaving animals. These offending artifacts not only misinterpret the original neural recordings but also sometimes saturate the recording electronics due to

their large magnitudes compared to neural signal of interest.

#### **1.1.1.1 Single and Multi-Unit Recording (Spikes)**

An electrode implanted into the brain of a living animal will detect electrical activity that is generated by the neurons adjacent to the electrode tip. If it is a micro-electrode, with a tip size of about  $1\ \mu\text{m}$ , the electrode will usually detect the activity of at most one neuron. Recording in this way is in general called 'single-unit' recording [9]. An action potential or spike is a short-lasting event in which the electrical membrane potential of neuron rapidly rises and falls, following a consistent trajectory. The extracellular action potentials are much smaller in amplitude (typically about  $100\ \mu\text{V}$  to  $1\ \text{mV}$ ) compared to intracellular recording [9]. Most recordings of the activity of single neurons in anesthetized and conscious animals are made in this way. Recordings of single neurons in living animals have provided important insights into how the brain processes information. For example, David Hubel and Torsten Wiesel recorded the activity of single neurons in the primary visual cortex of the anesthetized cat, and showed how a single neuron in this area responds to very specific features of a visual stimulus [10, 11]. If the electrode tip is slightly larger, then the electrode might record the activity generated by several neurons. This type of recording is often called "multi-unit recording", and is often used in conscious animals to record changes in the activity in a discrete brain area during normal activity. Recordings from one or more such electrodes that are closely

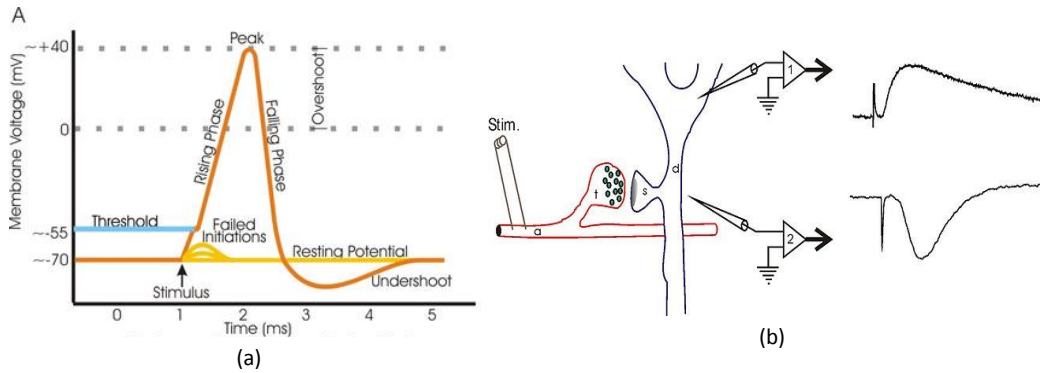


Figure 1.3: Illustration of an idealized intracellular action potential shows its various phases as the action potential passes a point on a cell membrane (a). A schematic diagram showing a field potential recording in response to a stimulus from rat hippocampus by an intracellular (1) and an extracellular electrode (2) (b).

spaced can be used to identify the number of cells around it as well as which of the spikes come from which cell. This process is called spike sorting and is suitable in areas where there are identified types of cells with well-defined spike characteristics. In general the activities of individual neurons cannot be distinguished even if the electrode tip is large, rather the electrode is still able to record a field potential generated by the activity of many neural cells.

#### 1.1.1.2 Local Field Potentials

Extracellular field potentials are local current sinks or sources that are generated by the collective activity of many neurons. Usually, a field potential is generated by the simultaneous activation of many neurons by synaptic transmission. Figure 1.3 (b) shows the recording of hippocampal synaptic field potentials which is adopted from [9, 12].

### 1.1.2 Electroencephalography (EEG)

Electroencephalography (EEG) is a non-invasive recording technique that measures the electrical activity of brain by placing electrodes on the scalp. It is the most commonly used brain recording technique for diagnosis of different neurological disorders along with other applications such as brain-computer interface. The EEG recordings are described in terms of rhythms and transients. The rhythmic activity of EEG is divided into bands of frequency. The most common EEG rhythms are Delta, Theta, Alpha and Beta waves [13]. Recently a relatively high frequency Gamma wave comes into EEG analysis in certain cases. On the other hand, artifacts are transient events, although epilepsy seizure events can also be transient but they are more oscillatory than artifacts.

To provide a model for recorded raw EEG data, let's denote the clean EEG background activity/rhythm as  $E_c$  with weight  $w_c$ ; Artifact event as  $A_{T_n}$  with weight  $w_{T_n}$  and time delay  $\tau_{T_n}$ ; where  $n = 0, 1, \dots, N$  denotes the type of artifact. For example, if it's a Type-1 artifact [7], then denoted by  $A_{T_1}$  with weight  $w_{T_1}$  and time delay  $\tau_{T_1}$ . Now the recorded raw EEG data,  $E_R$  can be modeled as the linear combination of these two signal components:

$$E_R(t) = w_c E_c(t) + \sum_{n=1}^N w_{T_n} A_{T_n}(t - \tau_{T_n}) \quad (1.1)$$

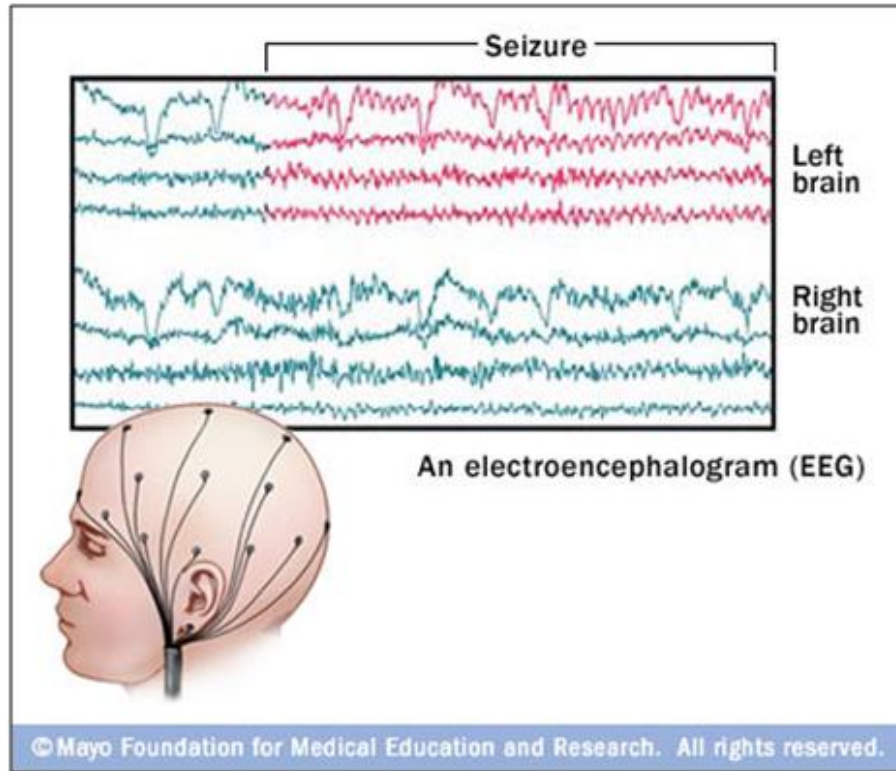


Figure 1.4: An illustration of EEG based epilepsy seizure monitoring and detection. Adopted from [14].

## 1.2 Thesis Motivation

### 1.2.1 Artifact Removal from *In-Vivo* Neural Recording

Many literatures [15, 16, 17, 18, 19, 20, 21, 22, 23, 24, 25, 26, 27] are found that propose various methods/algorithms to detect and remove artifacts in physiological signals (e.g. EEG, ECG, EMG, PPG, fNIRS, fMRI, recording of respiration), but there is hardly any literature found so far to the best of our knowledge that considers artifacts present in *in-vivo* neural signals except only one [28]. The artifact detection and removal for *in-vivo* neural recorded signal is a more challenging task due to the following facts:

### 1.2.1.1 The Signal and Artifact Characteristics

Many other physiological signal recordings mostly contain narrow-band neural data (e.g. bandwidths of EEG, ECG, and EMG in general range from sub Hz to no more than a few hundred Hz) while the *in-vivo* neural recordings have a broad spectral band, i.e. from sub-1 Hz to several kHz. Thus, spectral overlapping between artifacts and signals of interest for *in-vivo* recordings is larger. Apart from the wide bandwidth, the presence of different signal components (i.e. Local Field Potentials (LFP), neural spikes, synaptic activities, etc.) and their highly non-stationary properties [29, 30, 31, 32] compared with other recordings; make it more difficult for identifying artifacts.

When dealing with other physiological signals, often the appeared artifacts have certain stereotype waveforms or the artifact source itself can be recorded by a reference channel. This is not the case for *in-vivo* neural recordings. In fact, as it will be discussed later, the diversity in artifact types, their properties and the way they appear in the recordings make it more challenging in separating them from neural signals.

### 1.2.1.2 Deficiency of Available Algorithms

Many available algorithms for artifact detection and removal cannot be applied to *in-vivo* recordings. For example, a most frequent method to detect and remove artifacts in EEG signals is based on blind source separation (BSS), a technique for estimating/separating individual source com-

ponents/signals from their mixtures at multiple sensors/channels (i.e. observed signals) without knowing (or with very little information) about the source signals or the mixing process. One assumption of BSS is that the observations are linear mixing of the sources and the number of sources is equal or less than the number of observations. Another assumption is that the sources have to be either independent for Independent Component Analysis (ICA) based methods [15, 16, 17, 18, 19, 20] or maximally uncorrelated for Canonical Correlation Analysis (CCA) based methods [33, 34, 35, 36]. However, the mentioned assumptions most often do not match with the *in-vivo* neural recordings. For *in-vivo* neural data, spiking activities from the same neuron mostly appear in one or few adjacent channels, where in the rest of the channels, those activities merge into the noise floor. Therefore, spikes cannot be separated as an independent source if BSS-based algorithm is applied. Different from artifacts in EEG, the artifacts found here are sometimes localized in a single channel, which suggests that the cross-channel analysis cannot be directly applied. Again there could be some correlation present between neural spikes and Local Field Potentials (LFP) [6, 37] which violates the assumption of BSS as mentioned. Although, there are available algorithms in the literature, e.g. wavelet-based [24, 38, 39, 40] and Empirical Mode Decomposition (EMD)/Hilbert-Huang Transform (HHT)-based [22, 23] algorithms to remove such localized artifacts from individual single channel and they do not assume any independence/uncorrelation between sources unlike BSS. How-

ever, during applying for *in-vivo* data, not only their performances are inadequate but also the computational burden can be heavy (e.g. EMD/HHT based algorithms) [41].

### 1.2.2 Artifact Reduction from Scalp EEG

Artifact detection and reduction/removal is one of the most faced challenges for neural information processing applications and is an open research problem. Especially in EEG-based health-care applications, the electrodes being placed on the scalp are most prone to artifacts and interferences. The variety of artifacts and their overlapping with signal of interest in both spectral and temporal domains, even sometimes in spatial domain, make it difficult for simple signal preprocessing technique to identify them from EEG. Therefore, the use of simple filtering or amplitude threshold to remove artifacts often results in poor performance both in terms of signal distortion and artifact removal. The two major applications of Scalp-EEG based systems are: 1) epilepsy seizure detection during long-term patient monitoring and 2) in BCI experiments. In this thesis, we have proposed two different methods for artifact removal from EEG for these two distinct applications (i.e. seizure detection and BCI).

#### 1.2.2.1 Artifact Reduction for Seizure Detection

long-term EEG recording (as shown in Figure 1.4) is used during epilepsy patient monitoring for diagnosis of seizure. However, such recording is of-



ten contaminated by different types of artifacts and hence the signal quality gets degraded, as a result it can increase the false alarm during seizure detection. This scenario gets worse when the patient monitoring is performed under ambulatory environment where different types of movement-related artifacts are present. Considering this problem, we propose a method to reduce artifacts as much as possible without distorting the signal of interest which is found to be enhancing the later stage seizure detection performance significantly.

Although significant amount of efforts have been made to develop methods for artifact detection and removal in EEG applications, it is still an active area of research. Most of them handle single type of artifact, many of them cannot work for single-channel EEG, some of them require training data, some require a dedicated reference channel, some are designed for general purpose applications that often leads to overcorrection of data and some of them are not fully automated.

The proposed artifact reduction method for seizure detection application is automatic, independent of artifact types, does not require a reference channel, can work for both single and multi-channels and most importantly application-specific (i.e. epilepsy diagnosis). The method uses stationary wavelet transform with modified threshold parameters which relies on some a-priori spectral information of seizure events. In order to separate seizure from artifacts, it utilizes either a labeled real seizure epoch or a synthesized one simulated from a simple seizure model. The foremost priority of the

proposed method is to preserve the seizure events at all time and then to reduce artifacts as much as possible.

#### **1.2.2.2 Artifact Reduction for BCI Experiments**

Brain-Computer Interface (BCI) is a promising technique to establish a direct link between human brain and an external computerized device to allow communications for the person suffering from brain/spinal cord related injury/disease [42]. EEG is the most popular among the brain recording techniques in BCI research due to its mainly non-invasive nature along with other attractive features such as fine temporal resolution, simple to use, portability and lower cost [43]. In EEG-based BCI applications, the EEG recording is often contaminated by different types of artifacts that can misinterpret the BCI output. Although many attempts have been made to develop suitable methods for EEG artifact detection and removal with the help of recent advancement in signal processing techniques for algorithms; however, there has no universal and complete solution been proposed yet (e.g. some of them can only remove ocular artifacts, some of them require an additional reference channel whereas some of them cannot work on single-channel, etc.) which indicates the future need for removal algorithms to be application-specific such as brain-computer interface (BCI) applications.

This thesis also presents a unique artifact detection method for BCI application based on artifact probability mapping which quantifies an epoch

by a relative probability of being artifactual. This is achieved by considering the typical artifact characteristics in contrast to the background EEG rhythms with the help of four statistical measures namely entropy (measures the uncertainty), kurtosis (measures the peakedness), skewness (measures the symmetry) and Periodic Waveform Index, PWI (measures of periodicity). This unique probability mapping will allow the user to decide whether to correct the epoch or to remain as it is by choosing an appropriate probability threshold. Subsequently a removal method is also proposed which is based on stationary wavelet transform based denoising and relies on the desired spectral band of EEG rhythms in contrast to spectral bands of different artifacts particularly for BCI applications. The proposed method is demonstrated with both real and synthesized database and extensive quantitative measures show the efficacy of this method with obtained satisfactory results. Moreover, the proposed method is also compared with some of state-of-the-art methods and proves its superiority over others both in terms of performance and computational time. The effect of artifact removal on real BCI database has also been demonstrated to show that it can substantially improve the classifier accuracy in BCI experiments.

The above discussion clearly reveals that there is no artifact removal method for *in-vivo* neural data. In addition, the available EEG artifact removal methods have some practical limitations for applications like seizure monitoring or BCI experiments. The current research gap in this very important signal preprocessing stage to reliably detect and remove artifacts

from both invasive and non-invasive neural recordings mainly motivate the study presented in the thesis.

### 1.3 Thesis Objectives

Based on the problem definition mentioned above, the aim of this thesis is to provide methods for improving the quality of neural signals (both *in-vivo* neural recordings and scalp EEG) which are widely used in basic neuroscience studies, diagnosis of different neurological diseases (especially epilepsy seizure) and modern BCIs (both invasive and non-invasive). Accordingly, the specific objectives of this thesis are as follows:

- Study of artifacts present at *in-vivo* neural recordings and characterize them in a systematic way.
- Analysis of the effects of artifacts on *in-vivo* neural signals and study of the increased dynamic range due to artifacts for proper design of analog front-end recording technology.
- Propose a reliable artifact detection and removal method for preprocessing both *in-vivo* neural signal and scalp EEG.
- Observe the after-effects of artifact removal on later-stage signal processing applications (e.g. spike detection, seizure detection and BCI performance)

- Synthesis of an artifactual database for proper quantitative evaluation of both artifact removal and the aftereffect of removal to neural information processing. This is done in terms of neural spike detection accuracy and seizure classification performance.

## 1.4 Overview and Contributions

This section provides an overview of the organization of this thesis with its original contributions. This thesis contains four chapters of contributions and one chapter of extensive literature review on artifact removal from EEG. In the beginning of each chapter, we provide a detailed literature review of the topics discussed in that chapter.

### 1.4.1 Overview

In Chapter 2, we present a study of artifacts found in the *in-vivo* neural recordings including their possible sources, types and properties. We also provide the change in data dynamic range due to presence of such artifacts which is useful for designing the analog front-end (e.g. resolution of ADC) for recording the neural signals.

In Chapter 3, we present a detailed literature review on the existing state-of-the-art artifact removal methods/algorithms from EEG recordings by comparing their pros and cons along with their theoretical background.

Chapter 4 proposes an artifact detection and removal algorithm for *in-vivo* neural recording which has been compared with existing artifact

removal methods.

In Chapter 5, we introduce artifact removal method from scalp EEG for epilepsy seizure monitoring application and validation of proposed method by quantifying the performance metrics in comparison with some of the state-of-the-art methods.

In Chapter 6, we present another artifact detection and removal method from EEG for specifically BCI applications. The unique feature of this artifact detection is that we proposed a probability-mapping of an EEG epoch for being how much artifactual followed by user-dependent threshold selection scope for deciding whether the epoch should be denoised or not. This method is also quantitatively evaluated in comparison with other existing methods.

Finally, in Chapter 7, we summarize the results of the works presented in this thesis. We also described some of the possible directions of research that are left as open problems for future studies.

In addition to the main chapters, Appendix [A.1](#) presents the open source *MATLAB<sup>TM</sup>* code of the artifact removal algorithm from *in-vivo* neural signal and EEG signals. Appendix [A.2](#) presents the synthesized artifactual database with artifact templates to be able to download online for free.

### 1.4.2 Original Contributions

A summary of thesis contributions are discussed as follows:

- The thesis provides an investigation on the artifacts present in *in-vivo*

neural signals for the very first time which includes: i) Identifying artifact sources, ii) Characterizing them into four different types, iii) Studying the change in dynamic range due the presence of artifacts in neural recordings, and iv) Observing the artifacts' spectrum characteristics in comparison with neural signal of interest.

- An artifact database has been synthesized in order to allow realistic simulation of neural data contaminated with different artifact types for quantitative performance evaluation of any artifact removal algorithm/method.
- The thesis also proposes three different artifact detection and removal algorithms for three different applications: one for *in-vivo* neural recordings and two for EEG-based applications i.e. epilepsy seizure detection and BCI studies. Some of the beneficial features of the algorithms are: independence of artifact type, automated, application-specific solution, able to work for both single and multi-channel recordings, parameters can be optimized for best performance, almost no distortion to signal of interest, does not require any artifact reference channel, and so on.
  - The former proposed algorithm is the first ever attempt in the context of *in-vivo* neural recordings which is based on the stationary wavelet transform with selected frequency bands of neural signals.

- The second artifact reduction algorithm is for scalp EEG-based epilepsy seizure detection application where the proposed algorithm is based on stationary wavelet transform and by considering the spectral band of seizure events into account to separate artifacts from seizures.
- An unique artifact probability mapping for artifact detection and removal from EEG signals for BCI studies is proposed with a tuning parameter controlled by the user in removing specific type of artifacts as per application requirement.
- Finally all the proposed algorithms have been tested using both real and synthesized neural/EEG data to present quantification performance metrics in comparison with state-of-the-art algorithms. In addition, the later stage signal processing has also been quantified to observe the improvement in signal analysis/classification that is achieved through artifact removal.



## Chapter 2

### Artifacts

This chapter describes the study on artifacts, their origin and types, effects on dynamic range of the neural recording. The characterization of artifacts for *in-vivo* neural recording is the first ever study according to the best of our knowledge during time of this thesis writing.

#### 2.1 Characterization (*In-Vivo* Neural Recording)

We have investigated different artifacts that can be present in the *in-vivo* neural recordings from different databases and manually characterized those inspected artifacts to different types and also we make an effort to find the possible sources and mechanisms of such artifacts. The task of identification of different artifact segments from each recording sequence and from different datasets is non-trivial and expected to be useful for fu-

ture research given that there has not been any study so far to the best of our knowledge on investigation of such *in-vivo* artifacts.

### 2.1.1 Sources

Artifacts can be of external and internal types according to their origin. Internal artifacts arise from body activities that are either due to movements made by the subject itself or sudden changes of bioelectrical potentials, while external artifacts result from coupling with unwanted external interferences. A common case in rat recording experiments originates from the animal movements that include cable movement and fast head movement [20, 44, 45]. While it is also a frequent case that the interconnecting cable between recording site and preamplifier acts as an "antenna" and picks up unresolved interferences [45]. The differences in picked interferences (differential) appear as artifacts. A third type of artifacts relate to the momentary change in electrode interface, which can produce fast spike-like artifacts. Fourth, aggregated neural signals could be noisy: if they have good waveform repeatability (spikes) or differentiable spectrum property (field potentials), they are considered as useful signals. If there is no repeatability in some of recorded signals, they are more like outliers in processing and act as artifacts. The described four artifact sources are illustrated in Figure 2.1.

There are three general factors that are responsible mainly for the generation of artifacts [20]. They are as follows:

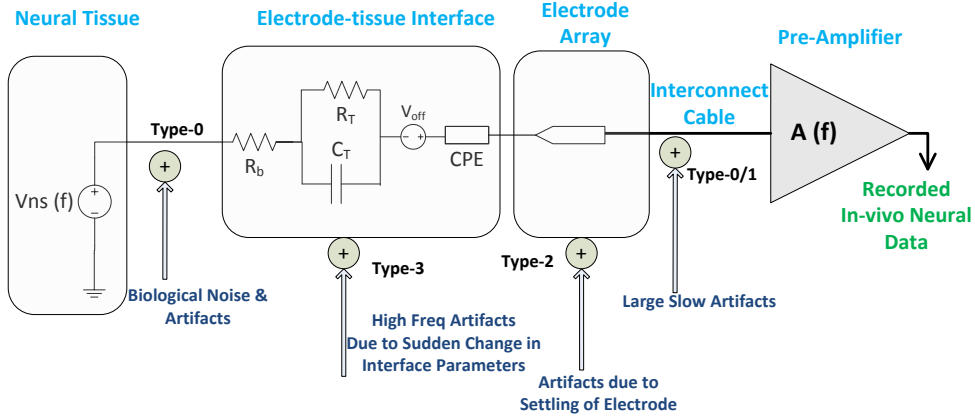


Figure 2.1: Illustration of different artifact sources for *in-vivo* neural recording.

- Environmental factors (e.g. power supply noise of 50/60 Hz and its harmonics, sound/optical interference, EM-coupling from earth: 7.82 Hz and harmonics [46], etc.)
- Experimental factors (e.g. alter of electrode position, movement of connecting wire, etc. due to mainly movement of the subject)
- Physiological factors (e.g. EOG, ECG, EMG, BCG, etc.)

The artifacts in broad sense can be classified into two categories: local and global. Local artifacts are localized in space, i.e. appear only in a single recording channel while global artifacts can be seen across all the channels of an electrode array at the same temporal window. An example of global artifacts appearing in all recording channels that present in two different datasets is shown in Figure 2.2.

On the other hand, the artifacts can be classified into external and internal types according to their origin. Internal artifacts arise from body activities that are either due to movements made by the subject itself or

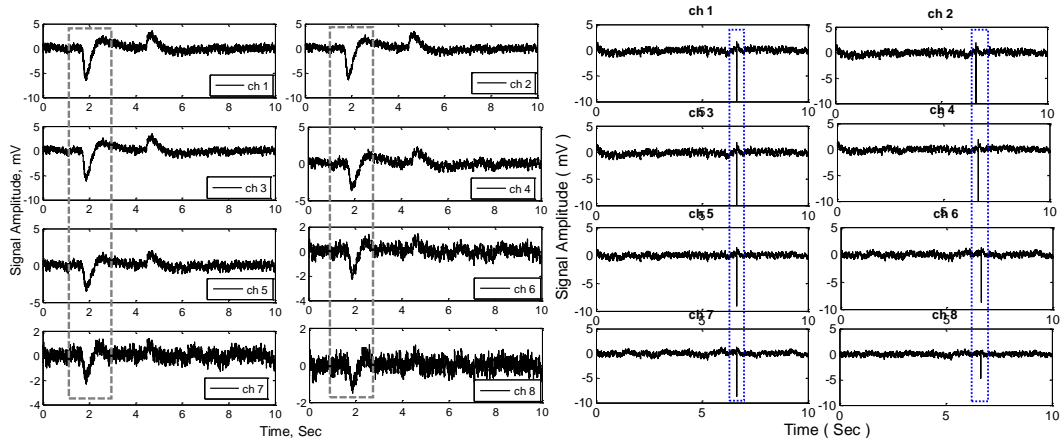


Figure 2.2: Example of global artifacts from two different datasets.

Table 2.1: Summary of artifact classification from different perspectives.

Perspective	Artifact Category/Class	
Repeatability	Irregular/No	Periodic/Regular/Yes
Origin	Internal	External
Appearance	Local	Global

sudden changes of bioelectrical potentials, while external artifacts result from coupling with unwanted external interferences. Sometimes the artifacts appear only once in the whole recording sequence (high entropy) while sometimes in a regular/periodic manner possibly due to some periodic motions of the subject. An example of such artifacts is shown in Figure 2.3.

Table 2.1 summarizes the artifact classes from different perspectives.

### 2.1.2 Types

As explained above that there are a number of factors and sources that generate artifacts, each could produce artifacts with different signatures

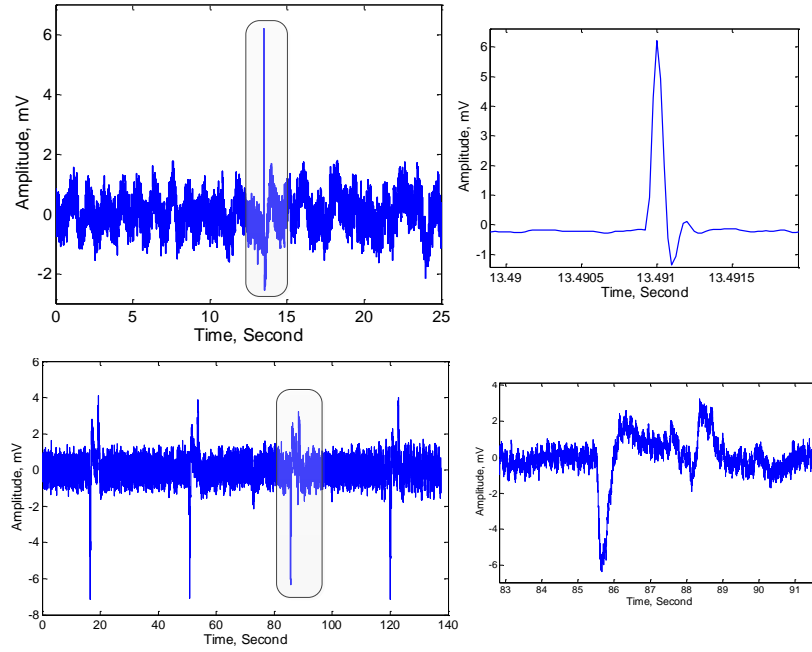


Figure 2.3: An example of irregular (top) and periodic (bottom) artifacts.

and waveform shapes. Therefore, we characterize majority of the artifacts observed from real *in-vivo* neural signals into four types based on different features, e.g. sharpness of edge, duration and waveform shape. The four types are described as follows (shown in Figure 2.4):

- Type-0: This type of artifacts usually has dominant power spectrum in low frequency region. They may appear as a single waveform or in a periodic fashion in recordings and over different channels. The artifact is similar to the vertical-EOG artifacts present in typical EEG recordings or may be generated from the muscle activities of the subject during movement.
- Type-1: This type of artifact segment starts with a large negative change in offset followed by some waveform similar to that of step

response of a second order system. Depending on the damping factor, individual artifacts may have different widths and different decaying spectra with frequency. However, due to the shape of edge, there always exist localized high frequency features.

- Type-2: Type-2 artifacts have been seen more frequently compared with both Type-0 and Type 1 artifacts. They usually have two fast ramp edges at two ends and can be modeled as the derivatives of the type-1 artifacts which suggest that type-2 artifacts are another form of type-1 artifacts possibly generated from the same source or factors.
- Type-3: Type-3 artifacts are often extremely large with narrow in duration (e.g.  $<200 \mu\text{Sec}$ ) and cause recording saturation. They could appear as individual waveforms and tend to appear simultaneously over different channels. Different from neural spikes, they have a wide spectrum characteristic with dominant power in the high frequencies (from few kHz up to the low pass corner frequency set by recording electronics).

### 2.1.3 Properties

- Usually the artifacts have very large magnitude and/or sharper transitions/edges compared to the neural data of interest, i.e. spike and local field potential.
- The frequency range for artifact may vary from very low (e.g. mo-

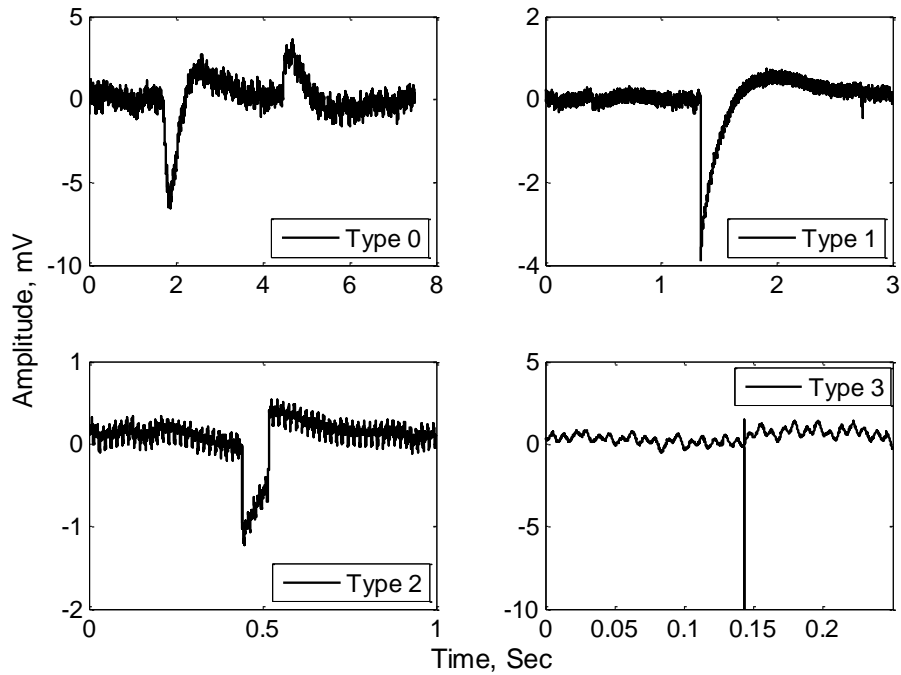


Figure 2.4: Different types of artifact present at *in-vivo* recordings.

tion artifact) to high frequency (e.g. artifacts due to residue charge on electrodes) range suggesting artifact spectra overlap with neural signal of interest.

## 2.2 Artifact Spectrum vs. Neural Signal

### Spectrum

In order to characterize the spectrum statistics of artifacts, we have analyzed neural data recorded from rat with a sampling frequency of 40 kHz using Plexon system <sup>1</sup> [47] (the high pass filter corner frequency is 0.1 Hz

<sup>1</sup>Plexon Inc. manufactures hardware and software for neurotechnology research. One of the products is Multichannel Acquisition Processor (MAP) Data Acquisition System which is Plexon's original standard for programmable amplification, filtering and real-time spike sorting of multi-channel signals acquired in neuroscience research.

and low pass filter corner frequency is 10 kHz). We have manually identified different artifact segments and labeled each into one of the four artifact categories as shown in Figure 2.4. Artifact envelopes are further extracted from the data segments to get the templates and artifact spectrum estimation is performed using windowed Fourier Transform. The results are summarized in Figure 2.5, where artifacts tend to exhibit varied spectrum shape and span from a few Hz to several KHz. As expected, type-1, type-2 artifacts have dominant power at low frequency range while type-3 has wide spectrum.

To characterize the spectrum statistics of local field potentials only, we have analyzed data recorded from rat superficial layer cortex where electrodes are away from any individual neurons. As a result there are less spiking activities. The average spectrum of local field potential is estimated from 8 different channels. From Figure 2.5(d), local field potential power spectrum drops to noise floor at frequency beyond 150 Hz <sup>2</sup>.

To derive neural spike spectrum, relatively large magnitude spikes are identified and grouped into different clusters. Spikes are smoothed and averaged to generate different spike templates. The power spectra of two spike templates are plotted in Figure 2.5(e), which drop to noise floor at frequency beyond 5 KHz<sup>3</sup>.

---

<sup>2</sup>Field potentials are aggregated or averaged from a large number of synaptic activities within a proximity region of the recording site and feature a  $1/f^x$  power spectrum distribution where  $x$  is in between 1 to 3. As a rule of thumb, at frequency beyond 150 Hz, the spectrum of field potential becomes insignificant.

<sup>3</sup>Extracellular neural spikes, on the other hand, are produced by ionic and displacement currents during the propagation of action potentials, which have clear low-cutoff and high-cutoff frequencies: the high-cutoff frequency is at several KHz, as sodium chan-



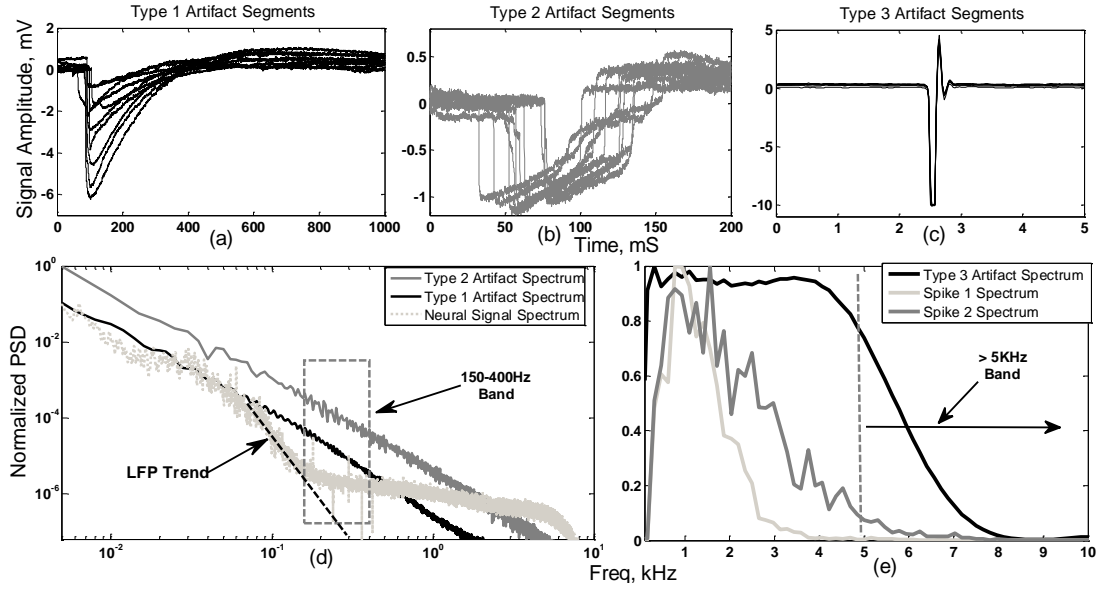


Figure 2.5: (a), (b), and (c): manually labeled type-1, type-2, and type-3 artifact segments collected from recorded data. (d), averaged type-1 and type-2 artifact power spectrum in comparison with LFP. (e), type-3 artifact spectrum and spike spectrum. Spikes are randomly selected from two different templates.

Consequently there are prospective frequency bands to detect artifacts.

One is at 150Hz - 400Hz region where both field potentials and spikes have insignificant power. The other one is beyond 5 KHz, which is too fast even for neural spikes.

## 2.3 Dynamic Range

In this study, we analyze how much dynamic range is actually increased due to the presence of artifacts for both real *in-vivo* data corrupted with artifacts recorded from different experimental set-ups and/or subjects/animals and for simulations with different synthesized artifact templates. We found

channels tend to open for a few hundred  $\mu$ s or even longer; the low-cutoff frequency is around several hundred Hz as potassium channels start to dominant after 1 ms and pull the transmembrane voltage back to its rest state.

that due to the presence of artifact, the dynamic range can increase as high as 20-30 dB compared to without artifact.

To study the dynamic range due to artifacts, we have analyzed neural data recorded from few subjects:

- Rat hippocampus data with a sampling frequency of 40 kHz provided by Dr Edward Keefer at Plexon Inc. (the high pass filter corner frequency is 0.1 Hz and low pass filter corner frequency is 10 kHz). The protocols can be found in [48].
- Human Epilepsy data with a sampling frequency of 32556 Hz (Low cut-off of 0.5 Hz and high cut-off of 9 kHz).

### 2.3.1 Real Data

The dynamic ranges of 134 and 64 full-spectrum *in-vivo* sequences of duration 15 min and 18 min from rat hippocampus and human Electrocor-ticography (ECoG) data respectively have been analyzed considering the amplifier circuit noise floor of both  $1 \mu V_{rms}$  and  $2 \mu V_{rms}$ <sup>4</sup>. The spike data dynamic range has also been studied in order to observe the effect of artifacts present in the recordings. The increase in dynamic range due to presence of artifacts for full-spectrum and spike data is on average 13 – 30 dB and 18 – 27 dB respectively. The detail result is given in the Table 2.2.

---

<sup>4</sup>The basis of these two noise floor values are based on the literature survey of state-of-the-art analog front-end amplifier circuits designed for typical neural recording.

Table 2.2: Summary of dynamic range change due to artifacts.

Subject (Fs in kHz) B.W.	No of Data Sequences (Data Length in min)	Amplif ier Circuit Noise Floor ( $\mu$ V rms)	DR without Artifact (Mean $\pm$ SD) (Full Spectrum Data in dB)	DR with Artifact (Mean $\pm$ SD) (Full Spectrum Data in dB)	Increase in DR (Full Spectrum Data in dB)	DR without Artifact (Mean $\pm$ SD) (Spike Data in dB)	DR with Artifact (Mean $\pm$ SD) (Spike Data in dB)	Increase in DR (Spike Data in dB)
<b>Rat</b> (40) 0.1 Hz – 10 kHz	134 (15)	1	69.01 $\pm$ 2.10	82.44 $\pm$ 4.21	13.43	59.21 $\pm$ 4.32	78.35 $\pm$ 8.26	19.14
		2	62.29 $\pm$ 1.85	75.84 $\pm$ 4.79	13.54	53.13 $\pm$ 4.32	71.33 $\pm$ 9.15	18.19
<b>Human</b> (32.5) 0.5 Hz – 9 kHz	64 (18)	1	34.45 $\pm$ 3.42	64.36 $\pm$ 3.42	29.90	28.82 $\pm$ 4.605	55.75 $\pm$ 6.94	26.92
		2	28.43 $\pm$ 3.42	58.34 $\pm$ 2.45	29.90	22.80 $\pm$ 4.60	49.73 $\pm$ 6.94	26.92

### 2.3.2 Synthesized Data

As described in [49], we have manually identified and extracted different artifacts (neural data segments contaminated with obvious visually detected artifacts) from real *in-vivo* data and categorized each into one of the mentioned three types, i.e. type-1, type-2 and type-3. Based on these extracted templates we simulated similar artifact templates with different amplitudes and durations as shown in Figure 2.7. We choose a real *in-vivo* raw data of 100 second duration which contains no visually detectable or obvious artifact and termed it as a reference signal. Then the simulated artifacts

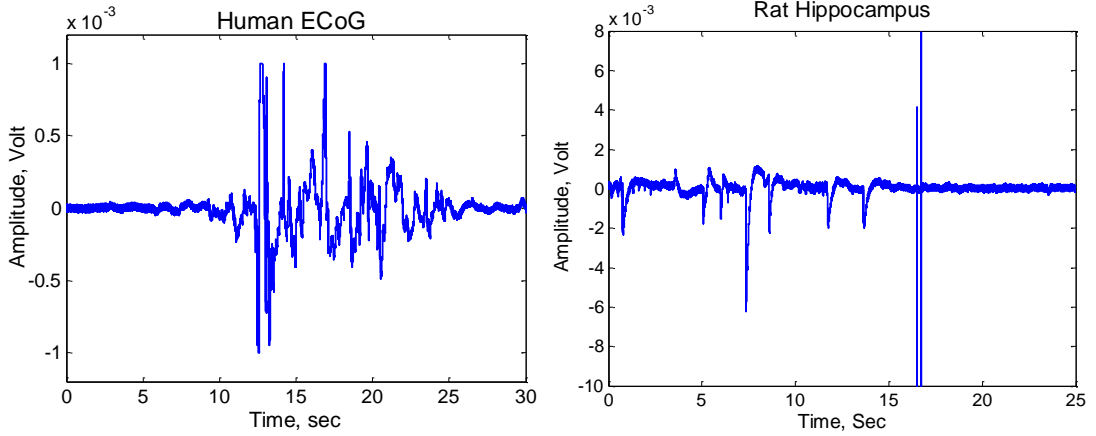


Figure 2.6: An example of effect of artifact on dynamic range can be seen in two time domain database of *in-vivo* neural data recorded from two different subjects. Left plot is from human epilepsy data and right plot is from rat hippocampus data.

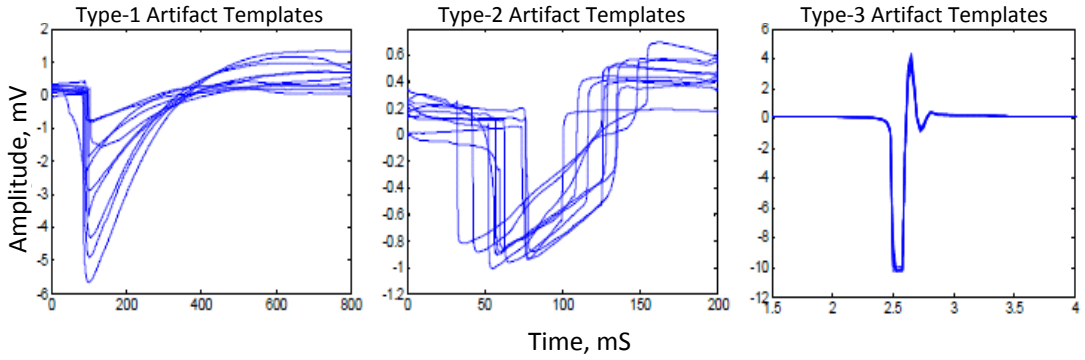


Figure 2.7: Synthesized artifact templates for type-1, type-2 and type-3.

are added to the reference signal in different random positions with different amplitudes, edge widths and durations to form a dataset that is contaminated with artifacts, we term it as an artifactual signal.

### 2.3.3 Calculation of Dynamic Range

Let's denote  $V_N$ ,  $V_{Ref(p-p)}$ , and  $V_{Art(p-p)}$  as RMS amplifier circuit noise floor, peak-to-peak reference signal, and peak-to-peak artifactual signal

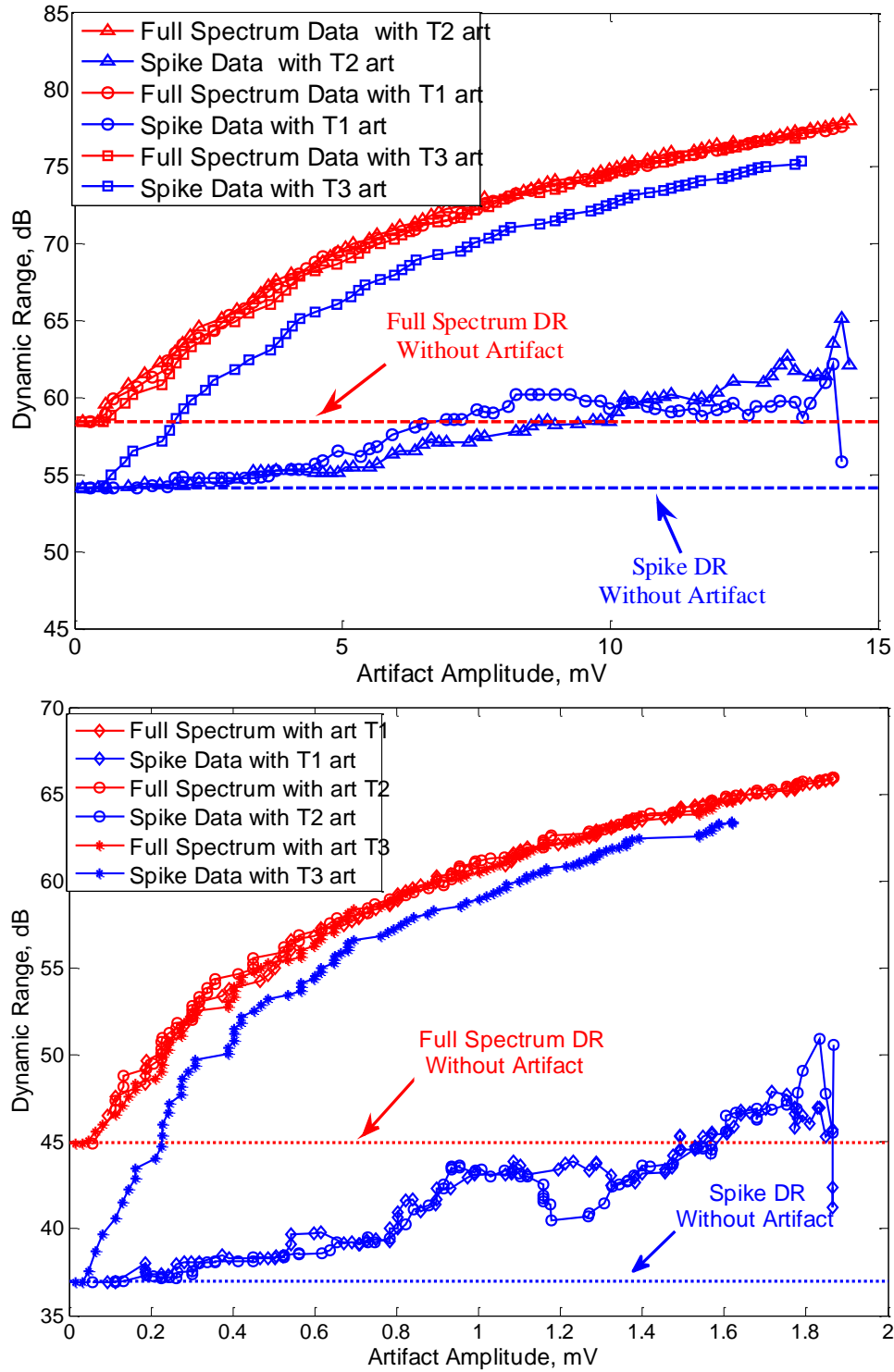


Figure 2.8: The simulation result for both full spectrum neural signal and spike signal contaminated with different artifact templates with respect to different artifact amplitudes. Top plot is for rat hippocampus data and bottom plot is for human epilepsy data.

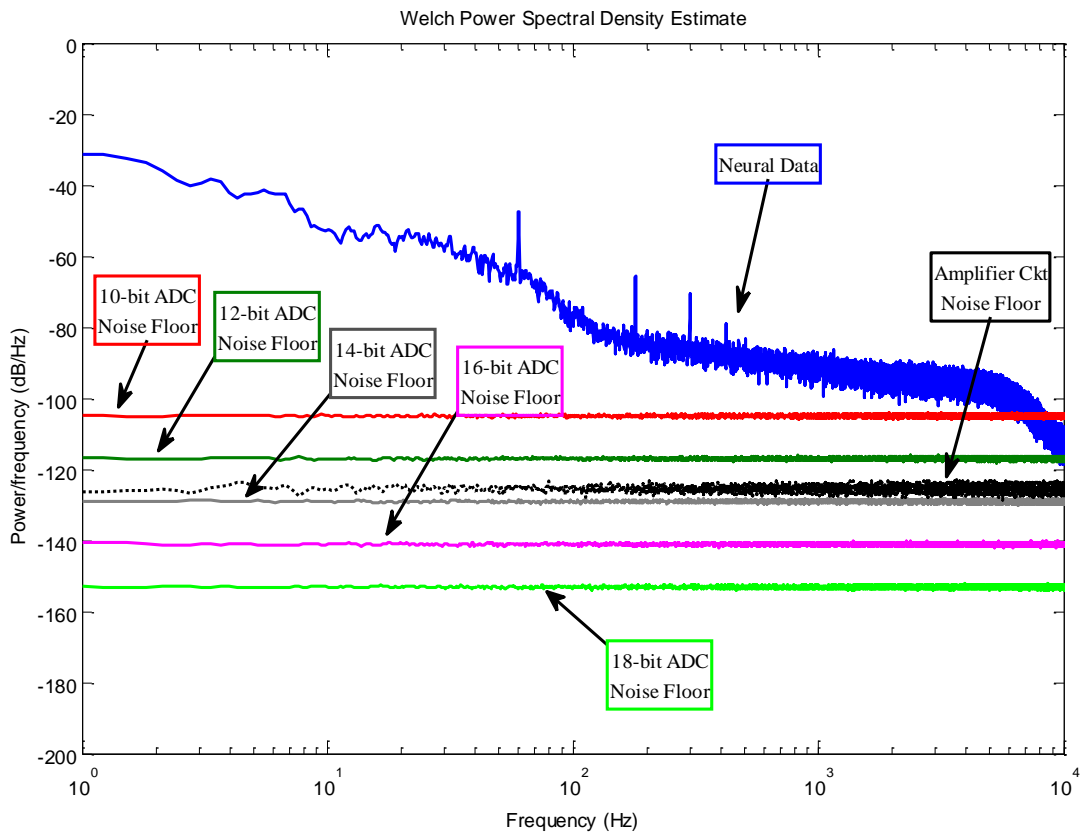


Figure 2.9: Illustration of different ADC resolution noise floor in comparison with neural signal power in spectral domain to choose the right ADC resolution in order to achieve minimum 10 dB SNDR for full-spectrum neural recording.

respectively. Then the dynamic range with and without artifact are  $DR_{Art}$  and  $DR_{Ref}$  respectively and are calculated using the following formula:

$$DR_{Art} = 20\log_{10}\left(\frac{V_{Art(p-p)}}{V_N}\right) \quad (2.1)$$

$$DR_{Ref} = 20\log_{10}\left(\frac{V_{Ref(p-p)}}{V_N}\right) \quad (2.2)$$

Therefore, the increase in dynamic range for full-spectrum signal due to presence of artifacts is calculated as follows:

$$\Delta DR = DR_{Art} - DR_{Ref} \quad (2.3)$$

Now, if we band-pass filter the reference and artifactual signal from 300 Hz to 5 kHz, we get the spike signal and assume  $S_{Art}$ ,  $S_{Ref}$  be the spike signal with and without artifact respectively. Then the corresponding dynamic ranges of spike signal are  $DR'_{Art}$  and  $DR'_{Ref}$  respectively and calculated similarly as follows:

$$DR'_{Art} = 20\log_{10}\left(\frac{S_{Art(p-p)}}{V_N}\right) \quad (2.4)$$

$$DR'_{Ref} = 20\log_{10}\left(\frac{S_{Ref(p-p)}}{V_N}\right) \quad (2.5)$$

Similarly, the increase in dynamic range for spike signal due to presence of artifacts is calculated as follows:

$$\Delta DR' = DR'_{Art} - DR'_{Ref} \quad (2.6)$$

In our simulation for dynamic range study, we assume two reasonable values for circuit noise floor,  $V_N$ : one is  $1 \mu V_{RMS}$  and another  $2 \mu V_{RMS}$ .

### 2.3.4 Spectral Domain Analysis

In this study, we consider both the amplifier circuit and ADC noise floor. The gain of the amplifier is adjusted in such a way that the input voltage swing to ADC is maximum 0.5V given that the supply voltage of ADC circuit is  $V_{DD} = 1V$ . We sweep the ADC resolution from 10 to 18-bit and calculate the corresponding ADC noise floor for reference signal of 1 V RMS by using following formula:

$$20\log_{10}\left(\frac{S_{Ref}}{V_{ADC}}\right) = 6.02N + 1.76 \quad (2.7)$$

where  $S_{Ref}$ ,  $V_{ADC}$  and  $N$  are the reference signal RMS, ADC noise floor RMS and no. of ADC-bit respectively. The amplifier circuit noise floor,  $V_{Amp}$  seen from the input of ADC if the amplifier's gain being  $A$ , is as follows:

$$V_{Amp} = AV_N \quad (2.8)$$

Then we plot the power spectral density of the full-spectrum neural data, amplifier circuit noise floor and ADC noise floor for different ADC-bit resolution to measure the required SNDR for successful neural data recording with at least 10 dB more with respect to ADC noise floor. We found that to get minimum 10 dB SNDR, the required resolution of the ADC should be at least 14-bit [50].



## 2.4 Artifact Characterization in EEG

The artifacts in EEG recording are of various types that come from different sources. In broad sense, artifacts in EEG can be originated from internal and external sources. The sources and types of artifacts are discussed below:

### 2.4.1 Internal/Physiological Artifacts

- **Ocular Artifacts:** The eyeball acts as an electrical dipole and therefore any movement in eyeball generates large-amplitude artifacts in EEG recordings. Ocular artifacts include eye blink, both horizontal and vertical eye movement, eye flutter, eye movement during REM sleep, eye saccade, etc.
- **Muscle Artifacts:** One of the most prominent physiological artifacts comes from muscle activity of the subject (EMG). Usually muscle artifacts are of high frequency range (e.g. from 20 Hz to 40 Hz) and are generated from activities like chewing, swallowing, clenching, sniffing, talking, scalp contraction, eyebrows raising, etc.
- **Cardiac Artifacts:** Cardiac artifacts are due to the electromagnetic field produced by heart and are of two types: ECG and pulse artifacts. ECG artifacts are rhythmic regular activities while the pulsation sometimes can cause slow waves which might mimic the EEG activity.

Table 2.3: Different types of artifacts and their origins.

Artifact Types and Sources						
Physiological / Internal				Extra-physiological / External		
Ocular	Cardiac	Muscle	Others	Instrumental	Interference	Movement
Eye blink, Eye movement, Eye flutter, REM sleep, etc.	ECG; Pulse.	Chewing; Swallowing; Clenching; Sniffing; Talking; Scalp contraction; etc.	Glossokinetic; Skin; Respiration; etc.	Electrode displacement and pop-up; Cable motion; Poor ground; etc.	Electrical; Magnetic; Sound; Optical; EM waves; etc.	Head movement; Body movement; Limbs movement; Tremor; Other movements, etc.

- **Respiration Artifacts:** Respiration artifacts originate from the movement of an electrode with inhalation or exhalation and can take the form of slow, rhythmic EEG activity.
- **Sweat Artifacts:** Electrodermal or sweat artifacts originate from changes in electrolyte concentration of electrode due to sweat secretion on the scalp and take the shape of a long, slow baseline drift in the spectral band of 0.25 -0.5 Hz [51].

#### 2.4.2 External Artifacts

- **Movement Artifacts:** Movement of patient especially in an ambulatory EEG monitoring system[52, 53, 54], generates a lot of motion artifacts. This artifact often has extremely high amplitude such that it can saturate the recordings. Head movement, body movement, limbs movement, tremor, walking, running, browsing PC, and many

other movements in daily activities are responsible for this type of artifact.

- Environmental Artifacts:
  - Interferences: This type of artifacts is due to the interferences coming from the surrounding electrical/electronic devices/machines that produce EM waves. Also any sound or optical interference may also be picked up by the EEG electrodes as artifacts.
  - Mains voltage: One of most common source of artifacts in any biomedical signal acquisition is the 50/60 Hz main voltage and its harmonics.
  - Loose electrode: Loose electrode contact with scalp can lead to impedance change on the tissue-electrode interface and results in prolonged EEG spike-like artifact.
  - Electrode Pop and Movement: Another common source of artifact is due to electrode pop which produces sudden change in impedance in the electrode-tissue interface and results in high amplitude sharp waveform-shaped artifacts. Electrode movement occurs when it moves with respect to the scalp and produces high-amplitude deflection in EEG generally in the low frequency range of 1-10 Hz.

A summary of different artifact types and their origins is provided in Table 2.3 [20, 51].

## Chapter 3

# Literature Review

This chapter presents an extensive literature review of the existing and state-of-the-art artifact handling methods and software tools including artifact avoidance, rejection, detection and removal. The methods are described briefly with their corresponding advantages and limitations. A comparative study between the methods is also provided at the end of the chapter in the form of table.

### 3.1 Introduction

Artifact detection and reduction/removal is one of the most faced challenges for EEG signal processing applications and is an open research problem. In EEG-based health-care applications, the electrodes are placed on the scalp and therefore, the recordings are most prone to artifacts and interferences. The variety of artifacts and their overlapping with signal of interest in both spectral and temporal domain, even sometimes in spatial domain,

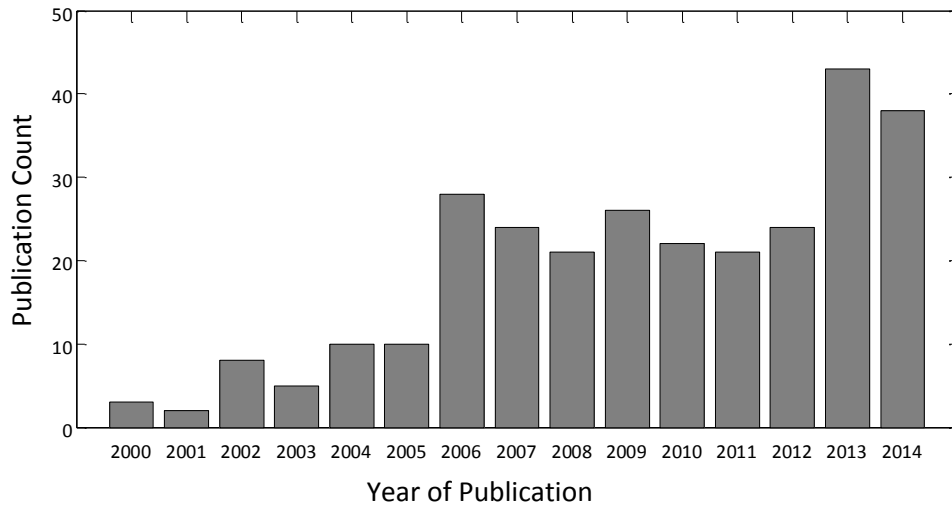


Figure 3.1: Trend of research on artifact detection and removal from EEG in terms of publication history since year 2000 until present indexed by Google Scholar. The search criteria include both the keywords Artifact(s)/Artefact(s) and EEG(s)/Electroencephalography/Electroencephalogram(s) that present in the title of published journal articles and conference papers.

make it difficult for simple signal preprocessing technique to identify them from EEG. Therefore the use of simple filtering or amplitude threshold to remove artifacts often results in poor performance both in terms of signal distortion and artifact removal.

Many attempts have been made and still being made to develop suitable methods for artifact detection and removal with the help of recent advancement in signal processing techniques/algorithms in the past decade and a half. Figure 3.1 shows the trend of EEG artifact research from year 2000 till last year which suggests an increasing trend of the no. of article published in the recognized journals and still counting. However, there is no universal complete solution yet and hence still an active area of research. After careful reviewing most of the relevant artifact detection

removal algorithms/methods in the literature, we realize there is a gap between designed algorithm and its target application. Most of the available techniques are not application-specific and therefore unnecessary computational burden arises. Considering this scenario, we present a comparative analysis of the existing methods/algorithms with their advantages, limitations and application-specific challenges.

## 3.2 Existing Artifact Handling Methods

First of all, we present the different artifact handling methods found from extensive literature review as follows:

### 3.2.1 Artifact Avoidance

Artifact avoidance is a preventive and precautionary way to avoid or minimize artifacts by instructing the subject to remain still and try to avoid unnecessary blinks, eye/body movements. Also by proper grounding of the EEG recorder, one can reduce the supply mains interference. Artifact avoidance is not the best way to get rid off artifacts completely, but by minimizing artifacts it can reduce both the data loss and the computational complexity. However, based on applications, sometimes this is a very unrealistic solution; e.g. in an ambulatory EEG monitoring or BCI applications. Moreover, there are several limitations to employ such approach since some of the physiological artifacts (e.g. ECG) are involuntary and therefore cannot be avoided. In addition, the subject cannot limit eye

blinking or movement for a long period of time, especially if the subject is neonatal or children. Therefore, there will always be some artifacts present in the recording and those should be handled in the digital signal processing domain.

### **3.2.2 Artifact Detection**

Identifying artifacts is the first and most important step for handling artifacts. Often the artifacts overlap with EEG signals in both spectral and temporal domain such that it becomes difficult to use simple filtering or straight forward signal processing technique. In many applications, it is required to identify or separate artifacts in real-time, therefore knowing both the artifact and signal characteristics is really necessary in order to detect them faster. Detection of artifacts may refer to detecting a particular epoch or detecting an independent component to be artifactual. Whether it should be detected in time domain or frequency domain or even in both by utilizing time-frequency analysis, this decision depends on the type of artifacts and/or type of applications. The detection method also varies depending on whether a reference artifact source is available or not, whether the no. of channels are enough, whether we want to remove the artifacts after detection and so on.

### 3.2.2.1 Machine Learning

Few existing methods adopted the idea of machine learning (mostly supervised learning) for artifact separation from useful EEG signal by training a classifier with (supervised) or without (unsupervised) labeled training datasets. Once artifactual epochs are identified by applying a machine learning algorithm, such epochs are either highlighted as artifact annotator to the clinicians for helping in decision making (e.g. seizure detection) or can be rejected before examination from clinician or before sending to automated signal processing system [55].

Machine learning techniques are mainly two types: supervised and unsupervised learning. Among supervised learning algorithms, two most popular methods used for classification between artifact and brain signals are ANN [56, 57, 58, 59, 60] and SVM [55, 61, 62, 63, 64, 65]. Among unsupervised learning, k-means clustering and outliers detection are most common in this particular area of research [55]. A basic approach to classify artifact from EEG by using the machine learning classifier is shown in Figure 3.2.

### 3.2.3 Artifact Rejection

The easiest way to remove the influence of artifacts after detection is to reject/cancel the epoch or segment of EEG data which is found to be artifactual. This process not only removes artifact but also removes important EEG information which results in the loss of data. This is the early days way of handling artifacts, but nowadays with the introduction of recent



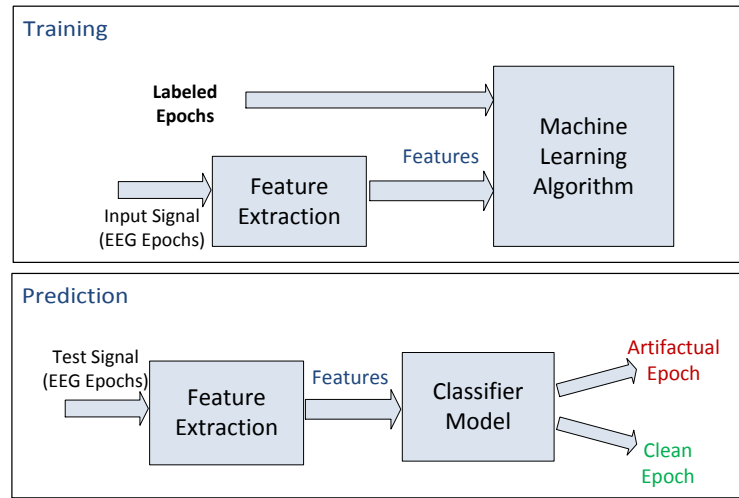


Figure 3.2: Machine learning classification for identifying artifactual epoch from clean EEG epoch.

signal processing techniques, the preference is more on the techniques for artifact removal or correcting them instead of rejecting the data epoch. However, in certain applications, this technique can still work reasonably well, e.g. offline analysis or during training of any classifier.

### 3.2.4 Artifact Removal

Artifact removal involves canceling or correcting the artifacts without distorting the signal of interest. This is primarily done in two ways: either by filtering and regression or by separating/decomposing the EEG data into other domains.

#### 3.2.4.1 Regression

Regression analysis using a multi-modal linear model between observed and a reference signal is a traditional way of identifying artifactual samples and consequently removing such sample that do not belong to the model.

Observed artifact-contaminated EEG signal and an artifact reference signal are common methods for removing some physiological artifacts such as ocular and cardiac artifacts. However, such regression analysis often fails when there is no reference channel available. In addition, EEG signal being non-linear and non-stationary process, linear regression is not the best choice for analysis in such applications. Moreover, it can only be used to treat few particular types of artifact, not all types.

#### 3.2.4.2 Blind Source Separation

One of the most popular artifact detection methods is based on BSS. Here the observed signals,  $X$  in multi-channel recordings are assumed to be linear mixture of the sources,  $S$  with additive white noise vector  $N$

$$X = AS + N \quad (3.1)$$

The objective is to find an estimate of the linear mixture matrix,  $A$  denoted by  $W$  by an iterative process and then estimate the source signals,  $S'$  by following formula:

$$S' = WX \quad (3.2)$$

The assumption with BSS is that the number of sources can be at most equal to that of observed channels (or lower) and the sources need to be independent (for ICA) or maximally uncorrelated (for CCA) from each other. A basic BSS technique is illustrated in Figure 3.3.

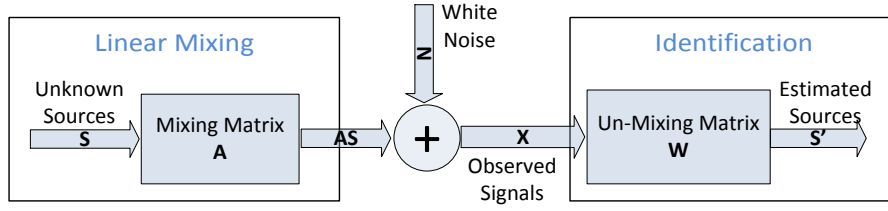


Figure 3.3: Illustration of blind source separation technique.

- ICA:** Independent Component Analysis (ICA) is based on blind source separation (BSS) technique where it is assumed that the sources are linearly independent. The major problem with ICA-based artifact detection and removal is that, it is often not automatic. It requires manual intervention to reject ICs with visually detected artifacts after decomposition. It (i.e. artifact detection and removal) can be made automatic by combining ICA with another complementary method such as Wavelet Transform or EMD or using classifier like SVM or even with a help of reference channel [66]. However, even in such case, the Independent Component with artifact(s) may also contain some residual neural signals. Therefore, during signal reconstruction after completely rejecting that particular IC, it introduces distortion to the neural signal. Another problem is that it cannot operate on single channel data, since the no. of recording channels must be at least equal to the no. of independent sources. The computational complexity is another factor that limits the choice of ICA for artifact removal in applications that require online/real-time implementation of the algorithm. Finally the involvement of iterative process in com-

puting ICA algorithm makes it difficult to perform robustly. E.g. ICA may be useful to remove global artifacts such as ocular artifacts [16, 19, 58, 67, 68] or sometimes other physiological artifacts, but not external artifacts. There are few works reported the use of modified [67] or constrained ICA [69, 64, 70, 71] for automated and better performance in artifact detection and removal.

- **CCA:** Canonical Correlation Analysis or CCA is another BSS method for separating a number of mixed or contaminated signals that uses second-order statistics (SOS) to generate components derived from their uncorrelated nature. By looking for uncorrelated components, the approach uses a weaker condition than statistical independence sought by the ICA algorithm. ICA does not take temporal correlations into account while CCA addresses this point by being capable of finding uncorrelated components that, in addition, have maximum spatial or temporal correlation within each component [21]. Both methods provide qualitatively the same results, but CCA method is more computationally efficient.
- **MCA:** Morphological Component Analysis (MCA) decomposes the recorded signal into components that have different morphological characteristics where each component is sparsely represented in an over-complete dictionary [21]. It is only applicable to certain known artifacts whose wave shape or morphology are known and stored in a

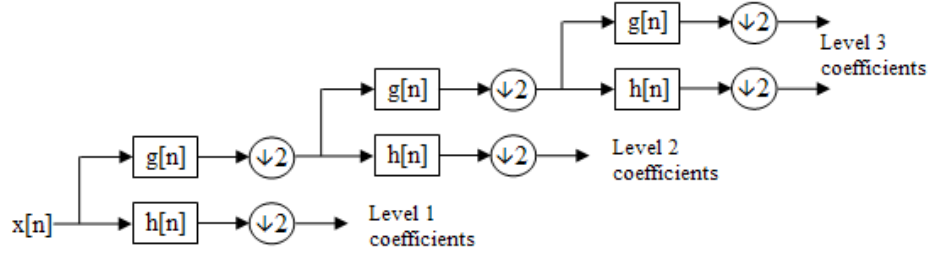


Figure 3.4: A 3-level DWT filter bank for decomposition (collected from [74]).

database. The efficacy of this method greatly depends on the available artifact-template database. In [72, 73], MCA is used to remove ocular artifacts and some of the muscle artifacts originating from jaw clenching, swallowing, and eye-brow raising.

### 3.2.4.3 Time-Frequency Representation

Time-frequency analysis of non-stationary time-series data is quite popular in biomedical signal processing, e.g. in EEG signal processing. The reason of using simultaneous time and frequency domain analysis is because of the non-stationary properties of this type of signal, i.e. frequency and statistics of time-series data vary with time. Therefore any momentary change in frequency values for any signal components (e.g. either artifact or seizure [75, 76] can be captured in a particular temporal window. [77] proposed a time-frequency analysis of ocular artifacts (OAs) including blinks and saccades found in EOG and observed that frequencies up to 181Hz can be present in a subject's EOG for certain tasks. This finding suggests that if EOG is used for ocular artifact removal from EEG, then EOG should be

sampled at least 362 Hz to avoid aliasing.

The common time-frequency representation is performed by short-window or short-time Fourier Transform (STFT). However, this method is not so effective as it has uniform time-frequency resolution at all frequency values. For EEG, since the bandwidth is around 0.5-120 Hz and most of the artifacts appear in the lower frequency region ( $< 10$  Hz), therefore, it's required to have high frequency resolution in lower frequency region which STFT cannot provide. A nice solution of this issue is to use wavelet transform since it provides a decent time-frequency resolution for EEG signals.

#### **3.2.4.4 Wavelet Transform**

Wavelets are localized in both time and frequency whereas the standard Fourier transform is only localized in frequency. Although the Short-time Fourier transform (STFT) is more similar to the wavelet transform, in a sense that it is also time and frequency localized, but wavelets provide a better signal representation using multi-resolution analysis, with balanced resolution at any time and frequency. The wavelet transform is a time-scale representation method that decomposes signal  $f(t)$  into basis functions of time and scale which are dilated and translated versions of a basis function  $\psi(t)$  which is called mother wavelet [78]. Translation is accomplished by considering all possible integer translations of  $\psi(t)$  and dilation is obtained by multiplying  $t$  by a scaling factor which is usually factors of 2. The following equation shows how wavelets are generated from the mother

wavelet:

$$\psi_{j,k}(t) = 2^{j/2} \psi(2^{j/2}t - k) \quad (3.3)$$

where  $j$  indicates the resolution level and  $k$  is the translation in time. This is called dyadic scaling, since the scaling factor is taken to be 2. Wavelet decomposition is a linear expansion and it is expressed as

$$f(t) = \sum_{k=-\infty}^{+\infty} [c_k \phi(t - k)] + \sum_{k=-\infty}^{+\infty} \sum_{j=0}^{+\infty} d_{j,k} \psi(2^j t - k) \quad (3.4)$$

where  $\phi(t)$  is called the scaling function or father wavelet and  $c_k$  and  $d_{j,k}$  are the coarse and detail level expansion coefficients, respectively. Theoretically, the expansion coefficients  $c_k$  and  $d_{j,k}$  are calculated from the inner product of  $f(t)$  with  $\phi(t)$  and  $\psi(t)$ , respectively. The power of wavelet transform is based on the fact that these coefficients are computed in a recursive manner. Once  $c_k$  is known in a starting scale  $J$ , all the coefficients for  $j = J, J+1, \dots$ , are found by a simple linear transform. A wide variety of functions could be chosen as the mother wavelet as long as following equation is satisfied:

$$\int_{-\infty}^{+\infty} \psi(t) dt = 0 \quad (3.5)$$

There are many techniques based on wavelet theory, such as wavelet packets, wavelet approximation and decomposition, discrete and continuous wavelet transform, and so forth. The most commonly used technique is

Discrete Wavelet Transform (DWT). The DWT is developed from continuous wavelet transform with discrete input, but it is simplified mathematical derivation. The relation between input and output can be represented as

$$x_{a,L}[n] = \sum_{k=1}^N x_{a-1,L}[2n-k]g[k] \quad (3.6)$$

$$x_{a,H}[n] = \sum_{k=1}^N x_{a-1,L}[2n-k]h[k] \quad (3.7)$$

where  $g[n]$  is a low pass filter just like scaling function and  $h[n]$  is a high pass filter just like mother wavelet function. Briefly, discrete wavelet transform is entering a signal into a low pass filter to get the low frequency component and into a high pass filter to get the high frequency component. The wavelet filter decomposition structure is shown in Figure 3.4 [78].

Once the signal is decomposed into detail and approximate coefficients, thresholding is applied on the decomposed coefficients to denoise the signal from artifacts. Then the new set of coefficients (all detail with final level approx. coefficients) are added up to reconstruct back the artifact-reduced signal.

#### 3.2.4.5 Empirical Mode Decomposition

EMD is an empirical and data-driven method developed to perform on non-stationary, non-linear, stochastic processes and therefore it is ideally suitable for EEG signal analysis and processing. However, the computational complexity of EMD is quite heavy, so may not be suitable for online



applications. Moreover, the theory behind EMD is still not complete and so far used in empirical studies, therefore it is difficult to predict its robustness in all EEG recordings.

EMD algorithm decomposes a signal,  $s(n)$  into a sum of the band-limited components/functions,  $d_m(n)$  called intrinsic mode functions (IMF) with well defined instantaneous frequencies [27, 33, 79]. There are two basic conditions to be an IMF: (i) the no. of extrema must be equal (or at most may differ by one) to the no. of zero crossings (ii) any point, the mean value of the two envelopes defined by the local maxima and the local minima has to be zero [27]. The general process flow of EMD algorithm is shown in Figure 3.10.

*EEMD*: It is an enhanced version of EMD (Enhanced Empirical Mode Decomposition) and inspired from the fact that EMD algorithm is very sensitive to noise which often leads to mode mixing complication. Therefore, EEMD is proposed which uses an average of no. of ensembles (IMFs) from EMD as the optimal IMFs thus it provides a noise-assisted data analysis method [33].

#### 3.2.4.6 Adaptive Filtering

An adaptive filter is a system with a linear filter that has a transfer function controlled by variable parameters and a means to adjust those parameters according to an optimization algorithm [81]. The filter weights can adapt based on the feedback from output of the system and it requires a reference

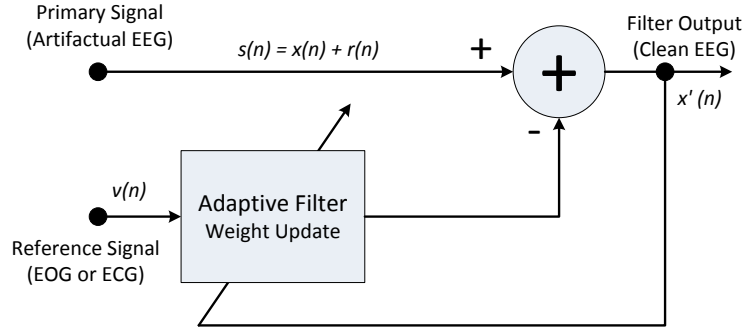


Figure 3.5: Typical use of adaptive filtering in canceling physiological artifacts with available artifact source channel as reference [80].

input to compare the desired output with the observed output.

Considering the observed signal,  $s(n)$  is composed of two signal components: original EEG,  $x(n)$  and additive artifact  $r(n)$ ; if the artifact source  $v(n)$  is available from a dedicated channel (e.g. EOG or ECG); then by an adaptive algorithm (e.g. LMS, RLS, etc.) the artifact-free EEG,  $x'(n)$  is possible to estimate given the assumption that the desired EEG and artifact signal are independent (or at least uncorrelated [82]). An illustration of the use of adaptive filter for EOG artifact removal is shown in Figure 3.5.

$$s(n) = x(n) + r(n) \quad (3.8)$$

#### 3.2.4.7 Wiener Filtering

Wiener filter which doesn't require the use of an external reference signal unlike adaptive filter, however, assumes that both the signal and artifact are stationary linear random processes with known spectral characteristics

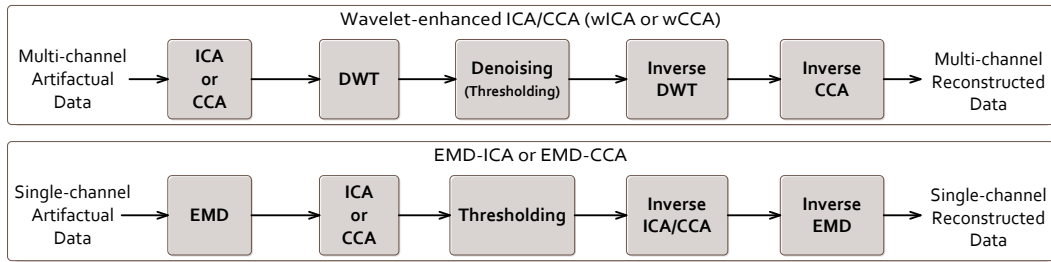


Figure 3.6: General process flow of EMD-BSS and Wavelet-BSS methods.

and also the signal and artifact are uncorrelated. But in fact, the neural signal exhibits non-stationary characteristics and is believed to originate from a complicated non-linear stochastic process. Again, although the spectral characteristics of EEG rhythms are known, due to the uncertainty of different types of artifact sources, the spectral characteristics cannot be determined accurately. In addition, the Wiener filter cannot be implemented in real-time, so it is not a good choice for artifact removal in applications that require real-time processing.

#### 3.2.4.8 Bayesian Filtering

- Kalman Filtering:** Kalman filter is another kind of Bayes filter which also doesn't require an external reference signal and is capable of operating in real-time. This method requires the filter models to be created prior to implementation of the algorithm and the model has to be linear. Besides, it also assumes that a-priori estimation is Gaussian and can work only with unimodal distribution. Now, the artifacts are of different waveform shapes and it is likely to be of

multi-modal distribution. The a-priori estimation may also not be valid due to non-stationary, nonlinear properties of EEG signals. So Kalman filter is not supposed to work robustly for such applications.

- **Particle Filtering:** Particle filter is a kind of filter based on Bayesian approach which overcomes the limitation of Kalman filter as it does not require the model to be linear or the distribution to be unimodal. But it still needs a-priori user input which may not be available always in EEG-based applications. And there has very little work been done so far to use particle filter to remove artifacts in EEG signals. Hence it is not guaranteed to be a successful choice, but one can definitely try to observe the outcome of such filter implementation in removing artifacts.

#### 3.2.4.9 Spatial Filtering

*Principal Component Analysis (PCA):* PCA is a type of spatial filter that transforms the time domain datasets into a different space by rotating axes in an  $N$ -dimensional space (where  $N$  is the no. of variables or EEG channels) such that each dimension in the new space has minimum variance and the axes are orthogonal to each other [83]. PCA reduces data dimension and highlights specific features of data which is usually difficult to identify in the spatially unfiltered data as the new components are created by weighted combinations of all EEG channels. Two recent articles have proposed artifact removal method based on PCA: [84] reported the use

of robust PCA after preprocessing is done based on wavelet denoising and band-pass-filtering; while [85] compared PCA with ICA for artifact removal and found ICA performs better than PCA. Both these articles have evaluated their method qualitatively, therefore, it's not possible to comment exclusively on the efficacy of PCA in detecting and removing artifacts. One important limitation of PCA (or SVD) is that it fails to separate/identify ocular or similar artifacts from EEG when amplitudes are comparable since PCA depends on the higher order statistical property [69].

#### 3.2.4.10 Hybrid Methods

In recent years, researchers are keen to utilize the advantages of different methods by combining them into a single method for artifact detection and removal, i.e. hybrid method which has two or more stages. Some of these methods are discussed below:

- **Wavelet-BSS:** This hybrid method formed by integrating two popular methods: wavelet transform and blind source separation is mainly inspired from the fact that only BSS based separation of artifactual components (e.g. ICs) is often erroneous since the separated artifactual component also contains residual neural information. Therefore, completely rejecting such component will introduce significant distortion in reconstructed EEG signal. Hence, the multi-channel datasets are transformed into ICs or CCs and then possible artifactual component is decomposed by wavelet transform to different frequency

bands of detail coefficients. After that, the artifactual coefficients are denoised by thresholding which eventually preserve the residual neural signals of low amplitude after thresholding the higher artifactual segments. The related articles are [38, 86, 87] for wavelet-ICA, [35, 36] for wavelet-CCA. On the other hand, there are similar hybrid methods that can be applied to single-channel EEG data by reversing the order of wavelet transform and BSS blocks. E.g. [88, 89] reported artifact removal by first decomposing signal into wavelet coefficients then artifactual coefficients are passed through BSS block to separate artifacts from neural signal. However, typically the prior way is more known to the research community as wavelet enhanced ICA or wavelet enhanced CCA. An example of such method is shown in Fig 3.6. Please note that the type of wavelet transform can be DWT, CWT, SWT or sometimes WPT [90].

- **EMD-BSS:** This hybrid method involves BSS with EMD instead of wavelet transform. The difference is that usually the first stage is to decompose the signal into IMFs by EMD or EEMD and then apply BSS (ICA or CCA) on the IMFs to identify artifactual component followed by rejecting the artifactual IC or CC. The general process flow of this hybrid method is also shown in the same Figure 3.6. Such methods are reported in [33, 66, 91]

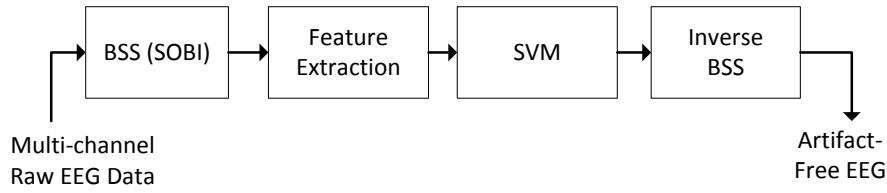


Figure 3.7: Process flow of the hybrid BSS-SVM algorithm.

- **BSS-SVM:** [64] reported a hybrid BSS-SVM algorithm for eye blink and ECG artifact removal where certain carefully chosen features are extracted from separated source components and then fed into a SVM classifier to identify artifact components followed by removing them. Finally the rest of the source components are re-projected to reconstruct artifact-free EEG. The whole system is illustrated in Fig 3.7.
- **REG-BSS:** [68] reported a hybrid methodology by combining BSS and regression based adaptive filtering (with vEOG and hEOG as reference channels) for rejection of ocular artifacts as shown in 3.8. Similar techniques have been used by [19] to remove ocular artifacts by combining ICA and adaptive filtering.

Another hybrid approach combining ICA and Auto-Regressive eXogenous (ARX) was proposed by [92] to remove ocular artifacts robustly as shown in Fig 3.9. In this method, ARX is used to reduce the negative effect induced by ICA by building the ARX multi-models based on the ICA correlated signals and the reference EEG that are

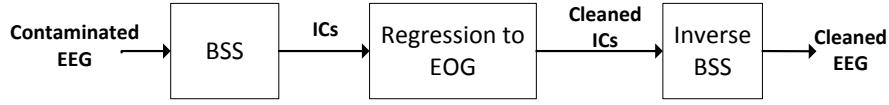


Figure 3.8: Process flow of the hybrid REG-BSS methodology.

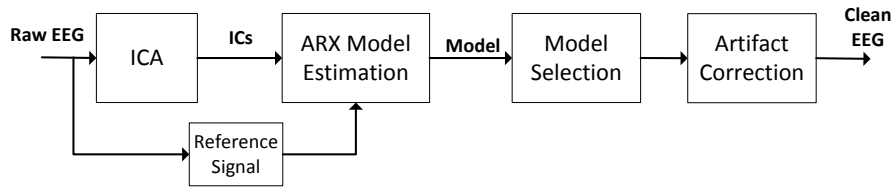


Figure 3.9: Process flow of the hybrid ICA-ARX methodology.

selected prior to the artifact-contamination.

- Other Hybrid Methods:** [93] reports EOG artifact removal using a hybrid method combined of Wavelet decomposition and Artificial Neural Network and termed as Wavelet Neural Network (WNN) where the reference EOG channel is only required during training of ANN classifier. A method combining DWT and ANC (Adaptive noise canceler) is proposed in [94] to remove ocular artifacts where the OA reference is derived from DWT decomposition and then used in the adaptive filter as reference. On the other hand, [95] used the combination of EMD and adaptive filter (with RLS algorithm) to remove ECG artifacts from EEG recordings. The authors in [60] presented a new way to remove EOG and EMG artifacts from EEG by using a hybrid combination of functional link neural network (FLNN) and



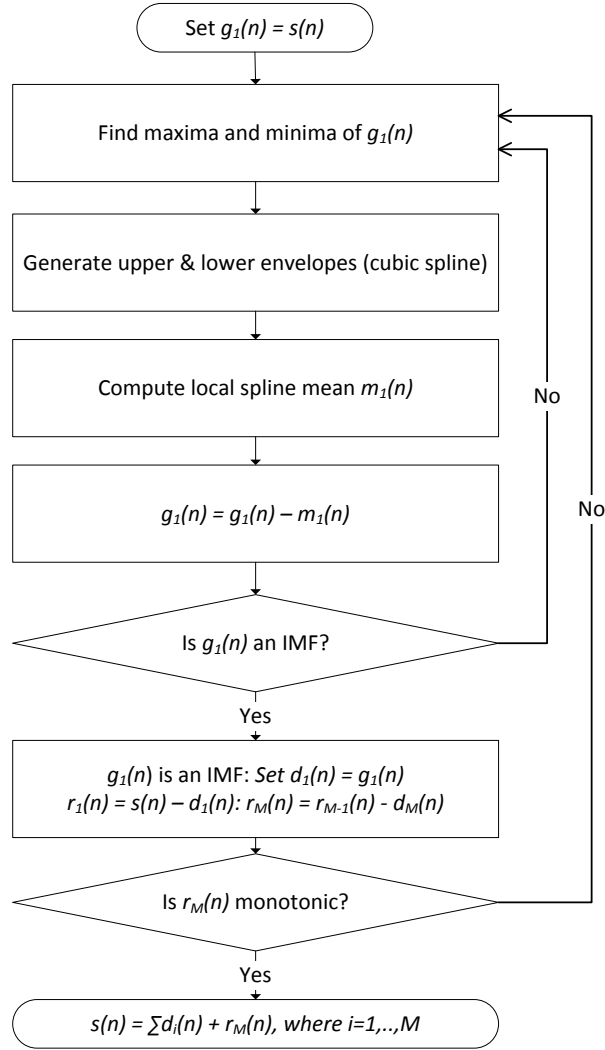


Figure 3.10: Process flow of EMD algorithm to generate IMFs.

adaptive neural fuzzy inference system (ANFIS). The ANFIS usually has two parts: a nonlinear antecedent and a linear consequent; however, in their proposed system, the second part is replaced with the FLNN to enhance the nonlinear approximation ability. Then an adaptive filtering algorithm adjusts the parameters of both ANFIS and FLNN.

### 3.2.4.11 Statistical Features

Several statistical features are used in machine learning classifier or during threshold calculation in wavelet/EMD/ICA based methods for separating or identifying artifacts from EEG signal of interest. Some of such features are discussed below:

- **Auto-regressive Features:** The autoregressive framework assumes that the EEG signal can be modeled as a linear combination of the signals at the previous time points. An autoregressive model of order  $p$  for a single channel can be written as:

$$y(t) = \sum_{i=1}^p a_i y(t-1) + \epsilon_t \quad (3.9)$$

where  $p$  denotes the number of times points in the past that are used to model the current time point and  $E_t$  denotes a zero-mean process with variance  $\sigma^2$ . The parameters of the AR model are the coefficients  $\alpha_i$ ,  $i = 1, \dots, p$  and the noise variance  $\sigma^2$ .

- **Time Domain Features:**

- **Entropy,  $H$ :** Entropy ( $H$ ), a measure of uncertainty of information content, of a discrete random variable  $x$  with possible values  $x_1, \dots, x_n$ , can be calculated as:

$$H(x) = E[-\ln(P(x))]. \quad (3.10)$$

Here  $E$  is the expected value operator and  $P(x)$  is the probability mass function of  $x$ .

- **Kurtosis**,  $Kr$ : Kurtosis is the measure of "peakedness" of probability distribution function and is calculated for a real-valued random variable  $x$  as follows:

$$Kr[x] = \frac{\mu^4}{\sigma^4}. \quad (3.11)$$

where  $\mu$  and  $\sigma$  are the mean and standard deviation of random variable  $x$ .

- **Line Length**,  $LL(n)$ : Line length, a signal feature for seizure onset detection as reported by [96], for a discrete time signal  $x[k]$  can be represented by,

$$LL(n) = \sum_{k=n-N}^n \text{abs}[x(k-1) - x(k)] \quad (3.12)$$

where  $N$  is the time window length. Here  $N = 1$  sec.

- **Maximum**,  $M$ : It is the maximum or peak value of an epoch and noted down as a feature.

$$M = \max(x(n)) \quad (3.13)$$

- **NEO**,  $\Psi$ : The ability of Non-linear Energy Operator (NEO) to enhance signal's transition or large amplitude [97, 98, 99] is sometimes considered as feature for seizure classification. The

NEO operator  $\psi$  applied to a discrete time variable  $x(n)$  is calculated as follows:

$$\psi[x(n)] = x(n)^2 - x(n+1)x(n-1) \quad (3.14)$$

In this thesis, we have taken the mean value of  $\psi[x(n)]$  for each epoch.

- **Variance,  $\sigma^2$ :** The variance of a random variable  $x$  is the expected value of the squared deviation from the mean,  $\mu = E[X]$ :

$$\sigma^2(x) = E[(x - \mu)^2] \quad (3.15)$$

where E is the expected value operator.

- **Frequency Domain Features:**

Spectral features along with temporal or spatial features are often used for EEG classification. As mentioned before that EEG rhythms have different spectral band, therefore sometimes the relative power in those bands are used as features for classifier training. It is important to note that apart from the rhythms, there are recently reported High Frequency Oscillations (HFO having band of 80 - 200 Hz), Ripple (200 - 600 Hz) bands present in EEG. In addition, the frequency band of typical Scalp EEG is 0.05 - 128 Hz while epileptic seizure appears in 0.5 Hz - 29 Hz [100]. These bands and their FFT or spectral power are useful features for separating artifacts from EEG.

- **FFT**,  $F$ : Fast Fourier Transform or FFT is the frequency representation of time domain signal values. For feature extraction, we have used the mean of the absolute of FFT values for each epoch computed over the entire frequency range of EEG signal (i.e. 0-128 Hz).

$$F = \text{mean}(\text{abs}[FFT(k)]) \quad (3.16)$$

- **Maximum FFT**,  $F_{max}$ : This feature is the maximum or peak value of the absolute of FFT values.

$$F_{max} = \text{max}(\text{abs}[FFT(k)]) \quad (3.17)$$

- **Spatial Features**: Spatial distribution or topographic mapping helps to identify the origin of many artifacts (e.g. ocular artifacts are dominant in frontal EEG channels). In addition some artifacts may appear in several nearby channels (global artifacts such as eye blink) where some only in one channel (i.e local artifacts). Therefore spatial features along with their spectral content are important to identify artifacts from EEG signals [56, 101].

### 3.3 Comparison between Methods

In order to compare different artifact handling methods qualitatively, several factors need to be considered that can evaluate the pros and cons of

these methods. Such factors are described as follows:

A detail comparison between the existing artifact detection and removal methods in the literature found from recognized journals is provided in tables 3.1, 3.2 and 3.3.

### **3.3.1 Removal Performance**

It is quite difficult to compare different artifact removal methods based on their ability to remove artifacts since very few quantitative evaluation have been reported in the literature. Most of the published articles evaluated their method in terms of some qualitative plots. In addition, very few of them quantified the distortion to desired EEG signals due to the removal effect. Therefore, it's not fair to tell which performs best based on the study.

### **3.3.2 Automatic or Semi-Automatic**

Most of the EEG based applications require automated information processing, specially it is an online/real-time implementation. In addition, manual identification of artifactual component or epoch is very time-consuming and laborious for multi-channel long-term data sequences. Therefore, many signal processing techniques have been proposed along with some useful a-priori signal or artifact statistics/characteristics have been utilized. Among them, BSS-based techniques sometimes can be semi-automated because of identification of artifactual component may require some training or param-

eter selection/tuning. Although there are few papers available that propose automated identification of ICs after ICA [102, 103]; however, they both require training samples for supervised classification and in addition requires an extra information in the form of contact impedance measurement [104]. If the method involves ICA for automatic detection of artifacts, then there has to be another stage (or method) in order to make the whole process automated.

### **3.3.3 Real-time/Online Implementation**

Online/Real-time implementation demands the algorithm to be fast enough and to have low-enough complexity for such application. Here, online implementation refers to the algorithms implemented in software platform capable of online/real-time processing, not in hardware platform. However, some EEG-based applications such as wireless ambulatory EEG monitoring, may require on-chip implementation of the artifact detection/removal algorithm. In such case the computational complexity has to be minimum which is a great challenge and so far according to best of our knowledge no real-time hardware implementation has been performed.

### **3.3.4 Single or Multi-Channel**

BSS-based methods require multi-channels to function, the more no. of channels the better for separating individual sources. Therefore, such methods cannot be used in low-channel (e.g. 4-6) or single-channel based ap-

plications (e.g. in ambulatory monitoring of epilepsy patient). On the other hand, Wavelet transform and EMD-based techniques can work with single-channel analysis by decomposing a single data sequence into multiple components (approx./detail coef. for wavelet decomposition and IMF for EMD).

### **3.3.5 Robustness**

Robustness is an important issue in developing any artifact removal algorithm as artifacts are of diverse types and contaminate the EEG differently in different recording environments. The factors that should be considered for robustness include artifact-SNR, type of artifact, subject-variability, environmental variability, application-specificity, etc.

### **3.3.6 Reference Channel**

Most of the available methods require a dedicated artifact channel to be functional. In order to remove ocular or cardiac artifacts, the reference channel often provide satisfactory complement information to identify ECG or EOG artifacts. Besides, real-time contact impedance measurement can provide the complement information about artifacts due to electrode pop-up, movement or loose connection. Some movement tracking devices such as motion captured camera, accelerometer and/or gyroscope can help to detect motion artifacts.



### 3.3.6.1 EOG

Several articles reported to remove EOG artifacts by the use of EOG reference channel [16, 68, 105]. [105] reported a hybrid de-noising method combining Discrete Wavelet Transformation (DWT) and an Adaptive Predictor Filter (APF) for automatic identification and removal of ocular artifacts for portable EEG applications which is found to achieve lower MSE and higher correlation between cleaned and original EEG in comparison with existing methods such as Wavelet Packet Transform (WPT) and Independent Component Analysis (ICA), Discrete Wavelet Transform (DWT) and Adaptive Noise Cancellation (ANC). Another article [68] reported an automated ocular artifact removal method using adaptive filtering and ICA with the help of vertical (vEOG) and horizontal (hEOG) EOG channel as reference. On the other hand, [16] proposed an ICA-based ocular artifact removal method from blind subjects EEG utilizing both vertical and horizontal EOG references.

### 3.3.6.2 ECG

[19, 95, 98] proposed removal/reduction of ECG/cardiac artifacts from EEG using a separate ECG reference channel. Among them, [19] proposed an automatic method based on a modified ICA algorithm that works for a single-channel EEG and the ECG (as reference) which gives promising results when compared with two popular methods that use a reference channel namely ensemble average subtraction (EAS) and adaptive filtering. The

other two articles proposed their methods for application in neonatal EEG monitoring. [98] reported an automated ECG artifact reduction method that mainly relies on ICA algorithm with the correlation-based thresholding to identify the ECG artifactual IC and shows that it can effectively reduce the false positives during neonatal seizure detection. Another paper [95] proposed a combination of EMD and Adaptive Filtering based method for ECG artifact removal in preterm EEG and reported up to 17% improvement in correlation coefficient between original and cleaned datasets compared with removal by only adaptive filtering.

### 3.3.6.3 Eye Tracker

Both [99, 106] reported techniques for removal of ocular artifacts by using an eye tracker as reference. The advantage of using eye tracker is that it can reduce the undesired EEG distortion produced by using an EOG channel as reference since EOG not only captures ocular events but also some frontal EEG events. Besides, in practical daily applications, the use of eye tracker removes the requirement of EOG electrodes attached to the face. [106] has shown to have significantly improved performance in removing of only eye movement artifacts by combining Kalman filter with the eye tracker information compared with three other popular methods namely Regression, PCA, and SOBI. On the other hand, [99] introduced an online algorithm for ocular artifacts (both movements and blink) removal from EEG by utilizing a high-speed eye tracker ( $> 400Hz$ ) along with the frontal-EEG as

reference instead of EOG channel. The article used two adaptive filters (RLS and  $H^\infty$ ) to prove the efficacy of their proposed technique which was shown to outperform the techniques using only EOG as reference.

#### **3.3.6.4 Accelerometer**

There are few articles reported to have used accelerometer recordings in conjunction with EEG recordings for detecting motion artifacts [44, 51]. [44] has shown that movement artifacts can be detected automatically using an accelerometer with a developed algorithm based on AR modeling and thus can increase the speed efficiency for automatic computation of EEG model parameters compared with manual detection of movement artifacts. Kevin reported in his PhD thesis [51] that the use of accelerometer as reference channel not only can detect motion artifacts but also can remove them with the use of different filtering techniques such as adaptive filtering, Kalman filtering and Wiener filtering.

#### **3.3.6.5 Gyroscope**

[61] reported to detect different head movement artifacts automatically by using a gyroscope as complementary features in fusion with EEG features and finally with the help of SVM, to classify artifacts from neural information. The method is inspired by the realization of an artifact detection system for implementing with the point-of-care REACT (Real-time EEG Analysis for event deTeCTion) technology that has potential application in

the detection of neurological events (e.g. seizure events) in adults. The artifacts were generated for 10 different types of head-related movements using 14-channel Emotiv EEG headset and the movement time was recorded for validation during artifact detection. The reported accuracy in terms of Avg. ROC areas was 0.802 and 0.907 for participant independent and dependent systems respectively.

#### **3.3.6.6 Contact Impedance Measurement**

[97, 104, 104] reported that by measuring the change in contact impedance due to head movements can help to estimate the motion artifacts and by utilizing this information with an adaptive filter in combination with band-pass filtering, the artifacts can be reduced significantly in real-time. The article also studies the effect of head movement artifacts on EEG recordings results in contaminating the spectral domain in  $< 20$  Hz frequency.

#### **3.3.6.7 Motion Captured Camera**

[107] proposed a channel-and-IC-based method to remove movement artifacts during walking and running from a high-density EEG recordings (248-channel) with the help of kinematics+kinetics information acquired from a 8-camera, 120 frames/s, motion capture system. The subject was asked to walk and run on a custom built, dual-belt, force measuring treadmill with two 24- belts mounted flush with the floor while simultaneously both brain and body dynamics were recorded. The findings conclude that

high-density EEG is possible to use in order to study brain dynamics during whole body movements; and the artifact from rhythmic gait events can be reduced by template regression procedure.

Table 3.1: Comparative analysis of artifact removal methods found in literature published in recognized journals: Part-A IEEE articles

Articles	Type of Artifacts	Method	Online/Real time	Automated	Reference	Multi/Single Channel	Application
Leor et al. '05 [64]	Eye blink & ECG	BSS-SVM (SOBI-SVM)	N/A	Y	N	Multi	General; e.g. ERP analysis
Park et al. '02 [147]	ECG	EIH-EAS	Y	Y	N	Single	General; e.g. sleep/wake state or epilepsy monitoring
Mehdi et al. '14 [87]	EKG	ICA-CWT	N/A	Y	Template	Multi	General; e.g. epilepsy monitoring
Shao et al. '09 [65]	Eye blink & ECG	ICA-Weighted PWC_PSVMM	N/A	Y	Template	Multi	General
Qinglin et al. '14 [105]	Ocular	DWT-APF	Y	Y	N	Single	monitor mental health (OPTIMI), portable applications
Wim et al. '06 [140]	Muscle	CCA	N	N	N	Multi	epilepsy monitoring; applied on ictal datasets
Slew-Cheok et al. '09 [138]	EOG + EMG	SOBI-SWT	N/A	Y	N	Multi	$\mu$ Rhythm Extraction
Javier et al. '13 [141]	Ocular	RBF based ANN	N/A	Y	EOG channel (vEOG+hEOG)	Single	General
Charles et al. '06 [137]	EOG & 60-Hz noise	GSVD-SFA	May Be	N	EOG channel	Multi	BCI; mental task
Wim et al. '05 [136]	Muscle & 50-Hz noise	SVD	N/A	N	N	Single/Multi	ictal EEG
Ian et al. '14 [113]	Head Movement	ICA	N	Semi-Automated	Accelerometer	Multi	General; BCI
Borna et al. '12 [99]	EOG & Blink	Adaptive Filter (RLS & H <sub>∞</sub> )	Y	Y	Eye Tracker	Multi	General
Hong et al. '13 [94]	Ocular	DWT-ANC	May Be	Y	N	Single	OPTIMI, portable applications
Kianoush et al. '08 [146]	Blink	STF_TS-RMVB	Y	Y	N	Multi	General
Christopher et al. '03 [71]	Ocular	dICA	Y	Y	Derived Reference	Multi	Seizure Analysis
Vitaly et al. '04 [57]	ECG, EOG, Muscle, & Electrode Noise	PNN_GMDH-DIT	N/A	Y	Template	Multi	Sleeping Newborns
Rashima et al. '15 [86]	Eye Blink	ICA-DWT with Statistics (MMSE, Kurtosis)	N/A	Y	N	Multi	General
Joep et al. '07 [106]	EOG	Kalman Filter	N/A	Y	Eye Tracker	Single	General
Kevin et al. '13 [33, 51]	Motion	EEMD-CCA	N/A	Y	N	Single	Ambulatory single channel applications

Table 3.2: Comparative analysis of artifact removal methods found in literature published in recognized journals: Part-B Elsevier articles

Articles	Type of Artifacts	Method	Online/Real time	Automated	Reference	Multi/Single Channel	Application
ZhenYu et al. '14 [92]	Ocular	ICA-ARX	N/A	Y	N	Multi	General
Burger et al. '15 [58]	EOG	ICA-WNN	N/A	N	N	Multi	General
Klados et al. '11 [68]	Ocular	REG-ICA	N	N	EOG	Multi	General
Simon et al. '13 [55, 61]	Head Movement	Feature Fusion (69) to SVM	N/A	Y	gyroscope	Single	Ambulatory EEG: seizure monitoring + BCI
Junshui et al. '11 [145]	Ocular	BSS based CSPA	N/A	Y	N	Multi	General
Junshui et al. '12 [148]	Muscle	ICA-SR	N/A	Y	N	Multi	General
Aysa et al. '13 [59]	Ocular, Muscular & ECG	adaptive FLN-RBFN-based filter (ANC)	N/A	Y	ECG, EOG, EMG	Single/Multi	General
Nguyen et al. '12 [93]	EOG	WNN	Y	Y, training required	EOG only for training	Single	Mental and Visual Task
Jing et al. '15 [60]	EOG & EMG	FLNN-ANFIS	May be	Y	EOG, EMG	Single/Multi	General
Hartmann et al. '14 [115]	Most types	Iterative Bayesian Estimation (MMSE)	N/A	Y	N	Single/Multi	Epilepsy Monitoring
Reza et al. '14 [135]	Ocular	generalized eigenvalue decomposition	N/A	Y	EOG	Multi	General
Muhammad et al. '12 [70]	Most types	Spatially cICA + Wavelet Denoising	N/A	Y	May be sometimes	Multi	
Molla et al. '12 [27]	EOG	data adaptive time domain filtering (EMD based filter)	N/A	Y	Fractional Gaussian noise (Simulated template)	Single	General
LeVan et al. '06 [139]	Ocular, EMG, Movement	ICA + Bayesian Classification	N/A	Y	ECG	Multi	Ictal Scalp EEG for Epilepsy Diagnosis



Table 3.3: Comparative analysis of artifact removal methods found in literature published in recognized journals: Part-C other articles

Articles	Type of Artifacts	Method	Online/Real time	Automated	Reference	Multi/Single Channel	Application
Vernon et al. '12 [62]	Ocular, Muscle, Movement	AR model (feature) + SVM	Possibly Yes	Y	N	Single	Real time EEG applications
Hallez et al. '09 [157]	Muscle & Ocular	BSS (CCA / Spatial cICA) + RAP-MUSIC	N/A	Semi-automated*	N	Multi	Ictal EEG Source Imaging
Sourya et al. '13 [63]	All of them	26D features + Bi-Classification (SVM)	N/A	Y	N	Single	neonatal seizure detection
Arnaud et al. '07 [176]	Most types (EMG, Blinks, electrical noise)	ICA + high order statistics	N	Y	N	Multi	General
Arthur et al. '05 [16]	Ocular	ICA	N/A	Semi-automated	N	Multi	Blind subjects
Teixeira et al. '06 [134]	EOG + baseline drifts	local SSA + Embedding Dimension	N/A	Y	N	Single	General
Sunan et al. '14 [133]	Ocular	FOOBI based on UBSS	N/A	Y	N	Multi	Only for healthy subjects; not for epilepsy
Nicolaou et al. '07 [96]	EOG, EMG & ECG	TDSEP + LAMIC	N/A	Y	EOG	Multi	discovery & analysis of ERP
Xun '14 [132]	Eye blink and EMG	SOBI	Y	Y	N	Multi	real-time application
Md. Et al. '13 [79]	Ocular	EMD	N/A	Y	Simulated	Multi	BCI
Guerrero et al. '12 [19]	Ocular	Adaptive Filtering + ICA		Y	Fp1, Fp2, F7 and F8 Electrodes	Multi	General
Nadia et al. '14 [88]	Ocular + Muscle + electrical shift + Linear trend	EAWICA (w/ICA)	N	Y	N	Multi	General
Irene et al. '11 [17]	EOG + EMG	TDSEP (based on ICA) + LPM	Y	Y	N	Multi	BCI
Xun et al. '14 [91]	Muscle	EEMD-JBSS	N/A	Y	N	Single	General + ictal EEG
Hong et al. '13 [66]	EOG	SSA (BSS)+ EMD	N	N	N	Multi	Diagnosis



## 3.4 Effects of Artifacts in EEG-Based Applications

The purpose of this section is to discuss the challenges faced in different EEG-based applications due to the presence of artifacts and how artifacts affect the outcome of any application. It also discusses the importance of developing an automated and reliable artifact removal algorithm for such applications.

### 3.4.1 Epilepsy Monitoring

During epilepsy patient monitoring for diagnosis of seizure, long-term EEG recording is used which is often contaminated by different types of artifacts and hence degrade the signal quality, particularly increase the false positives during seizure detection [100]. This scenario gets worse when the patient monitoring is performed under ambulatory environment [52, 53] where different types of movement-related artifacts are present.

### 3.4.2 BCI Applications

During BCI experiments or applications, artifacts can modify or alter the shape of a neurological event (e.g. ERP) that drives the BCI system. Moreover, they can also mistakenly result in an unintentional control of the device and hence consequence in a false positive [108]. Therefore, there is a strong urge to avoid the artifacts if possible, otherwise they must be

identified in order to reject or remove them from the neural signals to be analyzed or processed for the use of BCI system/device. In a self-paced BCI system, artifacts can negatively influence the performance of the system in following two ways:

- by altering the shape of the neural event during an intentional control (IC) period, resulting in the reduction of True Positives
- by imitating the shape/properties of the neural event during a non-intentional control (NC) periods, resulting in the increase of False Positives.

### **3.4.3 Patient Monitoring**

EEG monitoring of critical patients in intensive care unit (ICU) is a popular diagnostic tool for detection of brain injuries, which might result in epileptic seizures [44]. Critical illnesses due to brain injuries increases the risk of non-convulsive seizures [44] which does not affect the normal neuromuscular activity. In addition, the evolution of seizures for patients with critical condition is usually long-lasting which may contain slow frequencies and may not have obvious evolution in frequency, morphology or location. Therefore it is not possible to be sure that it represents seizure activity, which eventually demands for long-term EEG monitoring [44]. However, during long-term EEG monitoring, it's not feasible to restrict the patient without movement and hence a lot of motion artifacts along with other physiological artifacts contaminate the recording. As a result, the monitoring gets

difficult as the artifacts often misrepresent the recordings. Another application of EEG recording is during drug-effect monitoring or monitoring the right amount of dose during anesthesia.

#### **3.4.4 Sleep Study**

EEG, along with other physiological signals, are used to study and monitor different sleep stages and their associated patterns. For example, drowsiness, sleep apnea are some of the sleep-related disorders that are possible to monitor through EEG. The frequency bands of EEG during different sleep stages are different, however, as artifacts contaminate the recordings in both spectral and temporal domain, therefore the signal analysis becomes erroneous. However, to the best of our knowledge, unfortunately till now very few works [109, 110] have been done for artifact detection and removal on EEG during sleep study [44]. It is worth to mention that none of them emphasizes on the effects of artifacts and their removal on the sleep EEG and hence it is expected to be covered in near future, the sooner the better for such sleep study applications.

#### **3.4.5 Other Applications: Neurological Diseases**

EEG is also used in many other neurological applications, e.g. disease diagnosis, mental fatigue study, or even depression study. One of the neurological diagnosis applications is Alzheimer disease (AD). The article [111] reported the effects of artifact removal on the diagnosis of Alzheimer's dis-

ease. The authors applied three state-of-the-art artifact removal algorithms to observe the effect on disease diagnosis and reported their outcome as the fully-automated system can assist clinicians with early detection of AD, as well as disease severity progression assessment. In [112], a multi-scale entropy (MSE) based EEG complexity analysis was done for schizophrenia patients where the artifactual epochs have been manually identified (those are visually detectable) and rejected for calculating of MSE to extract EEG features. No doubt, has it been an automated and reliable artifact removal algorithm, the analysis could be more accurate and effective.

## 3.5 Discussion

### 3.5.1 Current Status

Although significant amount of efforts have been made to develop methods for artifact detection and removal in EEG applications, it is still an active area of research. Most of them handle single type of artifact, many of them cannot work for single-channel EEG, some of them require training data, some require a dedicated reference channel, some are designed for general purpose applications that often leads to overcorrection of data and some of them are not fully automated.

Currently available some of the major software plug-in GUIs are discussed below:

### 3.5.1.1 FORCe

Fully Online and automated artifact Removal for brain-Computer interfacing or FORCe is the most recent method reported in [113] that is based on a unique combination of WT, ICA and thresholding. Compared with two other state-of-the-art methods namely LAMIC and FASTER, FORCe has been shown to outperform them significantly and is capable of removing different types of artifacts including eye blink, EOG and EMG. One of salient features of FORCe is that it does not require any reference channel and can operate on fewer number of channels which makes it suitable for ambulatory EEG applications.

### 3.5.1.2 FASTER

FASTER stands for Fully Automated Statistical Thresholding for EEG artifact Rejection which is an unsupervised algorithm for parameter estimation in both EEG time series and in the ICs of EEG [114]. The achieved sensitivity and specificity is  $> 90\%$  for detection of EOG and EMG artifacts, linear trends and white noise in the contaminated channels.

### 3.5.1.3 LAMIC

Lagged auto-mutual information clustering (LAMIC) is a clustering algorithm developed for automatic artifact removal from EEG [96]. The method involves data decomposition by a BSS algorithm called TDSEP (Temporal De-correlation source SEparation) which is a temporal extension of ICA.

Then the components are clustered using the similarity of their lagged Auto-Mutual Information (AMI). This is inspired from the fact that EEG and artifacts are different from their temporal dynamics point of view. The clustering procedure follows the usual steps of hierarchical clustering.

#### **3.5.1.4 PureEEG**

This is an automatic EEG artifact removal algorithm for epilepsy monitoring that based on a neurophysiological model by utilizing an iterative Bayesian estimation scheme [115]. The method targets to remove most of the artifact types and does not require any manual intervention. The authors reported the performance of PureEEG from two independent clinical experts perspective and it's found to be significantly improving the readability of EEG recordings after artifact removal.

#### **3.5.1.5 OSET**

OSET is an Open-Source Electrophysiological Toolbox for biomedical signal generation, modeling, processing, and filtering [116]. It can remove cardiac artifacts from any bioelectrical signal including EEG. It can also handle and remove EOG artifacts from multichannel EEG using techniques based on semi-blind source separation.

#### **3.5.1.6 MARA**

Multiple Artifact Rejection Algorithm (MARA) is an open-source MATLAB based EEGLAB plug-in which automatically identify the artifact-

contaminated independent components for artifact rejection [17, 102]. The main part of MARA is a supervised machine learning algorithm that learns from labeled components by experts and utilizes six features based on spatial, spectral and temporal domain. It can handle any type of artifact.

#### **3.5.1.7 AAR**

Automatic Artifact Removal (AAR), a MATLAB toolbox which can be integrated as a plug-in into EEGLAB, includes several artifact removal methods for removing only EOG and EMG artifacts [117]. In order to remove only EOG artifacts, regression based methods such as Least Mean Squares (LMS), Conventional Re-cursive Least Squares (CRLS), Stable Recursive Least Squares (SRLS) and Algorithms based on the H norm are used. For removing both EOG and EMG artifacts, spatial filters based techniques have been adopted.

#### **3.5.1.8 ADJUST**

ADJUST, reported by [56] is an another EEGLab supported plug-in for automated EEG artifact detection. This algorithm is based on the combined use of stereotyped artifact-specific spatial and temporal features to automatically identify the artifactual ICs after ICA is performed. Four different artifact types (i.e. eye blink, vertical eye movement, horizontal eye movement and generic discontinuities) are chosen for extracting features such as temporal kurtosis, spatial average and variance difference, maximum epoch

variance, spatial eye difference, etc. The key feature of ADJUST is that it is entirely automated and unsupervised with reported accuracy of 95.2% in classifying all of the four artifacts. It can also successfully reconstruct the clean ERP topographies from heavy artifact contamination.

### **3.5.2 Future Direction**

Here we present the future direction for handling artifacts by raising realistic issues, proposing some ideas and providing recommendation based on reviewing existing solutions.

#### **3.5.2.1 Probability Mapping**

From the above literature review of existing solutions for artifact handling, one fact is obvious that artifacts are of different types and not all types will play major role in all EEG-based applications. Sometimes, the clinicians prefer manual event detection than automated algorithm for certain disease diagnosis (e.g. seizure detection). However, such manual analysis is also time-consuming. In such cases, if we can give the users an option to choose which particular artifacts they want to be detected and/or removed with what amount (%) for each epoch or data-segment of duration 1-sec (depends on application), then the process would still be automated with tuning facilities for the users either to turn-ON or remain OFF if not required. In order to implement such facility, a probability mapping of artifacts can be proposed (something similar to the idea of [118]) for each epoch of data



based on some statistical features to quantify the probability of an epoch to be artifactual. Then the user can opt for some threshold of probability above which he/she may want to remove artifacts while below the threshold, to preserve the epoch as it is. Thus it is possible to design automated artifact detection and removal algorithm which is application-specific with tuning facility for user. This would greatly enhance the signal analysis process by avoiding the chance of removing important signal information. In addition, it will reduce the unnecessary computational resources and time by focusing on the desired artifacts for detection/removal (i.e. only those types to be expected to affect the signal quality) and ignoring the rest of them.

### **3.5.2.2 Standard Performance Evaluation**

One of the important issues in evaluating the performance of any artifact detection or removal method is that there is no universal standard quantitative metric for the researchers to use. Most of the methods mentioned in the literature use some qualitative time/frequency domain plot to evaluate the artifact removal performance or evaluated by the clinical expert. Sweeney et al. [119] proposed a recording methodology for accurate evaluation and comparison between different artifact removal techniques/algorithms which presented the EEG recordings of two separate but highly-correlated channels that allow to record both artifact-contaminated and artifact-free signal simultaneously. It also presented a tagging algorithm employing two ac-

celerometer for generating a quality-of-signal (QOS) metric which can be used to for multiple purposes such as classification of motion artifacts, activation of artifact removal technique only when required and identification of the artifact-contaminated epochs. Thus this approach can provide accurate measurements of quantitative metrics for fair performance evaluation. However, such methodology still requires intervention to the recording technique and also extra reference channel for accelerometer data which may not be feasible in every application (e.g. portable EEG recordings). Although it is highly encouraged for the removal performance to be evaluated by the domain experts, however, such evaluation varies from one expert to another and still are manual and/or qualitative evaluation. Therefore, it's an urge to have a single standard evaluation method consists of both qualitative and more importantly quantitative metrics or ways for evaluating the performance in a more realistic and fair manner.

### **3.5.2.3 Ground Truth Data**

Another reason of not being able to evaluate artifact removal performance fairly is that the lack of availability of ground truth data. It's now equally important to have a public database with sufficiently long-term EEG recordings without or minimal artifacts to be used as a ground truth data. Besides such, an acceptable mathematical model to generate basic EEG rhythms and finally integrate them to simulate an EEG sequence with standard 10-20 system EEG channels is required for quantitative evaluation of any

existing/future artifact removal methods.

In addition, more study is necessary to characterize as much as possible of all artifact types, specially the motion artifacts for different movement in an ambulatory environment [52, 54]. Thus it will be easier to label both ground truth EEG and artifacts.

#### **3.5.2.4 Recommendation**

In order to choose the right artifact handling method, we need to consider the particular application, required specification to be satisfied given the computational resources and recording environment available. There are EEG applications where only one or two types of artifacts affect the later stage information decoding or processing, thus it's not wise to try to go for identifying and removing all the artifacts as other artifacts may not (or minimally) harm particular signal processing purpose. If any reference channel is available in the targeted application, then regression or adaptive filtering technique may be a preferred solution. In case of ambulatory EEG monitoring, when number of channels are fewer, no reference channel is available and wireless EEG transfer is preferred, then it is recommended to use computationally cheaper method that can work without reference and on single or few channels, e.g. wavelet based methods since BSS-based methods may not perform satisfactory with fewer number of channels. In some applications, if it's possible to have some a-priori knowledge about artifacts, some training data available, and if the application only requires

to identify artifacts but not to remove them, then machine learning based classifiers can be good choice. If the EEG recording involves high-density channels, then PCA may be preferred to reduce the dimensionality before applying any artifact removal methods, such as BSS-based methods. If the application is based on offline analysis then we can afford some computational expensive techniques such as ICA or EMD.

### 3.6 Conclusions

An extensive analysis of the existing methods for artifact detection and removal has been presented with their comparison, advantages and limitations. The work on artifacts present in the typical EEG recordings is still an active area of research and none of the existing methods can be considered as the perfect solution. Most of the solutions do not consider the particular application, therefore, not optimized for that application. Moreover, many of the removal algorithms, although provide good performance, are only suitable for offline analysis because of their high computational complexity and unsupervised nature. Some of them even require a dedicated reference channel which is not feasible for some applications. Further studies are required to characterize the properties of commonly encountered artifacts and to observe the effects of their contamination to the desired later-stage signal processing/analysis. Some applications may only require to identify artifacts and not to remove them, e.g. in applications where

classification/identification of two classes are required. In such cases, a more realistic mathematical model of the desired event(s) to be identified is essential in order to easily ignore other non-brain signals (i.e. artifacts or interferences). Finally, the future direction will be to provide application-specific solution with reasonable complexity and optimized performance.

## Chapter 4

# Artifact Detection and Removal from *In-Vivo* Neural Recording: Algorithm Design

This chapter introduces time series analysis of in-vivo neural recording and then describes the proposed algorithm for artifact detection and removal from such recordings. The algorithm relies on the spectrum characteristics of the neural signals (i.e. LFP and neural spikes) for artifact detection. It further applies stationary wavelet transform (SWT) to detect possible artifactual regions from the decomposed wavelet coefficients. Once artifacts have been detected, to restore neural signals, a modified version of the existing universal-threshold value is proposed, which makes the algorithm more robust.

## 4.1 Introduction

As mentioned before in chapter 1 that there is no method/algorithm found in the literature so far (to the best of our knowledge) to deal with artifacts present at in-vivo neural recordings. In addition, the available artifacts removal methods from other physiological signals (especially EEG) cannot be directly applied on in-vivo neural recordings due to few factors. One of them is the difference in signal characteristics (i.e. in-vivo neural signals have broad spectrum with two completely separate signal of interest types: spikes and LFP). Usually recording artifacts have large amplitudes, sharp edges, and varied durations up to hundreds of ms, which are important features for differentiating them from signals of interest, i.e. spikes and field potentials. The frequency span of artifacts tends to be wide (from a few Hz to several kHz) and the power spectra may exhibit significant variability, because there are different evoking mechanisms of artifacts. As a result, artifact waveforms do not tend to follow a specific template or a statistical distribution which makes reliable detection of artifacts quite challenging. In time domain, artifacts could have waveform features that are similar to field potentials or spikes; while in the frequency domain, their aggregated spectrum overlaps the signal frequency span (0.1 Hz to 5 kHz). Moreover, artifacts may appear globally over multiple channels, or locally over one single channel. Cross-channel analysis helps to identify and remove global artifact at the cost of computational burden and storage requirement.

Repeatability analysis will help to identify both local and global artifacts; however, it introduces processing latency and causes problems in real-time applications.

Therefore, in this chapter we first analyze the in-vivo neural recordings in both time and frequency domain simultaneously to understand the signal characteristics and then propose an automatic algorithm to detect and remove different types of artifacts from such neural recordings. Our wavelet based algorithm relies on the hypothesis through data modeling and real data analysis that the frequency bands of 150-400 Hz and  $>5$  kHz are the most prospective regions to detect artifacts. A synthesized database based on recorded neural data and manually labeled artifacts has been built to allow quantitative evaluations of the proposed algorithm. Some of the advantages of our proposed algorithm are: it is independent of artifact types, does not require any reference channel and brings almost no distortion to the signal of interest during artifact removal process. This chapter also includes optimum parameter selection to achieve the best performance of the algorithm.

## 4.2 Time Series Analysis of Neural Signal

Since neural signals are mainly non-stationary and non-linear time series signals, in order to detect possible artifactual activities from neural signal of interest it is necessary to analyze the recordings in both time and frequency



domains simultaneously. We have made significant observations to detect different types of artifacts and to justify the proposed method (e.g. band-pass filtering at 150-400 Hz from spectrogram and coherence analyses) from these time series analyses.

#### 4.2.1 Spectrogram

A spectrogram is a time-varying spectral representation that shows how the spectral density of a signal varies with time. The spectrogram of a signal  $s(t)$  can be estimated by computing the squared magnitude of the short-time Fourier transform (STFT) of the signal,  $S(t, f)$ , as follows:

$$S(t, f) = |STFT(s(t))|^2 \quad (4.1)$$

As the artifacts overlap with neural signal both in temporal and spectral domain, it is required to observe the spectrogram of the artifactual data to get more insight of the dominant power of artifacts at a particular time window. The spectrogram of a real artifact-contaminated neural data is shown in Figure 4.1. The challenges in using STFT based spectrogram are as follows:

- Spectrogram utilizes STFT in which both time and frequency are represented in limited precision. The precision is determined by the size of the window and the window size is fixed.
- Spectrogram requires huge amount of computational time and storage. Therefore, although good insight for offline artifact analysis but

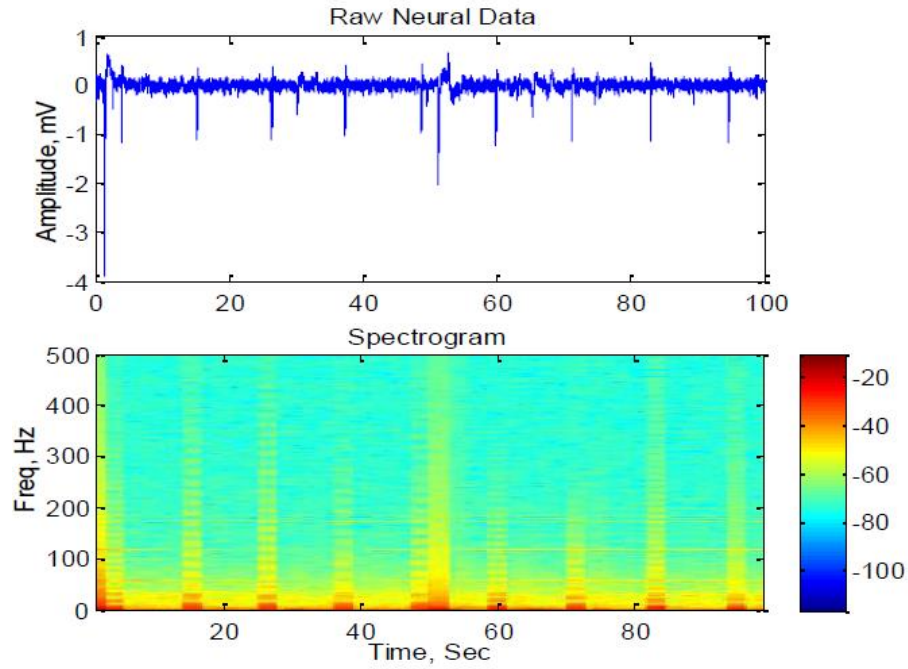


Figure 4.1: Upper trace: real neural data contaminated with both type-1 and type-2 artifacts; Lower trace: Spectrogram of that neural data showing the justification of using BPF at 150-400 Hz as there is significant artifact power in this band corresponding to the temporal location of artifacts.

the algorithm may not be suitable for online detection.

- Can only be used to detect artifacts, removal requires different method.

#### 4.2.2 Correlation Analysis

To detect the global artifact as shown in Figure 2.2 (left plot), if we observe the cross-correlation between all the channels in a particular electrode (cross-channel correlation analysis) for that simultaneous temporal window, the detection of such global artifact activities become obvious from their cross-correlation coefficient values as given in Table 4.1.

Table 4.1: Correlation coefficient between 8 different channels from a same electrode recording shown in Figure 2.2 (left plot) to detect global type-0 artifacts.

	<b>Ch1</b>	<b>Ch2</b>	<b>Ch3</b>	<b>Ch4</b>	<b>Ch5</b>	<b>Ch6</b>	<b>Ch7</b>	<b>Ch8</b>
<b>Ch1</b>	1.00	1.00	1.00	0.96	0.98	0.95	0.92	0.85
<b>Ch2</b>	1.00	1.00	1.00	0.98	0.99	0.95	0.92	0.84
<b>Ch3</b>	1.00	1.00	1.00	0.97	0.99	0.95	0.92	0.84
<b>Ch4</b>	0.96	0.98	0.97	1.00	0.99	0.94	0.88	0.82
<b>Ch5</b>	0.98	0.99	0.99	0.99	1.00	0.97	0.93	0.87
<b>Ch6</b>	0.95	0.95	0.95	0.94	0.97	1.00	0.98	0.95
<b>Ch7</b>	0.92	0.92	0.92	0.88	0.93	0.98	1.00	0.98
<b>Ch8</b>	0.85	0.84	0.84	0.82	0.87	0.95	0.98	1.00

### 4.2.3 Coherence Analysis

Coherence between two time series measures the association between them in frequency domain, in other words it is the cross-correlation in frequency domain instead of time domain. The coherence between two signals  $x(t)$  and  $y(t)$  is a real-valued function that is defined as:

$$C_{yy} = \frac{|G_{xy}|^2}{G_{xx}G_{yy}} \quad (4.2)$$

where  $G_{xy}$  is the cross-spectral density between  $x$  and  $y$ , and  $G_{xx}$  and  $G_{yy}$  the auto-spectral density of  $x$  and  $y$  respectively. The values of coherence will always satisfy . The coherence between artifactual and artifact-free neural data is plotted in Figure 4.2.

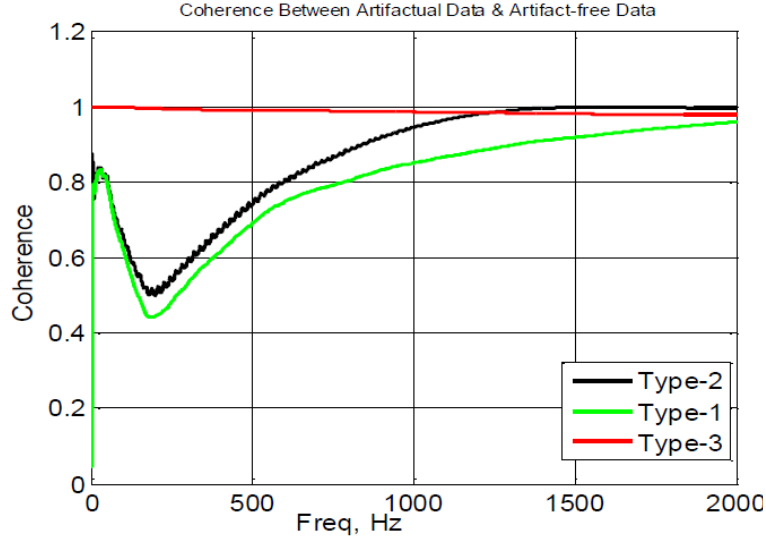


Figure 4.2: Coherence analysis between clean reference data and artifact-contaminated data which clearly shows that type-1 and type-2 artifacts can be detected between 150 Hz to 400 Hz as the coherence is minimum at this band while coherence for type-3 artifact becomes lower after few kHz.

### 4.3 Data Modeling

The recorded artifactual neural signal  $V(t)$  can be considered as superimposed from spikes, field potentials, neural interface noise, artifacts and interferences [120]. Where the neural interface noise itself is contributed by multiple sources including neuron noise, electrode-electrolyte interface noise, tissue thermal noise and electronic noise. Therefore  $V(t)$  can be written by the following formula:

$$V(t) = \sum_{i=1}^I V_i(t) + V_{LFP}(t) + N_n(t) + N_{Art}(t) + N_{int}(t) \quad (4.3)$$

where  $V_i(t)$  is the activity of  $i^{th}$  neuron within the recording radius  $r$  (spike power is much larger than noise power),  $I$  is the total no. of neurons,

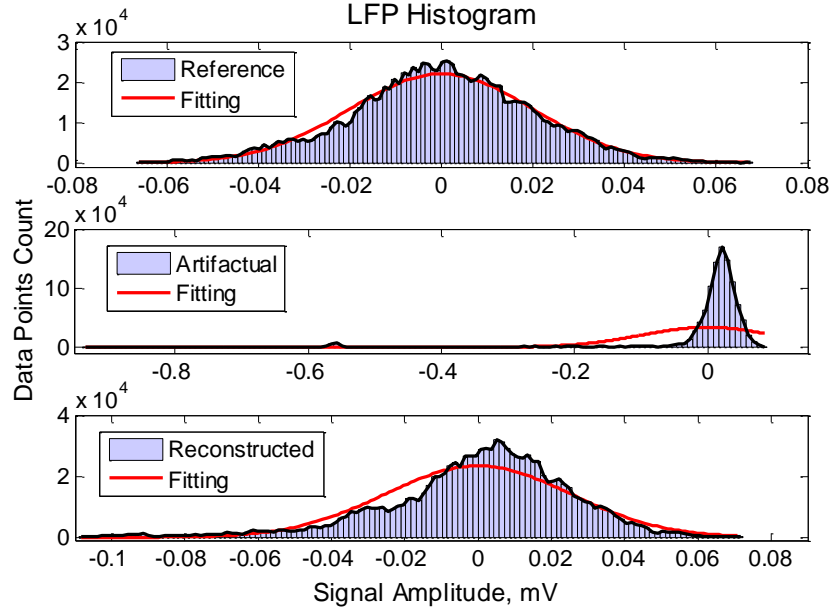


Figure 4.3: Comparison in amplitude histogram of LFP for reference, artifactual and reconstructed signal.

$V_{LFP}(t)$  is the field potential,  $N_n(t)$  is the neural interface noise,  $N_{Art}$  is the artifactual event and  $N_{int}$  is the power line interference.

The LFP distribution of an artifact-free reference signal has significant fluctuations due to non-stationary property but has a shape almost similar to that of Gaussian when curve fitting is done. While the artifactual histogram failed to fit anywhere near to Gaussian because of its large tail at one of the sides as shown in Figures 4.3 and 4.4. The reconstructed LFP signal histogram after artifact removal shows the significant improvement to fit the distribution almost similar to the original reference signal.

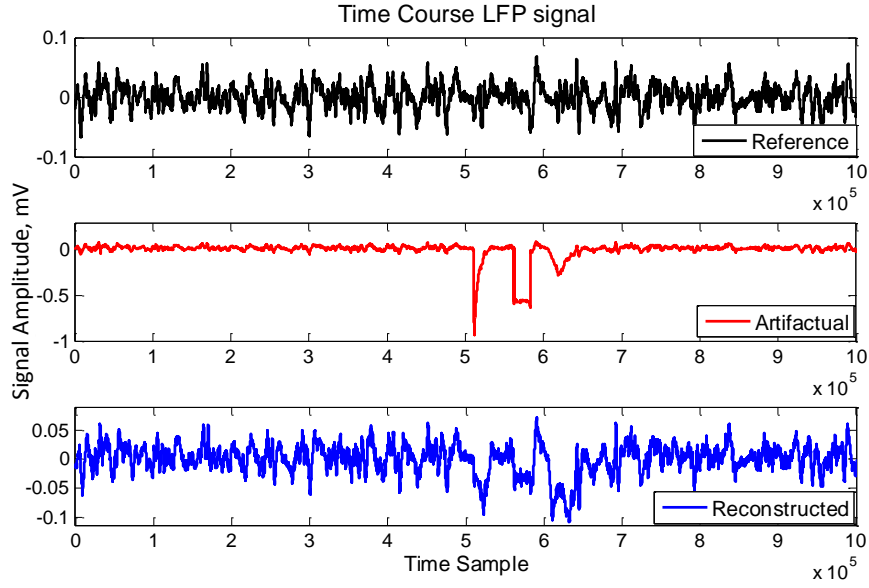


Figure 4.4: Corresponding time course data for the histogram of three signals shown in Figure 4.3.

## 4.4 Proposed Algorithm

Let's assume  $r(n)$  as the recorded neural data at discrete-time instant  $n$  and it can be expressed as:

$$r(n) = x(n) + a(n), \quad (4.4)$$

where  $x(n)$  and  $a(n)$  are actual neural signals (i.e. spikes and field potentials) and artifacts respectively. The proposed artifact removal algorithm is composed of four stages including artifact labeling, verification, detection, and reconstruction, as shown in Figure 4.5. In the following each stage of the proposed block diagram is described in more detail.

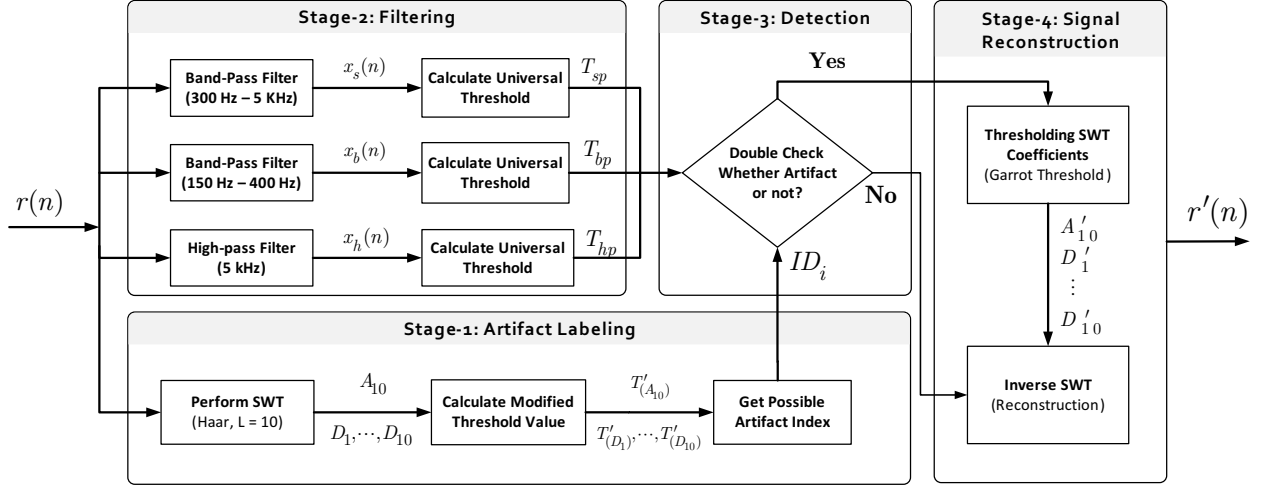


Figure 4.5: Overview of the proposed algorithm.

#### 4.4.1 Artifact Labeling

Wavelet transform has been chosen to assist labeling artifacts. The reason is that it is suitable for non-stationary signal analysis (e.g. neural signals) and is a powerful tool to detect abrupt changes or localized events mostly due to artifacts [78]. Among different wavelet transforms, the discrete wavelet transform (DWT) is the simplest one in terms of computational complexity<sup>1</sup>. However, the problem of DWT is that it is not translation invariant. Therefore small shifts in a signal can cause large changes in the wavelet coefficients and large variations in the distribution of energy in the different wavelet scales [27, 123]. Hence, denoising with DWT often introduces artifacts in the signal near discontinuities during signal reconstruction [34]. One solution is to use stationary wavelet transform (SWT)

<sup>1</sup>The computational complexity of DWT is  $\mathcal{O}(N)$  while the computational complexity of SWT is  $\mathcal{O}(NL)$  [121] using fast transform [122]. Here  $L$  is the number of decomposition level and  $N$  is the signal length.

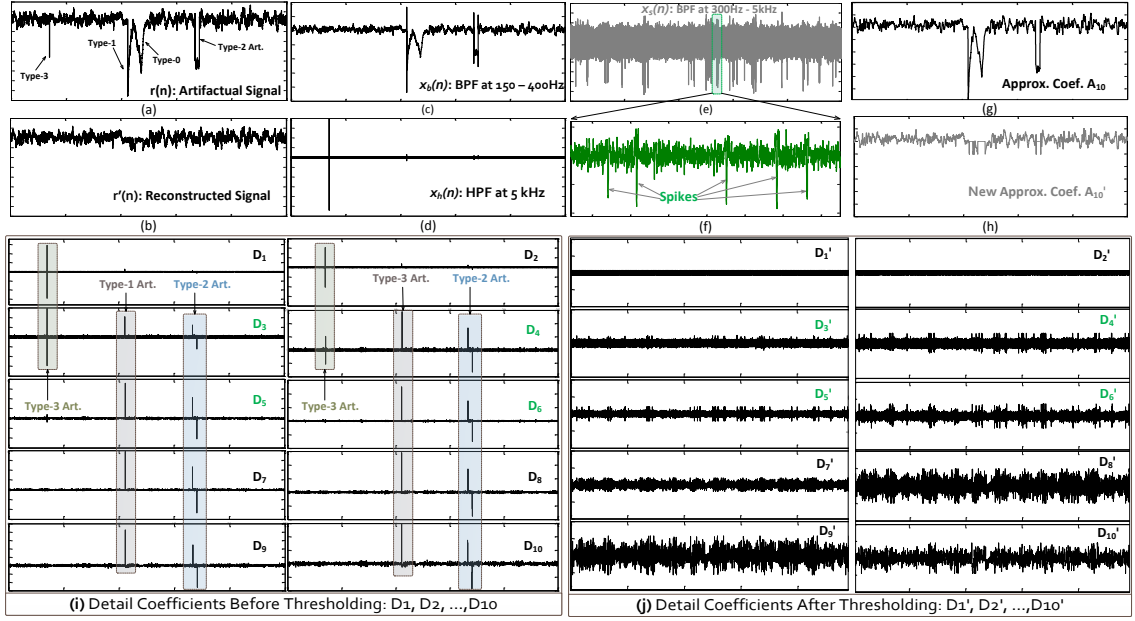


Figure 4.6: An example of all the signals at different stages (as mentioned in the proposed algorithm flow in Figure 4.5) in the same temporal domain is provided. A 10-level SWT decomposition is performed to an artifactual signal with Haar basis wavelet. (a): artifactual signal,  $r(n)$ ; (b): reconstructed signal,  $r'(n)$ ; (c):  $x_b(n)$  obtained from band-pass filtering  $r(n)$  at 300 Hz - 5 kHz; (d): A zoom-in version of (c) showing few spikes; (e):  $x_s(n)$  obtained from band-pass filtering  $r_n$  at 150 Hz - 400 Hz; (f):  $x_h(n)$  obtained from high-pass filtering  $r(n)$  at 5 kHz; (g)-(h): The final approximate coefficient before and after thresholding respectively; (i)-(j): The detail coefficients before and after thresholding respectively.

which is translation invariant, as there is no down sampling of data involved in the algorithm [27, 123, 34].

#### 4.4.1.1 SWT Decomposition

The SWT is performed on the artifactual signal  $r(n)$  at level  $L = 10$  with Haar as basis wavelet function<sup>2</sup>. Thus, two types of coefficients are

<sup>2</sup>A majority of motion artifacts appear in the form of abrupt changes in the amplitude of the signal. Therefore, Haar is used as basis wavelet since due to its waveform shape, it can possibly detect and localize such artifactual events and they appear with relatively high amplitudes in the decomposed coefficients. The choice of level-10 decomposition is done empirically by considering two facts: (i) the no. of signal components present in the raw recordings and (ii) the trade-off between latency/storage and amount of detail information extraction. Less than level-10 would give less detail information and more



generated: approximate and detail coefficients that contain low and high frequency information respectively as shown in Figure 4.2. The generated wavelet coefficients at different levels denote the correlation coefficients between artifactual signal and the wavelet function. The artifactual events will have larger coefficient values if they have higher correlation with the wavelet function while smaller coefficients will be generated corresponding to the actual neural activities. In order to perform thresholding, the selected coefficients are the final approximate coefficient,  $A_{10}$  and all the detail coefficients i.e.  $D_1, \dots, D_{10}$ .  $A_{10}$  consists of all low frequency components (from 0 Hz to 19.5 Hz), such as electrode offset, some part of information from LFPs, neuron noise and artifacts (e.g. type-0, type-1 and type-2). While,  $D_1, \dots, D_{10}$  contain the high frequency information such as neural spikes, type-3 artifacts and sharp edges from artifacts of type-1 or type-2. Table 4.2 illustrates the frequency bands of different level of coefficients and the corresponding neural signal bands. It reveals that even in the decomposed coefficients, the artifacts can overlap with the neural signals of interest. Therefore the threshold is chosen carefully in order to detect and suppress possible artifactual activities from the decomposed coefficients.

---

than level-10 would consume unnecessary time and storage.

Table 4.2: The frequency bands of the respective SWT coefficients and corresponding signal components for a 10-level decomposition. Here two typical sampling frequencies for extracellular neural recordings are considered (i.e. 40 kHz and 30 kHz) and the maximum recording bandwidth is assumed to be half of the sampling frequency.

SWT Coef. (L=10)	Fs (kHz)	$D_1$	$D_2$	$D_3$	$D_4$	$D_5$	$D_6$	$D_7$	$D_8$	$D_9$	$D_{10}$	$A_{10}$
Freq. Band		10 – 20 kHz	5 – 10 kHz	2.5 – 5 kHz	1.25 - 2.5 kHz	625 Hz – 1.25 kHz	312 - 625 Hz	156 - 312 Hz	78 - 156 Hz	39-78 Hz	19.5-39 Hz	0 - 19.5 Hz
	40											
	30	7.5 – 15 kHz	3.75 – 7.5 kHz	1.875 – 3.75 kHz	0.937 - 1.88 kHz	469 Hz – 937.5 Hz	234 - 469 Hz	117 - 234 Hz	58.5 - 117 Hz	29 - 58.5 Hz	14.5 - 29 Hz	0 - 14.5 Hz
Signal Component		Neural Spike						LFP				

#### 4.4.1.2 Threshold Calculation

The next step is to calculate a threshold value to detect the artifacts in the wavelet domain. The choice of threshold value will decide both the amount of artifact suppression and the amount of distortion to the neural signal at the same time. One possible solution is to use the universal threshold proposed by [34] which is given as follows:

$$T_j = \alpha_j \sqrt{2 \ln N}, \quad (4.5)$$

where  $N$  is the signal length and  $\alpha_j$  is the estimated noise variance for  $W_j$  which is usually calculated by following formula [34]

$$\alpha_j = \frac{\text{median}(|W_j|)}{0.6745}. \quad (4.6)$$

In (6.11)  $W_j$  is the wavelet coefficients at the  $j$ th decomposition level ( $W_j = A_j$  for approximation coefficient and,  $W_j = D_j$  for detail coefficient). Here,  $|\cdot|$  denotes the absolute value of elements in  $W_j$ . The constant denominator results in an unbiased estimate assuming the data

are normally distributed [124]. However, this particular threshold is fixed for each  $W_j$  and not optimal most of the time. By extensive testings, it has been found that this threshold is not suitable for our application as it may produce serious distortion to neural signals. Particularly for wavelet coefficients those contain components from spikes or when the neural recording has severe large artifacts such that the data distribution violates from the typical Gaussian fitting (a large tail in the histogram as shown in Figure 4.3)<sup>3</sup>. Hence it is proposed to include an extra parameter  $k$  to the original universal threshold formula in a following way and the resultant threshold modifies to

$$T'_j = k\alpha_j\sqrt{2\ln N}, \quad (4.7)$$

where  $k = \{k_A, k_D\}$ ,  $0 < k_A < 1$ ,  $1 < k_D < 5$ , which comes from the empirical observations (See sub-section 4.7.2). More precisely,  $k = k_A$  is selected for thresholding approximate coefficient at final level, here it is  $A_{10}$  and select  $k = k_D$  to threshold all the detail coefficients ( $D_j, j = 1, 2, \dots, 10$ ).

The tuning of parameter  $k_A$  depends on the data distribution as shown in Figure 4.3. Since  $A_{10}$  contains both the LFP and some low-frequency artifacts, so when the histogram of the data has large deviation from the standard deviation (large tail on the histogram on either one side or both), it is more likely due to presence of artifacts. Therefore a value less than 1

---

<sup>3</sup>The LFP distribution of an artifact-free reference data has significant fluctuations due to non-stationary property but has a shape almost similar to that of Gaussian when curve fitting is done. While the LFP distribution of an artifactual data fails to fit anywhere near to Gaussian because of its large tail at one of the sides as shown in Figure 4.3.

is chosen for  $k_A$  and if there is no such unusual tail present, then  $k_A = 1$  is chosen that makes the threshold exactly same as the original universal threshold, i.e.  $T'_i = T_1$ . The criterion for the choice of  $k_A$  is given below

$$k_A = \begin{cases} 1 & \text{if } \max(|A_{10}|) > m \times sd(A_{10}), \\ 0 \leq k_A < 1 & \text{otherwise,} \end{cases} \quad (4.8)$$

where  $sd$  denotes the standard deviation of  $A_{10}$ . The value of  $m$  is based on the parameter tuning and can be obtained from some initial several seconds of incoming raw *in-vivo* data samples to update the threshold value. From the empirical studies, the value of  $m$  is found as minimum of 5, i.e.  $5 < m < \infty$  (See sub-section 4.7.2).

In order to decide the value of  $k_D$ , power spectra of all detail coefficients are studied and it is found that coefficients at level 3, 4, 5 and 6, i.e.  $D_3$ ,  $D_4$ ,  $D_5$  and  $D_6$  have highest power around the neural spikes' spectra and hence these four levels contain spike information along with artifacts. Therefore it is chosen to put more weight ( $k_D > 1$ ) on these coefficients and less on the rest of the level of coefficients (i.e.  $D_1$ ,  $D_2$ ,  $D_7$ ,  $D_8$ ,  $D_9$  and  $D_{10}$ ) as follows

$$k_D = \begin{cases} 1 < k_i \leq 5 & i = 3, 4, 5 \text{ and } 6, \\ 1 & \text{otherwise,} \end{cases} \quad (4.9)$$

where  $i$  denotes the detail decomposition level and the constant parameter  $k_D$  is chosen from the spike data histogram. The spikes present in neural data with very large amplitudes influence the selection of  $k_D$  towards higher value while if the spike amplitude is normal, then from empirical studies it

is found that the value of  $k_D$  to be 2 to 3.

#### 4.4.2 Filtering

Once the time indices are obtained from the decomposed coefficients after applying modified threshold function,  $T'_i$ ; it is required to double check the possible artifactual segments in order to separate artifacts from signals of interest, especially from spikes. The use of filtering is inspired from the spectrum characteristics of neural signal components: LFP and spikes (as shown in Figure 2.5). Although the spectral band of *in-vivo* recordings has a wide spectrum, there are two prospective bands, i.e. 150-400Hz and >5kHz, where both LFP power and spike power are relatively low [49, 7]. Thus, band pass and high pass filtering are performed at 150-400Hz and 5kHz respectively for artifact detection<sup>4</sup>. It is assumed here that the recording does not contain ripple band oscillations, which appears around 100-300Hz, thus it is ignored [125].

The results after performing such filtering are shown in Figure 4.7. The result of high pass filtering at 5 kHz is shown in Figure 4.7(b) where it is

---

<sup>4</sup>We found out that artifacts tend to have a wide spectrum that overlaps both field potentials and neural spikes. Field potentials are aggregated or averaged from a large number of synaptic activities within a proximity region of the recording site and feature a  $1/f^x$  power spectrum distribution where  $x$  is in between 1 to 3 [120]. As a rule of thumb, at frequency beyond 150Hz, the spectrum of field potential becomes insignificant. Extracellular neural spikes, on the other hand, are produced by ionic and displacement currents during the propagation of action potentials, which have clear low-cutoff and high-cutoff frequencies: the high-cutoff frequency is at several kHz, as sodium channels tend to open for a few hundred  $\mu$ Sec or even longer; the low-cutoff frequency is around several hundred Hz as potassium channels start to dominant after 1 ms and pull the trans-membrane voltage back to its rest state. Consequently there are prospective frequency bands to detect artifacts. One is at 150Hz - 400Hz region where both field potentials and spikes have insignificant power. The other one is beyond 5kHz, which is too fast even for neural spikes

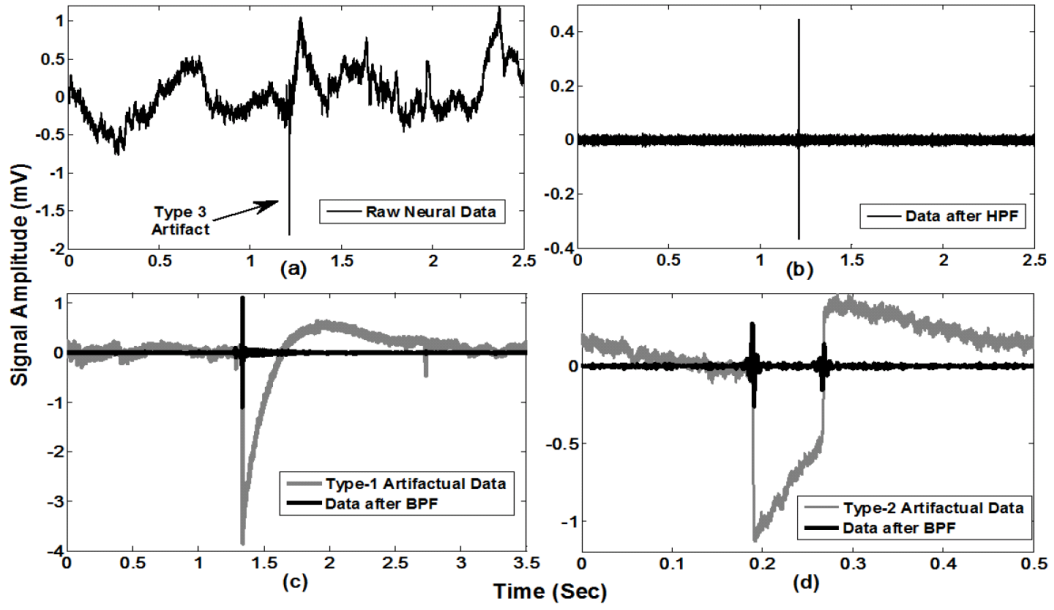


Figure 4.7: (a) Type-3 artifact contaminated neural data and (b) Effect of HPF at 5 KHz for detecting type-3 artifact; Effect of band pass filtering at 150-400 Hz for detecting type-1 (c) and type-2 (d) artifacts.

evident that after high pass filtering; the high frequency artifactual event becomes more separable from rest of the noise floor and hence can be detected easily. Band pass filtering at 150-400 Hz is applied to separate type-1 and type-2 artifacts from both LFP and spikes since artifact power is sufficiently large to be detectable compared to neural signal in this particular band. The result is illustrated in Figure 4.7(c) and 4.7(d) where the artifact edges become separable once band pass filtering is performed.

In order to detect spikes, the raw data is usually band-pass filtered from 300 Hz to 5 kHz [126]. Denoted by  $x_b(n)$ ,  $x_h(n)$  and  $x_s(n)$  as the band-pass filtered, high-pass filtered and spike signals respectively and their corresponding universal threshold values are calculated by

$$T_{bp, hp, sp} = \left( \frac{\text{median}(|x_{b,h,sp}|)}{0.6745} \right) \sqrt{2 \ln N}, \quad (4.10)$$

These threshold values  $T_{bp}$ ,  $T_{hp}$  and  $T_{sp}$  with the time indices of artifactual segments (provided by artifact labeling stage 4.4.1) are used to make the decision of whether artifacts or signals (Stage 2 from Figure 4.5).

#### 4.4.3 Detection

Denote  $ID_i$  the time index for artifactual segment at decomposition level  $i$  found from the earlier stage, the condition for separation of artifact from neural signals is given by the following pseudo code

Separation of Artifacts from Signals	
If $( x_b(ID_i)  < T_{bp})$ or $( x_h(ID_i)  < T_{hp})$	
If $( x_s(ID_i)  > T_{sp})$	
$ID_i$ is not artifact index	
else	
$ID_i$ is artifact index	
end	
else	
$ID_i$ is artifact index	
end	

#### 4.4.4 Signal Reconstruction

In the final stage, in order to reconstruct the signal, at first the coefficients are thresholded once it is confirmed as artifacts from stage-3. Thus a new set of coefficients, i.e.  $A'_{10}$ , and  $D'_1, \dots, D'_{10}$  are generated. Finally, inverse stationary wavelet transform is applied to the new coefficients to restore artifact-reduced neural signals.

The choice of threshold function is very important, as it influences the amount of attenuation to the SWT coefficients. A most popular threshold-

ing function is hard threshold that has a discontinuity which may produce large variance to the reconstructed signal or in other words, output estimate is very sensitive to small changes in the input data [124]. On the other hand, there is soft threshold function that is continuous but has larger bias in the estimated signal which results in larger errors. In order to overcome the disadvantages of these two threshold functions, the non-negative garrote shrinkage function is proposed in [124] which is a nice trade-off between hard and soft threshold function and is given by

$$\delta_{G_i} = \begin{cases} x & |x| \leq T'_i \\ x - \frac{T_i'^2}{x} & |x| > T'_i. \end{cases} \quad (4.11)$$

Where  $\delta_{G_i}$  is the garrote threshold function at each decomposition level of  $i$ . This function is less sensitive to input change, lower bias and more importantly continuous. Therefore garrote threshold function is chosen for our application. An illustration of better performance using Garrote threshold function over hard threshold function while spike detection is shown in Figure 4.8.

## 4.5 Experiments

To validate the proposed algorithm, extensive testings have been performed on both real and synthesized data to facilitate both qualitative and quantitative measurements and compared with other algorithms in the literature.

The data recording protocol is described below:



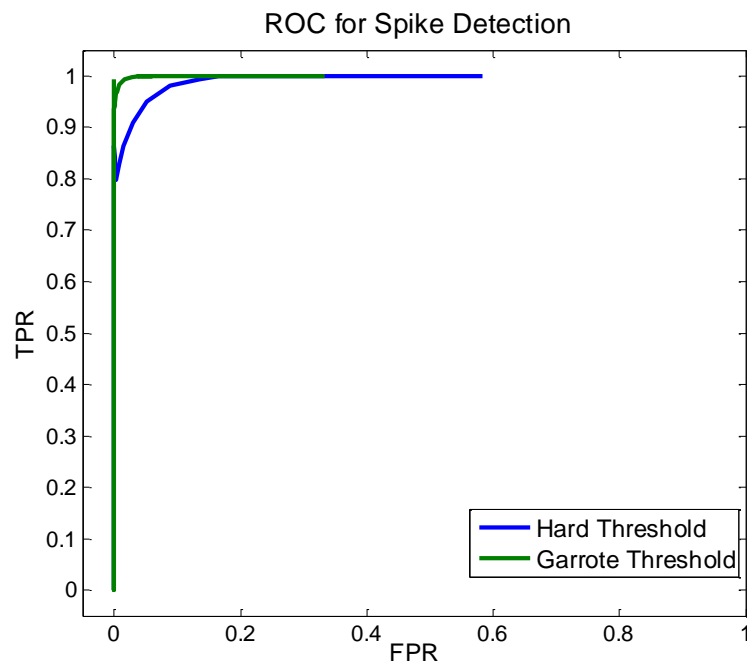


Figure 4.8: The comparison between two threshold functions: hard and garrote in terms of spike detection on the reconstructed signal where it is obvious that garrote outperforms the hard threshold.

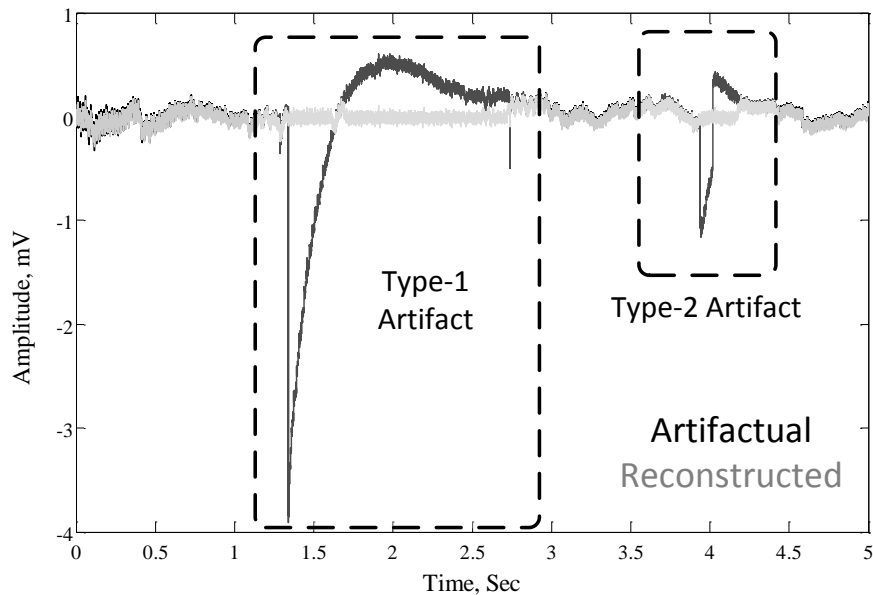


Figure 4.9: Artifact removal algorithm applied to a raw *in-vivo* data recorded from the hippocampus of a rat. The plot is the time course data where both type-1 and type-2 artifacts are present.

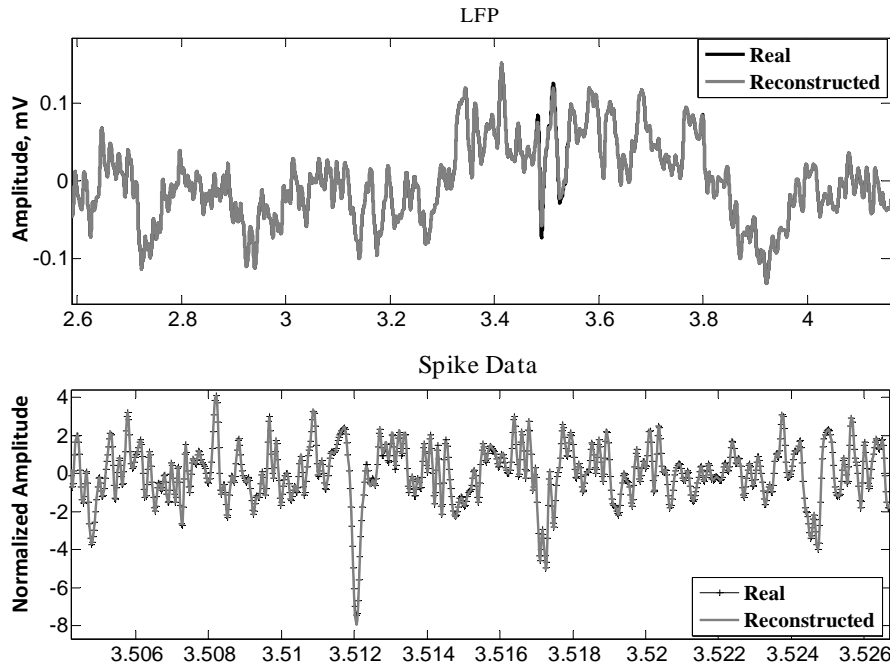


Figure 4.10: A Comparison in field potentials and spike data when there are no visually detectable artifacts (A small data segment from Figure 4.9 after low-pass filtering at 200 Hz and band-pass filtering at 300 Hz - 5 kHz are performed to get LFP and spike data respectively). The proposed algorithm nearly perfect reconstructs the original data when there is no artifact present.

Neural recording data from in-vivo preparations are provided by Edward Keefer at Plexon Inc/University of Texas Southwest Medical Institute and Victor Pikov at Huntington Medical Research Institute. For Keefers data, the protocols are similar to [48, 120], where the subjects (rats) have been anesthetized for acute experiments. CNT electrodes, microwire, and electrode array have been used in experiments and connected to Plexon OmniPlex neural data acquisition system. For Pikovs data: the 16-channel electrode arrays with a nominal geometric area of exposed electrode tips were purchased from Blackrock Microsystems. The array was chronically implanted in the sensorimotor cortex and connected to a percutaneous con-

nector mounted in the animal’s (monkey) head. The experiment protocols are in accordance with the Institutional Animal Care and in compliance with the United States Department of Agriculture (USDA) Animal Welfare Act. We have been authorized by Edward Keefer and Victor Píkov to utilize the recorded data for research and publication.

Synthesized data are prepared from in-vivo recordings. Data segments without artifacts are used as ground truth data. Labeled artifacts by a domain expert are used as artifact templates. Individual artifacts under different templates are then simulated with different amplitudes, widths and durations and finally superimposed onto the ground truth data for quantitative assessment of algorithm performance.

#### 4.5.1 Experiment on Real Data

Initially the proposed algorithm is tested on real *in-vivo* data sequences contaminated with artifacts. Then both the data sequences before and after artifact removal are plotted in the same trace of time domain (as shown in Figure 4.9.) to observe whether it has removed the artifact or not. The local field potentials and spikes are also plotted for both data sequences to observe qualitatively (shown in Figure 4.10) how much distortion it brings when there is no presence of visually detectable artifacts.

### 4.5.2 Experiment on Synthesized Data

Different artifacts have been manually identified and extracted (neural data segments contaminated with obvious visually detected artifacts) from real *in-vivo* data and categorized each into one of the mentioned four types, i.e. type-0, type-1, type-2 and type-3. Based on these extracted templates, similar artifact templates are simulated with different amplitudes and durations. An *in-vivo* neural data sequence of 100 second duration is chosen which does not contain any visually detectable artifacts and termed it as *reference signal*. Then the simulated artifacts are linearly added to the reference signal in different random positions with different amplitudes, edge widths and durations to form a data sequence that is contaminated with artifacts, it is referred to *artifactual signal*. The data synthesis process is illustrated in Figure 4.11. Finally the proposed artifact removal technique is applied on the artifactual signal and the resultant data sequence is termed as *reconstructed signal*. An example of artifact removal is shown in Figure 4.12. As mentioned that the proposed method is applied to the artifactual data to get the artifact-reduced reconstructed data which is more similar to the reference data.

#### 4.5.2.1 Efficiency Metrics

The measurement for quantitative evaluation of the algorithm is mainly two types: one is to measure how much artifact has been removed and the other one is to measure how much distortion it brings into the signal of

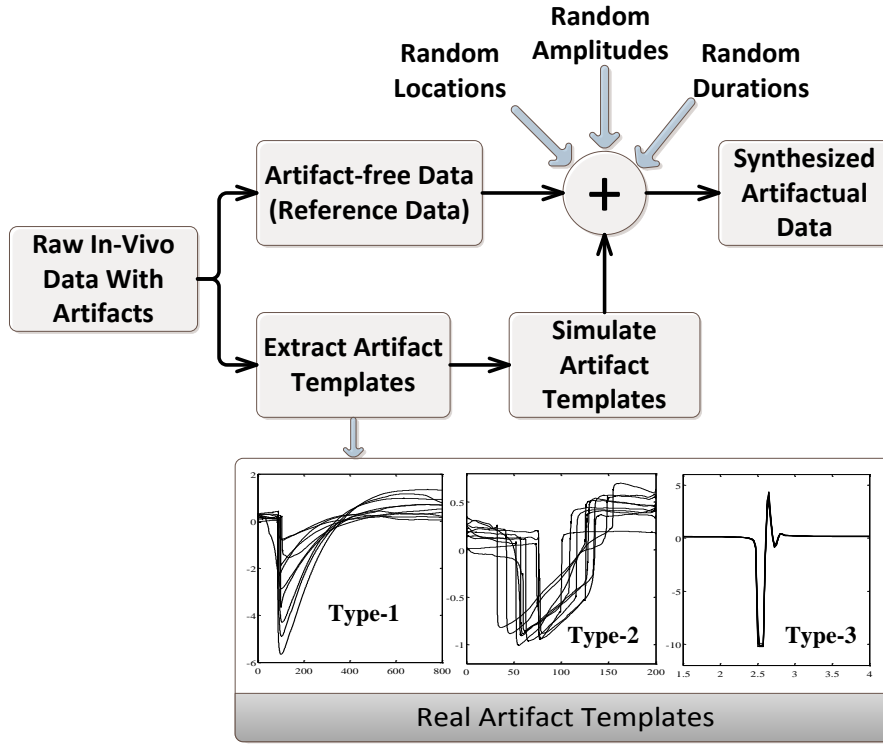


Figure 4.11: Illustration of the synthesis process to generate artifactual data.

interest. The first type of measurement includes two metrics: the amount of artifact reduction in percentage,  $\lambda$  as mentioned in [33] and the amount of increase in signal to noise ratio (SNR),  $\Delta\text{SNR}$  for different artifact amplitude or artifact SNR ( $\text{SNR}_{\text{Art}}$ ). The second type of measurement is to quantify the amount of signal distortion which includes: spectral distortion,  $P_{\text{dis}}$  as defined in [26] and root mean square error,  $\text{RMSE}$ . The former one refers to distortion in frequency domain and the later one measures the distortion in time domain. Also the efficacy of the algorithm is evaluated in terms of ROC (Receiver Operating Characteristics) plot for spike detection before and after artifact removal in comparison with the reference signal. The calculations of the mentioned metrics are discussed

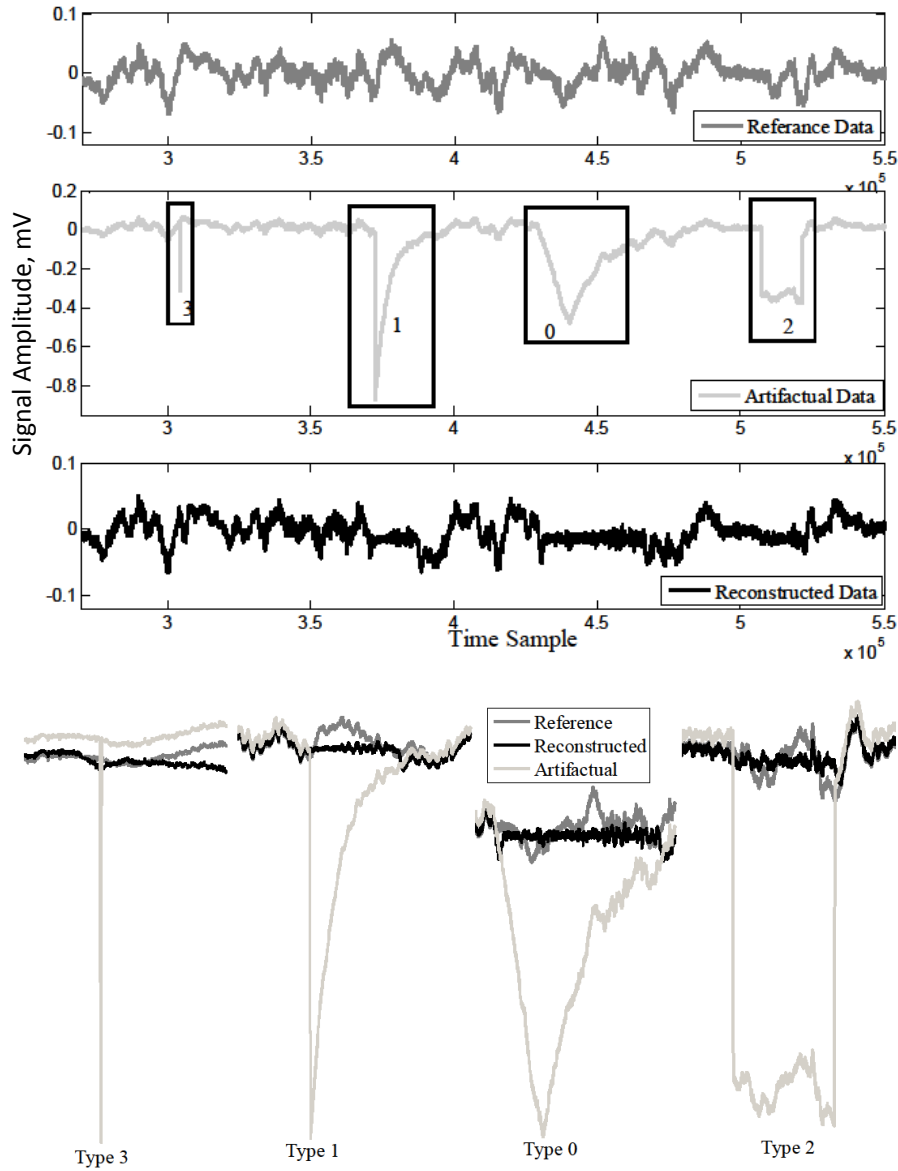


Figure 4.12: Artifact removal example by the proposed method where the artifactual signal (synthesized) is corrupted by all four types of artifact. The top plot shows the three different time course signals of reference, artifactual and reconstructed. The bottom plot is the zoom-in version of the previous plot highlighted on the artifact affected regions.

below. Note that the following calculations can only be performed on synthesized data. Assuming  $x(n)$ ,  $r(n)$  and  $r'(n)$  are the discrete time signals of length  $N$  representing reference, artifactual and reconstructed signal respectively. If the error signal before and after artifact removal are  $e_1$  and

$e_2$  respectively and calculated as follows:

$$e_1(n) = r(n) - x(n), \quad (4.12)$$

$$e_2(n) = r'(n) - x(n). \quad (4.13)$$

- $\lambda$ : The reduction in artifact,  $\lambda$  is calculated using the following formula [33]

$$\lambda = 100 \left( 1 - \frac{R_{ref} - R_{rec}}{R_{ref} - R_{art}} \right), \quad (4.14)$$

Here,  $R_{ref}$  denotes the auto-correlation of the reference signal at time lag 1,  $R_{art}$  and  $R_{rec}$  are the cross-correlation between reference signal with artifactual and reconstructed signal respectively.

- $\Delta\text{SNR}$ : Assuming the signals have zero mean, the  $\Delta\text{SNR}$  is the difference in SNR before and after artifact removal is given by the following formula [33]

$$\Delta\text{SNR} = 10 \log_{10} \left( \frac{\sigma_{ref}^2}{\sigma_{e_1}^2} \right) - 10 \log_{10} \left( \frac{\sigma_{ref}^2}{\sigma_{e_2}^2} \right), \quad (4.15)$$

where  $\sigma_{ref}^2$ ,  $\sigma_{e_1}^2$  and  $\sigma_{e_2}^2$  be the variance of reference signal, error signal before and after artifact removal respectively.

- $RMSE$ : The root mean square error,  $RMSE$  is calculated as follows:

$$RMSE = \sqrt{\frac{1}{N} \sum_{n=1}^N [e_2(n)]^2}. \quad (4.16)$$

- $P_{dis}$ : Denote  $PSD_{Ref}(f)$ ,  $PSD_{Art}(f)$  and  $PSD_{Recon}(f)$  the power spectral densities of reference signal, artifactual signal and reconstructed signal respectively, the spectral distortion  $P_{dis}$  is calculated

as follows

$$P_{dis} = \frac{\sum (PSD_{Recon}(f))^2}{\sum (PSD_{Ref}(f))^2}. \quad (4.17)$$

- $SNR_{Art}$ : Artifact SNR is calculated considering artifact as signal and reference neural signal as noise using the following formula

$$SNR_{Art} = 10 \log_{10} \left( \frac{\sigma_{e1}^2}{\sigma_{ref}^2} \right). \quad (4.18)$$

- $\Delta T_{Art}$ : It denotes the artifact duration out of total data length in percentage and calculated as follows:

$$\Delta T_{Art}(\%) = \frac{T_{Art}}{T_{Total}} \times 100, \quad (4.19)$$

where  $T_{Art}$  and  $T_{Total}$  are the time duration of artifact and whole data sequence respectively.

- **ROC Curve**: In order to evaluate the spike detection accuracy of a ROC curve, the simple amplitude threshold based detection method [127, 128, 129, 130] is used and compared with the reference signal. The true positive rate (TPR) and false positive rate (FPR) are calculated by following equations:

$$TPR = \frac{TP}{TP + FN}, \quad (4.20)$$

$$FPR = \frac{FP}{FP + TN}, \quad (4.21)$$

where  $TP$ ,  $TN$ ,  $FP$  and  $FN$  are the number of spikes detected as true positive, true negative, false positive and false negative respectively.



- $\Delta FPR(\%)$  and  $\Delta TPR(\%)$ : If  $FPR_{bef}$  and  $FPR_{aft}$  are the false positive rate before after artifact removal while  $TPR_{bef}$  and  $TPR_{aft}$  are the true positive rate before after artifact removal respectively, then the improvement in FPR,  $\Delta FPR(\%)$  and in TPR,  $\Delta TPR(\%)$  are given by

$$\Delta FPR(\%) = \frac{FPR_{bef} - FPR_{aft}}{FPR_{bef}} \times 100, \quad (4.22)$$

$$\Delta TPR(\%) = \frac{TPR_{aft} - TPR_{bef}}{TPR_{bef}} \times 100, \quad (4.23)$$

## 4.6 Results and Discussion

### 4.6.1 Effect of Filtering

In Figure 4.14, an example of a 'Receiver Operation Characteristic' (ROC) curve for spike detection is plotted where the improvement due to the inclusion of filtering along with SWT in comparison with only SWT is obvious. As mentioned in section 4.4.2, the reason for inclusion of filtering (i.e. HPF at 5 kHz and BPF at 150-400 Hz) is to preserve the spike information (i.e. spike time and shape both) and thus able to distinguish from artifacts. The decomposed wavelet coefficients are also thresholded adaptively and selectively in order to preserve the spikes according to section 4.4.4. The data corrupted with very large amplitude artifacts, especially type-3; result in a larger number of false negatives (FN). Since the presence of such

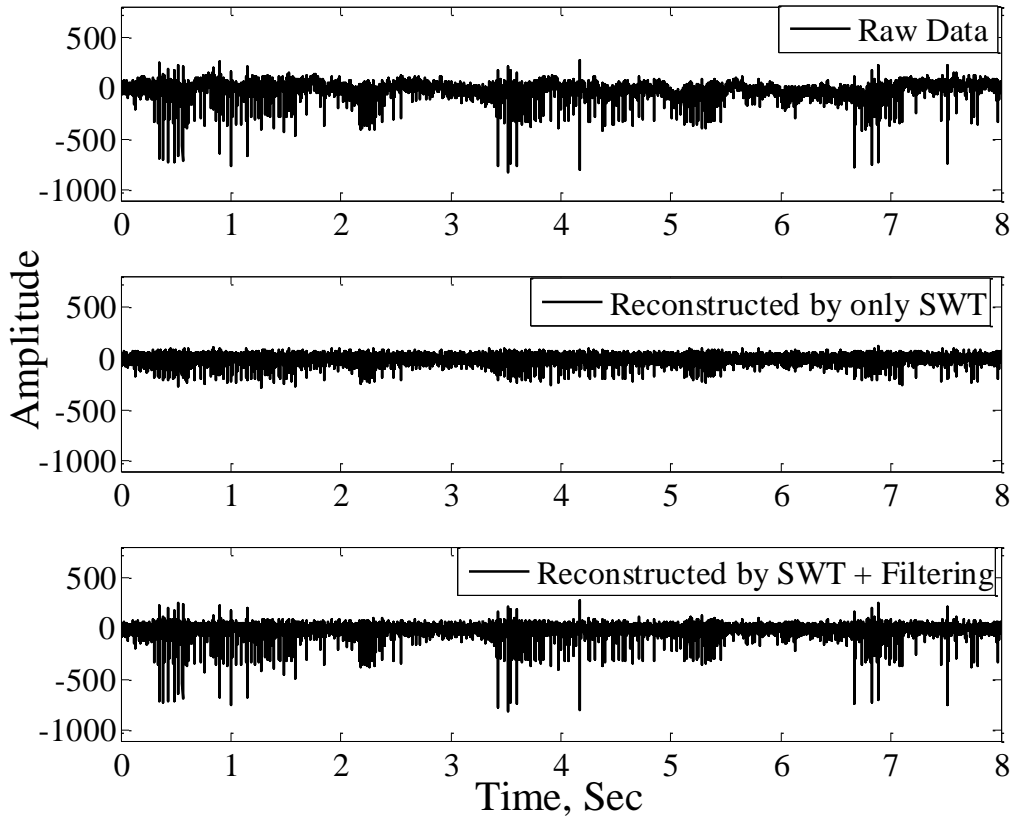


Figure 4.13: The effect of filtering along with SWT in comparison with only SWT during wavelet-denoising for artifact removal is obvious for the time course neural sequences presented in the plots for raw artifactual data with spikes, reconstructed with SWT only and reconstructed with SWT along with filtering respectively.

artifacts increases the data rms (root mean square) and so does the detection threshold which eventually misses some of the true spikes due to their relatively lower amplitude compared to artifacts. On the other hand, the presence of type-3 artifacts and edges of type-1, type-2 artifacts result in false positives (FP) during spike detection.

#### 4.6.2 Quantitative Evaluation

The simulation for quantitative evaluation is performed for 100 iterations where each iteration has random number of artifacts (ranging from 4-10)

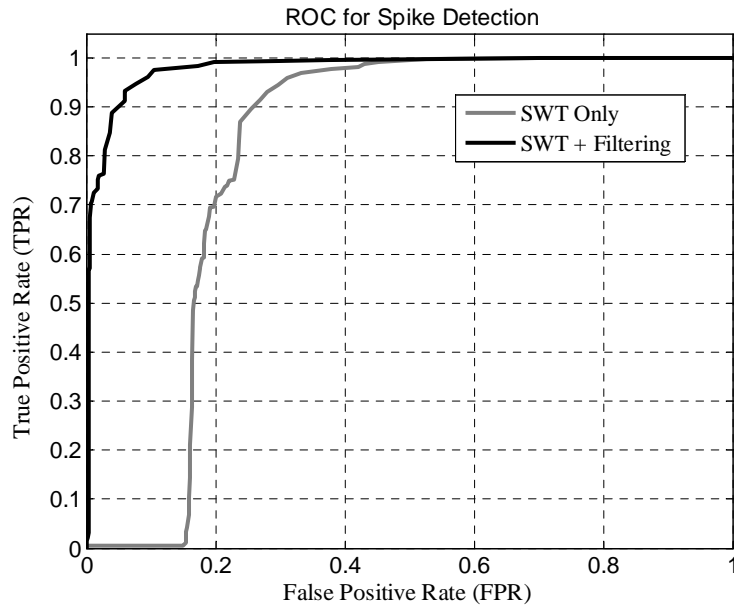


Figure 4.14: ROC curve evaluating neural spike detection accuracy to illustrate the effect of filtering in combination with SWT compared with only SWT.

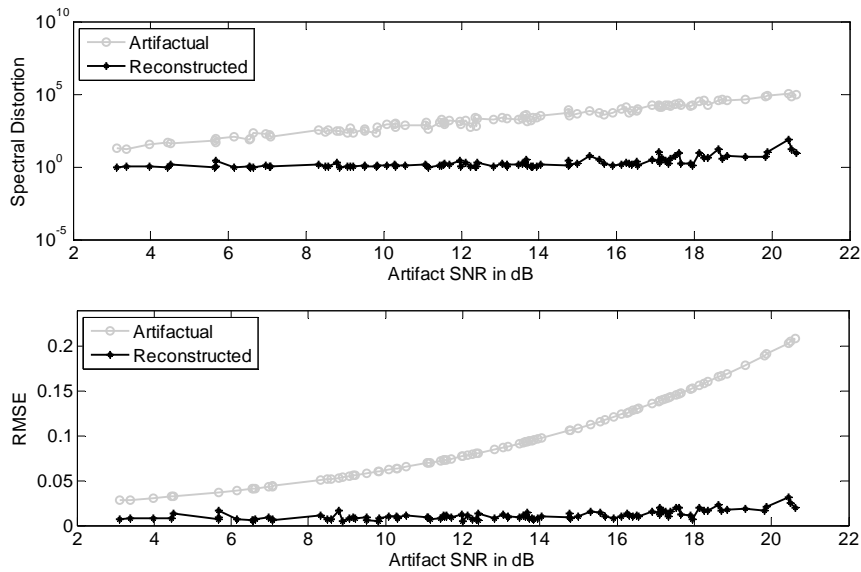


Figure 4.15: Amount of distortion to neural signal in terms of spectral distortion (top) and root mean square error, RMSE (bottom) before and after artifact removal for different artifact SNR.

with random time durations (ranging from  $200 \mu \text{ Sec}$  to  $1 \text{ Sec}$ ) placed in random locations on top of the reference signal. The artifact removal

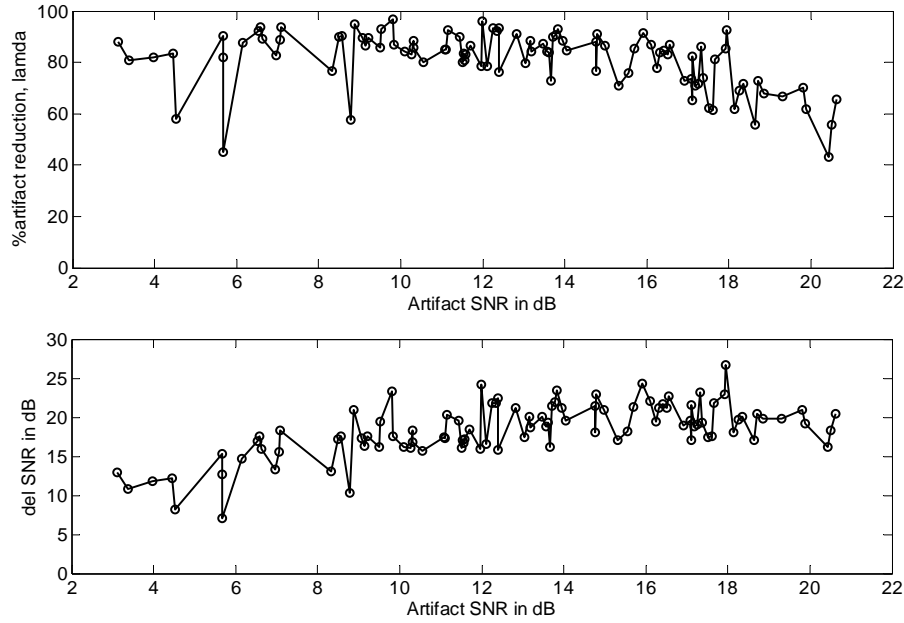


Figure 4.16: Amount of artifact removal in terms of Lambda,  $\lambda$  (top) and amount of SNR improvement,  $\Delta\text{SNR}$  (bottom) for different artifact SNR after artifact removal is performed.

performance has been evaluated at different artifact SNR,  $\text{SNR}_{\text{Art}}$  in order to observe the effects of artifact strength on the removal efficacy. Figure 4.15 shows the spectral distortion with respect to different artifact SNR for the data before and after artifact removal. The spectral distortion for artifactual data increases almost linearly in log scale as the artifact strength increase while the distortion for reconstructed data is somewhat constant up to 15 dB SNR of artifact and increases very slowly as artifact SNR further increases. The similar case can be seen for RMSE (which is temporal distortion) that the increase is logarithmically for artifactual data as artifact SNR increases while on the other hand, for reconstructed data it is more or less constant over the entire range of artifact SNR. It is worth to mention that in both cases, the improvement in terms of reduction in signal

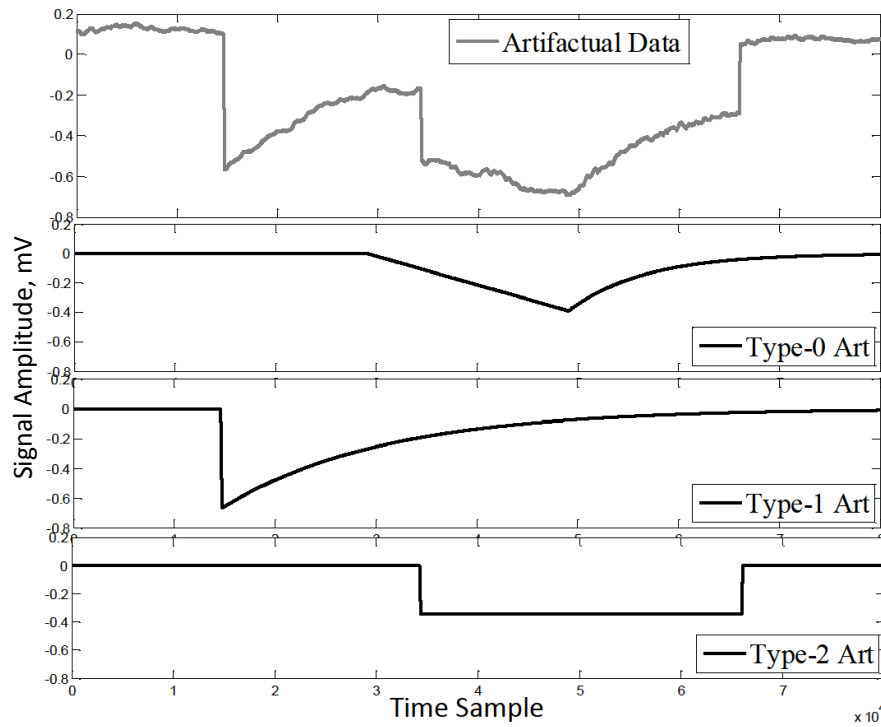


Figure 4.17: An example of overlapping of different artifact types in temporal domain in a synthesized artifactual data.

distortion is very impressive after artifact removal process is performed.

By observing the performance of artifact removal in Figure 4.16, it can be seen that, on average, approximately 80% of artifacts are removed over the wide range of artifact SNR. The reason of no particular trend in the graph may be due to the random positions of artifacts and their temporal overlapping as shown in Figure 4.17. In some iterations, in spite of artifact SNR being large, different types of artifact may overlap in temporal domain which slightly reduces the efficacy of the removal method. The increase in signal SNR with different artifact SNR follows somewhat linear trend with a positive offset probably due to the overcorrection in the artifact regions in some cases.

The mentioned four performance metrics are also evaluated with respect to the percentage of artifact duration out of the whole data segment duration in temporal domain in order to observe the algorithm's response or sensitivity to the amount of artifact duration. It is expected that, the higher the duration of artifacts (i.e. higher temporal overlapping with signals) present in a data sequence, the more difficult to remove them without distorting the signal of interest. The relevant plots are shown in Figure 4.19 and Figure 4.18 where the amount of artifact removal and signal distortions are plotted respectively with respect to the percentage artifact duration for data before and after artifact removal.

Figure 4.20 shows the average signal-to-noise-and-distortion ratio (SNDR) over the frequency band of neural signals for both artifactual and reconstructed data to illustrate the improvement in SNDR.

### 4.6.3 Qualitative Analysis

The proposed algorithm is also applied to the real *in-vivo* datasets which contain obvious artifacts. The reconstructed data after application of the removal process is plotted in time domain to compare with the real data qualitatively as previously shown in Figure 4.9.

### 4.6.4 Comparison with Other Methods

Table 4.3 summarizes the comparison between the proposed method and other available methods used for artifact removal in physiological signals

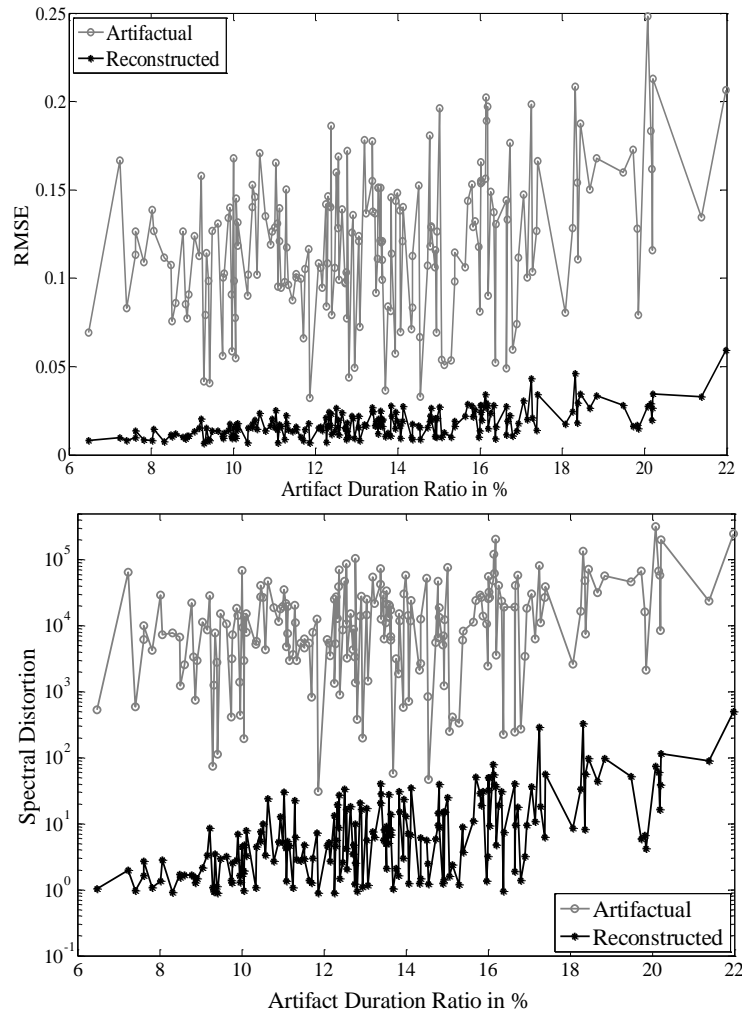


Figure 4.18: Amount of distortion to neural signal in terms of root mean square error, RMSE (top) and spectral distortion (bottom) before and after artifact removal for different artifact duration.

(e.g. EEG, fMRI, MEG, ECG, etc.). The recent review paper [82] reports the techniques used so far in artifact removal and made an extensive comparison between them. Among these techniques, the proposed algorithm is compared with wICA, wCCA, ICA, EMD-ICA and EMD-CCA (the methods are described in Figure 3.6). From the Table 4.3, it is evident that the proposed method outperforms all of these five methods most of the time in removal of the artifacts tested in this thesis. The possible rea-

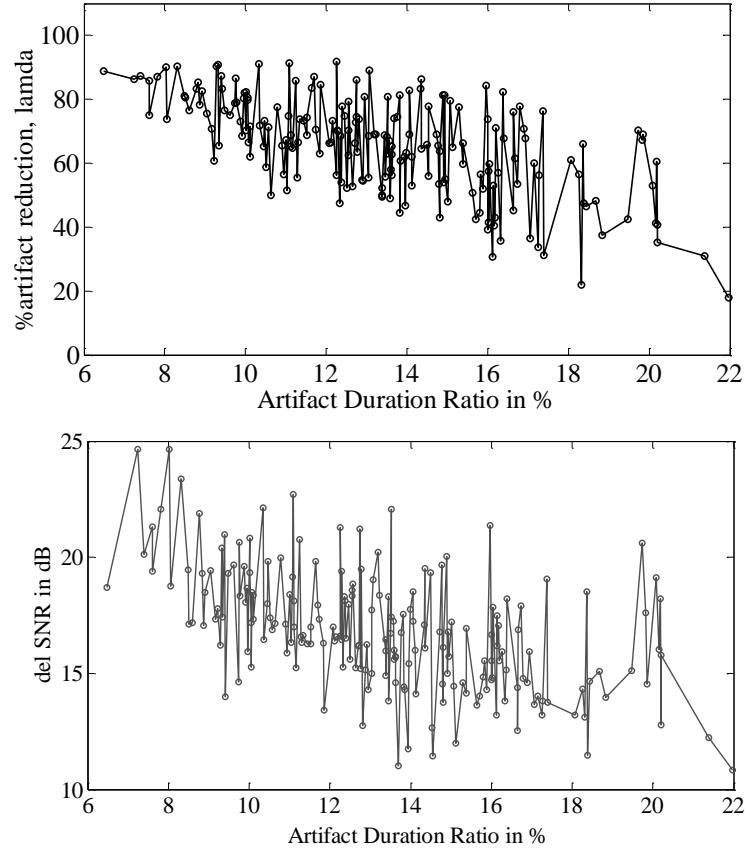


Figure 4.19: Amount of artifact removal in terms of lambda,  $\lambda$  (top) and amount of SNR improvement,  $\Delta\text{SNR}$  (bottom) for different artifact duration after artifact removal is performed.

sons are intuitive, ICA and CCA usually perform better for global artifacts and fail to identify the local ones [49, 7]. So even wICA and wCCA work satisfactory with EEG artifacts where at least few channels capture the global artifactual events, they fail in identifying the *in-vivo* artifacts which could also be local. The distortions brought by these algorithms are also higher compared with the proposed method. Since both wICA and wCCA are based on DWT, hence the algorithm induced spike-like artifacts are present after signal reconstruction (Figure 4.22). The best results among all the methods have been highlighted in blue for each  $\text{SNR}_{\text{Art}}$  level in



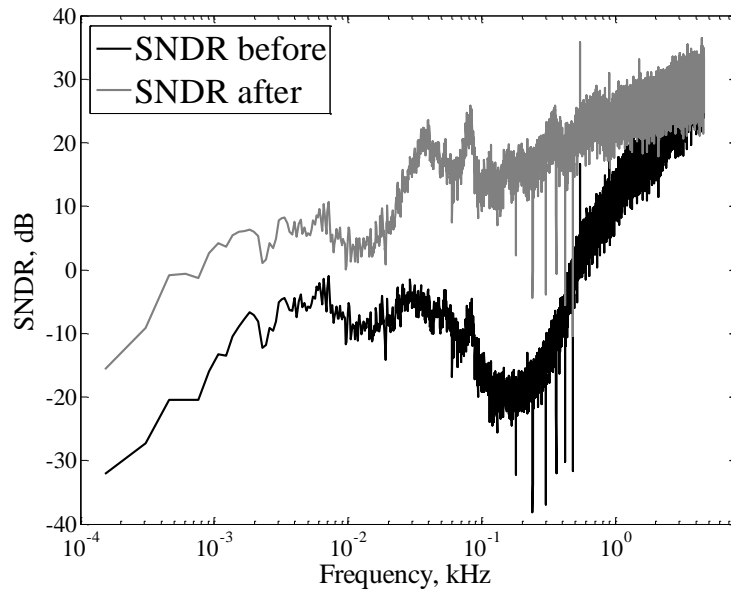


Figure 4.20: SNDR comparison between signals before (artifactual) and after (reconstructed) artifact removal. The SNDR values are averaged over 200 iterations.

Table 4.3.

Another problem with ICA and CCA related algorithms is the identification of artifacts from the independent components (ICs or CCs) which is first of all most of the time not automatic and secondly hard to identify as long as sufficient no. of recording channels is unavailable. However, wCCA seems to perform better than wICA since the sources are assumed to be maximally uncorrelated in CCA rather independent as in ICA which is a strong assumption. One important thing to note is that the performance of the algorithms do not follow any specific trend with respect to artifact SNR change, rather often it is found to be quite random. One possible reason of such random results is that because of the random locations of different artifact types, often they overlap in temporal domain, thus limits the outcome of the artifact removal method.

Table 4.4 presents the false positive rate and true positive rate for spike detection before and after artifact removal of different methods compared with the proposed one. It is also clear that the proposed method has higher TPR and lower FPR than the other available methods. The values are given in terms of improve in FPR and TPR. The improvement in FPR,  $\Delta\text{FPR}(\%)$  and in TPR,  $\Delta\text{TPR}(\%)$  suggests that the no. of false positive decreases and the no. of true positive increases after artifacts are removed. The high negative values of  $\Delta\text{FPR}(\%)$  in Table 4.4 in other methods at almost all threshold values indicate that those methods highly induce spike-like artifacts during the reconstruction process. However the proposed method significantly reduces the false positive rate except for threshold of 3 data RMS, even it is still much better than others. Regarding the improvement on TPR, the proposed method also outperforms all other methods significantly at all threshold levels. The best results have been highlighted in blue for each threshold level.

The comparative computational time required to process 1 second of in-vivo neural data is shown in Figure 4.21 where the proposed method takes the least processing time in comparison with other methods. The nearest competing time is from wCCA and the slowest of all methods are those involving EMD based methods.

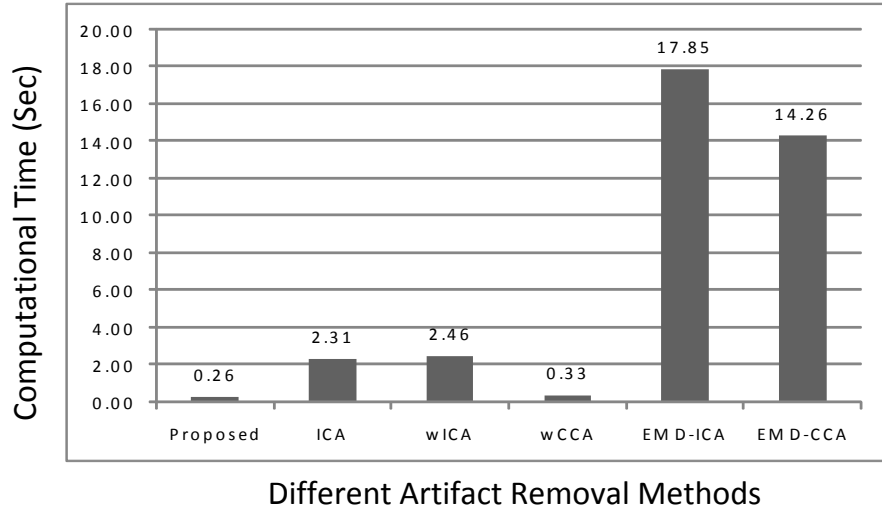


Figure 4.21: Comparison of computational latency for artifact removal from in-vivo neural recordings for processing of every 1 sec data segment.

## 4.7 Optimum Parameter Selection

We attempt to select the optimum mother wavelet and threshold parameters automatically in order to achieve best performance of the artifact removal algorithm. The parameter optimization process for our proposed algorithm includes three different steps including:

- 1) Optimization of Parameter Alpha for Best Mother Wavelet
- 2) Optimization of Parameter  $k_A$
- 3) Optimization of Parameter  $k_D$

### 4.7.1 Unsupervised Selection of Mother Wavelets

The purpose of parameterization is to optimize mother wavelet unsupervisedly in order to achieve the best performance both in terms of artifact removal and signal distortion.

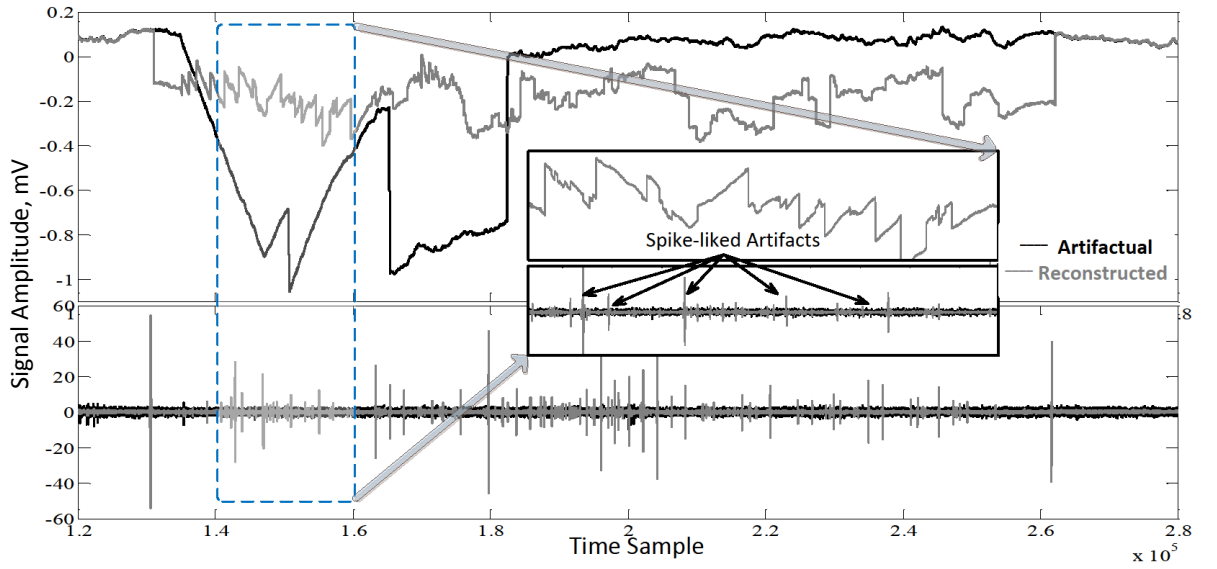


Figure 4.22: Example of spike-like artifacts produced after wICA algorithm is applied on artifactual signal. The upper trace is the superimposed representation of reconstructed signal on artifactual signal and the lower trace is the spike data after and before artifact removal derived from the upper-trace data after BPF is performed from 300 Hz to 5 kHz.

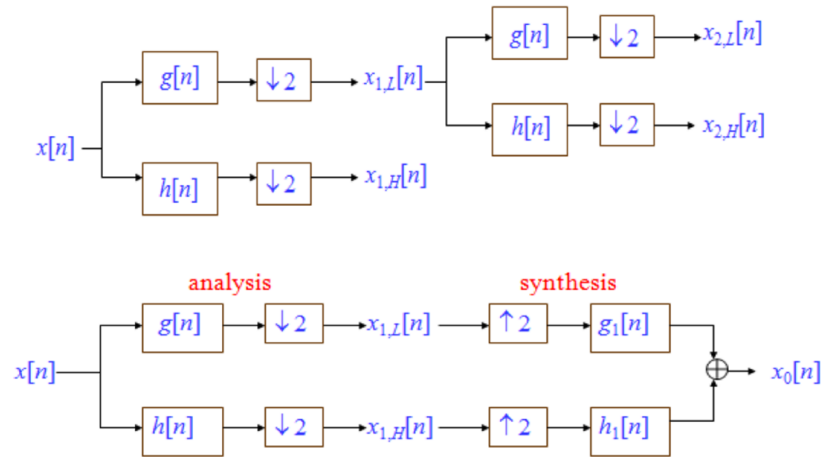


Figure 4.23: The decomposition and reconstruction structures of wavelet filters

As we know the stationary wavelet transform is a time-scale representation method that decomposes signal  $f(t)$  into basis functions of time and scale which are dilated and translated versions of a basis function  $\psi(t)$

which is called mother wavelet [78]. This  $\psi$  is defined by a low-pass filter,  $h$ ; and its corresponding high-pass filter, denoted by  $g$ ; such that in case of orthogonal wavelets,  $g$  can be calculated from  $h$  using the formula (The wavelet filter structure is shown in Figure 4.23):

$$g[n] = (-1)^{1-n}h[1-n] \quad (4.24)$$

The SWT approximation and detail coefficients are computed by following formula [131]:

$$a_{j+1}(t) = \sum_n h_j(n-t)a_j(t) \quad (4.25)$$

$$d_{j+1}(t) = \sum_n g_j(n-t)a_j(t) \quad (4.26)$$

If the design of wavelet low-pass filter,  $h$  is expressed by all filter coefficients in terms of  $L/2-1$  (where  $L$  is filter length) free parameters then it can follow unconstrained optimization, e.g. if  $L = 4$  then only a single parameter  $\alpha$  is required for the filter design [131]. The low-pass filter  $h$  can be expressed as:

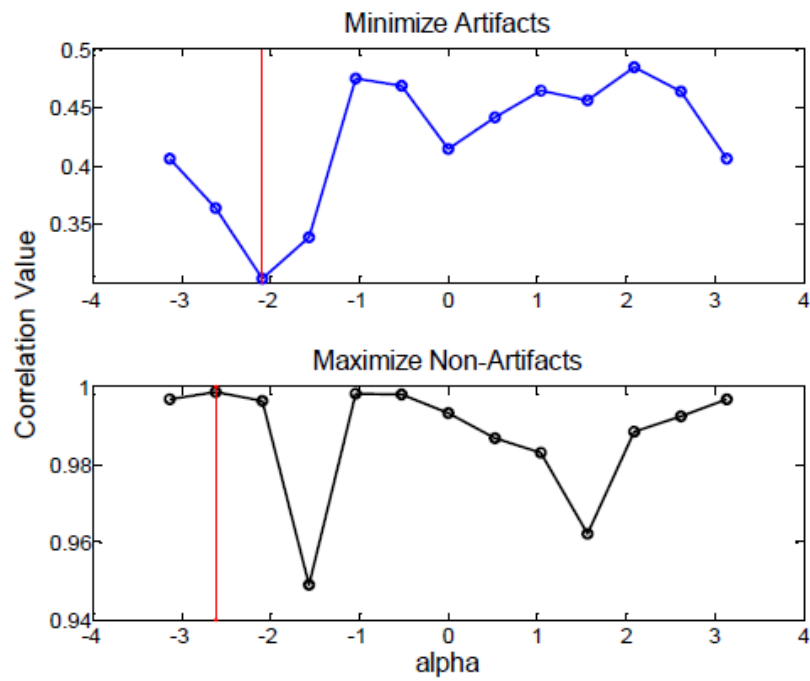
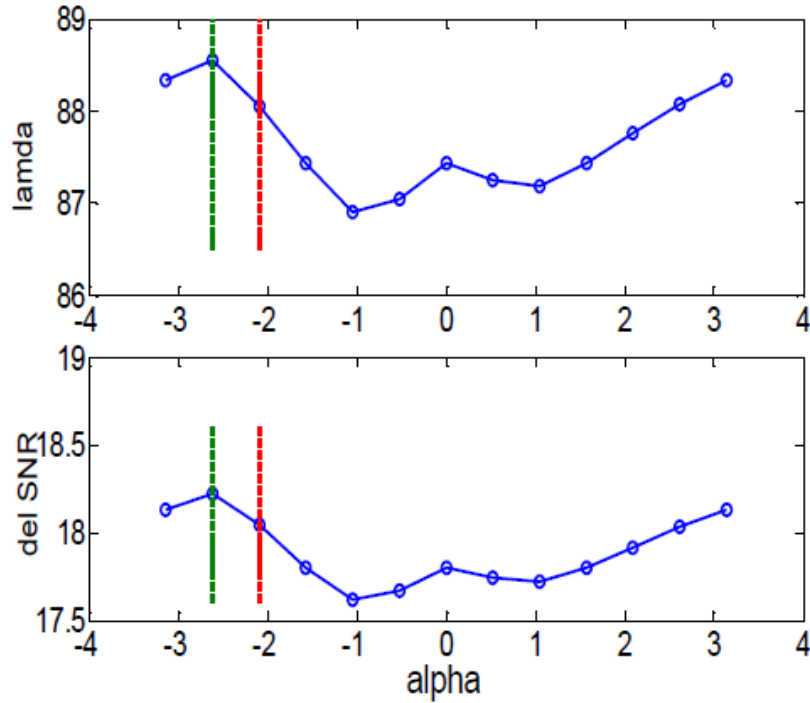
$$h[0] = [1 - \cos \alpha + \sin \alpha]/(2\sqrt[3]{2}) \quad (4.27)$$

$$h[1] = [1 + \cos \alpha + \sin \alpha]/(2\sqrt[3]{2}) \quad (4.28)$$

$$h[2] = [1 + \cos \alpha - \sin \alpha]/(2\sqrt[3]{2}) \quad (4.29)$$

$$h[3] = [1 - \cos \alpha - \sin \alpha]/(2\sqrt[3]{2}) \quad (4.30)$$

The steps for optimizing the wavelet parameter  $\alpha$  are as follows:

Figure 4.24: Correlation value vs.  $\alpha$ Figure 4.25: Performance metrics (amount of artifact removal) vs.  $\alpha$

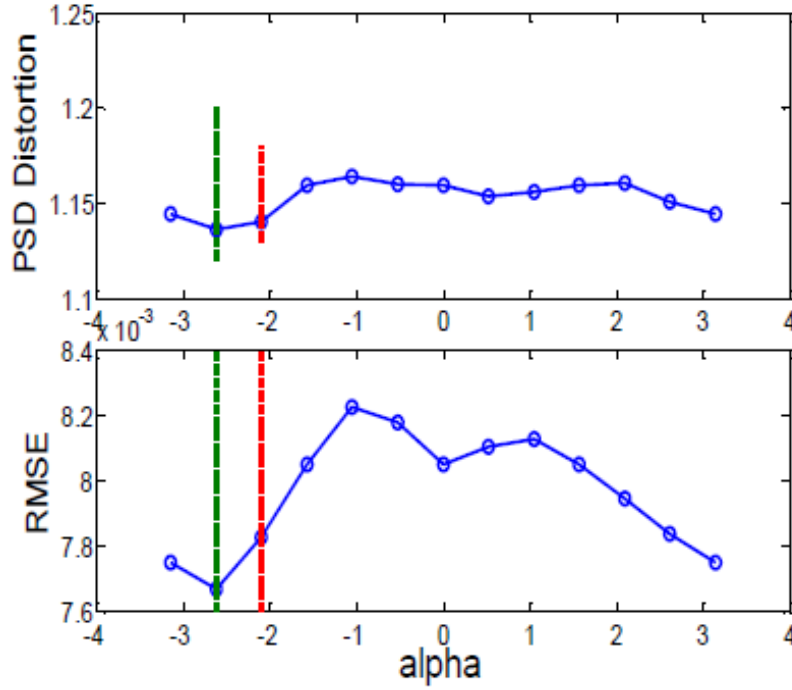


Figure 4.26: Performance metrics (amount of distortions) vs.  $\alpha$

- Sweeping  $\alpha$  from  $-\pi$  to  $+\pi$  with increment of  $\pi/6$
- Computation of the filter coefficients,  $h^\alpha$  and  $g^\alpha$  for each
- Performing proposed artifact removal process with the wavelet filters,  $h^\alpha$  and  $g^\alpha$
- Select an optimization criterion either semi-supervised
  - Measure the performance metrics and plot them against  $\alpha$ . The value of  $\alpha$  corresponds to the best performance metrics is chosen as optimal  $\alpha$ ,  $\alpha_{opt}$ . Or unsupervised as below
  - Minimize the correlation between artifactual,  $x_{art}(n)$  and reconstructed  $x_{rec}(n)$  signals only in the artifact-index regions to find

optimal  $\alpha$ ,  $\alpha_{opt1}$  Or

- Maximize the correlation between artifactual,  $x_{art}(n)$  and reconstructed  $x_{rec}(n)$  signals only in the non-artifact-index regions to find optimal  $\alpha$ ,  $\alpha_{opt2}$

The results for choosing optimum  $\alpha$  are shown in Figures 4.24, 4.25 and 4.26.

#### 4.7.2 Calculation and Optimization of Threshold Parameters

The threshold parameters  $k_A$  and  $k_D$  are chosen based on artifact removal results from few initial trial/training cycles. If we sweep both these two parameters and evaluate the corresponding artifact removal performance in terms of the correlation value between signals before and after artifact removal, then we can get a rough idea of choosing the optimal values for  $k_A$  and  $k_D$ . In order to do so, we assume that the correlations between artifactual and reconstructed signals are higher in non-artifactual regions and lower in artifact-contaminated regions.

If  $R_{XY_{Art}}$  and  $R_{XY_{Non-Art}}$  are the correlation values between artifactual and reconstructed signals for artifact-contaminated regions (i.e.  $ID_i$  is artifact index) and non-artifact-contaminated regions (i.e.  $ID_i$  is not artifact index) respectively, then the optimization problem will be as follows:

- Find  $k_A$  for maximum  $R_{XY_{Non-Art}}$  and minimum  $R_{XY_{Art}}$ .
- Find  $k_D$  for maximum  $R_{XY_{Non-Art}}$  and minimum  $R_{XY_{Art}}$ .



Now if  $k_{A_{max}}$  be the value when  $R_{XY_{Non-Art}}$  is maximum and  $k_{A_{min}}$  be the value when  $R_{XY_{Art}}$  is minimum, then the optimal value of  $k_A$  (i.e.  $k_{A_{opt}}$ ) is chosen as the average of these two values as given by following equation.

$$k_{A_{opt}} = \frac{k_{A_{max}} + k_{A_{min}}}{2} \quad (4.31)$$

Similarly the optimal value of  $k_D$ , (i.e.  $k_{D_{opt}}$ ) is calculated as follows:

$$k_{D_{opt}} = \frac{k_{D_{max}} + k_{D_{min}}}{2} \quad (4.32)$$

The value of  $m$  can be averaged over few initial trials of 1-sec data segment from the following equation:

$$m = \frac{1}{N} \sum_{j=1}^N \frac{\max(|A_{10}|_j)}{(sd(A_{10}))_j}. \quad (4.33)$$

#### 4.7.2.1 Optimization of $k_A$ and $k_D$

In order to optimize the threshold parameter  $k$ , we follow the below steps:

- Sweep parameter  $k_A$  from 0 to 1 and calculate the threshold  $T_i$  to apply for approximate coefficient,  $A_{10}$ .
- Apply the artifact removal process for each value of  $T_i$  (in other word for each value of  $k_A$ )
- Sweep parameter  $k_D$  from 1 to 5 and calculate the threshold  $T_i$  to apply for detail coefficients,  $D1 - D10$ .

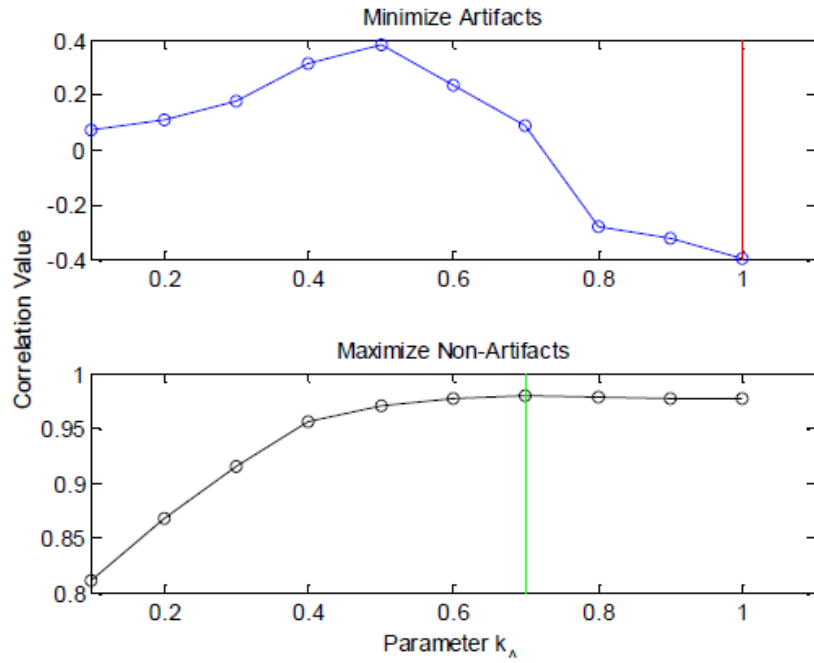


Figure 4.27: Correlation value vs.  $k_A$

- Apply the artifact removal process for each value of  $T_i$  (in other word for each value of  $k_D$ )
- Find the values of  $k_A$  and  $k_D$  correspond to the best performance metrics and hence choose the optimal  $k_{A_{opt}}$  and  $k_{D_{opt}}$

The results for choosing optimum  $k_A$  are shown in Figures 4.27 and 4.28 while for parameter  $k_D$ , the results are found in Figures 4.29 and 4.30.

## 4.8 Conclusion

In this chapter, we proposed an algorithm for artifact detection and removal which is based on the stationary wavelet transform with selected frequency bands of neural signals. The selection of frequency bands is based

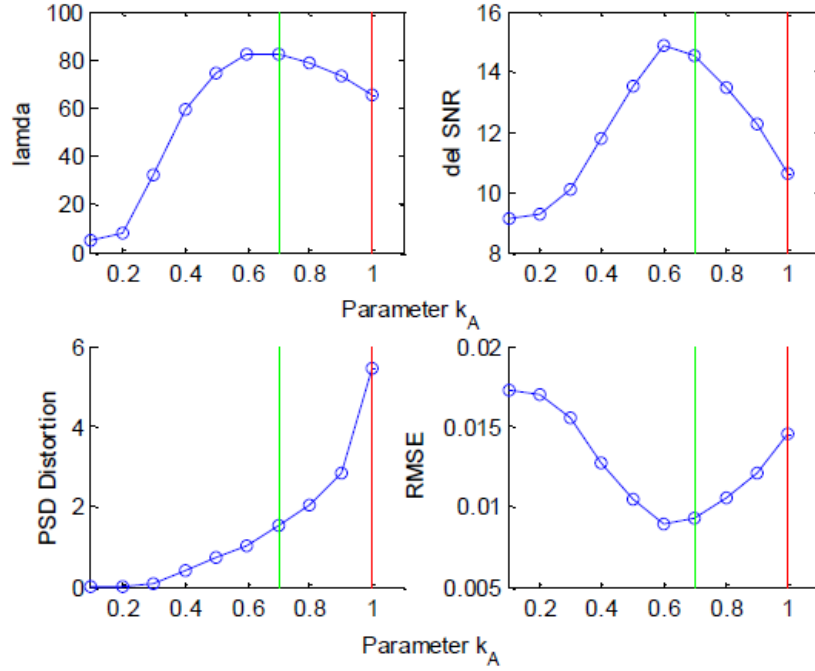


Figure 4.28: Performance metrics vs.  $k_A$

on the spectrum characteristics of in-vivo neural data. Robustness of the proposed algorithm is further improved by a modified universal-threshold value. Both real and synthesized data have been used for testing the proposed algorithm in comparison with other available algorithms. Quantitative results showed that the proposed algorithm outperforms the others in removing artifacts reliably without distorting neural signals. Therefore, this work is expected to be useful for future research on proper preprocessing of *in-vivo* neural signals. However, it also requires for further observations on experimental data to identify other artifacts (if any) and more importantly to model their sources, which is a non-trivial task. Our future work includes further optimization of the proposed algorithm and implementation for real-time applications.

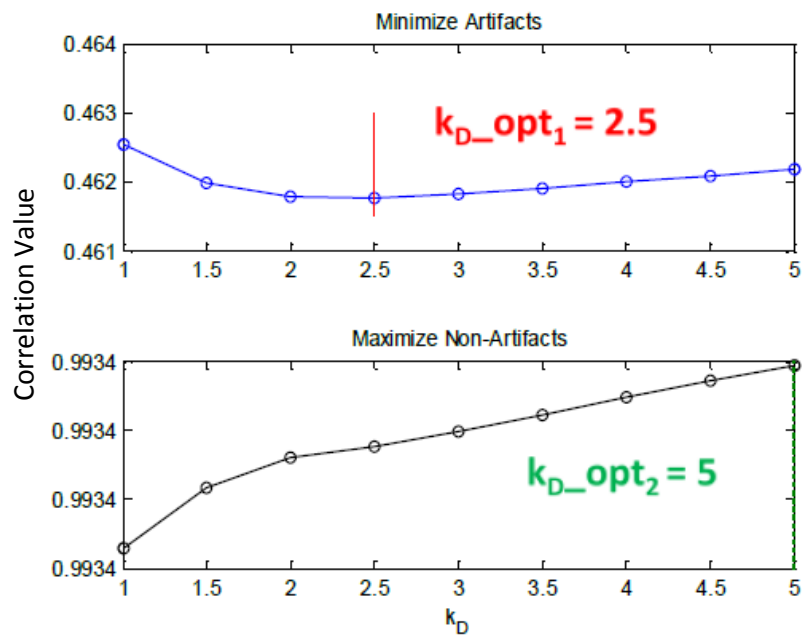
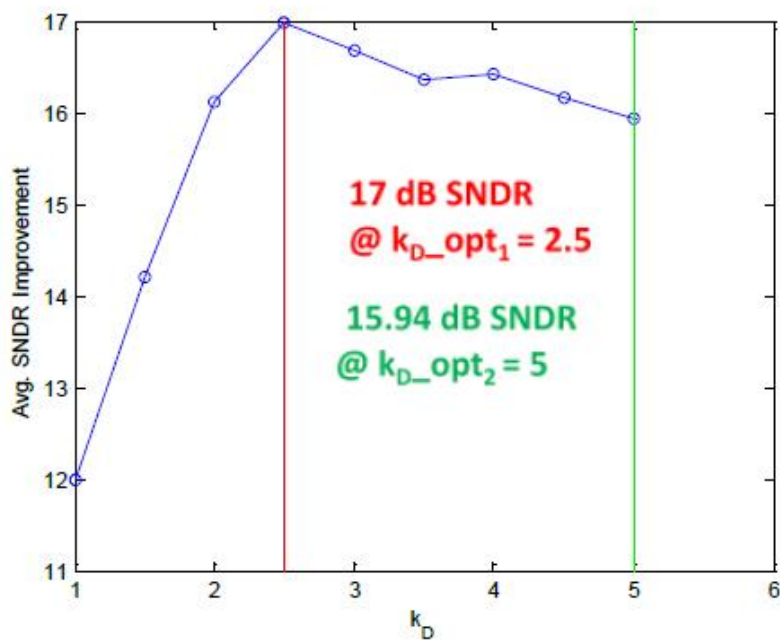
Figure 4.29: Correlation value vs.  $k_D$ Figure 4.30: Performance metric,  $SNDR$  vs.  $k_D$ .

Table 4.3: Quantitative comparison of proposed method with other methods on artifact removal for different artifact SNR ( $SNR_{Art}$ ).

$SNR_{Art}$ (dB)	Artifact Reduction, $\lambda$ , (Ideal value = 100)					
	<b>Proposed</b>	wICA	wCCA	ICA	EMD-ICA	EMD-CCA
5	58	30	45.5	46.45	-1.82	9
10	85	8	40	33.1	-3.8	3.4
15	90	-1	37	38.2	22.25	1.3
20	60	5	29	25.1	26	16
25	18.5	-3.5	8.85	17.25	-5.5	4.2
$SNR_{Art}$ (dB)	Signal SNR Improvement, $\Delta SNR$					
	<b>Proposed</b>	wICA	wCCA	ICA	EMD-ICA	EMD-CCA
5	7.5	4	0.5	6.67	0.02	0.6
10	16	6.2	5	8	0.05	2.93
15	20	5	9.8	12.3	12.4	3.05
20	18	5.5	15.2	13.9	9.5	4.58
25	17.6	5.4	13.1	13.3	3.5	5.1
$SNR_{Art}$ (dB)	Improve in Spectral Distortion					
	<b>Proposed</b>	wICA	wCCA	ICA	EMD-ICA	EMD-CCA
5	49.5	- 13.03	-4.17	-1.21	-5.35	-3.5
10	184	- 23	-7	-2.2	-10.5	-9
15	4.88e3	-25	-3.95	-2.52	-1.0	-70
20	5.34e4	-36.4	-1.92	-1.4	-9.6	-37.5
25	5.65e5	-40	16.15	5.69	-164.5	-60.48
$SNR_{Art}$ (dB)	Improve in RMSE					
	<b>Proposed</b>	wICA	wCCA	ICA	EMD-ICA	EMD-CCA
5	0.02	0.06	2.1e-3	0.023	1.6e-4	3.6e-3
10	0.044	0.082	-0.05	0.037	0.002	7e-3
15	0.102	0.10	0.07	0.085	0.08	0.016
20	0.17	0.098	0.145	0.164	0.137	0.06
25	0.32	0.114	0.28	0.243	0.031	0.12

Table 4.4: Improvement in FPR and TPR for proposed method in comparison with other methods for different data RMS thresholds.

Trh, Data RMS	Improve in Avg. FPR (%)					
	<b>Proposed</b>	wICA	wCCA	ICA	EMD-ICA	EMD-CCA
3	73.89	-1.68e3	-833.3	-241.17	-185.71	-57.14
4	95.24	-1.4e3	-699.6	-783.33	-587.5	-553.85
5	93.41	-1.28e3	-522.2	-1.02e3	-400	-1.16e3
6	90.91	-1.1e3	-474.7	-880.0	-337.5	-1.19e3

Trh, Data RMS	Improve in Avg. TPR (%)					
	<b>Proposed</b>	wICA	wCCA	ICA	EMD-ICA	EMD-CCA
3	30.63	-92.21	-98.54	-84.93	-16.16	-5.93
4	14.93	-76	-98.0	-27.45	-34.37	-10.71
5	1.5	-91.43	-97.14	-56.41	-31.82	-31.82
6	10.46	-97.35	-96.3	-85.71	-71.43	-44.83

## Chapter 5

# Artifact Reduction from Scalp

# EEG for Epilepsy Seizure

# Monitoring: Algorithm Design

This chapter introduces a method to reduce artifacts from scalp EEG recordings to facilitate seizure diagnosis/detection for epilepsy patients. The proposed method is primarily based on stationary wavelet transform and takes the spectral band of seizure activities (i.e. 0.5 - 29 Hz) into account to separate artifacts from seizures. Different artifact templates have been simulated to mimic the most commonly appeared artifacts in real EEG recordings. The algorithm is applied on three sets of synthesized data including fully simulated, semi-simulated and real data to evaluate both the artifact removal performance and seizure detection performance. The EEG features responsible for the detection of seizures from non-seizure epochs

have been found to be easily distinguishable after artifacts are removed and consequently the false alarms in seizure detection are reduced. Results from an extensive experiment with these datasets prove the efficacy of the proposed algorithm, which makes it possible to use it for artifact removal in epilepsy diagnosis as well as other applications regarding neuroscience studies.

## 5.1 Introduction

Approximately 2% of the world population suffer from epilepsy seizures. The occurrence of seizure is almost uncertain which is the main cause of disability associated with epilepsy [100]. To reduce this uncertainty, a recording system that provides early and accurate seizure detection with immediate warning is highly desired. One way to achieve that is to use long-term EEG recording to detect the characteristic EEG waveforms during seizures. The prolonged EEG recordings not only can increase the chance of detecting an ictal event (seizure) or an interictal epileptic discharge, but also useful in the diagnosis of non-epileptic paroxysmal disorders compared to a routine EEG. Unfortunately, EEG recordings are often contaminated by different forms of artifacts such as artifacts due to electrode displacement and pop-up, motion artifacts, ocular artifacts and EMG artifacts from muscle activity, which reduce the accuracy of recorded EEG signal. Besides, some artifacts may increase the false positive rate during seizure



detection while some certain types of seizures can be misdiagnosed as non-epileptic events when they are submerged/masked under artifacts. Thus, in order to correctly diagnose epilepsy, it is extremely important to remove such offending artifacts automatically, prior to seizure detection. However, automatic detection and removal of artifacts in such applications is a great challenge since the artifacts overlap with background EEG rhythms and seizure events in both temporal and spectral domain. On the other hand, the artifacts are of various types related to their origins, waveform shapes, frequency characteristics which make it difficult to differentiate them from the signal of interest.

Many traditional approaches have been proposed to remove or attenuate artifacts from recorded EEG signals [19, 22, 23, 26, 27, 33, 36, 35, 34, 38, 39, 40, 22, 23, 44, 55, 58, 59, 60, 64, 65, 66, 67, 68, 77, 84, 85, 69, 86, 87, 88, 89, 90, 91, 92, 93, 94, 95, 103, 109, 132, 133, 134, 135, 136, 137, 138]. The most widely used methods for attenuating artifacts in EEG signals are based on blind source separation such as independent component analysis (ICA) and canonical correlation analysis (CCA) [19, 33, 36, 35, 34, 38, 58, 87, 88, 89, 90, 91, 92, 103, 109, 139, 140]. The BSS-based algorithms assume that the observations are linear mixing of the sources and the number of sources is equal or less than the number of observations. Another assumption is that the sources have to be either independent for ICA based methods or maximally uncorrelated for CCA based methods. Beside these assumptions, the usefulness of BSS-based methods are affected

by some issues as follows:

- Some ictal events can only be found in few channels if it is a focal seizure.
- Some of the artifacts are localized in a single channel, resulting in failure to identify the artifact source in the cross-channel analysis.
- Detection of artifactual independent component is not automatic or semi-automatic given that the reference channel that records the artifactual source separately is available [104, 141].
- The artifactual independent component is often found to be mixed with neural signals and therefore complete rejection of such IC results in serious signal distortion. Hence, over correcting the EEG recordings.

The methods in [19, 59, 95, 97, 142, 143] rely on adaptive filtering to remove artifacts from EEG signal. These methods are applicable only when there is any reference artifact channel available. However, due to diversity of artifacts for different movements and in different surrounding environments, such reference channel is not feasible. Other filtering methods like Kalman, Wiener and Particle filters, however, do not require an extra reference channel, but they need a-priori user input to function which may not be feasible always [82]. In addition, some other limitations of the existing artifact removal methods are:

- Most of the methods remove single type of artifact and unable to handle other types e.g. ocular artifact [40, 16, 19, 36, 144, 145, 146, 141], motion artifact [51], ecg artifact [147] and muscle artifact [34, 148, 140].
- Many studies have proposed methods to remove artifacts for general purpose [65, 141, 86, 106, 92, 58, 68, 60] and they do not consider specific target application. As a result, it brings unnecessary complexity in their algorithms and also results in over-correction of data.

In this chapter, we develop an automated algorithm to remove artifacts as much as possible without distorting the signal of interests. The proposed algorithm is based on the stationary wavelet transform (SWT) and takes the spectral band of seizure activities into account to separate artifacts from seizures. The reason of choosing wavelet transform over other methods (e.g. BSS, EMD, Adaptive Filtering, etc.) is its ability to decompose single-channel EEG data into different frequency bands with high temporal resolution followed by easier denoising technique[78]. This is done with reasonable computational complexity compared with BSS or EMD and without requiring any reference channel unlike adaptive filtering. In addition, the choice of SWT (also known as Undecimated Wavelet Transform) over discrete wavelet transform (DWT) is because of the fact that SWT is translational-invariant since it involves up-sampling of the filter coefficients instead of down-sampling unlike in DWT [149]. Therefore small shifts in a signal can't cause large changes in the wavelet coefficients

and large variations in the distribution of energy in the different wavelet scales in SWT unlike in DWT and consequently denoising with DWT often results in introducing of artifacts in the signal near discontinuities during signal reconstruction [27, 123, 34].

The proposed method is evaluated for both real and simulated EEG data where both data consist of epileptic seizures and artifacts. By extensive testing, it has been shown that the proposed algorithm can reduce artifacts to an extent that can significantly increase the performance of a seizure detector/classifier, which proves its suitability to use in such EEG applications for epilepsy diagnosis.

The rest of this chapter is organized as follows. A brief introduction to EEG signals with epileptic seizures is described in Section 5.2. Section 5.4 provides the methods of data collection and synthesis. Section 5.3 describes the proposed method. In Section 5.5, formulation and analysis for performance evaluation are presented. Section 5.6 provides the simulation results and discusses about the performance of the proposed algorithm. Optimum parameter selection is mentioned in Section 5.8. Section 5.8 gives concluding remarks.

## 5.2 EEG Characteristics

EEG is the recording of the electrical activities from surface/scalp of the brain and typically described in terms of *rhythms* and *transients*. It is

Table 5.1: The frequency bands of EEG rhythms and seizure activities.

Rhythm or Transient	EEG Signal Component	Freq. Band (Hz)
Rhythm	Delta	< 4
	Theta	4 – 8
	Alpha	8 – 13
	Beta	14 – 30
	Gamma	> 30
	Mu	7.5 – 12.5
Transient	Seizure Activities	0.5 – 30

usually corrupted by different noise/interferences and artifacts. Although seizure and artifacts both are fallen into *transient* category, seizure has more rhythmic oscillation than artifacts or in other words, artifacts are more transient than seizure events.

### 5.2.1 EEG Rhythm

The rhythmic activity of EEG is divided into bands by frequency. The most common EEG rhythms are *Delta*, *Theta*, *Alpha* and *Beta* waves. Recently a relatively high frequency *Gamma* wave comes into EEG analysis in certain cases. Also *Mu* wave is considered as 'normal variant' because of its disassociation with dysfunction or disease in spite of having uncommon statistics. The corresponding frequency bands of these waves are given in Table. 5.1.

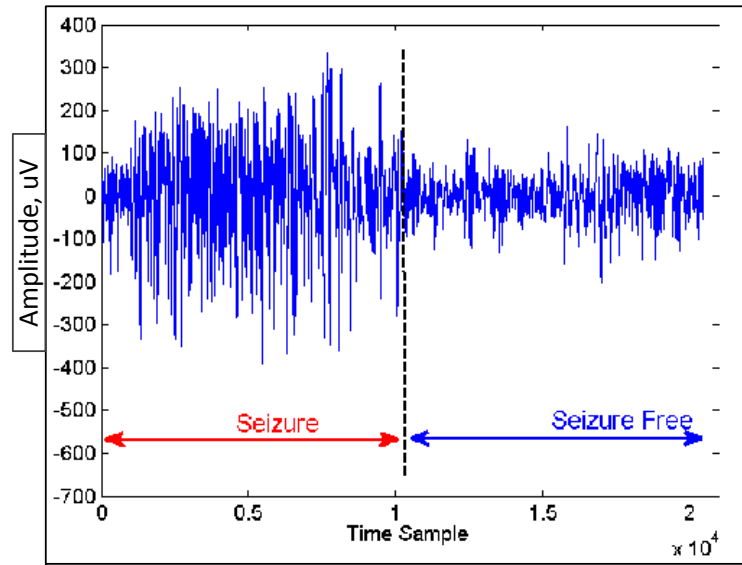


Figure 5.1: An example of real seizure segment marked by the epilepsy specialist from MIT-CHB database.

### 5.2.2 Epileptic Seizures

Epileptic seizure is a recurrent, unprovoked, brief event of abnormal or excessive synchronous activity in the brain which may last from few seconds to few minutes [100]. The waveform pattern of epileptic seizures differ from seizure type to type, even may differ from patient to patient of same seizure type. The most familiar epileptic seizure pattern is the spike-and-wave oscillation. In general, the seizure event is characterized by its rhythmicity, waveform morphology and evolution of both amplitude and frequency over time. The frequency band of most of the seizure types lies between 0.5 Hz and 29 Hz [150, 151]. Although some recent literatures report the presence of high-frequency oscillation (HFO: band 80 - 200 Hz) and fast ripple (200 - 600 Hz) as an indication of seizure characteristics and detection [152, 153], however such signal components are difficult to record/sample with the

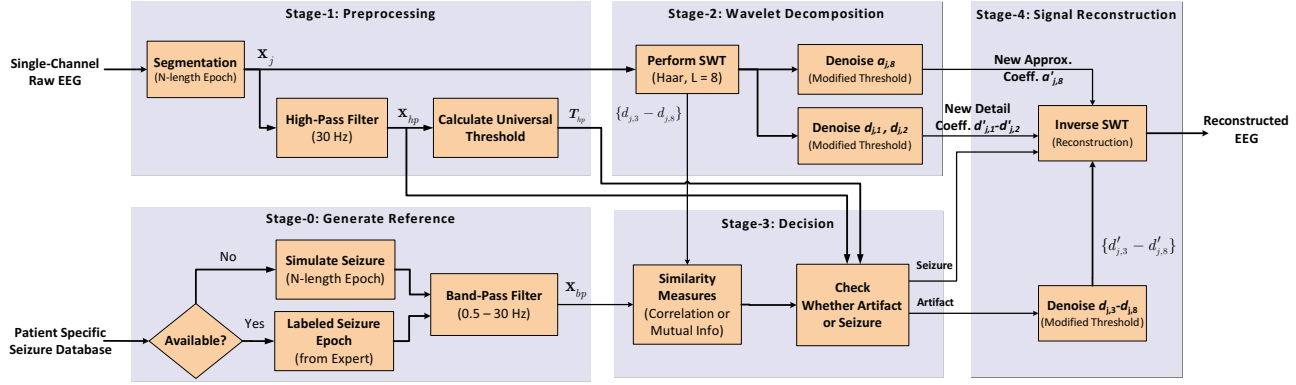


Figure 5.2: The overall process flow of the proposed method.

typical routine scalp-EEG setting which has a sampling frequency of the order of few hundred Hz (e.g. usually 256 Hz). In this thesis, since we only consider the sampling frequency no more than 512 Hz in routine scalp EEG, therefore such HFO and fast ripples are ignored. An example of epileptic seizure marked by clinician is shown in Figure 5.1.

### 5.3 Proposed Algorithm

The first priority of the proposed artifact removal algorithm is not to distort any seizure waveforms at any cost and then (i.e. next priority) to remove artifacts as much as possible. The proposed algorithm has total four stages out of which stage-0, i.e. *reference generation* can be obtained offline prior to the incoming of EEG data. A block diagram for process flow of the whole method is shown in Figure 5.2. The rest of the stages can only function during the incoming stream of data. The description of the stages are given below.

### 5.3.1 Reference Generation

This stage generates a reference seizure epoch of length  $N$  (i.e. duration of  $N/F_s$  second) either from an available seizure-type specific labeled seizure database or can be obtained from simulating a particular seizure-type epoch by simple mathematical model. For example, the neonatal seizure events can be simulated from a free online database available at [154]. This EEG simulator has mainly two parts: a background simulator and a seizure simulator [75, 76]. On the other hand, if a seizure-type specific database (epilepsy patient database) is available where the seizure events are labeled by the clinicians, then we can also use such database to generate the reference seizure to be used for subsequent stages. However, some preprocessing steps are necessary before starting to use such database. One of them is to band-pass filter the raw database from 0.5 Hz to 30 Hz to eliminate other signal components and to amplify the desired seizure activities (since frequency band of seizure is 0.5~29 Hz [150, 151]). Let  $x_{bp}$  be the bandpass-filtered epoch which will be utilized in stage-3 for similarity check.

### 5.3.2 Preprocessing

To begin with, let  $x_{\text{raw}}(n)$  denote the sampled raw EEG signal which is sampled at  $F_s$  Hz where  $n = \{0, 1, 2, \dots\}$  is the discrete-time index. We assume that the power-line interference of 50/60 Hz and the baseline of raw EEG have already been removed prior to this preprocessing stage. In the preprocessing, the incoming signal is firstly divided into *non-overlapping*



epochs with size of  $N$ . Then, the  $j$ th epoch ( $j \geq 1$ ) is given by

$$x_j = \begin{bmatrix} x_{\text{raw}}(jN - 1) \\ x_{\text{raw}}(jN - 2) \\ \vdots \\ x_{\text{raw}}(jN - N) \end{bmatrix} \quad (5.1)$$

Note that the choice of epoch duration plays an important role in both amount of artifact removal and amount of distortion made to the signal of interest (i.e. seizure events)<sup>1</sup>. If  $N$  is too low (e.g.  $\frac{N}{F_s} < 1$  sec.), then such short duration epoch may not represent seizure waveform properly (the typical duration of seizure event may be several seconds in general) and likely to be confused with artifact waveform (artifacts tend to be more transient than seizure). When  $N$  is too high (e.g.  $\frac{N}{F_s} > 5$  sec.), then there is high chance that lot of artifacts will be missed to be detected and hence will lower the amount of artifact removal. In our algorithm, we have found  $\frac{N}{F_s}$  as 3-sec to be optimum after trying different values empirically <sup>2</sup>


After segmentation, each epoch is passed through a high-pass filter of

---

<sup>1</sup>In addition, in case of automated seizure detection method to work after our proposed algorithm is applied, the value of  $N$  will determine the minimum time delay for seizure detection after its onset. This epoch by epoch processing will allow almost no distortion to signal of interest with the penalty of less amount of artifacts to be removed.

<sup>2</sup>although EEG signal is non-stationary but it can be considered as stationary for shorter duration epochs (e.g. 1 sec). Therefore for each of such epoch, the statistical properties of time-frequency representation achieved by SWT can be considered as stationary too. Now, sometimes there are some slow artifacts (e.g. ocular or movement artifacts) that last for  $> 1$  sec, e.g. 2-3 sec. So in order to capture the full duration of artifacts the epoch size may be required to more than 1 sec, i.e. 2 or 3 sec. Again, if the epoch size is too large (e.g.  $> 3$  sec), then the stationary assumption of EEG will no longer valid, and consequently brings unavoidable errors in detection followed by removal of artifacts. Another point to note that, in order for automated seizure detection to work in real-time processing of epilepsy data, the epoch size cannot be too long; otherwise it would create non-acceptable amount of delay in seizure detection applications.

Table 5.2: The frequency bands of wavelet coefficients after performing level-8 SWT on the raw EEG data which has a typical sampling frequency of 256 Hz. Coefficients that correspond to the seizure activities (0.5 Hz  $\sim$  30 Hz) are from  $d_3$  to  $d_8$ .

SWT Coeff.	Fs (Hz)	$D_1$	$D_2$	$D_3$	$D_4$	$D_5$	$D_6$	$D_7$	$D_8$	$A_8$
Freq. Band (Hz)	256	64 – 128	32 – 64	16 – 32	8 – 16	4 – 8	2 – 4	1 – 2	0.5 – 1	0 – 0.5
Signal Component										

30 Hz to obtain signals which likely to have least seizure information<sup>3</sup> but contain high frequency artifacts and gamma waves. Then, for every filtered epoch  $_{hp}$  its corresponding universal threshold [34] is calculated. The reason, computation and use of such threshold will be discussed in stage-3. Finally, both the high-pass filtered epoch and threshold value are passed to stage-3 for double check to decide whether an epoch is artifactual or seizure.

### 5.3.3 Wavelet decomposition

Wavelet decomposition and subsequently removing unwanted artifacts by applying threshold is a familiar denoising process in biomedical signals [123]. Usually, the denoising process refers to removing high frequency noise by thresholding the detail coefficients after wavelet decomposition. However, in this thesis, by using the term denoising, we refer to removing artifactual components from neural signals in the wavelet domain, irrespective of whether it is high-frequency or low-frequency artifacts. The objective of this stage is to decompose and analyze the raw epoch with a

<sup>3</sup>This is because seizure activities lie between 0.5-29 Hz band [150, 151].

reasonable time-scale resolution in wavelet domain for possible identification of artifactual components in the later stage. To this end, stationary wavelet transform is performed on the epochs  $\{x_j\}_{j \geq 1}$  with level-8 decomposition by *Haar* as basis wavelet which results in final approximate  $a_{j,8}$  and detail coefficients  $d_{j,1}, d_{j,2}, \dots, d_{j,8}$ . Although there are many types of wavelet transform (e.g. DWT, CWT, SWT, etc.), we chose SWT for its advantage of being translational invariant [123]. The choice for level of decomposition is mainly inspired from the bandwidth of EEG signal (i.e. 0.05 - 128 Hz) and dominant frequency band of seizure activities (i.e. 0.5 - 29 Hz) in order to have enough number of frequency sub-bands to make decisions on where to denoise carefully and where not. Figure 5.2 shows the frequency sub-bands of the decomposed detail coefficients and the final-stage approximate coefficient after 8-level SWT is performed on the raw EEG data. It is clear that  $\{d_{j,3}, \dots, d_{j,8}\}$  correspond to the seizure frequency band and hence during denoising process, we need to be very careful to handle these coefficients. The other three coefficients, i.e.  $d_{j,1}$ ,  $d_{j,2}$  and  $a_{j,8}$  can be denoised by applying the modified universal threshold directly without requiring the decision stage.

#### 5.3.4 Denoising

We use non-negative *garrote shrinkage function* during denoising since it has some appealing properties of being less sensitive to input change, having lower bias and being continuous [124]. This is a nice trade-off between soft

Table 5.3: Pseudo code for the separation of seizures from artifacts. The decision is made by the similarity based thresholding.

Decision Making	Remarks/Comment
$If  C_i  \geq T_{C_{high}}$ $k_i = 3$	Don't denoise the epoch
$Else if T_{C_{low}} \leq  C_i  \leq T_{C_{high}}$ $if  x_{hp}  > T_{hp}$ $k_i = 1$ $Else$ $k_i = 1.5$	Denoise carefully
$Else$ $k_i = 1$ $End$	Fully denoise

and hard threshold function in terms of amount of artifact removal and signal distortion<sup>4</sup> and is given by

$$g(j, \ell) = \begin{cases} d_{i,j} & |d_{j,\ell}| \leq t_{j,\ell} \\ \frac{t_{j,\ell}^2}{d_{j,\ell}} & |d_{j,\ell}| > t_{j,\ell}. \end{cases} \quad (5.2)$$

where  $g(j, \ell)$  is the garrote threshold function at each decomposition level of  $\ell$  for epoch  $j$ , and  $t_{j,\ell}$  denotes the threshold value. To denoise the critical coefficients  $\{d_{j,3}, \dots, d_{j,8}\}$ , we have used modified universal threshold reported by [7]

$$t'_{j,\ell} = K \alpha_{j,\ell} \sqrt{2 \ln N}, \quad (5.3)$$

<sup>4</sup>It is from the fact that hard threshold function is discontinuous that produces large variance (i.e. very sensitive to small changes in the input data) and hence it induces artifact itself when there is a spike-like transient artifacts. On the other hand, soft threshold has large bias in the denoised signal which results-in under-correction of artifacts. Therefore we decided to choose Garrote threshold function which is a balanced approach between hard and soft threshold and does not have the mentioned disadvantages [124].

where in (6.10)  $N$  is the length of epoch and  $\alpha_{j,\ell}$  is the estimated noise variance for  $w_{j,\ell}$  which is usually calculated by following formula [34]

$$\alpha_{j,\ell} = \frac{\text{median}(|w_{j,\ell}|)}{0.6745}. \quad (5.4)$$

where  $w_{j,\ell}$  is the wavelet coefficient at the  $\ell$ th decomposition level (i.e.  $w_{j,\ell} = a_{j,\ell}$  for approximation coefficient and  $w_{j,\ell} = D_{j,\ell}$  for detail coefficient.). The new parameter  $K$  in (6.11) comes from the empirical observations [7]. It is given as

$$K = \begin{cases} K_A \ (0 < K_A < 1) & \text{for thresholding } a_{j,8} \\ K_D \ (1 < K_D < 3) & \text{for thresholding } d_{j,\ell} \end{cases} \quad (5.5)$$

where,  $K = K_A$  is selected for thresholding approximate coefficient  $a_{j,8}$  and select  $K = K_D$  to threshold all the detail coefficients ( $d_{j,\ell}$ ,  $\ell = 1, 2, \dots, 8$ ). The tuning of parameter  $K$  is discussed in the previous Chapter-4 under sub-section 4.7.2.

### 5.3.5 Decision

The most important part of our artifact removal algorithm is stage-3, i.e. *Decision*. Depending upon this stage, the decision of whether an epoch is to be detected as artifactual or seizure is made. In addition, if there is possibility for an epoch to be both artifactual and seizure, how carefully that particular epoch to be denoised to remove artifacts, is also decided in this stage. The first step of this stage is to measure the similarity between epochs of decomposed coefficients  $\{d_{j,3}, \dots, d_{j,8}\}$  coming from stage-2 and reference epochs of  $x_{bp}$  coming from stage-0. The similarity is measured

in terms of either correlation value or mutual information. Depending on the similarity values, we choose two levels of threshold: one is upper limit  $T_{high}$  and the other one is lower limit  $T_{low}$ . Hence three conditions arise which results in three decisions: if it is high likelihood to be a seizure, then denoising is not performed on that epoch; if it is in between seizure and artifacts, then we carefully denoise the epoch and finally if it is least likely to be seizure then we fully denoise that epoch. A pseudo code for this decision stage is provided in Table 5.3. To double check apart from the similarity based decision, we also take input from the output of stage-1 where we have a high-pass filtered epoch and its threshold value. Since we assume that the epoch  $x_{hp}$  is less likely to be seizure and most likely to be artifacts if the value exceeds the calculated threshold value  $T_{hp}$ , so if any of the three decisions made from similarity based condition contradicts with this hypothesis, then to be in the safe side, the epoch is not denoised in order to preserve the seizure events all the time. However, in such case, where the epoch is actually artifactual and not seizure, but due to the decision made not to denoise the epoch, we pay the penalty of less artifact reduction.

### 5.3.6 Reconstruction

In the final stage of reconstruction, based on the decision stage, we either apply thresholding (fully or carefully) or let the coefficients  $\{d_{j,3}, \dots, d_{j,8}\}$  remain same. Finally with all the new set of coefficients obtained from

stage-2 (i.e.  $d'_{j,1}$  -  $d'_{j,2}$  and  $a'_{j,8}$ ) and the ones obtained from the first step of this stage (i.e.  $\{d'_{j,3}, \dots, d'_{j,8}\}$ ), we apply inverse SWT to reconstruct the EEG epochs. Thus a new sequence of data so called *reconstructed data* is obtained.

### 5.3.7 Overall Process Flow

Artifact removal steps are described in brief as below:

- Segmentation of single-channel raw EEG data sequence into epochs of length  $N$ .
- Performing SWT with Haar basis on the epoch to generate 8 levels of decomposed coefficients
- Denoising the final approximate coefficient ( $a_{j,8}$ ) with modified universal threshold to get a new coefficient  $a'_{j,8}$
- Generating a simulated seizure segment of length  $N$  to use as a reference. This epoch is band-pass filtered at 0.5~30 Hz.
- Selecting some specific detail coefficients (i.e.  $\{d_{j,3}, \dots, d_{j,8}\}$ ) to be eligible for correlation-based thresholding whose frequency bands correspond to the bandwidth of seizure activities (i.e. 0.5~29 Hz). Such selection is dependent on both the sampling frequency of the scalp EEG (i.e.  $F_s = 256$  Hz in this thesis) and the number of decomposition level (i.e. in our case it is 8).

- Calculating the cross-correlation coefficient or mutual information between each epoch of detail coefficients from level 3 to 8 ( $\{d_{j,3}, \dots, d_{j,8}\}$ ) and the reference seizure epoch.
- Thresholding the detail coefficients ( $\{d_{j,3}, \dots, d_{j,8}\}$ ) based on the correlation coefficients calculated with the condition that for higher/significant values of correlation, we carefully denoise the epochs to remove artifacts (i.e. higher value of threshold) and for lower/insignificant values of correlation, we perform as much thresholding as possible (i.e. lower values of threshold).
- Denoising the 1st two-levels of detail coefficients ( $d_{j,1}$  and  $d_{j,2}$ ) directly with the modified universal threshold
- Performing the inverse transform of SWT with the new set of wavelet coefficients ( $a'_{j,8}$  and  $\{d'_{j,3}, \dots, d'_{j,8}\}$ ) to reconstruct the EEG epochs with reduced artifacts.

## 5.4 Methods and Experiments

### 5.4.1 Data Collection

Real EEG recordings are downloaded from CHB-MIT Scalp EEG Database [155] which was collected from the Children's Hospital Boston. The database consists of EEG recordings from pediatric subjects with intractable seizures and the patients were monitored for up to several days. The signals are



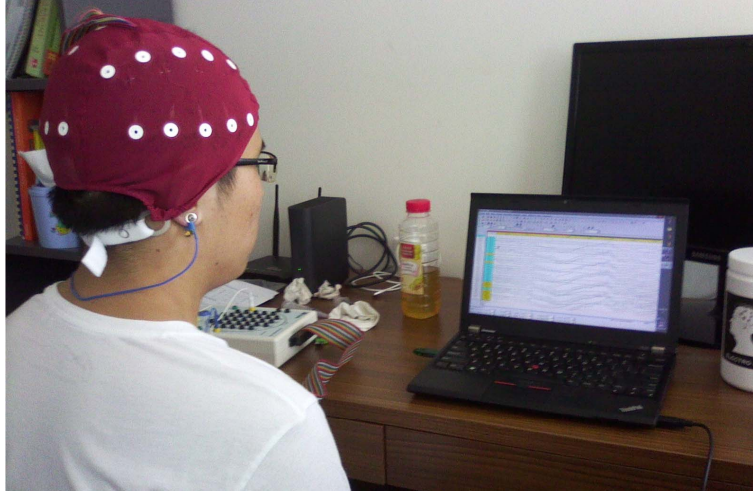


Figure 5.3: EEG experiment performed.

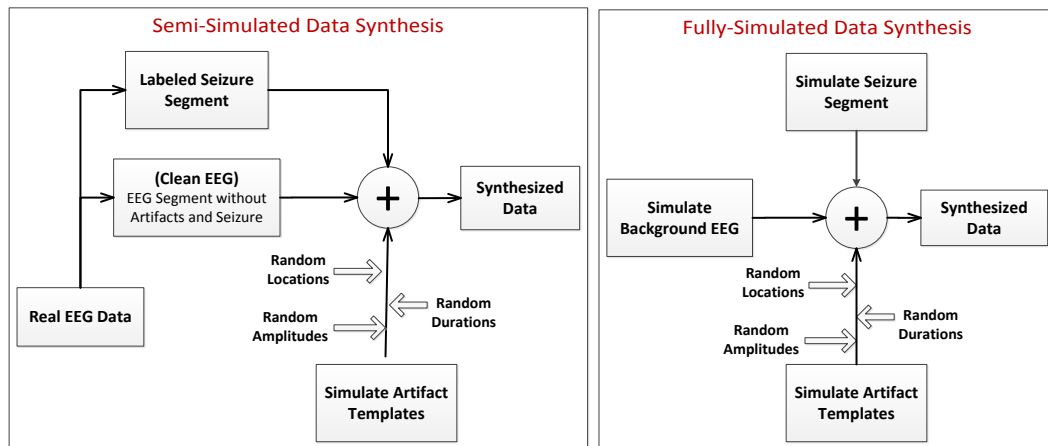


Figure 5.4: Illustration of the synthesis process to generate artifactual EEG data with seizure segment.

sampled at 256 Hz with 16-bit resolution. Apart from that, we have also performed some simple experiments to record 32-channel EEG data with a healthy subject by using the commercial Mitsar-EEG-202 recorder as shown in Figure 5.3. The subject is asked to perform specific task in order to record and characterize some common artifacts, e.g. chewing, swallowing, head movement, body movement, eye blinking, eye movement, etc. The timing of those tasks are noted down and later confirmed with the



Figure 5.5: Process flow for validation of seizure detection.

corresponding recorded signals.

## 5.4.2 Data Synthesis

### 5.4.2.1 Semi-Simulated

We have synthesized an artifact-free EEG sequence of 5 min long from real EEG collected from CHB-MIT database as ground truth and different types of simulated artifact waveforms to test our artifact removal algorithm. The process of data synthesis is shown in Figure 5.4.

### 5.4.2.2 Fully-Simulated

In this dataset, we have simulated all three data components: artifacts, seizure event and EEG background activity (i.e. EEG rhythm), and then combined them together to make artifactual EEG dataset with seizure events. The simulated EEG data have been generated according to the classical theory of Event Related Potentials (ERP) as described in [156]. The MATLAB code we used to generate such simulated EEG is available to download for free from [154].

## 5.5 Performance Evaluation

A fair performance evaluation of any artifact removal algorithm has often been an issue because of few reasons; e.g. lack of ground truth data, insufficient amount of data used, casual choice of performance metrics and so on. Therefore, it is often seen that only qualitative evaluation is available in time domain plot and/or in spectral domain in terms of PSD plot [16, 27, 157, 144]. In order to have a fair and complete evaluation, enough quantitative results are required along with the traditional qualitative approach. In addition, further analysis of later stage signal processing is required to observe the aftereffect of artifact removal. Hence this section deals on the way of performance evaluation for both artifact removal and seizure detection accuracy by quantitatively as well as in qualitative manner.

To define the quantitative metrics used for artifact removal and seizure detection, we define  $x_{\text{ref}}(n)$ ,  $x_{\text{art}}(n)$  and  $x_{\text{rec}}(n)$  as the discrete time signals of length  $L$  representing clean reference signal (artifact-free), artifactual and reconstructed signal respectively. Then, the error signal before and after artifact removal can be defined respectively as

$$e_{\text{br}}(n) = x_{\text{art}}(n) - x_{\text{ref}}(n), \quad (5.6)$$

$$e_{\text{ar}}(n) = x_{\text{rec}}(n) - x_{\text{ref}}(n). \quad (5.7)$$

In the sequel, we introduce the metrics used for artifact removal and seizure

detection in more detail.

### 5.5.1 Metrics for Artifact Removal

The performance of the proposed algorithm on the artifact removal has been evaluated both in terms of the amount of artifact reduction and the amount of distortion it brings into the signal of interest, specially to the seizure events. Several efficiency metrics have been calculated in both time and spectral domain to quantify such evaluation. In order to have fair evaluation and clear idea we also have considered the amount and duration of artifacts present in the signals. Some of the metrics (such as  $\lambda$ ,  $\Delta SNR$ ,  $RMSE$ ,  $P_{dis}$ ,  $SNR_{art}$ ,  $\Delta T_{art}$ ) have already been defined in Chapter-4 under sub-section 4.5.2. Thus rest of the metrics are described here as follows:

1.  $\Delta\text{Cor}$ : Correlation is the measure of similarity between two time series in time domain. In order to calculate the improvement in correlation  $\Delta\text{Cor}$  due to artifact removal, the following equation is used

$$\Delta\text{Cor}(\%) = \frac{c_{\text{rec}} - c_{\text{art}}}{c_{\text{art}}} \times 100 \quad (5.8)$$

where  $c_{\text{art}}$  and  $c_{\text{rec}}$  are the cross-correlation coefficients between reference signal with artifactual and reconstructed signal respectively.

2.  $\Delta\text{Coh}$ : Coherence is the measure of similarity between two time series in frequency domain and it is defined between two signals  $x(t)$  and  $y(t)$  as:

$$\Delta\text{Coh} = \frac{|\mathcal{G}_{xy}|^2}{\mathcal{G}_{xx}\mathcal{G}_{yy}}, \quad (5.9)$$

where  $|\mathcal{G}_{xy}|$  is the cross-spectral density between  $x(t)$  and  $y(t)$ ;  $\mathcal{G}_{xx}$  and  $\mathcal{G}_{yy}$  are the auto-spectral density of  $x(t)$  and  $y(t)$  respectively. Now, we assume  $\text{Coh}_{\text{bef}}$  be the coherence between reference and artifactual signal while  $\text{Coh}_{\text{aft}}$  be the coherence between reference and reconstructed signal, then the average improvement in coherence due to artifact removal denoted by  $\Delta\text{Coh}$  is calculated by following equation:

$$\Delta\text{Coh}(\%) = \frac{\text{Coh}_{\text{aft}} - \text{Coh}_{\text{bef}}}{\text{Coh}_{\text{bef}}} \times 100 \quad (5.10)$$

3. SNDR: Signal to noise and distortion ratio in frequency domain is calculated as follows:

$$\text{SNDR} = 10 \log_{10} \left( \frac{P_{\text{sig}} + P_{\text{dis}}}{P_{\text{dis}}} \right). \quad (5.11)$$

where  $P_{\text{sig}} = \sum (\mathcal{P}_{\text{ref}}(f))^2$ .

### 5.5.2 Metrics for Seizure Detection

Seizure detection/classification still is an active research problem in the epilepsy research community. There are several seizure detection methods available in the literature and none of them can claim to be robust for every patient and in every recording/surrounding environment as most of them are evaluated based on small quantity of dataset and do not consider the effects of all types of artifacts. However, since the purpose of this study is not to develop a seizure detection algorithm but to verify the performance of seizure analysis after the proposed artifact removal algorithm is applied,

therefore in this section we will show some examples of simple seizure analysis or measurement available in the literature to prove the efficacy of the artifact removal algorithm.

#### 5.5.2.1 Feature Extraction

Feature extraction is an important stage for classification in machine learning on which both classification performance and classifier complexity greatly depends. There are many ways of extracting EEG features for seizure classification that are mentioned in the literature [158, 159, 160, 161]. Most of them use the statistical features (e.g. entropy [162, 163], kurtosis, skewness, line length [158], variance, min, max, maxima count, etc.) either from directly time domain, or from both time and frequency domain or even some combined spatial (channel-wise) domain based features along with time and frequency. Some recent literatures also use wavelet domain based features to extract the desired frequency sub-bands [160, 161]. In this thesis, we use a single-dimension feature so called Sample Entropy which is described below.

- Sample Entropy: Sample entropy or SampEn which was introduced by [162], quantifies the complexity of a time series data and recently it has become an attractive measure in analyzing non-linear physiological signals [163]. Unlike other entropy or complexity measures (e.g. approximate entropy or ApEn), the advantage of SampEn is that it is resistant to the short-duration transient interferences like

spikes. It is the negative natural logarithm of an estimate of the conditional probability that if two sets of simultaneous data points of length  $m$  match point wise within a tolerance  $r$  then two sets of simultaneous data points of length  $m + 1$  also match point-wise within the tolerance  $r$  and represented as  $SampEn(m, r, N)$  where  $m$ ,  $r$  and  $N$  are the embedding dimension, tolerance and number of data points respectively [162].

We assume a time-series data epoch of length  $N = x_1, x_2, x_3, \dots, x_N$ ; a template vector of length  $m$ , such that  $X_m(i) = x_i, x_{i+1}, x_{i+2}, \dots, x_{i+m-1}$  and the distance function  $d[x_m(i), x_m(j)]$  for  $i \neq j$ . Now the number of vector pairs in template vectors of length  $m$  and  $m + 1$  having  $d[x_m(i), x_m(j)] < r$  are denoted by  $B$  and  $A$  respectively. Thus the sample entropy is defined as

$$SampEn = -\log_e\left(\frac{A}{B}\right) \quad (5.12)$$

where,  $A$  = no of template vector pairs having  $d[x_m(i), x_m(j)] < r$  of length  $m + 1$

and  $B$  = no of template vector pairs having  $d[x_m(i), x_m(j)] < r$  of length  $m$

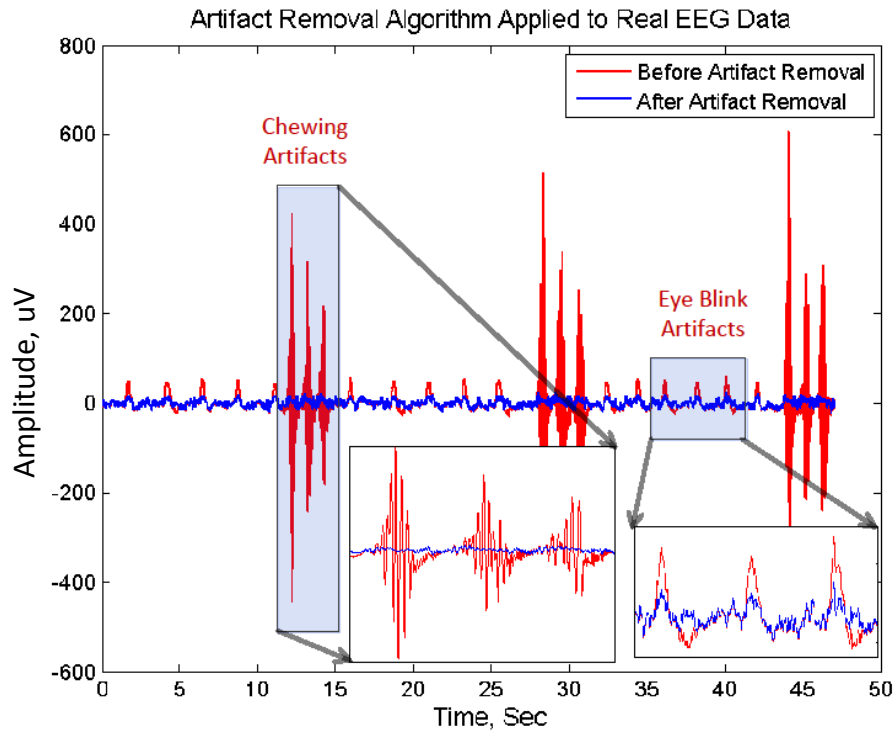


Figure 5.6: The removal result after the proposed algorithm is applied on our recorded EEG.

### 5.5.2.2 SVM Classification

Support vector machine is a supervised learning based classifier which is widely used in simple binary linear classification [164]. In our problem of classifying seizure epoch from non-seizure epoch, we have used a simple SVM classifier whose input is the extracted SampEn feature. Initially the classifier is trained with the SampEn values calculated from each epoch as training samples. The benchmark epochs are obtained from reference signal where both artifact free seizure and artifact-free non-seizure epochs have known label. Then the classifier is tested with SampEn values calculated from artifactual signal epochs. Finally the same designed classifier is again tested with the SampEn values calculated from reconstructed signal epochs.



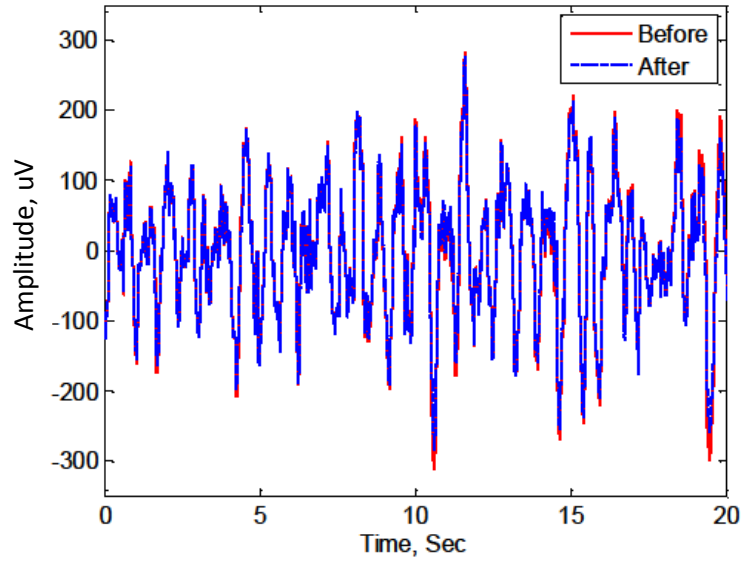


Figure 5.7: The removal result after the proposed algorithm is applied on an artifact-free seizure segment labeled and collected from MIT-CHB dataset. The reconstruction is almost perfect when there is no visible artifact.

In both cases, the no. of true positives and false positives are recorded. The process flow of seizure detection after artifact removal is shown in Figure 5.5.

- $\Delta F(\%)$ : If  $F_{\text{bef}}$  and  $F_{\text{aft}}$  denote the number of false positives for seizure classification before and after artifact removal respectively, then the improvement in number of false positives, i.e.  $\Delta F(\%)$  is given by

$$\Delta F(\%) = \frac{F_{\text{bef}} - F_{\text{aft}}}{F_{\text{bef}}} \times 100 \quad (5.13)$$

## 5.6 Results and Discussion

### 5.6.1 Qualitative Evaluation

#### 5.6.1.1 Real Data

The proposed algorithm is applied to our recorded EEG data from a healthy subject with labeled *chewing* and *eye-blink* artifacts. The artifact removal result in terms of time-domain plot is shown in Figure 5.6 for qualitative evaluation which suggests a satisfactory removal of both types of artifacts without distorting the background EEG signals in the non-artifactual region.

Another example of artifact removal result is illustrated in Figure 5.7 where there is an artifact-free seizure segment is present. It is obvious from the time-course data that almost perfect reconstruction of seizure activities occurs.

#### 5.6.1.2 Semi Simulated

An example of artifact removal algorithm applied on semi-simulated data is presented in Figure 5.10. The artifactual data sequence is made up with real seizure and real background EEG data where simulated artifacts are superimposed. It's obvious that the algorithm can't remove all of the artifacts all the time, but can reduce them significantly most of the time and more importantly can still preserve the desired seizure activities pretty

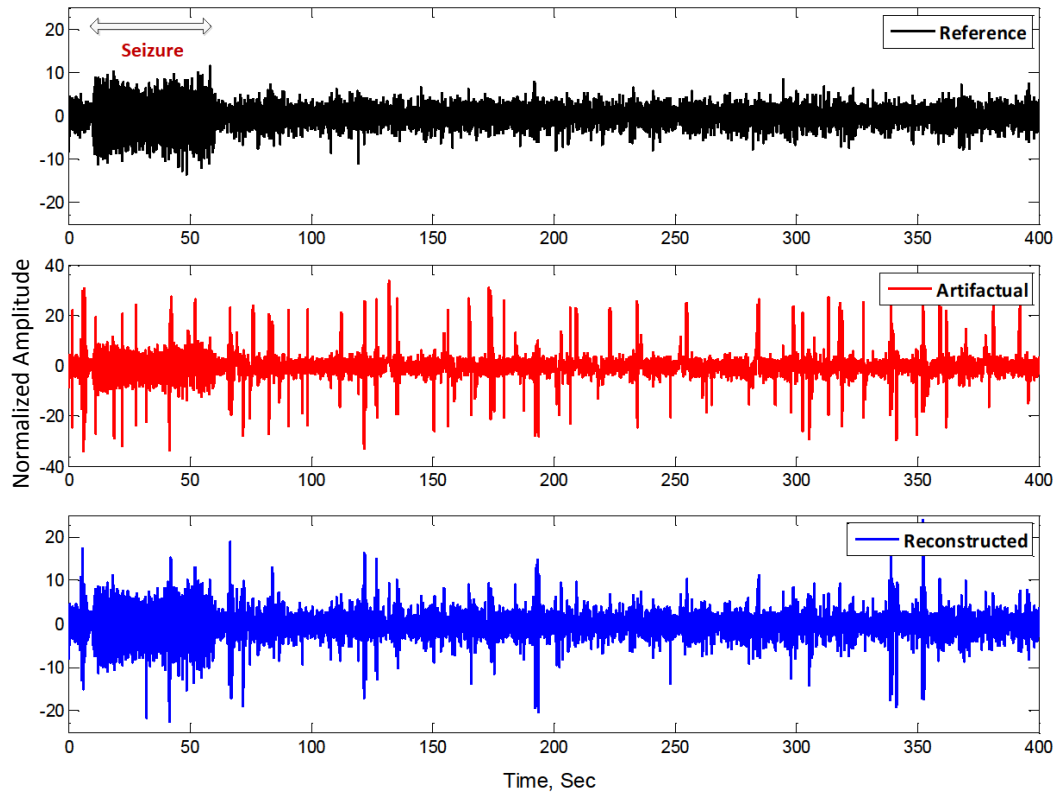


Figure 5.8: Artifact removal result applied to fully-simulated dataset-1. The plot is a time course data where all six types of artifacts are present. Note that, not all of the artifacts are removed or attenuated. The reason is that in order to preserve the seizure events, the amount of artifact reduction has been compromised.

well. This qualitative illustration in time domain data shows a better visualization to detect seizure offline after significant reduction of most of the artifacts as usually done by the clinicians.

### 5.6.1.3 Fully Simulated

The artifact removal result from a fully simulated data is illustrated in Figure 5.8 where all three signal components are simulated. The synthesized artifactual data is severely contaminated with different types of artifacts and thus makes it difficult to detect the segment of seizure activities prop-

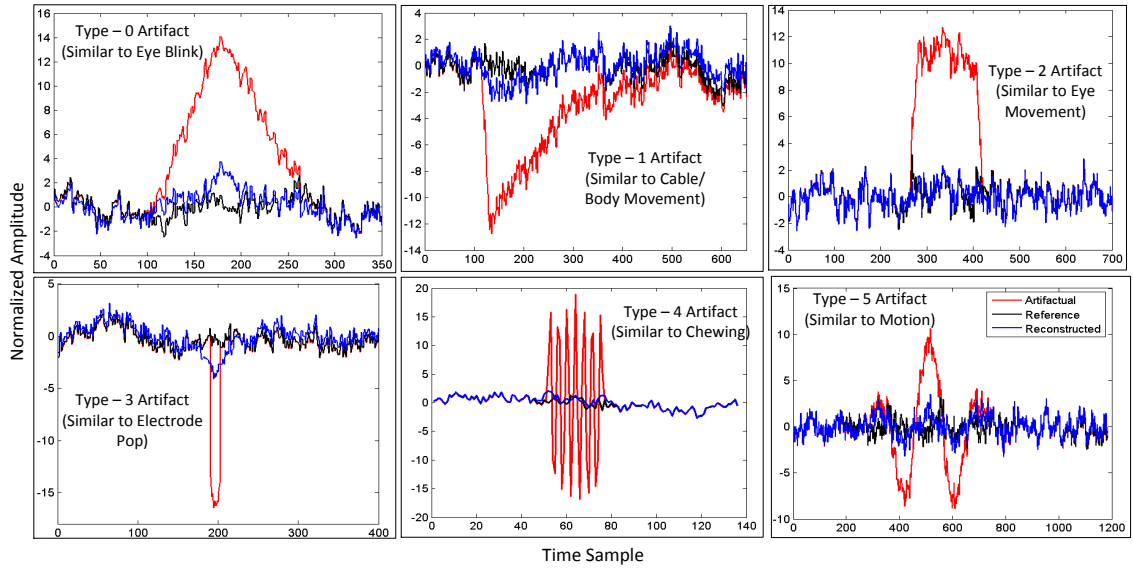


Figure 5.9: Six types of different simulated artifacts that mimicking real artifacts found in the typical scalp EEG recording environments. The application of proposed artifact removal algorithm can almost successfully remove such artifacts most of the time without distorting the background EEG signals. The black, red and blue traces denoting reference, artifactual and reconstructed simulated EEG data respectively.

erly. Once most of the artifacts are reduced, it's now easy to detect seizure segment which also increases the true positive detection.

Another example of all six types of simulated artifacts and their reduction is shown in Figure 5.9. Here each plot shows each type of artifact contaminated segment before and after artifacts are removed along with the reference artifact-free segment. This qualitative illustration proves that most of the time when there is no seizure, the algorithm can significantly reduce each type of artifacts.

### 5.6.2 Quantitative Evaluation

This sub section quantifies the results obtained both in terms of artifact removal and the consequence of artifact removal, i.e. improvement in seizure

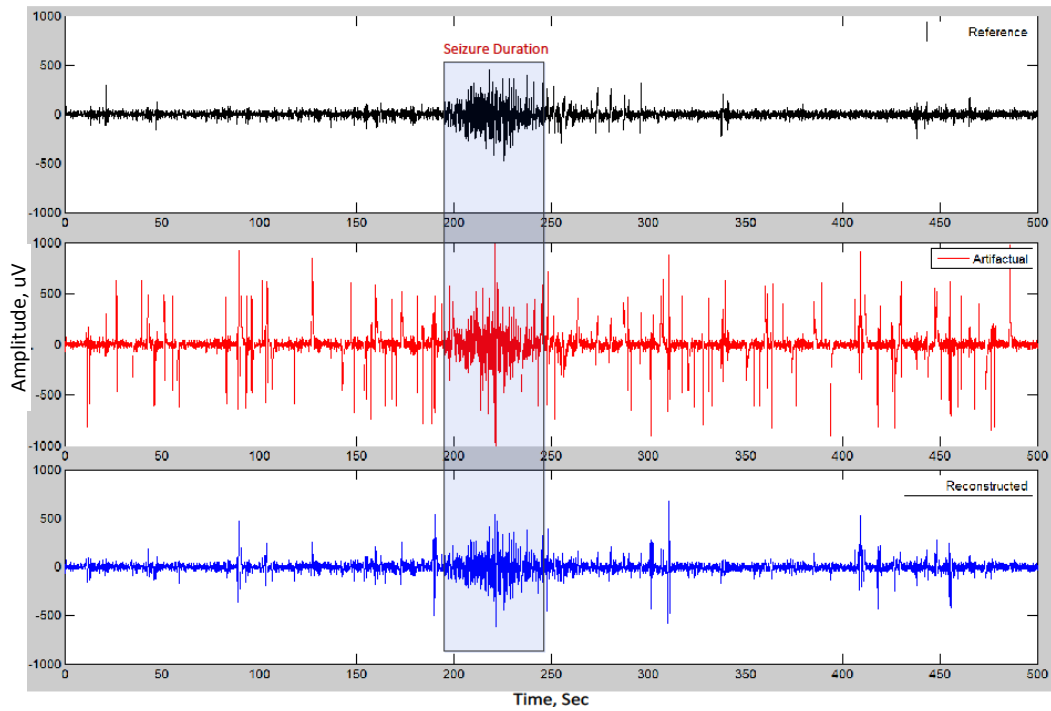


Figure 5.10: The removal result after the proposed algorithm is applied on the semi-simulated EEG data.

detection.

### 5.6.2.1 Artifact Removal Results

As discussed in sub-section-5.5.1, we have calculated several time and frequency domain metrics to quantify both amount of artifacts removed as well as amount of distortion made with respect to both amount and intensity of artifacts present in the data. Figure 5.11 shows the calculated SNDR over the entire frequency bandwidth of EEG data for fully simulated data sequence as in Figure 5.8 before and after artifacts are removed. It is clearly seen that a significant improvement of SNDR on an average of 5-10 dB over the entire frequency is made due to artifact removal which proves the efficacy of the proposed algorithm. Table 5.4 presents the quantitative

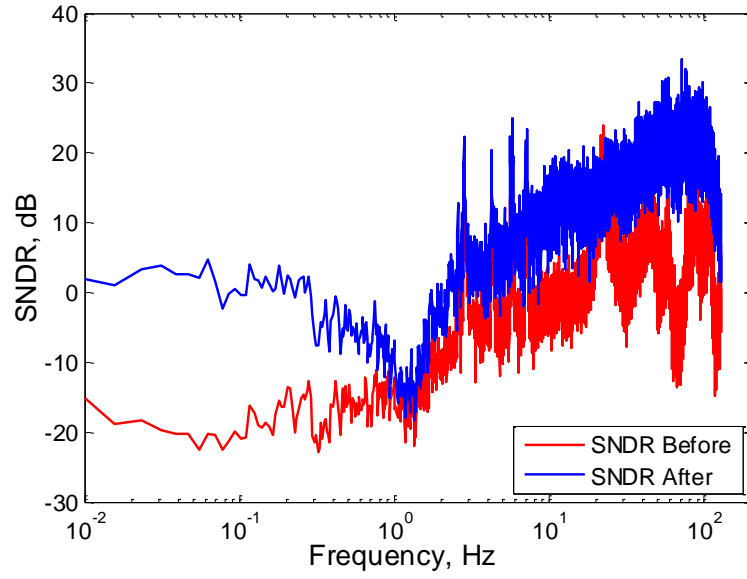


Figure 5.11: SNDR for signals before and after artifact removal clearly shows the improvement in signal quality over the entire frequency band.

metrics of artifact removal with respect to the strength of artifacts, i.e. different artifact SNR  $\text{SNR}_{\text{art}}$ . Table 5.5 presents the quantitative metrics of artifact removal with respect to different artifact duration  $\Delta T_{\text{art}}$ .

#### 5.6.2.2 Comparison with Other Methods

We have compared the performance our proposed method with few state-of-the-art artifact removal methods (i.e. wavelet-BSS and EMD-BSS based methods) in terms of both quantitative removal metrics (Figure 5.12) and computational time (Figure 5.13) to roughly illustrate the superior efficacy of our method in comparison with others. As we can see that the amount of artifact removal, i.e.  $\lambda$  is around 40% which means more than half of the artifacts have not been removed in order to protect the unwanted removal of seizure events. Even with such limitation, the increment in signal quality

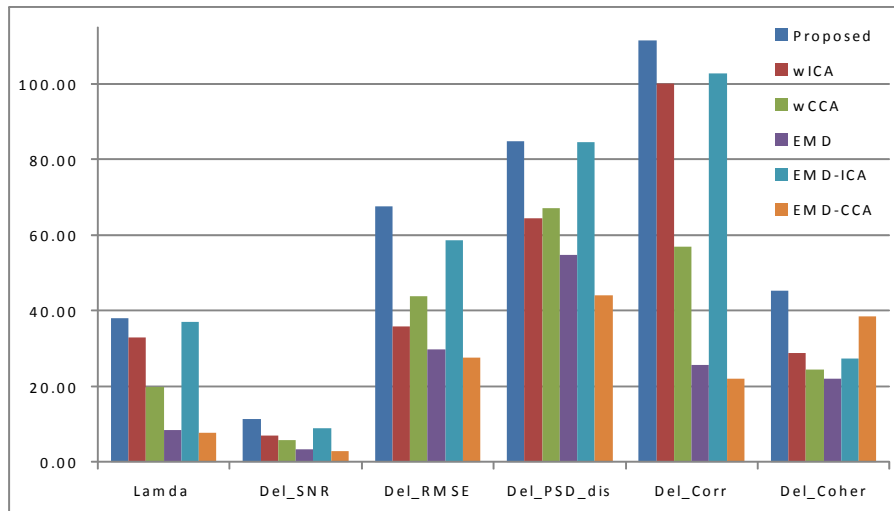


Figure 5.12: Comparison of proposed method with respect to few available artifact removal methods in terms of the quantitative metrics.

is significant. The comparison of computational time to process roughly 1s of data for the proposed method is about 1.8 ms which is lowest among all others. However, in order to achieve online processing, further reduction of computational time is necessary by optimizing the algorithm. The process flows of wavelet-BSS and EMD-BSS based methods are shown in Figure 3.6.<sup>5</sup>

### 5.6.2.3 Seizure Detection Results

In order to show that artifact removal by this proposed algorithm not only makes offline analysis during seizure detection easier and more accurate, but also helps the available automated seizure detector (ASD) to improve their performance significantly. An example of false alarms due to arti-

<sup>5</sup>Note that the epoch-by-epoch processing is only applied for our proposed method and for others we just process the whole sequence at once as it's difficult for BSS-based methods to function properly to separate components with small duration of data (i.e. epoch).

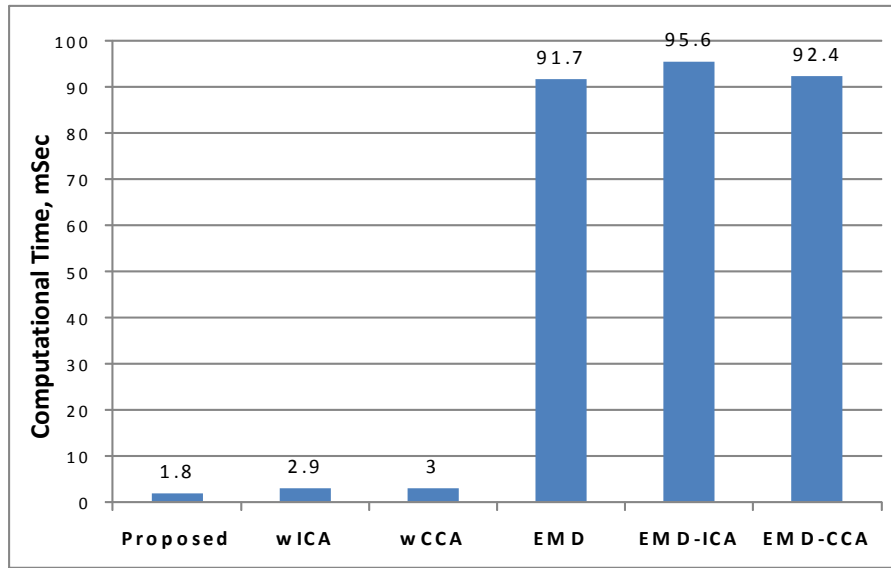


Figure 5.13: Comparison of proposed method with respect to few available artifact removal methods in terms of the computational time required to process each 1 second of data in MATLAB simulation.

facts is presented in Figure 5.14. Here we present three sequences of fully simulated EEG data: reference, artifactual, reconstructed and their corresponding SamEn values calculated with 2-sec time window. For an ideal case, i.e. without artifact, seizure and non-seizure segments can be easily separated by comparing their average sample entropy. However, in practice, EEG sequence is always contaminated with different artifacts and hence it may introduce some false alarms due to artifacts. Once most of the artifacts are reduced, the no. of false alarms is also reduced significantly as illustrated clearly in the Figure 5.14.

A quantitative representation of amount of improvement in seizure detection is illustrated in Figure 5.15 where the no. of false positives are plotted for both before and after artifact removal. In addition the corresponding improvement in  $\Delta F(\%)$  which suggests that on average 20-80%



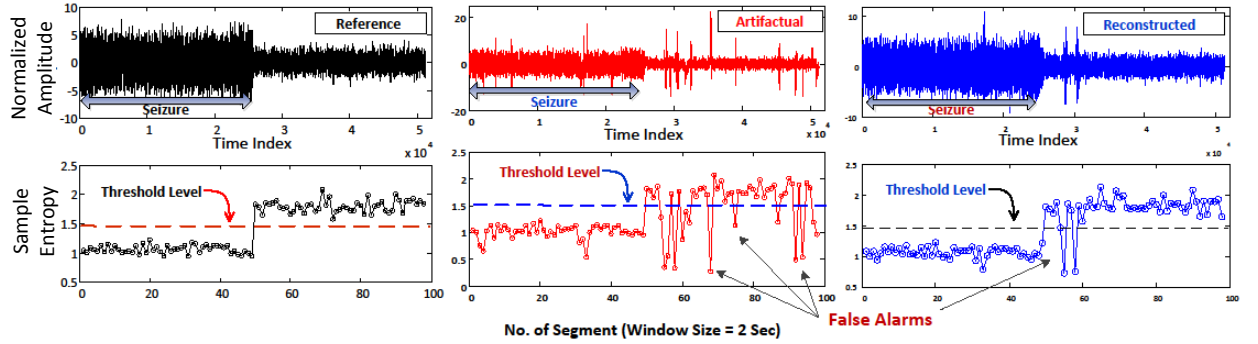


Figure 5.14: An example of false alarms due to artifacts is illustrated where sample entropy is chosen as a feature to separate seizure from non-seizure (normal) events. Artifact removal can significantly reduce the false alarms by reducing the amount of artifacts.

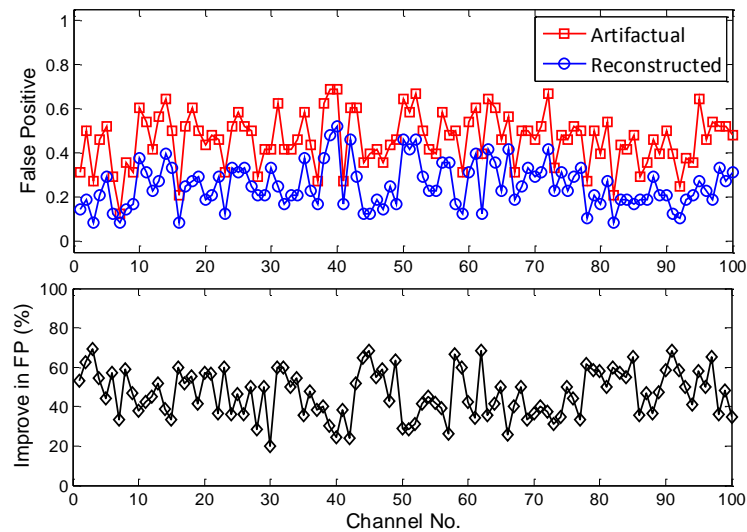


Figure 5.15: False positive ( $FP$ ) before and after artifact removal (shown on top) and improvement of false positive ( $\Delta FP$ ) in percentage (shown on bottom) are plotted with respect to different data sequence/channel no. For seizure detection purpose, SampEn is used as feature and SVM as classifier.

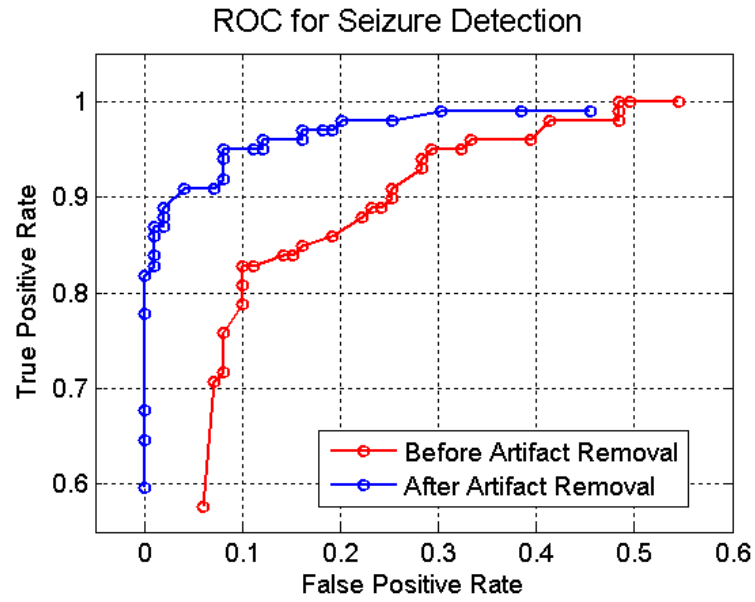


Figure 5.16: ROC curve for seizure detection in scalp EEG to illustrate the effect of artifact removal on the seizure detection performance.

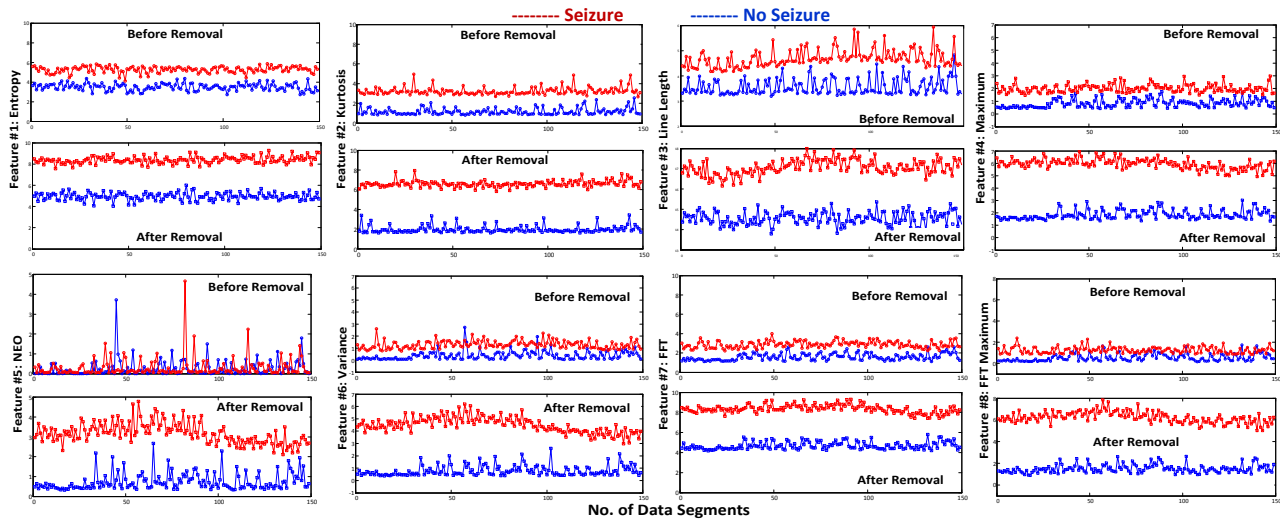


Figure 5.17: Different features from EEG data for seizure and non-seizure events calculated for each data segment of time window 1 sec.

improvement is possible after artifacts are reduced by proposed algorithm. Please note that, for this quantification we have simulated 100 different data sequences each of 200-sec duration where 100-sec is seizure and rest 100-sec is non-seizure segment. Then for each epoch of 2-sec, SampEn is calculated and used as a feature for SVM classification to quantify the no. of *FP*. The no. of *TP* in this simulation remains always 100% due to the single feature selection. However, these values are not absolute and may differ depending on the type and size of features, type of classifier used, length of the seizure segment, epoch duration and so on. The results are given only for simple understanding of the fact that artifacts removal with proposed algorithm can significantly improve the performance of seizure detection. Figure 5.16 shows the receiver operating characteristics (ROC) curve for seizure detection before and after artifact removal.

Figure 5.17 shows some common statistical features used in literature for differentiating seizure epochs from non-seizure ones for both before and after artifact removal. It is obvious from the plots that after artifact removal, the features are easier to distinguish than before artifact removal. Hence the proposed algorithm can also be useful in improving seizure detector performance in other seizure detection algorithms where combination of different statistical features are used for classification.

## 5.7 Optimum Parameter Selection

Similar attempts to sub-section 4.7 of Chapter-4 have been followed to select the best mother wavelet and threshold parameters automatically for performance. The filter parameter  $\alpha$  and threshold parameters  $k_A$  and  $k_D$  have been swept across wide range of values to find the optimal ones where both the amount of artifact removal and signal distortion is achieved as best. The process flow for algorithm optimization is shown in 5.18.

The performance metrics (quantitative) are plotted against the parameters  $\alpha$ ,  $k_A$  and  $k_D$  in Figure 5.19, 5.20 and 5.21 respectively to be able to select the best/optimal values of parameters correspond to the best performances.

Another Figure 5.22 shows the average SNDR improvement after artifact removal w.r.t the threshold parameters and obvious from the graph to be able to choose the optimal values of  $k_A$  and  $k_D$ .

## 5.8 Conclusions

The purpose of this research was to develop an artifact removal method in order to make the seizure analysis process easier for the clinicians and also to improve the performance of the available automated seizure detection algorithm. In addition, such artifact removal which preserves the seizure events, can greatly reduce the labor and complexity of seizure detection

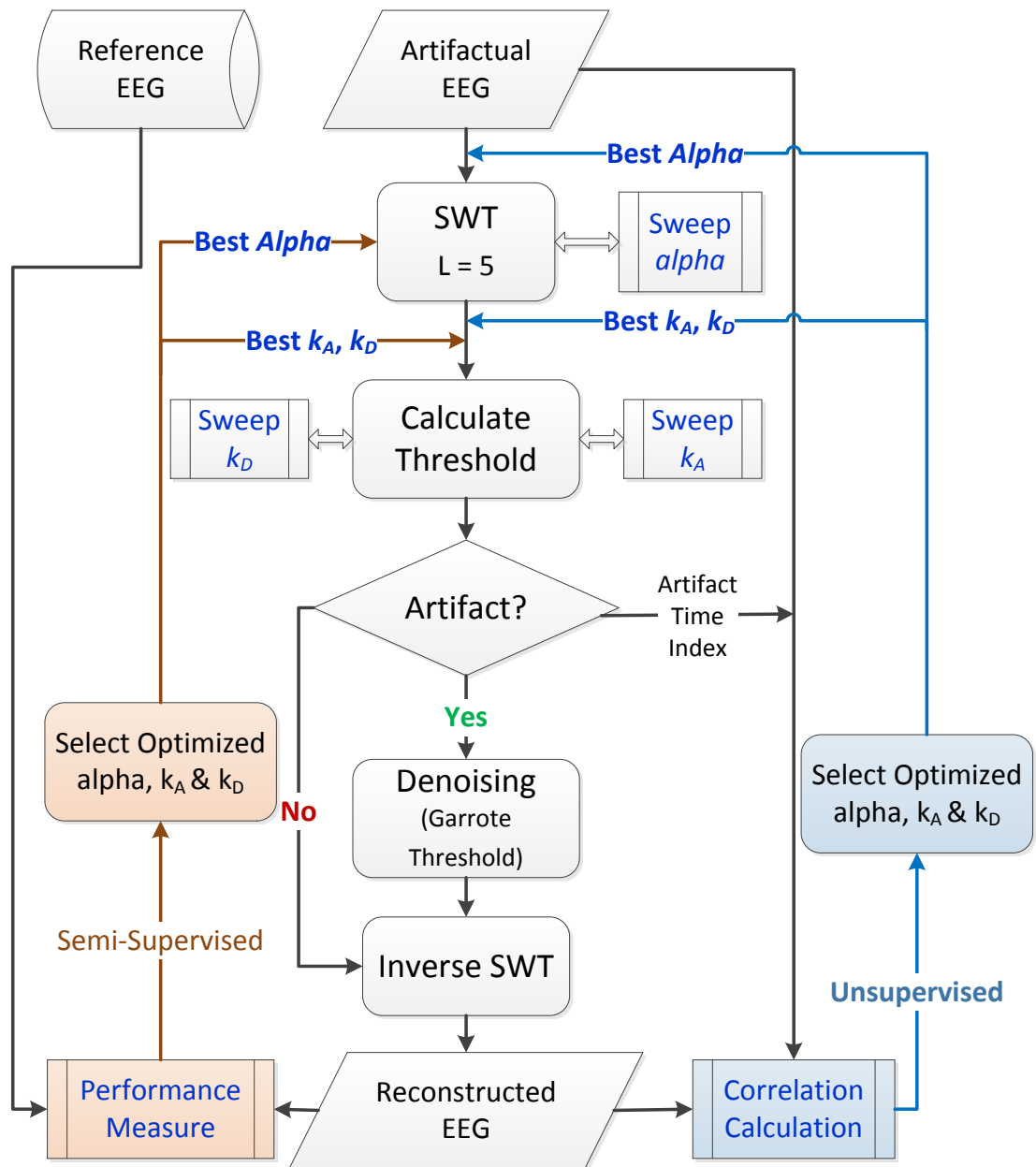


Figure 5.18: Process flow for automatically selection of wavelet parameters for algorithm optimization in terms of best performance metrics.

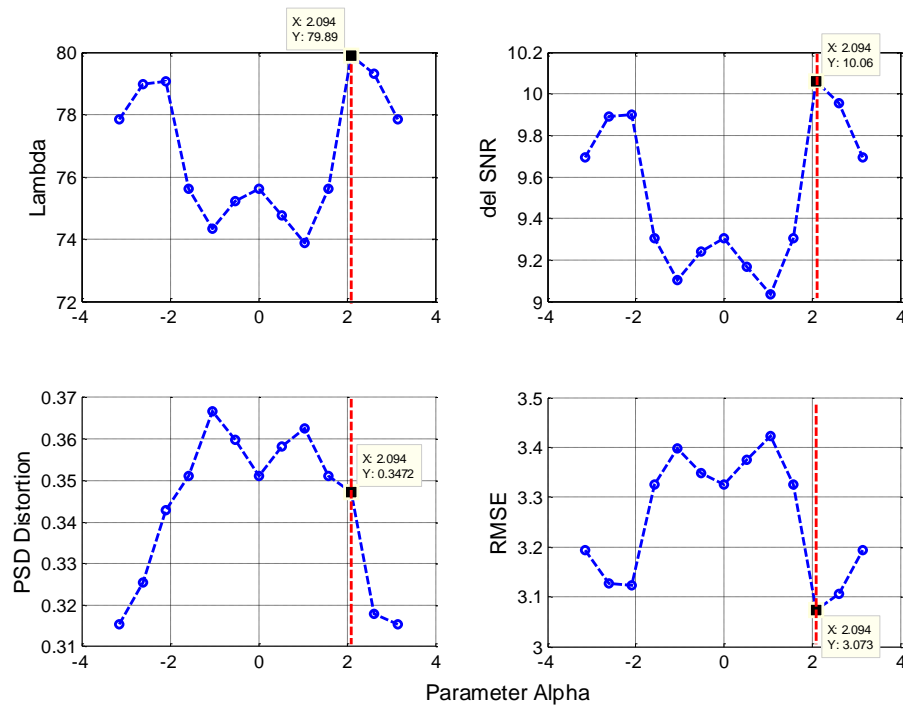


Figure 5.19: An illustration of selecting the best mother wavelet by optimizing the parameter alpha with the help of performance metrics vs. alpha plot.

by making it easy to analyze underlying signal of interest. To ensure a fair performance evaluation of the proposed method, we performed extensive simulations on both real and synthesized data with several metrics to quantify results. Also an analysis of a simple seizure detection proves the efficacy of the method that seizure detection accuracy can be significantly improved. The results are impressive and further improvement of the current algorithm to be able to remove artifacts in real-time will surely be a breakthrough in epilepsy patients monitoring. It is, therefore, expected to have more analysis on this particular research to enhance the quality of epilepsy patients by ensuring proper seizure diagnosis and treatment.

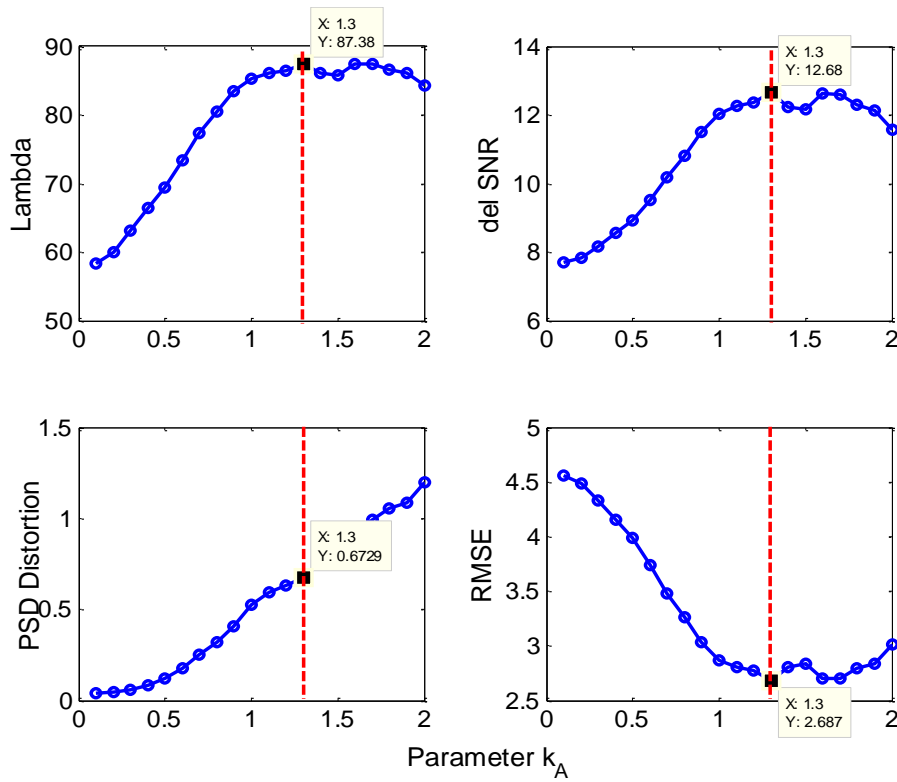


Figure 5.20: An illustration of selecting the best threshold parameter  $k_A$  by the help of performance metrics vs.  $k_A$  plot.

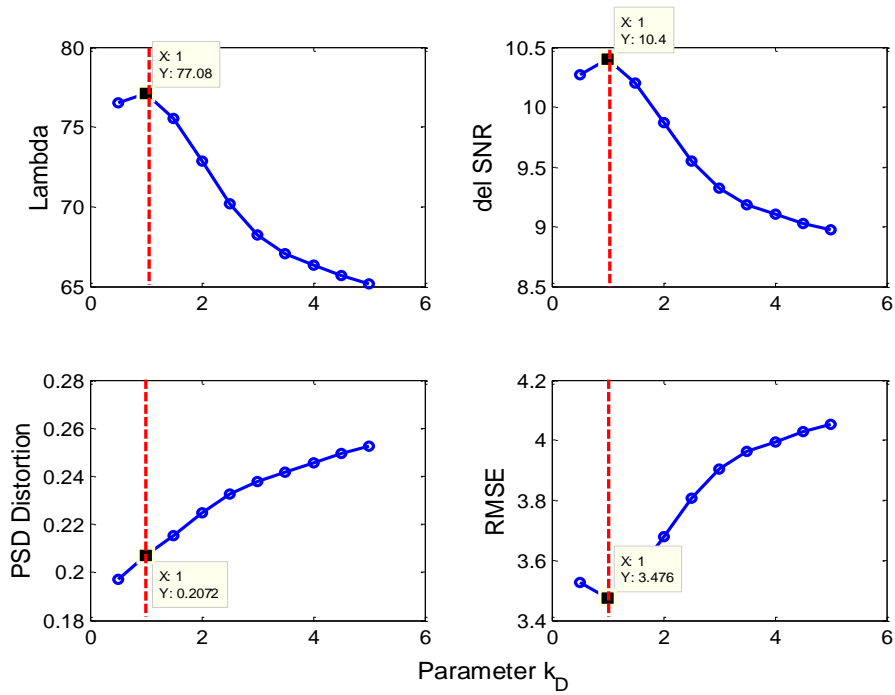


Figure 5.21: An illustration of selecting the best threshold parameter  $k_D$  by the help of performance metrics vs.  $k_D$  plot.

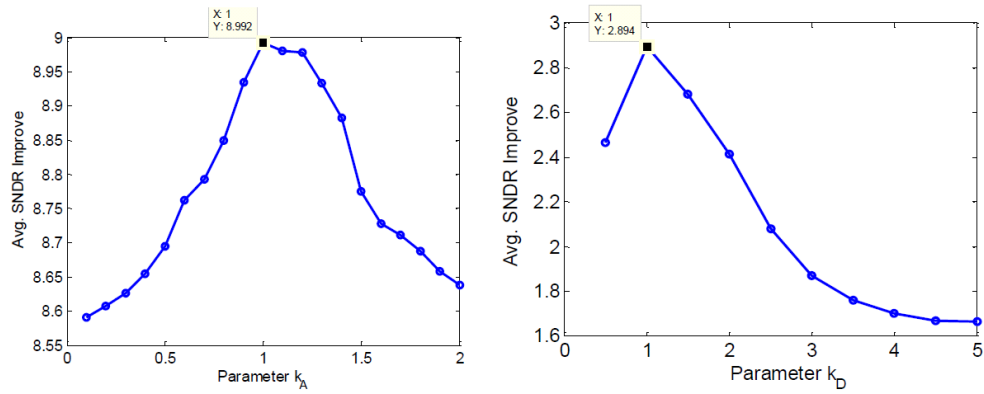


Figure 5.22: An illustration of selecting the best threshold parameter  $k_A$  and  $k_D$  by the help of performance metric (Avg. SNDR Improvement) vs.  $k_A$  or  $k_D$  plot.

Table 5.4: Quantitative metrics of artifact removal results for different artifact SNR ( $SNR_{Art}$ ).

$SNR_{Art}$ (dB)	Performance Metrics					
	$\lambda$	$\Delta SNR$	$\Delta RMSE$ (%)	$\Delta PSD_{dis}$ (%)	$\Delta Corr$ (%)	$\Delta Coher$ (%)
5	62.3	8.5	62.2	90.5	63.8	25.5
10	48.5	9.6	67.1	98.8	110.5	53.8

Table 5.5: Quantitative metrics of artifact removal results for different artifact durations ( $\Delta T_{Art}$ ). The mean values are highlited with bold face in the final row.

$\Delta T_{Art}$ (%)	Performance Metrics					
	$\lambda$	$\Delta SNR$	$\Delta RMSE$ (%)	$\Delta PSD_{dis}$ (%)	$\Delta Corr$ (%)	$\Delta Coher$ (%)
20	44.3	7.8	75.9	98.8	84.5	46.7
25	57.0	8.6	66.5	97.8	75.5	29.8
30	66.2	9.1	51.7	86.3	67.9	30.2
35	57.8	10.8	49.9	99.9	139.7	45.9
40	68.8	11.1	61.1	99.6	113.5	30.7
<b>30.87%</b>	<b>54.71%</b>	<b>8.27%</b>	<b>63.92%</b>	<b>97.55%</b>	<b>98.91%</b>	<b>43.05%</b>



## Chapter 6

# Artifact Reduction for EEG-based BCI Application: Algorithm Design

This chapter discusses about artifact detection and removal for different BCI applications and proposes a unique idea of mapping the probability of artifact contamination in each epoch of a data sequence for BCI applications. Finally, an algorithm is proposed to remove artifacts based on the probability mapping with a tuning parameter controlled by the user in removing specific type of artifacts in specific BCI application.

## 6.1 Introduction

Brain-Computer Interface (BCI) is a promising technique that establishes a direct link between human brain and an external computerized device by-passing the normal pathway that is not functional due to any brain/spinal related injury [42]. This technology thus allows severely disabled persons suffering from brain or spinal cord injury to communicate with outside world by controlling certain computerized device, e.g. computer, wheel chair, neural prosthetics, etc. It is also used as a rehabilitation tool for stroke patients and people with spinal cord injury. Apart from clinical needs, it has recently been popular in some other applications as well, such as virtual augmentation, cognitive study, human-computer interaction (HCI), etc. Although, there are different brain recording techniques (starting from non-invasive to invasive ones) to measure the electrical activity of brain to process and use in BCI applications, scalp EEG is the most popular among them in BCI research due to its mainly non-invasive nature with other attractive features such as fine temporal resolution, simple to use, portability and lower cost [43]. However, scalp EEG is very much prone to undesirable artifacts that come from non-cerebral origin. The artifacts often severely contaminate the EEG recordings and modify the shape of a particular neurological event that drives the BCI system affecting the accuracy of the BCI performance. For example, artifacts can mistakenly cause an unintentional control of the BCI device [108].

Therefore, handling of such offending artifacts is critical in BCI research for satisfactory performance and consequently many ways have been developed to get rid off artifacts that create misinterpretation in the signal analysis. The first step of handling artifacts is to avoid them by instructing the BCI user not to make unnecessary blink or body movement. Although this is the easiest way to avoid the occurrence of only few types of artifacts, there are always some involuntary and uncontrolled movements associate with the user that can never be avoided, such as eye blink, ECG, etc. Another way of getting rid off artifacts is to reject the epochs that are highly contaminated with artifacts. However, this doesn't mean that the other epochs are completely free of artifacts. Often such rejection involves manual interpretation of the EEG data by clinical experts and thus requires intensive human labor. Sometime automated rejection is also carried out but often not accurate as the manual one. Rejection of epochs sometimes don't work when it requires the real-world applications that involve online signal processing [165]. Recent advances in signal processing techniques has now allowed the researchers to design automatic artifact identification and removal algorithms to be able to implement online for real-world BCI applications.

There have been several methods proposed in the literature to detect and remove artifacts particularly for BCI applications. One of the most common is the use of Blind Source Separation based algorithm (e.g. ICA [15, 18, 19, 84, 92, 166, 167, 168]) which separates multi-channel EEG

recordings into independent or maximally uncorrelated sources and then rejecting the artifact source before reconstructing the signals. However, ICA is an offline technique and often requires manual intervention to identify the artifactual source (ICs). Moreover, it cannot operate on few or single-channel datasets thus not suitable for portable ambulatory BCI applications. Another popular method to remove physiological artifacts is linear regression (e.g. using adaptive filter [19, 59]) with the availability of a dedicated reference artifact channel such as EOG or ECG. In many BCI applications, such reference channel may not be available thus not possible to use regression technique. In recent times, two methods namely wavelet transform [34, 35, 40, 51] and empirical mode decomposition (EMD) [27, 33, 34], that are suitable for nonlinear and nonstationary biomedical signal processing, have been introduced to detect and remove artifacts from EEG. Among these two, wavelet based techniques combining with another technique such as ICA/CCA [35, 38] or neural network [59] have been very popular and stated to have decent performance in artifact removal. On the other hand, EMD is more computationally expensive and still an empirical method that doesn't have complete theoretical background.

In this chapter, we propose a unique artifact detection method based on artifact probability mapping which quantifies an epoch by a relative probability of being artifactual. This is achieved by considering the typical artifact characteristics in contrast to the background EEG rhythms

with the help of four statistical measures namely entropy (measures the uncertainty), kurtosis (measures the peakedness), skewness (measures the symmetry) and Periodic Waveform Index, PWI (measures of periodicity) as described in detail in the later section of this chapter. This unique probability mapping will allow the user to decide whether to correct the epoch or to remain as it is by choosing an appropriate probability threshold. Subsequently a removal method is also proposed which is based on stationary wavelet transform based denoising and relies on the desired spectral band of EEG rhythms in contrast to spectral bands of different artifacts particularly for BCI applications. The proposed method is demonstrated with both real and synthesized database and extensive quantitative measures show the efficacy of this method with obtained satisfactory results. Moreover, the proposed method is also compared with some of state-of-the-art methods and proves its superiority over others both in terms of performance and computational time. Finally, the effect of artifact removal on real BCI database has also been demonstrated to show that it can substantially improve the classifier accuracy in BCI experiments.

The rest of this chapter is organized as follows. Section 6.2 introduces the proposed artifact probability mapping followed by proposed removal method. Section 6.3 briefly describes the data collection and data synthesis process. Section 6.4 provides the metrics to evaluate the performance of proposed artifact removal method. Section 6.5 presents and discusses the results for both artifact removal and its effect on BCI performance. Finally,

section 6.6 gives concluding remarks.

## 6.2 Proposed Method

The whole process flow of our proposed method starting from preprocessing to probability mapping and finally artifact removal is shown in Figure 6.2.

### 6.2.1 Artifact Detection: Probability Mapping

The proposed artifact probability mapping is similar to the idea of spike probability mapping described in [118] where the authors proposed a probability mapping for separation/identification of neural action potential or spike from background noise for in-vivo neural recordings. Here we attempt to separate artifacts from background EEG rhythms by representing each epoch of 1-sec duration by the relative probability of artifact contamination. Figure 6.1 shows the segmentation process of EEG sequence into epochs and calculation of its corresponding artifact probability. This probability of artifact contamination depends on four measures as

- Entropy of the epoch that represents the randomness of the samples in an epoch
- Kurtosis of the epoch that represents the peakedness of the samples in that epoch
- Skewness of the epoch representing the symmetry of distribution of the samples in the epoch

- Periodic waveform index (PWI) that represents the periodicity of the samples in that epoch

The above mentioned four measures are described below:

1. **Entropy,  $H$** : Entropy ( $H$ ), a measure of uncertainty of information content, of a discrete random variable  $x$  with possible values  $x_1, \dots, x_n$ , can be calculated as:

$$H(x) = E[-\ln(P(x))]. \quad (6.1)$$

Here  $E$  is the expected value operator and  $P(x)$  is the probability mass function of  $x$ .

2. **Kurtosis,  $Kr$** : Kurtosis is the measure of "peakedness" of probability distribution function and is calculated for a real-valued random variable  $x$  as follows:

$$Kr[x] = \frac{\mu^4}{\sigma^4}. \quad (6.2)$$

where  $\mu$  and  $\sigma$  are the mean and standard deviation of random variable  $x$ .

3. **Skewness,  $\gamma_1$** : Skewness is a measure of the asymmetry of the probability distribution of a real-valued random variable,  $x$  about its mean and calculated as

$$\gamma_1 = \frac{\mu^3}{\sigma^3}. \quad (6.3)$$

where  $\mu$  and  $\sigma$  are the mean and standard deviation of random variable  $x$ .

**4. Periodic Waveform Index,  $PWI$ :** Periodic Waveform Index is the measure of the rhythmicity or periodicity pattern in a signal  $x$  proposed by [169]. Suppose the total harmonic energy at time point  $n$  is  $E_\tau[n]$  and the signal energy corresponding to a cycle duration  $\tau$  is  $N_\tau[n]$  then  $PWI$  is defined as

$$PWI[n] \triangleq \frac{E_{\hat{\tau}}[n]}{N_{\hat{\tau}}[n]}. \quad (6.4)$$

where

$$N_\tau[n] \triangleq \frac{1}{\tau} \sum_{n'=-\infty}^{\infty} (x[n']\psi[n' - n])^2 \quad (6.5)$$

and

$$E_\tau[n] \triangleq \sum_{k>0} \left| \frac{1}{\tau} \sum_{n'=-\infty}^{\infty} (x[n']\psi[n' - n]) \exp(-2i\pi \frac{kn'}{\tau}) \right|^2 \quad (6.6)$$

here  $\psi$  is a window of bounded energy centered around 0 of length  $\alpha/\tau$  and  $\hat{\tau} = \arg.\max_\tau E_\tau$ .

**Probability of Artifact,  $Pr$ :** Probability of an epoch being artifact-contaminated depends on four above mentioned measures. By studying the artifact characteristics, we know that artifact tends to be more random



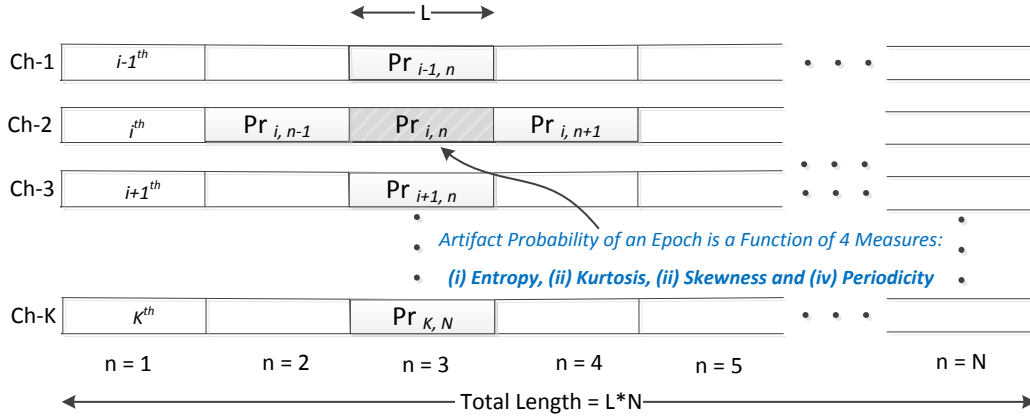


Figure 6.1: Segmenting EEG sequences into epochs and calculating corresponding probability of being artifactual

(i.e. lower entropy values) with higher amplitude (i.e. higher kurtosis) than background EEG, more likely to be transient (i.e. lower PWI) than rhythmic (i.e. unlike EEG rhythms) and artifact makes the data distribution to be asymmetrical e.g. longer tail on either side of data histogram (i.e. higher skewness). Therefore, keeping in mind of these facts, we propose an equation as follows to measure the probability of being artifactual for an epoch

$$Pr = \frac{[k_H(1 - \hat{H})] + [k_{Kr}\hat{K}r] + [k_{\gamma_1}|\hat{\gamma}_1|] + [k_{PWI}(1 - \hat{PWI})]}{4}. \quad (6.7)$$

where  $k_H$ ,  $k_{Kr}$ ,  $k_{\gamma_1}$ , and  $k_{PWI}$  are the weights of the measures  $\hat{H}$ ,  $\hat{K}r$ ,  $\hat{\gamma}_1$ , and  $\hat{PWI}$  respectively that are normalized by their corresponding maximum values.

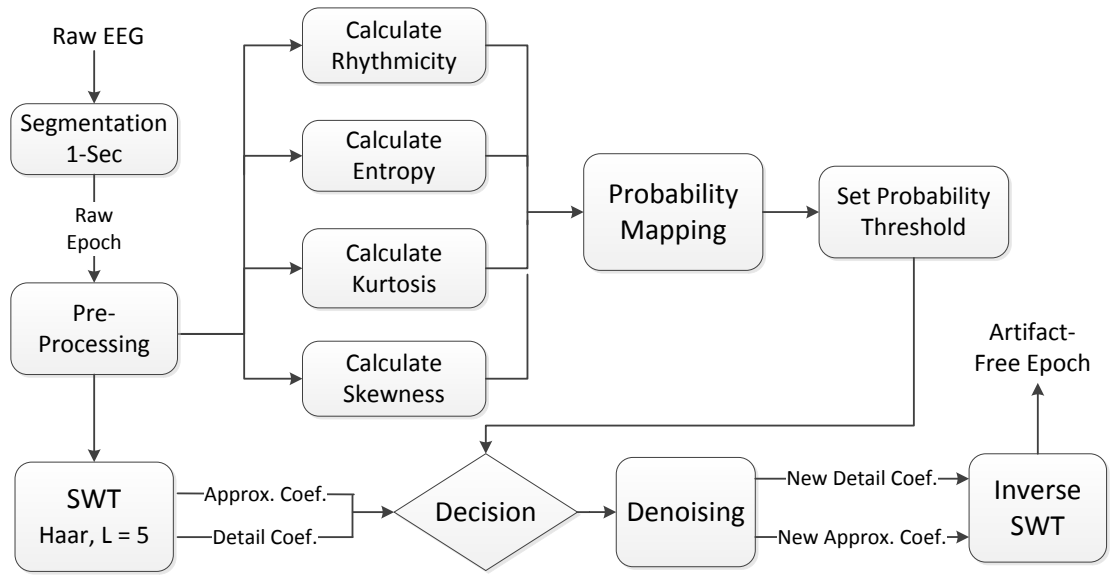


Figure 6.2: Proposed structure to create probability mapping and subsequently to remove artifacts from EEG

## 6.2.2 SWT-Based Artifact Removal

### 6.2.2.1 Preprocessing

To begin with, let  $x_{\text{raw}}(n)$  denotes the sampled raw EEG signal which is sampled at  $F_s$  Hz where  $n = \{0, 1, 2, \dots\}$  is the discrete-time index.

We assume that the power-line interference of 50/60 Hz and the offset of raw EEG have already been removed prior to this preprocessing stage.

In the preprocessing, the incoming signal is firstly divided into into *non-overlapping* epochs epochs with size of  $N$ . Then, the  $j$ th epoch ( $j \geq 1$ ) is

Table 6.1: Illustration of SWT coefficients in relation to EEG rhythms, artifacts and relevant BCI studies in their corresponding frequency bands.

SWT Coeff.	Fs (Hz)	$D_1$	$D_2$	$D_3$	$D_4$	$D_5$	$A_5$
Freq. Band (Hz)	256	64 – 128	32 – 64	16 – 32	8 – 16	4 – 8	<b>0 – 4</b>
EEG Rhythms			<b>Gamma</b>	<b>Beta</b>	<b>Mu Alpha</b>	<b>Theta</b>	<b>Delta</b>
Relevant BCI Studies				Motor Imagery BCI		ERP (P300)	
					SSVEP		
Artifact Type			EMG (Muscle Artifacts) Electrode Pop			Cardiac	EOG Blink
						Movement	

given by

$$x_j = \begin{bmatrix} x_{\text{raw}}(jN - 1) \\ x_{\text{raw}}(jN - 2) \\ \vdots \\ x_{\text{raw}}(jN - N) \end{bmatrix} \quad (6.8)$$

Note that the choice of epoch duration plays an important role in both amount of artifact removal and amount of distortion made to the signal of interest. In addition, in case of automated BCI classification algorithm to work after our proposed artifact removal method is applied, the value of  $N$  will determine the minimum time delay for BCI signal processing. In our algorithm, we have found  $N$  as 1-sec to be optimum after trying different values empirically.

### 6.2.2.2 Wavelet Decomposition

Wavelet decomposition and subsequently removing unwanted artifacts by applying threshold is a familiar denoising process in non-linear, non-stationary biomedical signals [78]. Usually, the denoising process refers to removing high frequency noise by thresholding the detail coefficients after wavelet decomposition. However, in this thesis, by using the term denoising, we refer to removing artifactual components from neural signals in the wavelet domain, irrespective of whether it is high-frequency or low-frequency artifacts. The objective of this stage is to decompose and analyze the raw epoch with a reasonable time-scale resolution in wavelet domain for possible identification of artifactual components in the later stage. To this end, stationary wavelet transform is performed on the epochs  $\{x_j\}_{j \geq 1}$  with level-5 decomposition by *Haar* as basis wavelet which results in final approximate  $a_{j,5}$  and detail coefficients  $d_{j,1}, d_{j,2}, \dots, d_{j,5}$ . Although there are many types of wavelet transform (e.g. DWT, CWT, SWT, etc.), we chose SWT for its advantage of being translational invariant [78]. The choice for level of decomposition is mainly inspired from the bandwidth of EEG signal (i.e. 0.05 - 128 Hz) and the frequency bands of EEG rhythms relevant to BCI studies such as *mu*(7 – 13Hz) and *beta*(14 – 30Hz) for MI-based BCI [170]; *delta*( $< 4Hz$ ) for ERP-based BCI; e.g. P300 [171]; and SSVEP (12-18 Hz) [172] in order to have enough no. of frequency sub-bands to make decisions on where to denoise carefully and where not. Table 6.1 shows the

frequency sub-bands of the decomposed detail coefficients and the final-stage approximate coefficient after 5-level SWT is performed on the raw EEG data. It is clear that  $D_3$ ,  $D_4$  and  $A_5$  correspond EEG rhythms *beta*, *mu* and *delta* respectively and hence during denoising process, we need to be very careful to handle these coefficients. The other three coefficients, i.e.  $D_1$ ,  $D_2$  and  $D_5$  can be denoised directly and fully without any further consideration as most likely they contain artifacts and non-relevant EEG rhythms in such BCI applications.

### 6.2.2.3 Denoising

We use non-negative garrote shrinkage function during denoising since it has some appealing properties of being less sensitive to input change, having lower bias and being continuous [124]. This is a nice trade-off between soft and hard threshold function in terms of amount of artifact removal and signal distortion [124] and is given by

$$g(j, \ell) = \begin{cases} d_{i,j} & |d_{j,\ell}| \leq t_{j,\ell} \\ \frac{t_{j,\ell}^2}{d_{j,\ell}} & |d_{j,\ell}| > t_{j,\ell}. \end{cases} \quad (6.9)$$

where  $g(j, \ell)$  is the garrote threshold function at each decomposition level of  $\ell$  for epoch  $j$ , and  $t_{j,\ell}$  denotes the threshold value. To denoise the critical coefficients  $d_{j,3} - d_{j,4}$  for MI-BCI and  $d_{j,5}$ ,  $a_{j,5}$  for P300-based BCI, and  $d_{j,4}$  for SSVEP-based BCI, we have used modified universal threshold reported by [7]

$$t'_{j,\ell} = K\alpha_{j,\ell}\sqrt{2\ln N}, \quad (6.10)$$

where in (6.10)  $N$  is the length of epoch and  $\alpha_{j,\ell}$  is the estimated noise variance for  $w_{j,\ell}$  which is usually calculated by following formula [38]

$$\alpha_{j,\ell} = \frac{\text{median}(|w_{j,\ell}|)}{0.6745}. \quad (6.11)$$

where  $w_{j,\ell}$  is the wavelet coefficient at the  $\ell$ th decomposition level (i.e.  $w_{j,\ell} = a_{j,\ell}$  for approximation coefficient and  $w_{j,\ell} = D_{j,\ell}$  for detail coefficient.). The new parameter  $K$  in (6.11) comes from the empirical observations [7]. It is given as

$$K = \begin{cases} K_A \ (0 < K_A < 1) & \text{for thresholding } a_{j,5} \\ K_D \ (0 < K_D < 1) & \text{for thresholding } d_{j,\ell} \end{cases} \quad (6.12)$$

where,  $K = K_A$  is selected for thresholding approximate coefficient  $a_{j,5}$  and select  $K = K_D$  to threshold all the detail coefficients ( $d_{j,\ell}$ ,  $\ell = 1, 2, \dots, 5$ ). The tuning of parameter  $K$  is discussed at the end of this chapter under section 6.7 as an example for particularly MI-based BCI studies.

#### 6.2.2.4 Decision

The most important part of the algorithm is *Decision*. Depending upon this stage, the decision of whether an epoch is to be denoised or not is made from the probability threshold set by user. In addition, once the decision of denoising is made, then how carefully that particular epoch to be denoised to remove artifacts without affecting the signal of interest, is also decided in this stage. Therefore the performance of artifact removal and consequent improvement of BCI performance is highly dependent on this stage.

Table 6.2: Pseudo-code for the decision stage during denoising SWT coefficients.

Decision Making	Remarks/Comment
<p><i>If (P300 ERP Study)</i></p> <p><math>k_{A_5} = 1,</math>  <math>k_{D_5} = 1</math>  <math>k_{D_i} = 0.75, \quad i = 2,3,4</math>  <math>k_{D_1} = 0.5</math></p> <p><i>End</i></p>	<p><b>Denoise <math>D_5, A_5</math> carefully</b></p>
<p><i>If (MI Study)</i></p> <p><math>k_{A_5} = 0.5, k_{D_5} = 0.75</math>  <math>k_{D_i} = 1, \quad i = 3,4</math>  <math>k_{D_2} = 0.75, k_{D_1} = 0.5</math></p> <p><i>End</i></p>	<p><b>Denoise <math>D_3-D_4</math> carefully</b></p>
<p><i>If (SSVEP Study)</i></p> <p><math>k_{A_5} = 0.5, k_{D_5} = 0.75</math>  <math>k_{D_4} = 1</math>  <math>k_{D_3} = 0.75, k_{D_2} = 0.75, k_{D_1} = 0.5</math></p> <p><i>End</i></p>	<p><b>Denoise <math>D_4</math> carefully</b></p>

The first step of this stage is to find whether the epoch is truly artifactual based on response from both probability mapping and from measuring the modified universal threshold for each level of decomposed wavelet coefficients: if both of them are affirmative, then the epoch is decided to denoise fully. Otherwise we let the epoch as it is. The parameters are chosen as we discuss in the previous part of *Wavelet Decomposition*. As we denoise primarily based on the user's set probability threshold, some epochs still being found artifactual from both probability mapping and wavelet coefficients, they remain untouched and therefore we pay the penalty of less amount of artifact removal.

### 6.2.2.5 Reconstruction

In the final stage of reconstruction, based on the decision stage, we either apply thresholding (fully) or let the coefficients  $D_3 - D_4$  remain same. Finally with all the new set of coefficients obtained (i.e.  $D'_1 - D'_5$  and  $A'_5$ ), we apply inverse SWT to reconstruct the EEG epochs. Thus a new sequence of data so called *reconstructed data* is obtained.

## 6.3 Methods/Data Collection

### 6.3.1 Data Collection

Real EEG recordings are downloaded from BCI competition-IV Scalp EEG Database: dataset-1 from [43], dataset-2a and dataset-2b from [43, 173, 174]. The dataset-1 has 64 EEG channels (0.05-200 Hz) and sampled at 1000 Hz recorded from 7 subjects for MI-BCI study. Dataset-2a has 22 EEG channels (0.5-100 Hz) with 3 EOG channels recorded from 9 subjects having 4 classes whereas dataset-2b has 3 bipolar EEG channels + 3 EOG channels collected from 9 subjects having 2 classes for MI-based BCI experiment. Both of them were sampled at 250 Hz.

Apart from that as mentioned in previous chapter under sub-section 5.3.1 Data Collection, we performed simple EEG experiments to record some specific artifact types from healthy subject.



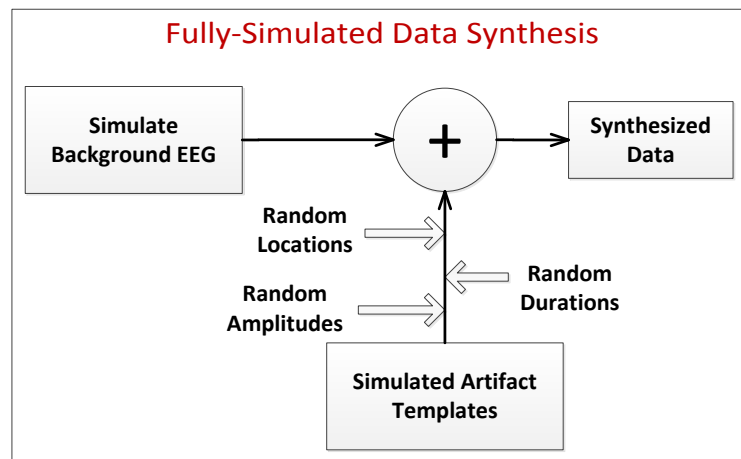


Figure 6.3: Illustration of the synthesis process to generate artifactual EEG data for quantitative evaluation of proposed artifact removal.

### 6.3.2 Data Synthesis

In this dataset, we have simulated two data components: artifacts and EEG background activity (i.e. EEG rhythm), and then combined them together to make artifactual EEG dataset. The simulated EEG data have been generated according to the classical theory of Event Related Potentials (ERP) as described in [156]. The MATLAB code we used to generate such simulated EEG is available to download for free from [154]. The process of data synthesis is shown in Figure 6.3.

## 6.4 Performance Evaluation

### 6.4.1 Artifact Removal Performance Metrics

As we mentioned in the previous chapter 5 that it is quite difficult to compare different artifact removal methods based on their ability to remove

artifacts since very few quantitative evaluation have been reported in the literature. Most of the published articles evaluated their method in terms of some qualitative plots. In addition, very few of them quantified the distortion to desired EEG signals due to the removal effect. Therefore, it's not fair to tell which performs best based on the study.

The performance of the proposed algorithm on the artifact removal has been evaluated both in terms of the amount of artifact reduction and the amount of distortion it brings into the signal of interest. Several efficiency metrics have been calculated in both time and spectral domain to quantify such evaluation. In order to have fair evaluation and clear idea we also have considered the amount and duration of artifacts present in the signals. We have incorporated the similar performance metrics reported in chapter 5 for evaluating artifact removal outcome.

#### 6.4.2 BCI Performance Metrics

**ROC Curve:** In order to evaluate the BCI performance accuracy for the classifier in terms of ROC curve, the required two metrics i.e. true positive rate (TPR) and false positive rate (FPR) are calculated by following equations:

$$TPR = \frac{TP}{TP + FN}, \quad (6.13)$$

$$FPR = \frac{FP}{FP + TN}, \quad (6.14)$$

where  $TP$ ,  $TN$ ,  $FP$  and  $FN$  are the number of epochs detected as true positive, true negative, false positive and false negative for a particular BCI task respectively.

## 6.5 Results and Discussion

### 6.5.1 Qualitative Evaluation

#### 6.5.1.1 Real Data

The proposed algorithm is applied to our recorded EEG data from a healthy subject with labeled *chewing* and *eye-blink* artifacts. The artifact removal result in terms of time-domain plot is shown in 6.4 for qualitative evaluation which suggests a satisfactory removal of both types of artifacts without distorting the background EEG signals in the non-artifactual region.

Another example of artifact removal result is illustrated in Figure 6.5 where real EEG data from BCI competition dataset-IV is contaminated with ocular artifact. It is obvious from the time-course data that the artifacts are corrected without much distorting the signal of interest.

#### 6.5.1.2 Simulated

The artifact removal result from a fully simulated data is illustrated in Figure 6.6 where both signal components (artifacts and background EEG) are simulated. The synthesized artifactual data is severely contaminated with different types of artifacts and its corresponding probability mapping

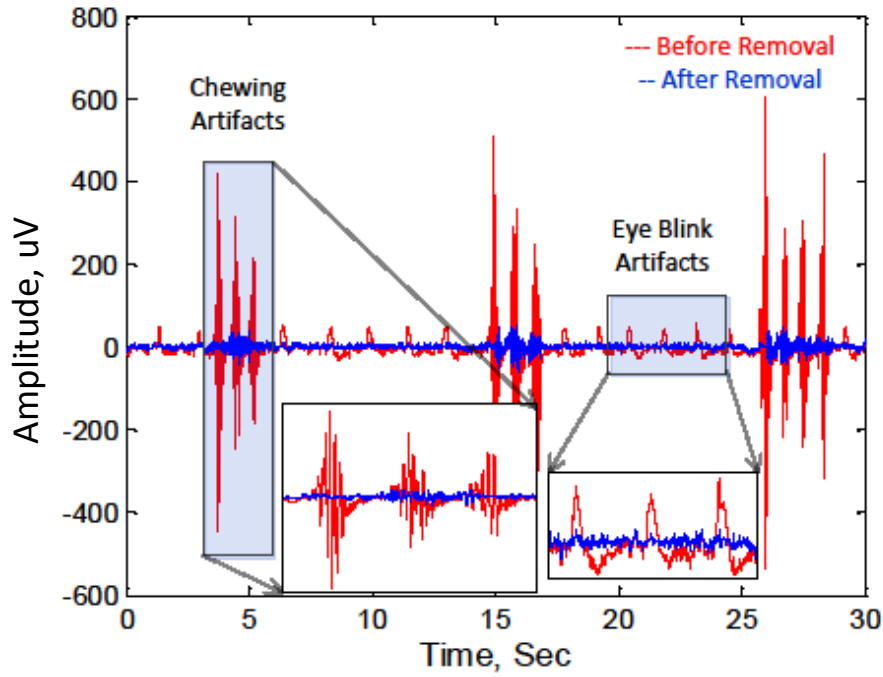


Figure 6.4: The removal result after the proposed algorithm is applied on our recorded EEG.

is also shown. Once the artifact removal is performed, the probability of being artifactual for previously contaminated epochs have been reduced significantly as it is obvious from the lower part of the plot. Please note that it's not possible to remove all the artifacts completely (i.e. 100%  $\lambda$ ), but the purpose is to reduce artifact contamination as much as possible without distorting the signal of interest.

Another example of all six types of simulated artifacts and their reduction is shown in Figure 6.7. Here each plot shows each type of artifact contaminated segment before and after artifacts are removed along with the reference artifact-free segment. This qualitative illustration proves that most of the time the algorithm can significantly reduce each type of artifact.

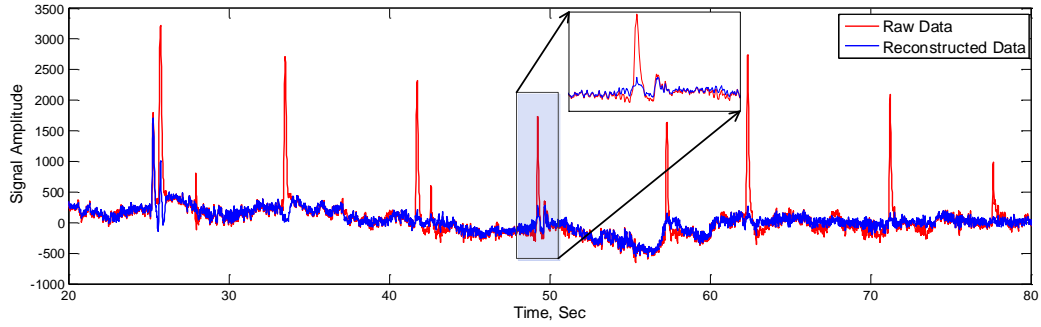


Figure 6.5: The removal result after the proposed algorithm is applied on real BCI dataset collected from BCI Competition-IV.

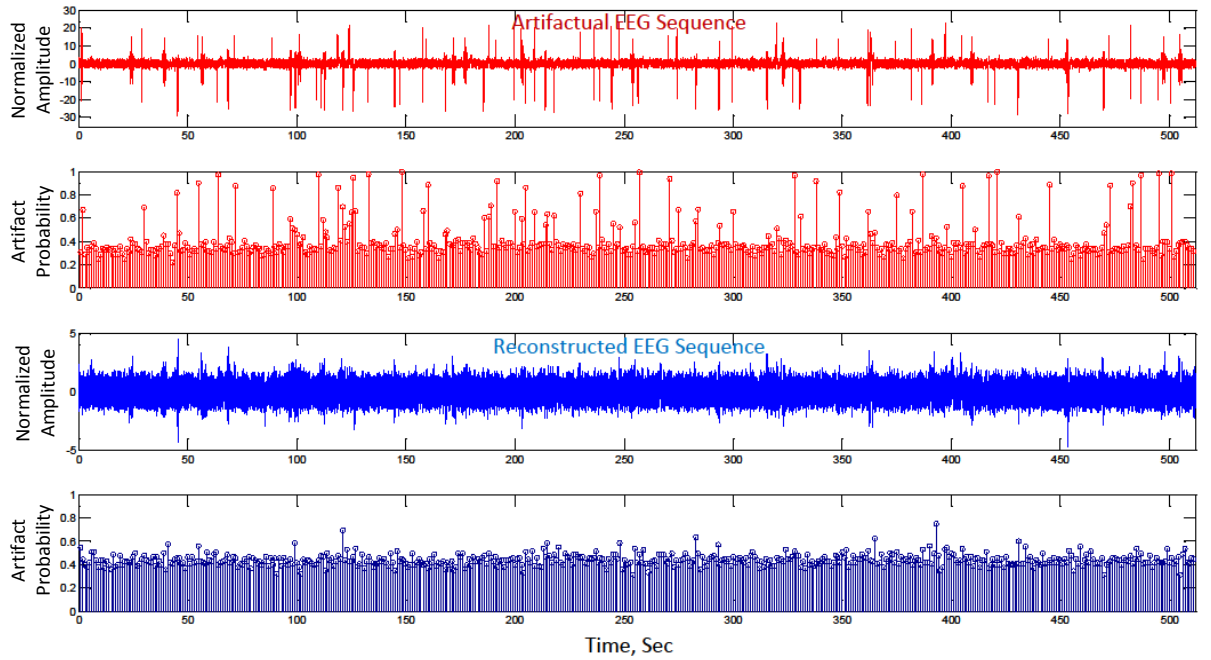


Figure 6.6: Fully simulated EEG data sequence with different types of artifacts before and after artifact removal (upper plot) and their corresponding probability map (lower plot). The time window duration in this case is chosen as 1 sec

### 6.5.2 Quantitative Evaluation

This sub section quantifies the results obtained both in terms of artifact removal and the consequence of artifact removal, i.e. improvement in BCI classification.

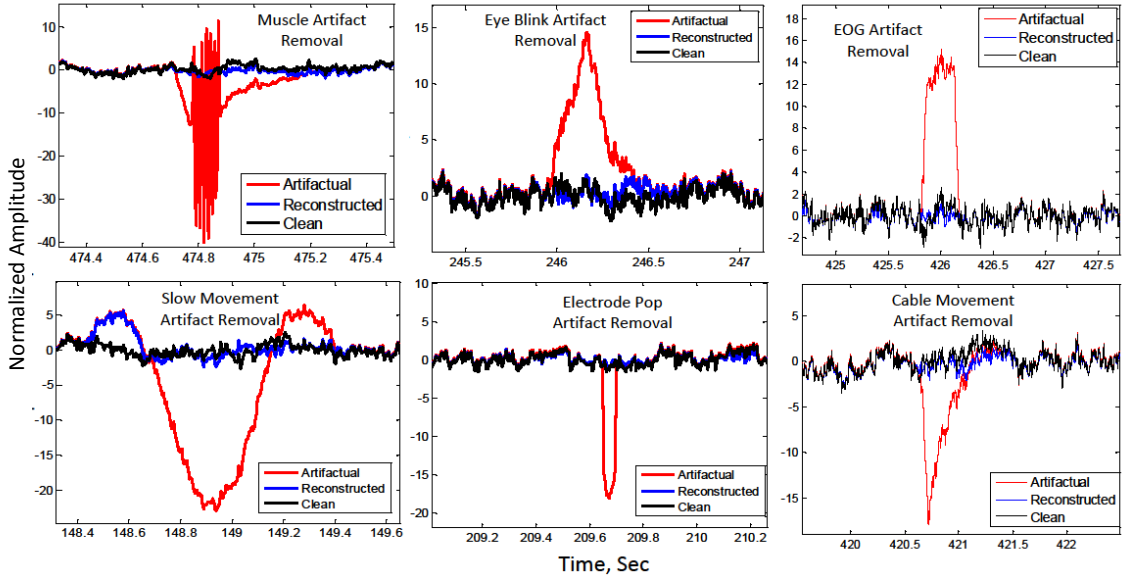


Figure 6.7: Six types of different simulated artifacts that mimicking real artifacts found in the typical scalp EEG recording environments. The application of proposed artifact removal algorithm can almost successfully remove such artifacts most of the time without distorting the background EEG signals. The black, red and blue traces denoting reference, artifactual and reconstructed simulated EEG data respectively.

#### 6.5.2.1 Artifact Removal

As discussed in Section 6.4, we have calculated several time and frequency domain metrics to quantify both amount of artifacts removed as well as amount of distortion made with respect to both amount and intensity of artifacts present in the data. Figure 6.9 shows the calculated  $SNDR$  over the entire frequency bandwidth of EEG data for fully simulated data sequence as in Figure 6.6 before and after artifacts are removed. It is clearly seen that a significant improvement of  $SNDR$  on an average of 5-10 dB over the entire frequency is made due to artifact removal which proves the efficacy of the proposed algorithm. Figure 6.8 shows the amount of artifact removal for those epochs that exceed the probability threshold set manually

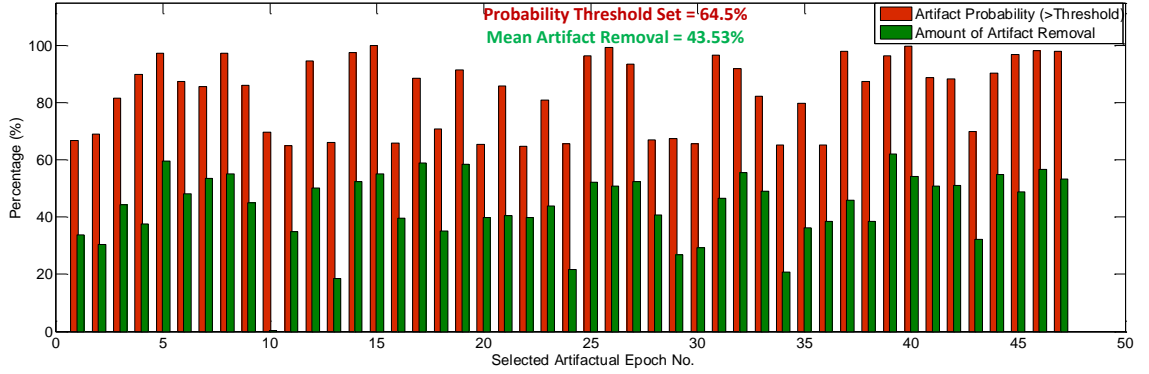


Figure 6.8: Selected epochs with probability more than threshold for artifact correction and their corresponding amount of artifact removal in %.

as  $1.5 * RMS(Pr)$  (i.e. 0.645 and the corresponding artifact probability which shows that the average artifact removal is 43.53% and thus it's a reasonable removal performance.

Table 5.4 presents the quantitative metrics of artifact removal with respect to the strength of artifacts, i.e. different artifact SNR  $SNR_{Art}$  and different artifact duration  $\Delta T_{Art}$ . The upper part (i.e. row) of the table represents the quantitative values without considering the set probability threshold while the lower row represents after considering the probability mapping and its probability threshold.

### 6.5.2.2 Comparison with Other Methods

We have compared the performance our proposed method with few state-of-the-art artifact removal methods (i.e. wavelet-BSS and EMD-BSS based methods) in terms of both quantitative removal metrics (Figure 6.10) and computational time (Figure 6.11) to roughly illustrate a comparison the efficacy of our method compared with others. The process flow of wavelet-

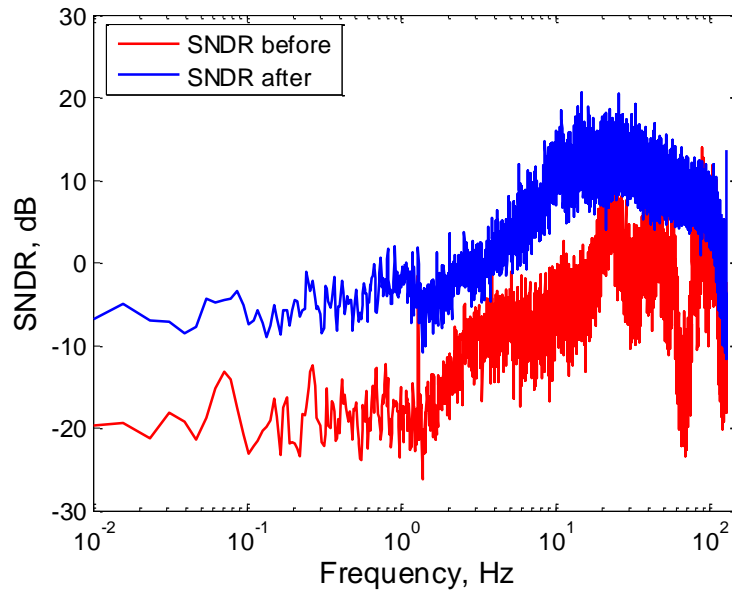


Figure 6.9: SNDR improvement in frequency domain for signals before and after artifact removal.

BSS and EMD-BSS based methods is shown in Figure 3.6 from chapter 3.

One of the very few limitations of the proposed method is that its low  $\lambda$  which suggests that it cannot remove all the artifacts at all time. However, still it achieves better performance compared to others not only in amount of artifact removal but also in signal quality improvement. Another limitation of the proposed method in its current form is that the algorithm can only process offline. But for real BCI application, it requires online data processing, which can be achieved through automated threshold parameter selection during decision making for denoising from artifact probability map achieved in the first stage of the proposed method.



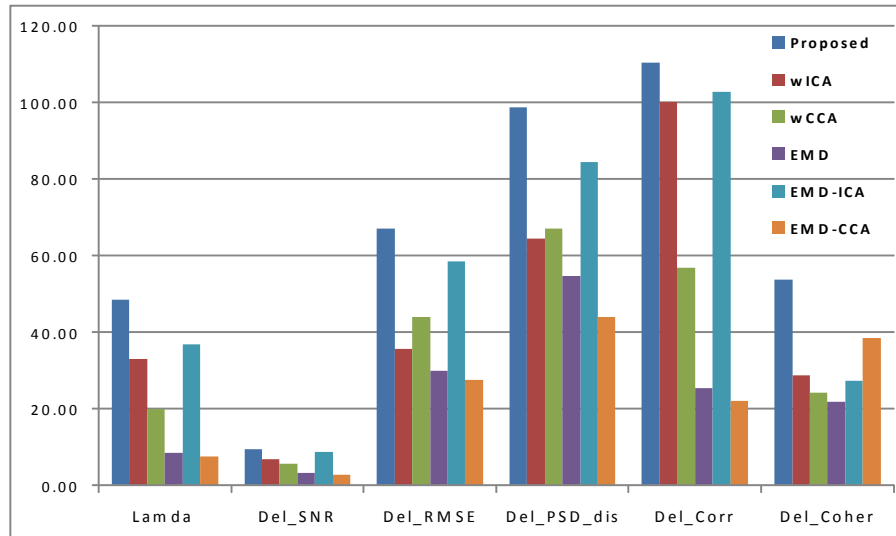


Figure 6.10: Comparison of proposed method with respect to few available artifact removal methods in terms of the quantitative metrics.

### 6.5.2.3 BCI Performance

During BCI experiments or applications, artifacts can modify or alter the shape of a neurological event (e.g. ERP) that drives the BCI system. Moreover, they can also mistakenly result in an unintentional control of the device and hence consequence in a false positive [108]. Therefore, there is a strong urge to avoid the artifacts if possible, otherwise they must be identified in order to reject or remove them from the neural signals to be analyzed or processed for the use of BCI system/device. In a self-paced BCI system, artifacts can negatively influence the performance of the system in following two ways:

- by altering the shape of the neural event during an intentional control (IC) period, resulting in the reduction of True Positives
- by imitating the shape/properties of the neural event during a non-

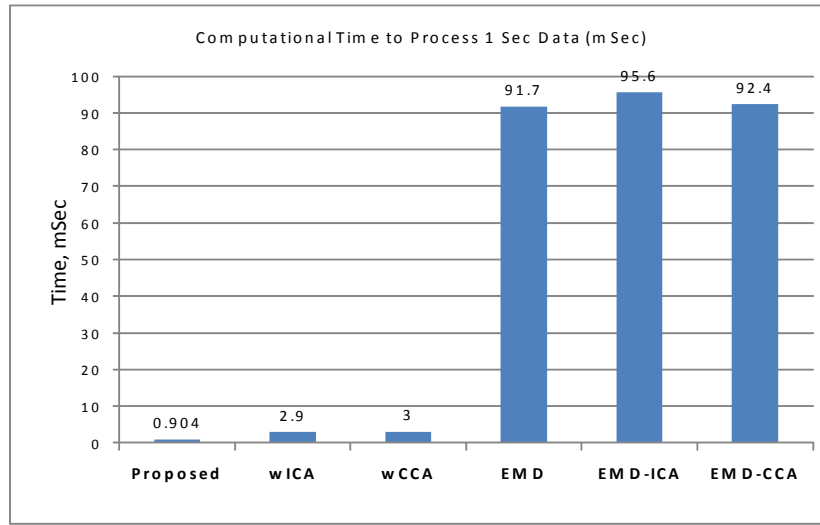


Figure 6.11: Comparison of proposed method with respect to few available artifact removal methods in terms of the computational time required to process each 1 second of data in MATLAB simulation.

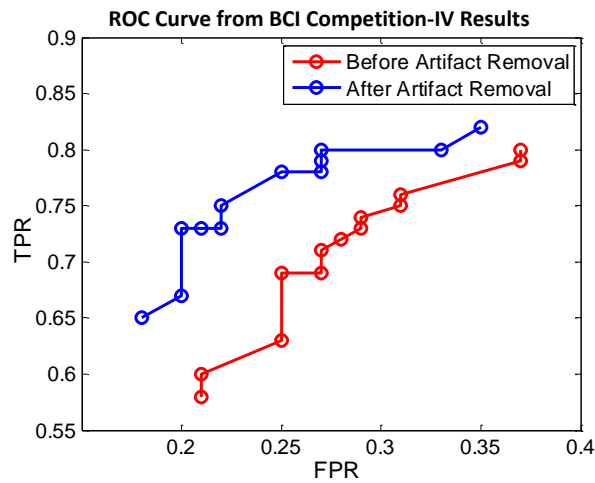


Figure 6.12: ROC curve plotted for signals before and after artifact removal from the BCI output using LDA Classifier and Windowed Means as features from BCILAB tool.

intentional control (NC) periods, resulting in the increase of False Positives.

We have used BCILAB [175] which is a open source toolbox compatible with EEGLAB [176] for BCI performance evaluation. The BCI-IV com-

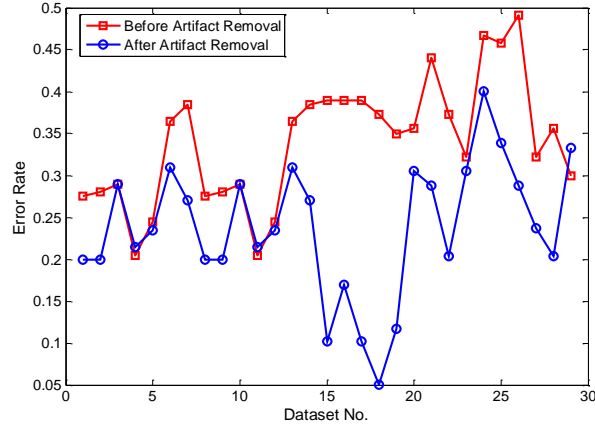


Figure 6.13: Error Rate for signals before and after artifact removal from the BCI output using LDA Classifier and Windowed Means as features from BCILAB tool.

Table 6.3: Quantitative metrics of artifact removal results for corresponding artifact SNR ( $SNR_{Art}$ ) and artifact duration ratio ( $T_{Art}(\%)$ ) for two different cases: one is without considering probability mapping and the other is after considering probability mapping.

$SNR_{Art}$ (dB)	$T_{Art}(\%)$	$\Lambda$ (%)	$\Delta SNR$ (dB)	$\Delta RMSE$ (%)	$\Delta PSD_{dis}$ (%)	$\Delta Corr$ (%)	$\Delta Coh$ (%)	$\Delta SNDR$ (dB)
11.39 (1.95)	20.15 (3.66)	43.37 (8.09)	12.85 (1.53)	76.87 (4.21)	96.64 (0.05)	126.88 (39.89)	51.45 (20.51)	11.26 (1.84)
$SNR_{Art}$ (dB)	$T_{Art}(\%)$	$\Lambda$ (%)	$\Delta SNR$ (dB)	$\Delta RMSE$ (%)	$\Delta PSD_{dis}$ (%)	$\Delta Corr$ (%)	$\Delta Coh$ (%)	$\Delta SNDR$ (dB)
15.93 (2.17)	14.06 (2.39)	48.45 (6.88)	14.84 (1.67)	81.77 (3.57)	99.85 (0.14)	109.73 (34.82)	8.22 (4.79)	16.54 (1.58)

petition dataset (motor-imagery experimental BCI) was used to observe the classification results for both before and after artifact removal signals. Windowed means features with LDA classifier is used for such evaluation. The test results (by the model after training the classifier with some selective epochs) from whole data is shown in terms of both ROC curve in Figure 6.12 and error rate in Figure 6.13 suggest that BCI classifier outputs get better after artifact removal is applied and hence it can be used to improve the BCI experience for the users.

## 6.6 Conclusions

The presented probability mapping of artifact for each EEG epoch will allow the user to choose whether to denoise any epoch or not and hence providing the flexibility in artifact handling for different BCI applications. Also the use of wavelet transform in artifact removal provides the use of single-channel BCI applications that has recently been popular [177, 178, 179] and also eliminate the requirement of a reference artifact channel. The scope of employing the proposed artifact removal for both ERP-based and MI-based BCI application is another advantage of this presented work. The quantitative results proof that it can not only remove artifacts satisfactory but also improves the BCI performance significantly. Although the current method has been tested for offline analysis, but since it is consistent with the typical epoch-by-epoch handling of BCI processing, we expect this method to be able to implement online after necessary modification.

## 6.7 Tuning of Parameter $K$ for MI-BCI

### Application

The tuning of parameter  $k_A$  depends on the data distribution of  $A_5$  epoch which contains both the  $\delta$  wave, ocular artifacts and some low-frequency artifacts (mostly large amplitude slow movement artifacts). This coefficient is usually irrelevant for MI-based BCI applications, so when the histogram

of the data has large deviation from its standard deviation (large tail on the histogram on either one side or both), it is more likely due to presence of such artifacts. Therefore a value less than 1 is chosen for  $k_A$  and if there is no such unusual tail present, then  $k_A = 1$  is chosen that makes the threshold exactly same as the original universal threshold, i.e.  $T'_i = T_1$ .

The criterion for the choice of  $k_A$  is given below

$$k_A = \begin{cases} 0 \leq k_A < 1 & \text{if } \max(|A_5|) > m \times sd(A_5), \\ 1 & \text{otherwise,} \end{cases} \quad (6.15)$$

where  $sd$  denotes the standard deviation of  $A_5$ . The value of  $m$  is based on the parameter tuning and can be obtained from some initial several seconds of incoming raw *EEG* data samples to update the threshold value. From the empirical studies, the value of  $m$  is found as minimum of 2, i.e.  $2 < m < \infty$  (See Chapter-4 under sub-section 4.7.2).

In order to calculate the value of  $k_D$ , *Decision* stage helps. Since  $D_1$  contains higher frequency activities (see Table 6.1), while  $D_2$  and  $D_5$  contain gamma and theta frequency bands respectively but they don't affect much on the MI-based BCI study; therefore value of  $k_D$  for first detail coefficient  $D_1$  is selected as 0.5 – 0.75, while for  $D_2$  and  $D_5$  it is selected as 0.75 – 0.9. For rest of the detail coefficients, (i.e.  $D_3$  -  $D_4$ ) the value is chosen as 1 i.e. same as universal threshold.

$$k_D = \begin{cases} 0.5 < k_i \leq 0.75 & i = 1 \\ 0.75 & i = 2, 5 \\ 1 & i = 3, 4 \end{cases} \quad (6.16)$$

## Chapter 7

# Conclusion and Future Work

This chapter summarizes the overall contribution of this thesis and highlights their significances in neural information processing system. In addition we also present the future prospect of this work.

### 7.1 Contributions

This study explored one of the major problems in neural signal preprocessing: artifact detection and removal. Two contributions were made by studying and characterizing the artifact for *in-vivo* neural data for the first time along with an intensive literature review of existing EEG artifact removal methods/algorithms with detailed comparative analysis from several points of view. A synthesized database with several artifact templates has been generated and made available online for quantitative performance evaluation of any artifact removal method. Then three separate artifact removal algorithms are proposed for three different application purposes:

*in-vivo* neural signal analysis and processing, epilepsy seizure detection and BCI studies. All three algorithms have been evaluated with several quantitative metrics and compared with some of the available state-of-the-art methods. The results suggest that in every case, the proposed algorithms outperform their respective competing algorithms with an obvious margin most of the times. In addition, the after-effect of artifact removal from neural signals on the later-stage signal analysis is also measured quantitatively and found to achieve substantial improvement in all three cases. Thus this work is expected to be useful for neural signal processing and analysis community in the long run and will provide platform to further improve the understanding of our brain for different applications, both in clinical and non-clinical applications.

## 7.2 Future Works

The work presented in this thesis can be further continued and improved in future in different ways. Here, we suggest some of the possible directions and potential approaches for future works which could be useful for further improvements.



## 7.2.1 Improvements on Current Work

### 7.2.1.1 Artifact Removal from *In-Vivo* Neural Signals

Artifact removal algorithm for *in-vivo* neural recordings requires further improvement to be able to implement on hardware for real-time applications e.g. spike detection and sorting on the fly. The rooms for improvement are discussed below:

- Automatic Parameter Adaptation: The algorithm should be able to adapt its parameters automatically and that may require having some training data. Once the training of the system is completed, the algorithm should tune the parameters according to incoming input signals and to different recording conditions.
- Complexity Reduction and Optimization of Algorithm: The complexity of the algorithm should be further reduced in order to be able to perform online signal processing. After extensive validation with more real neural recordings, some parameters can be hard-coded like a look-up table if possible and necessary.
- Hardware Implementation: The algorithm must be optimized further for hardware efficient design during implementing in an ASIC. Due to the invasive nature of the recording, the recorder must be worn by the subject which demand on-chip signal processing in real time. Therefore the digital signal processing algorithm here is not feasible

to be implemented in FPGA or DSP chip, it must be implemented in an ASIC. This would require several stages of algorithm optimization before hardware implementation. Once ASIC is done, measurement results followed by animal experiments need to be performed in near future.

#### **7.2.1.2 Artifact Removal from EEG**

The other two artifact removal algorithms for scalp EEG also has room for further improvement for real-life applications.

- Online Processing: For obvious reasons during seizure detection or BCI applications in real-life, the signal must be processed in real-time which also demand the artifact removal algorithm to be online. However, if the number of channels of EEG recorder increases, the complexity of the algorithm also increases linearly. Therefore, further attempt to reduce the algorithm complexity in terms of wavelet filter implementation must be considered seriously.
- Validation with Patient/User Data: In order to tune the threshold parameters properly during seizure detection applications, experiments should be performed to get more real long-term EEG data from several patients so that decision can be made whether the algorithm is patient-specific or can be termed general. Our group is in collaboration with few epilepsy experts (i.e. clinicians) and we expect to get some patient data from them. We expect to validate our algo-

rithm and further tune its parameters by applying on those datasets.

The same applies to BCI experiments also that we require recording more EEG from different BCI paradigms from different users to validate our proposed algorithm-3.

- Further Optimization and Tuning: Both the algorithms for EEG artifact removal require further optimization for best performance and automatic tuning of parameters for online processing. A stage of automatic parameter tuning can be included in the algorithm architecture according to application's requirement. Although the added stage would increase computational cost but it will be worth if the algorithm is to be used by a non-expert or for general purpose applications.

## 7.2.2 Other Possible Applications of Current Work

In addition to the improvement of current work; similar idea of artifact removal by wavelet-denoising along with utilizing the known signal characteristics, can be applied with some modification on other biomedical signal processing/analysis application areas. The signal of interest could be either neural or non-neural biomedical signals.

### 7.2.2.1 Neural Signals

- Artifact removal from ECoG/iEEG and sub-scalp EEG data for epilepsy seizure monitoring

- Motion artifact removal from Ambulatory EEG
- Metallic interferences and artifact removal from MEG
- Artifact removal from peripheral nerve recordings for neural prostheses applications.
- Stimulation artifact removal from DBS or any other stimulation during simultaneous neural recording and stimulation.

#### **7.2.2.2 Non-Neural Biomedical Signals**

- Artifact removal from ambulatory ECG or PCG for wearable health-care monitoring applications.

#### **7.2.2.3 Software GUI for Complete Solution**

A software GUI is possible to develop like the kinds of EEGLAB or BCILAB and make it available in online for free as a part of neuroinformatics tools initiative taken by International Neuroinformatics Coordinating Facility (INCF). Two types of software tool can be developed as follows:

- Signal-specific artifact removal from neural signals (e.g. intracortical/*in-vivo*, intra-cranial/ECoG, sub-scalp EEG and scalp EEG)
- Application-specific artifact removal (e.g. Seizure detection, mental fatigue detection, BCI applications, Alzheimer diagnosis, sleep studies, depression studies, general neuroscience studies, etc.).

# Bibliography

- [1] Howard Eichenbaum. The hippocampus and declarative memory: cognitive mechanisms and neural codes. *Behavioural brain research*, 127(1):199–207, 2001.
- [2] G Foffani and KA Moxon. Decoding the spatio-temporal localization of behavioral events in populations of neurons. In *Neural Engineering, 2003. Conference Proceedings. First International IEEE EMBS Conference on*, pages 24–27. IEEE, 2003.
- [3] Shun-ichi Amari. Mathematical neuroscience - an overview.
- [4] William W Lytton. *From computer to brain: foundations of computational neuroscience*. Springer Science & Business Media, 2007.
- [5] Partha Mitra and Hemant Bokil. *Observed brain dynamics*. Oxford University Press, 2007.
- [6] György Buzsáki, Costas A Anastassiou, and Christof Koch. The origin of extracellular fields and currents - eeg, ecog, lfp and spikes. *Nature reviews neuroscience*, 13(6):407–420, 2012.

- [7] Md Kafiul Islam, Amir Rastegarnia, Anh Tuan Nguyen, and Zhi Yang. Artifact characterization and removal for in vivo neural recording. *Journal of neuroscience methods*, 226:110–123, 2014.
- [8] Farzaneh Shahrokhi, Karim Abdelhalim, Demitre Serletis, Peter L Carlen, and Roman Genov. The 128-channel fully differential digital integrated neural recording and stimulation interface. *Biomedical Circuits and Systems, IEEE Transactions on*, 4(3):149–161, 2010.
- [9] [online]. available. <http://en.wikipedia.org/wiki/Electrophysiological>.
- [10] David H Hubel and Torsten N Wiesel. Receptive fields of single neurons in the cat's striate cortex. *The Journal of physiology*, 148(3):574–591, 1959.
- [11] David H Hubel and Torsten N Wiesel. Receptive fields, binocular interaction and functional architecture in the cat's visual cortex. *The Journal of physiology*, 160(1):106, 1962.
- [12] [online]. available. [http://en.wikipedia.org/wiki/Action\\_potential](http://en.wikipedia.org/wiki/Action_potential).
- [13] [online]. available. <https://en.wikipedia.org/wiki/Electroencephalography>.
- [14] [online]. available. <http://www.mayoclinic.org/>

[tests-procedures/EEG/multimedia/EEG-brain-activity/img-20005915.](#)

- [15] M Ungureanu, C Bigan, R Strungaru, and V Lazarescu. Independent component analysis applied in biomedical signal processing. *Measurement Science Review*, 4(2):18, 2004.
- [16] Arthur Flexer, Herbert Bauer, Jürgen Pripfl, and Georg Dorffner. Using ica for removal of ocular artifacts in eeg recorded from blind subjects. *Neural Networks*, 18(7):998–1005, 2005.
- [17] Irene Winkler, Stefan Haufe, and Michael Tangermann. Automatic classification of artifactual ica-components for artifact removal in eeg signals. *Behavioral and Brain Functions*, 7(1):30, 2011.
- [18] Arnaud Delorme, Terrence Sejnowski, and Scott Makeig. Enhanced detection of artifacts in eeg data using higher-order statistics and independent component analysis. *Neuroimage*, 34(4):1443–1449, 2007.
- [19] Carlos Guerrero-Mosquera and Angel Navia-Vázquez. Automatic removal of ocular artefacts using adaptive filtering and independent component analysis for electroencephalogram data. *IET signal processing*, 6(2):99–106, 2012.
- [20] Antti Savelainen. An introduction to eeg artifacts. *Aalto University School of Science: Systems Analysis Laboratory*, 20, 2010.

- [21] Bill Scott. Developments in eeg analysis, protocol selection, and feedback delivery. *Journal of Neurotherapy*, 15(3):262–267, 2011.
- [22] Lihong Zhang, Dingyun Wu, and Lianhe Zhi. Method of removing noise from eeg signals based on hht method. In *Information Science and Engineering (ICISE), 2009 1st International Conference on*, pages 596–599. IEEE, 2009.
- [23] Yan Long Wang, Jin Hua Liu, and Yuan Chun Liu. Automatic removal of ocular artifacts from electroencephalogram using hilbert-huang transform. In *Bioinformatics and Biomedical Engineering, 2008. ICBBE 2008. The 2nd International Conference on*, pages 2138–2141. IEEE, 2008.
- [24] Behnam Molavi and Guy A Dumont. Wavelet-based motion artifact removal for functional near-infrared spectroscopy. *Physiological measurement*, 33(2):259, 2012.
- [25] Frances C Robertson, Tania S Douglas, and Ernesta M Meintjes. Motion artifact removal for functional near infrared spectroscopy: a comparison of methods. *Biomedical Engineering, IEEE Transactions on*, 57(6):1377–1387, 2010.
- [26] Xinyi Yong, Mehrdad Fatourehchi, Rabab K Ward, and Gary E Birch. Automatic artefact removal in a self-paced hybrid brain-computer interface system. *Journal of neuroengineering and rehabilitation*, 9(1):50, 2012.



- [27] Md Khademul Islam Molla, Md Rabiul Islam, Toshihisa Tanaka, and Tomasz M Rutkowski. Artifact suppression from eeg signals using data adaptive time domain filtering. *Neurocomputing*, 97:297–308, 2012.
- [28] Ivan Gligorijevic, Marleen Welkenhuysen, Dimitar Prodanov, Silke Musa, Bart Nuttin, Wolfgang Eberle, Carmen Bartic, and Sabine Van Huffel. Neural signal analysis and artifact removal in single and multichannel in-vivo deep brain recordings. In *in Proc. of 4th Annual Symposium of the IEEE-EMBS Benelux Chapter (IEEE-EMBS)*, pages 79–82, 2009.
- [29] George J Tomko and Donald R Crapper. Neuronal variability: non-stationary responses to identical visual stimuli. *Brain research*, 79(3):405–418, 1974.
- [30] Michael S Lewicki. A review of methods for spike sorting: the detection and classification of neural action potentials. *Network: Computation in Neural Systems*, 9(4):R53–R78, 1998.
- [31] Hidekazu Kaneko, Hiroshi Tamura, and Shinya S Suzuki. Tracking spike-amplitude changes to improve the quality of multineuronal data analysis. *Biomedical Engineering, IEEE Transactions on*, 54(2):262–272, 2007.
- [32] Aharon Bar-Hillel, Adam Spiro, and Eran Stark. Spike sorting:

- Bayesian clustering of non-stationary data. *Journal of neuroscience methods*, 157(2):303–316, 2006.
- [33] Kevin T Sweeney, Sean F McLoone, and Tomas E Ward. The use of ensemble empirical mode decomposition with canonical correlation analysis as a novel artifact removal technique. *Biomedical Engineering, IEEE Transactions on*, 60(1):97–105, 2013.
- [34] Doha Safieddine, Amar Kachenoura, Laurent Albera, Gwénaél Birot, Ahmad Karfoul, Anca Pasnicu, Arnaud Biraben, Fabrice Wendling, Lotfi Senhadji, and Isabelle Merlet. Removal of muscle artifact from eeg data: comparison between stochastic (ica and cca) and deterministic (emd and wavelet-based) approaches. *EURASIP Journal on Advances in Signal Processing*, 2012(1):1–15, 2012.
- [35] BS Raghavendra and D Narayana Dutt. Wavelet enhanced cca for minimization of ocular and muscle artifacts in eeg. *World Academy of Science, Engineering and Technology*, 57(6):1027–32, 2011.
- [36] Chunyu Zhao and Tianshuang Qiu. An automatic ocular artifacts removal method based on wavelet-enhanced canonical correlation analysis. In *Engineering in Medicine and Biology Society, EMBC, 2011 Annual International Conference of the IEEE*, pages 4191–4194. IEEE, 2011.
- [37] Yiwen Wang, Justin C Sanchez, Jose C Principe, Jeremiah D Mitzelfelt, and Aysegul Gunduz. Analysis of the correlation between

- local field potentials and neuronal firing rate in the motor cortex. In *Engineering in Medicine and Biology Society, 2006. EMBS. 28th Annual International Conference of the IEEE*, pages 6185–6188. IEEE, 2006.
- [38] Nazareth P Castellanos and Valeri A Makarov. Recovering eeg brain signals: artifact suppression with wavelet enhanced independent component analysis. *Journal of neuroscience methods*, 158(2):300–312, 2006.
- [39] M Zima, P Tichavský, K Paul, and V Krajča. Robust removal of short-duration artifacts in long neonatal eeg recordings using wavelet-enhanced ica and adaptive combining of tentative reconstructions. *Physiological measurement*, 33(8):N39, 2012.
- [40] Wei-Yen Hsu, Chao-Hung Lin, Hsien-Jen Hsu, Po-Hsun Chen, and I-Ru Chen. Wavelet-based envelope features with automatic eeg artifact removal: Application to single-trial eeg data. *Expert Systems with Applications*, 39(3):2743–2749, 2012.
- [41] Rui Fonseca-Pinto. *A new tool for nonstationary and nonlinear signals: The Hilbert-Huang Transform in biomedical applications*. INTECH Open Access Publisher, 2011.
- [42] Robert Leeb, Felix Lee, Claudia Keinrath, Reinhold Scherer, Horst Bischof, and Gert Pfurtscheller. Brain–computer communication:

- motivation, aim, and impact of exploring a virtual apartment. *Neural Systems and Rehabilitation Engineering, IEEE Transactions on*, 15(4):473–482, 2007.
- [43] Benjamin Blankertz, Guido Dornhege, Matthias Krauledat, Klaus-Robert Müller, and Gabriel Curio. The non-invasive berlin brain-computer interface: fast acquisition of effective performance in untrained subjects. *NeuroImage*, 37(2):539–550, 2007.
- [44] Antti Savelainen. *Movement artifact detection from electroencephalogram utilizing accelerometer*. PhD thesis, Citeseer, 2011.
- [45] Jozsef Csicsvari, Darrell A Henze, Brian Jamieson, Kenneth D Harris, Anton Sirota, Péter Barthó, Kensall D Wise, and György Buzsáki. Massively parallel recording of unit and local field potentials with silicon-based electrodes. *Journal of neurophysiology*, 90(2):1314–1323, 2003.
- [46] Bruce L Cathie. *The Harmonic Conquest of Space*. Aware Journalism, 1995.
- [47] [online]. available. <http://www.plexon.com/products/plexon-systems>.
- [48] EW Keefer, BR Botterman, MI Romero, AF Rossi, and GW Gross. Carbon nanotube-coated electrodes improve brain readouts. *Nat Nanotech*, 3:434–439, 2008.

- [49] Md Islam, Nguyen Anh Tuan, Yin Zhou, Zhi Yang, et al. Analysis and processing of in-vivo neural signal for artifact detection and removal. In *Biomedical Engineering and Informatics (BMEI), 2012 5th International Conference on*, pages 437–442. IEEE, 2012.
- [50] Jian Xu, Md Islam, Shuo Wang, Zhi Yang, et al. A  $13\mu\text{w}$  87db dynamic range implantable  $\delta\sigma$  modulator for full-spectrum neural recording. In *Engineering in Medicine and Biology Society (EMBC), 2013 35th Annual International Conference of the IEEE*, pages 2764–2767. IEEE, 2013.
- [51] Kevin Sweeney. *Motion Artifact Processing Techniques for Physiological Signals*. PhD thesis, National University of Ireland Maynooth, 2013.
- [52] Gregory L Holmes, Solomon L Moshé, and H Royden Jones. *Clinical neurophysiology of infancy, childhood, and adolescence*. Butterworth-Heinemann, 2005.
- [53] Udaya Seneviratne, Armin Mohamed, Mark Cook, and Wendyl D’Souza. The utility of ambulatory electroencephalography in routine clinical practice: A critical review. *Epilepsy research*, 105(1):1–12, 2013.
- [54] Bernard S Chang, Steven C Schachter, and Donald L Schomer. *Atlas of ambulatory EEG*. Academic Press, 2005.

- [55] Simon H ORegan. Artefact detection and removal algorithms for eeg diagnostic systems. 2013.
- [56] Andrea Mognon, Jorge Jovicich, Lorenzo Bruzzone, and Marco Buiatti. Adjust: An automatic eeg artifact detector based on the joint use of spatial and temporal features. *Psychophysiology*, 48(2):229–240, 2011.
- [57] Vitaly Schetinin and Joachim Schult. The combined technique for detection of artifacts in clinical electroencephalograms of sleeping newborns. *Information Technology in Biomedicine, IEEE Transactions on*, 8(1):28–35, 2004.
- [58] Christiaan Burger and David Jacobus van den Heever. Removal of eeg artefacts by combining wavelet neural network and independent component analysis. *Biomedical Signal Processing and Control*, 15:67–79, 2015.
- [59] Aysa Jafarifarmand and Mohammad Ali Badamchizadeh. Artifacts removal in eeg signal using a new neural network enhanced adaptive filter. *Neurocomputing*, 103:222–231, 2013.
- [60] Jing Hu, Chun-sheng Wang, Min Wu, Yu-xiao Du, Yong He, and Jinhua She. Removal of eeg and emg artifacts from eeg using combination of functional link neural network and adaptive neural fuzzy inference system. *Neurocomputing*, 151:278–287, 2015.

- [61] Simon O'Regan, Stephen Faul, and William Marnane. Automatic detection of eeg artefacts arising from head movements using eeg and gyroscope signals. *Medical engineering physics*, 35(7):867–874, 2013.
- [62] Vernon Lawhern, W David Hairston, Kaleb McDowell, Marissa Westerfield, and Kay Robbins. Detection and classification of subject-generated artifacts in eeg signals using autoregressive models. *Journal of neuroscience methods*, 208(2):181–189, 2012.
- [63] Sourya Bhattacharyya, Arunava Biswas, Jayanta Mukherjee, Arun Kumar Majumdar, Bandana Majumdar, Suchandra Mukherjee, and Arun Kumar Singh. Detection of artifacts from high energy bursts in neonatal eeg. *Computers in biology and medicine*, 43(11):1804–1814, 2013.
- [64] Leor Shoker, Saeid Sanei, and Jonathon Chambers. Artifact removal from electroencephalograms using a hybrid bss-svm algorithm. *Signal Processing Letters, IEEE*, 12(10):721–724, 2005.
- [65] Shi-Yun Shao, Kai-Quan Shen, Chong Jin Ong, Einar PV Wilder-Smith, and Xiao-Ping Li. Automatic eeg artifact removal: a weighted support vector machine approach with error correction. *Biomedical Engineering, IEEE Transactions on*, 56(2):336–344, 2009.
- [66] Hong Zeng, Aiguo Song, Ruqiang Yan, and Hongyun Qin. Eeg artifact correction from eeg recording using stationary subspace analysis

- and empirical mode decomposition. *Sensors*, 13(11):14839–14859, 2013.
- [67] Yandong Li, Zhongwei Ma, Wenkai Lu, and Yanda Li. Automatic removal of the eye blink artifact from eeg using an ica-based template matching approach. *Physiological measurement*, 27(4):425, 2006.
- [68] Manousos A Klados, Christos Papadelis, Christoph Braun, and Panagiotis D Bamidis. Reg-ica: A hybrid methodology combining blind source separation and regression techniques for the rejection of ocular artifacts. *Biomedical Signal Processing and Control*, 6(3):291–300, 2011.
- [69] Vandana Roy and Shailja Shukla. Automatic removal of artifacts from eeg signal based on spatially constrained ica using daubechies wavelet. *International Journal of Modern Education and Computer Science (IJMECS)*, 6(7):31, 2014.
- [70] Muhammad Tahir Akhtar, Wataru Mitsuhashi, and Christopher J James. Employing spatially constrained ica and wavelet denoising, for automatic removal of artifacts from multichannel eeg data. *Signal Processing*, 92(2):401–416, 2012.
- [71] Christopher J James and Oliver J Gibson. Temporally constrained ica: an application to artifact rejection in electromagnetic brain signal analysis. *Biomedical Engineering, IEEE Transactions on*, 50(9):1108–1116, 2003.



- [72] Xinyi Yong, Rabab K Ward, and Gary E Birch. Artifact removal in eeg using morphological component analysis. In *Acoustics, Speech and Signal Processing, 2009. ICASSP 2009. IEEE International Conference on*, pages 345–348. IEEE, 2009.
- [73] Xinyi Yong, Rabab K Ward, and Gary E Birch. Generalized morphological component analysis for eeg source separation and artifact removal. In *Neural Engineering, 2009. NER. 4th International IEEE/EMBS Conference on*, pages 343–346. IEEE, 2009.
- [74] [online]. available. [http://commons.wikimedia.org/wiki/File:Wavelets\\_-\\_SWT\\_Filter\\_Bank.png#/media/File:Wavelets\\_-\\_SWT\\_Filter\\_Bank.png](http://commons.wikimedia.org/wiki/File:Wavelets_-_SWT_Filter_Bank.png#/media/File:Wavelets_-_SWT_Filter_Bank.png).
- [75] Luke Rankine, Nathan Stevenson, Mostefa Mesbah, and Boualem Boashash. A nonstationary model of newborn eeg. *Biomedical Engineering, IEEE Transactions on*, 54(1):19–28, 2007.
- [76] N Stevenson, L Rankine, M Mesbah, and B Boashash. Newborn eeg seizure simulation using time-frequency signal synthesis. In *Proc. APRS Workshop on Digital Image Computing*, pages 145–151, 2005.
- [77] Borna Nouredin, Peter D Lawrence, and Gary E Birch. Time-frequency analysis of eye blinks and saccades in eeg for eeg artifact removal. In *Neural Engineering, 2007. CNE. 3rd International IEEE/EMBS Conference on*, pages 564–567. IEEE, 2007.

- [78] Stephane Mallat. *A wavelet tour of signal processing: the sparse way*. Academic press, 2008.
- [79] Md Rashed-Al-Mahfuz, Md Rabiul Islam, Keikichi Hirose, and Md Khademul Islam Molla. Artifact suppression and analysis of brain activities with electroencephalography signals. *Neural regeneration research*, 8(16):1500, 2013.
- [80] J Gerardo Avalos, Jose Velazquez, and Juan C Sanchez. *Applications of Adaptive Filtering*. INTECH Open Access Publisher, 2011.
- [81] Samuel D Stearns. *Adaptive signal processing*. Prentice Hall, 1985.
- [82] Kevin T Sweeney, Tomás E Ward, and Seán F McLoone. Artifact removal in physiological signals practices and possibilities. *Information Technology in Biomedicine, IEEE Transactions on*, 16(3):488–500, 2012.
- [83] Mike X Cohen. *Analyzing neural time series data: theory and practice*. MIT Press, 2014.
- [84] Arjon Turnip. Automatic artifacts removal of eeg signals using robust principal component analysis. In *Technology, Informatics, Management, Engineering, and Environment (TIME-E), 2014 2nd International Conference on*, pages 331–334. IEEE, 2014.
- [85] Arjon Turnip and Edy Junaidi. Removal artifacts from eeg signal using independent component analysis and principal component analysis.

- sis. In *Technology, Informatics, Management, Engineering, and Environment (TIME-E), 2014 2nd International Conference on*, pages 296–302. IEEE, 2014.
- [86] Rashima Mahajan, Bashir Morshed, et al. Unsupervised eye blink artifact denoising of eeg data with modified multiscale sample entropy, kurtosis, and wavelet-ica. *Biomedical and Health Informatics, IEEE Journal of*, 19(1):158–165, 2015.
- [87] Mehdi Bagheri Hamaneh, Numthip Chitravas, Kitti Kaiboriboon, Samden D Lhatoo, Kenneth Loparo, et al. Automated removal of ekg artifact from eeg data using independent component analysis and continuous wavelet transformation. *Biomedical Engineering, IEEE Transactions on*, 61(6):1634–1641, 2014.
- [88] Nadia Mammone and Francesco C Morabito. Enhanced automatic wavelet independent component analysis for electroencephalographic artifact removal. *Entropy*, 16(12):6553–6572, 2014.
- [89] Salvatore Calcagno, Fabio La Foresta, and Mario Versaci. Independent component analysis and discrete wavelet transform for artifact removal in biomedical signal processing. *American Journal of Applied Sciences*, 11(1):57, 2014.
- [90] Valentina Bono, Wasifa Jamal, Saptarshi Das, and Koushik Maharatna. Artifact reduction in multichannel pervasive eeg using hybrid wpt-ica and wpt-emd signal decomposition techniques. In *Acous-*

- tics, Speech and Signal Processing (ICASSP), 2014 IEEE International Conference on*, pages 5864–5868. IEEE, 2014.
- [91] Xun Chen, Chen He, and Hu Peng. Removal of muscle artifacts from single-channel eeg based on ensemble empirical mode decomposition and multiset canonical correlation analysis. *Journal of Applied Mathematics*, 2014, 2014.
- [92] ZhenYu Wang, Peng Xu, TieJun Liu, Yin Tian, Xu Lei, and DeZhong Yao. Robust removal of ocular artifacts by combining independent component analysis and system identification. *Biomedical Signal Processing and Control*, 10:250–259, 2014.
- [93] Hoang-Anh T Nguyen, John Musson, Feng Li, Wei Wang, Guangfan Zhang, Roger Xu, Carl Richey, Tom Schnell, Frederic D McKenzie, and Jiang Li. Eog artifact removal using a wavelet neural network. *Neurocomputing*, 97:374–389, 2012.
- [94] Hong Peng, Bin Hu, Qiuxia Shi, Martyn Ratcliffe, Qinglin Zhao, Yanbing Qi, and Guoping Gao. Removal of ocular artifacts in eegan improved approach combining dwt and anc for portable applications. *Biomedical and Health Informatics, IEEE Journal of*, 17(3):600–607, 2013.
- [95] Xavier Navarro, Fabienne Porée, and Guy Carraault. Ecg removal in preterm eeg combining empirical mode decomposition and adaptive

- filtering. In *Acoustics, Speech and Signal Processing (ICASSP), 2012 IEEE International Conference on*, pages 661–664. IEEE, 2012.
- [96] N Nicolaou and Slawomir J Nasuto. Automatic artefact removal from event-related potentials via clustering. *The Journal of VLSI Signal Processing Systems for Signal, Image, and Video Technology*, 48(1-2):173–183, 2007.
- [97] Vojkan Mihajlovic, Shrishail Patki, and Bernard Grundlehner. The impact of head movements on eeg and contact impedance: An adaptive filtering solution for motion artifact reduction. In *Engineering in Medicine and Biology Society (EMBC), 2014 36th Annual International Conference of the IEEE*, pages 5064–5067. IEEE, 2014.
- [98] Wouter Deburchgraeve, PJ Cherian, Maarten De Vos, RM Swarte, JH Blok, GH Visser, P Govaert, and Sabine Van Huffel. Automated ecg artefact reduction in eeg as a preprocessing step for neonatal seizure detection. 2008.
- [99] Borna Nouredin, Peter D Lawrence, and Gary E Birch. Online removal of eye movement and blink eeg artifacts using a high-speed eye tracker. *Biomedical Engineering, IEEE Transactions on*, 59(8):2103–2110, 2012.
- [100] Robert S Fisher, Barbara G Vickrey, Patricia Gibson, Bruce Hermann, Patricia Penovich, Ann Scherer, and Steven Walker. The

- impact of epilepsy from the patients perspective i. descriptions and subjective perceptions. *Epilepsy research*, 41(1):39–51, 2000.
- [101] Ana M Skupch, Peter Dollfuss, F Furbass, Gerhard Gritsch, Manfred M Hartmann, Hannes Perko, Ekaterina Pataraiia, Gerald Lindinger, and Tilmann Kluge. Spatial correlation based artifact detection for automatic seizure detection in eeg. In *Engineering in Medicine and Biology Society (EMBC), 2013 35th Annual International Conference of the IEEE*, pages 1972–1975. IEEE, 2013.
- [102] Irene Winkler, Stephanie Brandl, Franziska Horn, Eric Waldburger, Carsten Allefeld, and Michael Tangermann. Robust artifactual independent component classification for bci practitioners. *Journal of neural engineering*, 11(3):035013, 2014.
- [103] Yao Zou, Viswam Nathan, and Roozbeh Jafari. Automatic identification of artifact-related independent components for artifact removal in eeg recordings. 2014.
- [104] Alexander Bertrand, Vojkan Mihajlovic, Bernard Grundlehner, Chris Van Hoof, and Marc Moonen. Motion artifact reduction in eeg recordings using multi-channel contact impedance measurements. In *Biomedical Circuits and Systems Conference (BioCAS), 2013 IEEE*, pages 258–261. IEEE, 2013.
- [105] Qinglin Zhao, Bin Hu, Yujun Shi, Yang Li, Philip Moore, Minghou Sun, and Hong Peng. Automatic identification and removal of ocular

- artifacts in eeg - improved adaptive predictor filtering for portable applications. *NanoBioscience, IEEE Transactions on*, 13(2):109–117, 2014.
- [106] Joep JM Kierkels, Jamal Riani, Jan WM Bergmans, and Geert JM Van Boxtel. Using an eye tracker for accurate eye movement artifact correction. *Biomedical Engineering, IEEE Transactions on*, 54(7):1256–1267, 2007.
- [107] Joseph T Gwin, Klaus Gramann, Scott Makeig, and Daniel P Ferris. Removal of movement artifact from high-density eeg recorded during walking and running. *Journal of neurophysiology*, 103(6):3526–3534, 2010.
- [108] Theresa M Vaughan, WJ Heetderks, LJ Trejo, WZ Rymer, M Weinrich, MM Moore, A Kübler, BH Dobkin, N Birbaumer, E Donchin, et al. Brain-computer interface technology: a review of the second international meeting. *IEEE transactions on neural systems and rehabilitation engineering: a publication of the IEEE Engineering in Medicine and Biology Society*, 11(2):94–109, 2003.
- [109] Maite Crespo-Garcia, Mercedes Atienza, and Jose L Cantero. Muscle artifact removal from human sleep eeg by using independent component analysis. *Annals of biomedical engineering*, 36(3):467–475, 2008.
- [110] Shayan Motamedi-Fakhr, Mohamed Moshrefi-Torbati, Martyn Hill, Catherine M Hill, and Paul R White. Signal processing techniques

- applied to human sleep eeg signals - a review. *Biomedical Signal Processing and Control*, 10:21–33, 2014.
- [111] Raymundo Cassani, Tiago H Falk, Francisco J Fraga, Paulo AM Kanda, and Renato Anghinah. The effects of automated artifact removal algorithms on electroencephalography-based alzheimer’s disease diagnosis. *Frontiers in aging neuroscience*, 6, 2014.
- [112] Tetsuya Takahashi, Raymond Y Cho, Tomoyuki Mizuno, Mitsuru Kikuchi, Tetsuhito Murata, Koichi Takahashi, and Yuji Wada. Antipsychotics reverse abnormal eeg complexity in drug-naïve schizophrenia: a multiscale entropy analysis. *NeuroImage*, 51(1):173–182, 2010.
- [113] Ian Daly, Rafal Scherer, Martin Billinger, and Gernot Muller-Putz. Force: fully online and automated artifact removal for brain-computer interfacing. 2014.
- [114] H. Nolan, R. Whelan, and R.B. Reilly. Faster: Fully automated statistical thresholding for {EEG} artifact rejection. *Journal of Neuroscience Methods*, 192(1):152 – 162, 2010.
- [115] MM Hartmann, K Schindler, TA Gebbink, G Gritsch, and T Kluge. Pureeeg: Automatic eeg artifact removal for epilepsy monitoring. *Neurophysiologie Clinique/Clinical Neurophysiology*, 44(5):479–490, 2014.



- [116] [online]. available. <http://spc.shirazu.ac.ir/products/Featured-Products/oset/>.
- [117] Germán Gómez-Herrero. Automatic artifact removal (aar) toolbox v1. 3 (release 09.12. 2007) for matlab. *Tampere University of Technology*, 2007.
- [118] Zhi Yang, Wentai Liu, Mohammad Reza Keshtkaran, Yin Zhou, Jian Xu, Victor Pikov, Cuntai Guan, and Yong Lian. A new ec-pc threshold estimation method for in vivo neural spike detection. *Journal of neural engineering*, 9(4):046017, 2012.
- [119] Kevin T Sweeney, Hasan Ayaz, Tomás E Ward, Meltem Izzetoglu, Seán F McLoone, and Banu Onaral. A methodology for validating artifact removal techniques for physiological signals. *Information Technology in Biomedicine, IEEE Transactions on*, 16(5):918–926, 2012.
- [120] Zhi Yang, Qi Zhao, Edward Keefer, and Wentai Liu. Noise characterization, modeling, and reduction for in vivo neural recording. In *Advances in neural information processing systems*, pages 2160–2168, 2009.
- [121] Gregory Beylkin. On the representation of operators in bases of compactly supported wavelets. *SIAM Journal on Numerical Analysis*, 29(6):1716–1740, 1992.

- [122] Hanne Moen. Wavelet transforms and efficient implementation on the gpu. 2007.
- [123] Ronald R Coifman and David L Donoho. *Translation-invariant denoising*. Springer, 1995.
- [124] Hong-Ye Gao. Wavelet shrinkage denoising using the non-negative garrote. *Journal of Computational and Graphical Statistics*, 7(4):469–488, 1998.
- [125] Matthias Mölle, Oxana Yeshenko, Lisa Marshall, Susan J Sara, and Jan Born. Hippocampal sharp wave-ripples linked to slow oscillations in rat slow-wave sleep. *Journal of neurophysiology*, 96(1):62–70, 2006.
- [126] Andrei Belitski, Arthur Gretton, Cesare Magri, Yusuke Murayama, Marcelo A Montemurro, Nikos K Logothetis, and Stefano Panzeri. Low-frequency local field potentials and spikes in primary visual cortex convey independent visual information. *The Journal of Neuroscience*, 28(22):5696–5709, 2008.
- [127] Reid R Harrison. A low-power integrated circuit for adaptive detection of action potentials in noisy signals. In *Engineering in Medicine and Biology Society, 2003. Proceedings of the 25th Annual International Conference of the IEEE*, volume 4, pages 3325–3328. IEEE, 2003.
- [128] Xiaowei Yang, Shihab Shamma, et al. A totally automated system

- for the detection and classification of neural spikes. *Biomedical Engineering, IEEE Transactions on*, 35(10):806–816, 1988.
- [129] RK Snider and AB Bonds. Classification of non-stationary neural signals. *Journal of neuroscience methods*, 84(1):155–166, 1998.
- [130] Rishi Chandra and Lance M Optican. Detection, classification, and superposition resolution of action potentials in multiunit single-channel recordings by an on-line real-time neural network. *Biomedical Engineering, IEEE Transactions on*, 44(5):403–412, 1997.
- [131] Ernest Nlandu Kamavuako, Winnie Jensen, Ken Yoshida, Mathijs Kurstjens, and Dario Farina. A criterion for signal-based selection of wavelets for denoising intrafascicular nerve recordings. *Journal of neuroscience methods*, 186(2):274–280, 2010.
- [132] Xun Chen, Aiping Liu, Hu Peng, and Rabab K Ward. A preliminary study of muscular artifact cancellation in single-channel eeg. *Sensors*, 14(10):18370–18389, 2014.
- [133] Sunan Ge, Min Han, and Xiaojun Hong. A fully automatic ocular artifact removal from eeg based on fourth-order tensor method. *Biomedical Engineering Letters*, 4(1):55–63, 2014.
- [134] Ana Rita Teixeira, Ana Maria Tomé, Elmar Wolfgang Lang, Peter Gruber, and A Martins da Silva. Automatic removal of high-amplitude artefacts from single-channel electroencephalograms.

- Computer methods and programs in biomedicine*, 83(2):125–138, 2006.
- [135] Reza Sameni and Cédric Gouy-Pailler. An iterative subspace denoising algorithm for removing electroencephalogram ocular artifacts. *Journal of neuroscience methods*, 225:97–105, 2014.
- [136] Wim De Clercq, Bart Vanrumste, J-M Papy, Wim Van Paesschen, and Sabine Van Huffel. Modeling common dynamics in multichannel signals with applications to artifact and background removal in eeg recordings. *Biomedical Engineering, IEEE Transactions on*, 52(12):2006–2015, 2005.
- [137] Charles W Anderson, James N Knight, Tim O’Connor, Michael J Kirby, and Artem Sokolov. Geometric subspace methods and time-delay embedding for eeg artifact removal and classification. *Neural Systems and Rehabilitation Engineering, IEEE Transactions on*, 14(2):142–146, 2006.
- [138] Siew-Cheok Ng and Paramesran Raveendran. Enhanced rhythm extraction using blind source separation and wavelet transform. *Biomedical Engineering, IEEE Transactions on*, 56(8):2024–2034, 2009.
- [139] P LeVan, E Urrestarazu, and J Gotman. A system for automatic artifact removal in ictal scalp eeg based on independent component anal-

- ysis and bayesian classification. *Clinical Neurophysiology*, 117(4):912–927, 2006.
- [140] Wim De Clercq, Anneleen Vergult, Bart Vanrumste, Wim Van Paesschen, and Sabine Van Huffel. Canonical correlation analysis applied to remove muscle artifacts from the electroencephalogram. *Biomedical Engineering, IEEE Transactions on*, 53(12):2583–2587, 2006.
- [141] Javier Mateo, Ana Maria Torres, Maria Garcia, et al. Eye interference reduction in electroencephalogram recordings using a radial basic function. *Signal Processing, IET*, 7(7):565–576, 2013.
- [142] Ping He, G Wilson, and C Russell. Removal of ocular artifacts from electro-encephalogram by adaptive filtering. *Medical and biological engineering and computing*, 42(3):407–412, 2004.
- [143] Sadasivan Puthusserypady and Tharmalingam Ratnarajah.  $h^\infty$  adaptive filters for eye blink artifact minimization from electroencephalogram. *Signal Processing Letters, IEEE*, 12(12):816–819, 2005.
- [144] Carrie A Joyce, Irina F Gorodnitsky, and Marta Kutas. Automatic removal of eye movement and blink artifacts from eeg data using blind component separation. *Psychophysiology*, 41(2):313–325, 2004.
- [145] Junshui Ma, Sevinç Bayram, Peining Tao, and Vladimir Svetnik. High-throughput ocular artifact reduction in multichannel electroen-

- cephalography (eeg) using component subspace projection. *Journal of neuroscience methods*, 196(1):131–140, 2011.
- [146] Kianoush Nazarpour, Yodchanan Wongsawat, Saeid Sanei, Jonathon Chambers, Soontorn Orintara, et al. Removal of the eye-blink artifacts from eegs via stf-ts modeling and robust minimum variance beamforming. *Biomedical Engineering, IEEE Transactions on*, 55(9):2221–2231, 2008.
- [147] Hae-Jeong Park, Do-Un Jeong, and Kwang-Suk Park. Automated detection and elimination of periodic eeg artifacts in eeg using the energy interval histogram method. *Biomedical Engineering, IEEE Transactions on*, 49(12):1526–1533, 2002.
- [148] Junshui Ma, Peining Tao, Sevinç Bayram, and Vladimir Svetnik. Muscle artifacts in multichannel eeg: characteristics and reduction. *Clinical neurophysiology*, 123(8):1676–1686, 2012.
- [149] Haitao Guo and C Sidney Burrus. Convolution using the undecimated discrete wavelet transform. In *ICASSP*, pages 1291–1294. IEEE, 1996.
- [150] J Gotman. Automatic recognition of epileptic seizures in the eeg. *Electroencephalography and clinical Neurophysiology*, 54(5):530–540, 1982.

- [151] ME Saab and Jean Gotman. A system to detect the onset of epileptic seizures in scalp eeg. *Clinical Neurophysiology*, 116(2):427–442, 2005.
- [152] Maeike Zijlmans, Premysl Jiruska, Rina Zelmann, Frans SS Leijten, John GR Jefferys, and Jean Gotman. High-frequency oscillations as a new biomarker in epilepsy. *Annals of neurology*, 71(2):169–178, 2012.
- [153] Greg A Worrell, Andrew B Gardner, S Matt Stead, Sanqing Hu, Steve Goerss, Gregory J Cascino, Fredric B Meyer, Richard Marsh, and Brian Litt. High-frequency oscillations in human temporal lobe: simultaneous microwire and clinical macroelectrode recordings. *Brain*, 131(4):928–937, 2008.
- [154] [online]. available. [https://www.som.uq.edu.au/media/285423/EEG\\_simulator.zip](https://www.som.uq.edu.au/media/285423/EEG_simulator.zip).
- [155] [online]. available. <http://physionet.nlm.nih.gov/pn6/chbmit/>.
- [156] Nick Yeung, Rafal Bogacz, Clay B Holroyd, and Jonathan D Cohen. Detection of synchronized oscillations in the electroencephalogram: an evaluation of methods. *Psychophysiology*, 41(6):822–832, 2004.
- [157] Hans Hallez, Maarten De Vos, Bart Vanrumste, Peter Van Hese, Sara Asseconi, Koen Van Laere, Patrick Dupont, Wim Van Paesschen, Sabine Van Huffel, and Ignace Lemahieu. Removing muscle and eye artifacts using blind source separation techniques in ictal eeg source imaging. *Clinical Neurophysiology*, 120(7):1262–1272, 2009.

- [158] Rosana Esteller, Javier Echauz, T Tcheng, Brian Litt, and Benjamin Pless. Line length: an efficient feature for seizure onset detection. In *Engineering in Medicine and Biology Society, 2001. Proceedings of the 23rd Annual International Conference of the IEEE*, volume 2, pages 1707–1710. IEEE, 2001.
- [159] Nathan J Stevenson, John M OToole, Luke J Rankine, Geraldine B Boylan, and Boualem Boashash. A nonparametric feature for neonatal eeg seizure detection based on a representation of pseudo-periodicity. *Medical engineering & physics*, 34(4):437–446, 2012.
- [160] Deng Wang, Duoqian Miao, and Chen Xie. Best basis-based wavelet packet entropy feature extraction and hierarchical eeg classification for epileptic detection. *Expert Systems with Applications*, 38(11):14314–14320, 2011.
- [161] Nidal Rafiuddin, Yusuf Uzzaman Khan, and Omar Farooq. Feature extraction and classification of eeg for automatic seizure detection. In *Multimedia, Signal Processing and Communication Technologies (IMPACT), 2011 International Conference on*, pages 184–187. IEEE, 2011.
- [162] Joshua S Richman and J Randall Moorman. Physiological time-series analysis using approximate entropy and sample entropy. *American Journal of Physiology-Heart and Circulatory Physiology*, 278(6):H2039–H2049, 2000.



- [163] Yuedong Song, Jon Crowcroft, and Jiaxiang Zhang. Automatic epileptic seizure detection in eegs based on optimized sample entropy and extreme learning machine. *Journal of Neuroscience Methods*, 210(2):132–146, 2012.
- [164] Nello Cristianini and John Shawe-Taylor. *An introduction to support vector machines and other kernel-based learning methods*. Cambridge university press, 2000.
- [165] [online]. available. <http://mlpr.wikidot.com/artifacts-in-bci-systems>.
- [166] Stéphanie Devuyst, Thierry Dutoit, Patricia Stenuit, Myriam Kerkhofs, and Etienne Stanus. Cancelling eeg artifacts in eeg using a modified independent component analysis approach. *EURASIP Journal on advances in signal processing*, 2008:180, 2008.
- [167] Chiu-Kuo Chen, Ericson Chua, Zong-Han Hsieh, Wai-Chi Fang, Yu-Te Wang, and Tzyy-Ping Jung. An eeg-based braincomputer interface with real-time artifact removal using independent component analysis. In *Consumer Electronics-Berlin (ICCE-Berlin), 2012 IEEE International Conference on*, pages 13–14. IEEE, 2012.
- [168] Yijun Wang and Tzyy-Ping Jung. Improving brain-computer interfaces using independent component analysis. In *Towards Practical Brain-Computer Interfaces*, pages 67–83. Springer, 2013.

- [169] Manfred Hartmann, Andreas Graef, Hannes Perko, Christoph Baumgartner, and Tilmann Kluge. A novel method for the characterization of synchronization and coupling in multichannel eeg and ecog. *WASET Proceedings*, 34:6–11, 2008.
- [170] Gang Wang, Chaolin Teng, Kuo Li, Zhonglin Zhang, and Xiangguo Yan. The removal of eeg artifacts from eeg signals using independent component analysis and multivariate empirical mode decomposition.
- [171] Rafał Kuś, Anna Duszyk, Piotr Milanowski, Maciej Łabecki, Maria Bierzyńska, Zofia Radzikowska, Magdalena Michalska, Jarosław Żygierewicz, Piotr Suffczyński, and Piotr Jerzy Durka. On the quantification of ssvep frequency responses in human eeg in realistic bci conditions. *PloS one*, 8(10), 2013.
- [172] II Goncharova, Dennis J McFarland, Theresa M Vaughan, and Jonathan R Wolpaw. Emg contamination of eeg: spectral and topographical characteristics. *Clinical Neurophysiology*, 114(9):1580–1593, 2003.
- [173] C Brunner, R Leeb, G Müller-Putz, A Schlögl, and G Pfurtscheller. Bci competition 2008–graz data set a. *Institute for Knowledge Discovery (Laboratory of Brain-Computer Interfaces), Graz University of Technology*, pages 136–142, 2008.
- [174] R Leeb, C Brunner, GR Müller-Putz, A Schlögl, and G Pfurtscheller.

- Bci competition 2008–graz data set b. *Graz University of Technology, Austria*, 2008.
- [175] Christian Andreas Kothe and Scott Makeig. Bcilab: a platform for brain–computer interface development. *Journal of neural engineering*, 10(5):056014, 2013.
- [176] Arnaud Delorme and Scott Makeig. Eeglab: an open source toolbox for analysis of single-trial eeg dynamics including independent component analysis. *Journal of neuroscience methods*, 134(1):9–21, 2004.
- [177] Christopher J James and Suogang Wang. Blind source separation in single-channel eeg analysis: an application to bci. In *Conference proceedings:... Annual International Conference of the IEEE Engineering in Medicine and Biology Society. IEEE Engineering in Medicine and Biology Society. Annual Conference*, pages 6544–6547, 2005.
- [178] Xiao Guixian and Yan Wei. Achieve single-channel bci: The choice of electrode position and signal characteristics. In *Information Management and Engineering (ICIME), 2010 The 2nd IEEE International Conference on*, pages 190–192. IEEE, 2010.
- [179] Sheng Ge, Ruimin Wang, and Dongchuan Yu. Classification of four-class motor imagery employing single-channel electroencephalography. 2014.

# Appendix A

## Source Codes and Artifact Templates

### A.1 Open Source MATLAB Codes for Artifact Removal

#### A.1.1 Artifact Removal from *In-Vivo* Neural Signals

MATLAB source code for artifact removal from *in-vivo* neural signals can be found from following link

[https://drive.google.com/open?id=0B\\_SqwPnI9VgBeTIXUVJEdGs3e1U](https://drive.google.com/open?id=0B_SqwPnI9VgBeTIXUVJEdGs3e1U)

### A.1.2 Artifact Removal from EEG for Seizure Detection

#### Application

MATLAB source code for artifact removal from EEG signals for epilepsy seizure monitoring application can be found from following link

[https://drive.google.com/open?id=0B\\_SqwPnI9VgBNm01ZTJoZ0h1SFk](https://drive.google.com/open?id=0B_SqwPnI9VgBNm01ZTJoZ0h1SFk)

### A.1.3 Artifact Detection and Removal from EEG for BCI

#### Application

MATLAB source code for artifact removal from EEG signals for BCI application can be found from following link

[https://drive.google.com/open?id=0B\\_SqwPnI9VgBcFh5YjJ5cEM3T00](https://drive.google.com/open?id=0B_SqwPnI9VgBcFh5YjJ5cEM3T00)

## A.2 Artifact Templates

### A.2.1 *In-Vivo* Neural Recording

Sample neural recording and synthesized datasets with artifact templates can be found from

<https://www.dropbox.com/sh/k200ofw17vm3rg1/AADlFiVU3Qic40qUoAL5aHPaa?dl=0>

### A.2.2 EEG Recording

Some EEG artifact templates and synthesized EEG data can be found from the shared link

[https://drive.google.com/folderview?id=0B\\_SqwPnI9VgBZ1MzNVFrQlBWRnM&usp=sharing](https://drive.google.com/folderview?id=0B_SqwPnI9VgBZ1MzNVFrQlBWRnM&usp=sharing)

# Author's Publications

## Journal Papers:

1. M. K. Islam, A. Rastegarnia, A. T. Nguyen, and Z. Yang. Artifact characterization and removal for in vivo neural recording. Published in *Journal of Neuroscience Methods* 226:110-123, 2014.
2. M. K. Islam, A. Rastegarnia, and Z. Yang. A Wavelet-Based Artifact Reduction from Scalp EEG for Epileptic Seizure Detection. In *IEEE Journal of Biomedical and Health Informatics*, 2015, accepted (in-press).
3. M. K. Islam, A. Khalili, and Z. Yang. Probability Mapping based Artifact Detection and Wavelet Denoising based Artifact Removal from Scalp EEG for Brain-Computer Interface (BCI) Applications. 2015, under review.
4. M. K. Islam, and Z. Yang. Artifact Characterization, Detection and Removal from Scalp EEG - A Review. 2015, under review.
5. M. K. Islam, and Z. Yang. Unsupervised Selection of Mother Wavelet

and Parameter Optimization during Wavelet Denoising Based Artifact Removal from EEG Signal. 2015, under review.

6. Jian Xu, Menglian Zhao, Xiaobo Wu, M. K. Islam, and Zhi Yang. A High Performance Delta-Sigma Modulator for Neurosensing. *Sensors* 2015, 15(8), 19466-19486; doi: <http://dx.doi.org/10.3390/s150819466>.

## Conference Papers:

1. Islam, MK, Tuan NA, Zhou Y, Yang Z. Analysis and processing of *in-vivo* neural signal for artifact detection and removal. Published in *the 5th International Conference on Biomedical Engineering and Informatics (BMEI)*, p. 43742, 2012, China.
2. Xu, J., Islam, M. K., Wang, S., and Yang, Z. A  $13\mu\text{W}$  87dB dynamic range implantable  $\Delta$ - $\Sigma$  modulator for full-spectrum neural recording. Published in *the 35th Annual International Conference of the IEEE Engineering in Medicine and Biology Society (EMBC)*, pp. 2764-2767), July, 2013.